The Science and Practice of Rubber Mixing

Nobuyuki Nakajima

RAPRA
TECHNOLOGY LTD.

Contents

Preface

Manufacturing rubber products requires the use of many additives. Therefore, mixing is a very important step in rubber processing. There have been extensive research efforts to understand the relationships between formulation and the product properties.

On the other hand processes such as mixing and shaping have only recently become the focus of systematic inquiry. Recognising that there are more than 100 years history in the rubber industry and a number of possible combinations of ingredients in the rubber formulation, the accumulated knowledge of processing must be enormous. However, the knowledge of processing exists in fragments scattered as in-house 'know-how' among manufacturers and more likely as the personal experience of the individual operator.

This work is an effort to summarise systematically the above fragmented knowledge within a unifying scheme, which is based on scientific principles. However, there are difficulties: first, there are so many variables that it is impossible to include every phase of the subject. Therefore, the treatment must be limited to highlights.

Another difficulty is that information from practical experience is usually incomplete. For example, a decrease of Mooney index on milling is interpreted as a decrease of molecular weight, resulting from breaking of polymer chains. The chain-break, however, does not necessarily result in the decrease of molecular weight. It might create a larger molecule by generating long branches. Such a structure sometimes causes a decrease of Mooney index.

Another lack of information is in the description of processability. Some rubber is reported to be poorly processed on the mill. However, there are at least three different causes of this problem. Unless the circumstances are known, the poor mixing cannot be explained. Along with a systematic treatment of the practical experience, the gap in knowledge as well as misconceptions must be pointed out.

In the very beginning we must recognise the fact that there are two different definitions of 'rubber'. One is based on the chemical make-up, such as natural rubber and polybutadiene. The other is based on its physical behaviour. Sometimes a statement is made, 'after a long time (gum) rubber flows'. In this statement the 'rubber' is chemical by definition. The physical description is 'after a long time the material is no longer a rubber because it flows'.

The Mooney index is usually measured under the conditions, i.e., time and temperature, where the material behaviour is rubbery and not flow. Therefore, what is measured is not a viscosity. Yet, it is erroneously called Mooney viscosity. The deformation and fracture may be observable using coloured markers on the rubber specimen.

The rubber behaviour in mixing is also in most cases, deformation and fracture instead of flow. Viscosity contributes only as a frictional heat generation. Namely, the material behaviour is viscoelastic, but the interpretation of mixing has by and large ignored viscoelasticity. One of the objectives of this book is to introduce viscoelasticity to those who are not familiar with this subject.

The misconceptions and lack of understanding are not limited to the material behaviour, but also include molecular architecture. Although the importance of molecular weight and its distribution are well recognised, the subject of branching has been less critically examined. Often the presence of branches has a dominant influence on the rubber behaviour. In addition there are two aspects of this subject which are not well recognised. The first is a crossover phenomenon, in that the presence of long branches has an opposite effect depending upon the imposed conditions. For example, at long times or at low frequencies, the presence of long branches increases modulus, but at short times or high frequencies, it decreases the modulus. There are many examples of the crossover phenomena so that a statement like 'the long branch does this or does that', cannot be made.

Another problem concerns various branch patterns. The behaviour of one pattern may be quite different from that of another. For example, a long branch may be so long that it gives strain-hardening upon stretching but if the other long branch is not as long, it will give strain-softening under the same conditions. Long branching with equal arm-stars or combs is a very special type and findings from these cannot be generalised to all branch patterns.

Another subject of importance is a 'gel', which is present in many rubbers. The definition of the term is unique in the field of rubber and is different from that used in physical chemistry. In physical chemistry, gel is a solvent-swollen polymer, which is capable of supporting a finite stress. In the field of rubber, gel is a gigantic molecule but comes in different structures. This subject has not been explored sufficiently, but influence of gels on the mixing has been recognised to be important.

Even when the relationship between the molecular architecture and the mixing behaviour are carefully investigated, a knowledge gained from one type of rubber, for example, ethylene-propylene-diene copolymer can not entirely be used to interpret the relationship in other types of rubber, such as butadiene-acrylonitrile copolymer.

In order to understand mixing of rubber one has to have a breadth and depth of knowledge, including polymerisation processes and post-mixing processes such as extrusion and injection moulding.

This book is written for students, teachers and those outside of the rubber industry. It is also written for those in rubber industry, who wish to acquire a scientific viewpoint. Last but not least it is written for the researchers in this field. In this regard subjects for future research are pointed out wherever appropriate. With varied readers in mind, each chapter is written in such a way that it may be read independently from others.

The author wishes to thank many people who generously shared their experience and his former colleagues for their contributions.

Professor N Nakajima
The University of Akron
December 1999

1 Introduction

1.1 Polymerisation and molecular architecture

Listed in Table 1.1 are a representative selection of commercially available rubbers. The commercial rubbers are those confined within the cost-performance window and there are other rubbers which may be synthesised, if needs arise. Some rubbers are used to perform mechanical functions only and others are used because of additional special features. Such features may be the outdoor- and chemical-stability, oil resistance and high temperature stability.

Within each rubber there are many variations, i.e., commercial grades, which are fine-tuned for specific applications. Because each grade of rubber has its own processing characteristics, those who handle them need to know the properties of the rubbers that they use.

Even for those who purchase rubbers for processing, some knowledge of their manufacture is helpful. For those who are in the marketing of rubbers, relationships between manufacturing conditions and processability must be understood for technical as well as economic reasons. Even though the description of the manufacturing of rubbers is outside of the scope of this book, some highlights need to be given. This will be done with selected group of rubbers. For further information on this topic, readers are referred to encyclopaedia [1] and review [2].

1.1.1 Natural rubber

NR is the only natural product amongst those in Table 1.1. It is a *cis*-polyisoprene but contains a variety of impurities such as proteins and resins. It crystallises much more readily upon stretching compared to synthetic *cis*-polyisoprene, IR, which does not contain the impurities. NR has a very high molecular weight (MW) and contains long branches.

1.1.2 Styrene-butadiene copolymer

SBR comes in two distinctly different forms. One is emulsion-polymerised, E-SBR and the other is solution-polymerised, S-SBR.

Table 1.1 Abbreviations of Representative Commercial Rubbers	
Natural Rubbers	NR
Styrene-butadiene copolymer	SBR
Styrene-isoprene-butadiene terpolymer	SIBR
Polyisoprene	IR
Acrylonitrile-butadiene copolymer	NBR
Polychloroprene	CR
Ethylene-propylene copolymer	EPM
Ethylene-propylene-diene terpolymer	EPDM
Polyisobutylene	IIR
Polyethylacrylate	ACM
Chlorosulphonated polyethylene	CSM
Polydimethylsiloxane	MQ
Vinylidene fluoride type polymer	FKM
Tetrafluoroethylene-propylene	TFEP
Tetrafluoroethylene-perfluoromethyl vinylether	FFKM
Fluorosilicone	FQ
Epichlorohydrin rubber	CO
Epichlorohydrin-ethyleneoxide	ECO
Polysulphide	T
Polyurethane	U
Chlorinated polyethylene	CPE
Ethylene vinylacetate polymer	EVA

Most of the E-SBR contains about 24% by weight of styrene and it is a random copolymer with butadiene. Some specific grades contain as much as 40~46% styrene, and are much stiffer. The polymerisation is by free radical initiator and there is a finite probability of chain-transfer reaction, which generates long branches. Because the chain-transfer targets

existing polymer chains, a larger molecule offers a better target. It results in a branched molecule becoming more branched.

At the high conversion the polymer concentration within the emulsion droplets becomes very high and the long branches are more readily formed. The extensive formation of branches results in a gigantic molecule, which is called gel. The definition of the term 'gel' is unique to rubber technology and different from the one defined in physical chemistry; in the latter the gel is a solvent-swollen network, which is capable of supporting a finite stress. To a rubber technologist the gel is a constituent of gum rubber, and usually it has the same chemical composition to other parts of the rubber. Because the term has been used for so many years one has to accept it as is, but should not be confused with the definition of gel outside of the field of rubber. The determination of the amount of gel requires a good solvent for the rubber and subsequent filtration. Sometimes the presence of long branches and gel are ignored and the MW and its distribution are reported. Such information is misleading. The subject of the molecular architecture has a critical importance on the mixing behaviour and will be discussed later in more detail.

Another important feature is the sequence [3] by which butadiene polymerises; it is called a 'microstructure', resulting from different ways of addition. A typical value for E-SBR is 13% *cis*-1,4, 69% *trans*-1,4 and 18% 1,2 addition. The 1,2 addition results in vinyl pendent group. A pendent group is a small side group, which usually has a different chemical composition from that of the main chain, e.g., the phenyl-group in SBR. If the composition is the same and it has a polymeric sequence it will be called a 'branch' in this book.

E-SBR is one of the first commercial rubbers; in the early days of manufacture the polymerisation temperature was high and many long-branches and gels were formed. The rubber was stiff and difficult to mill. It was called 'hot rubber'. Later polymerisation at a lower temperature became possible, giving less branches and gels; this is called 'cold rubber'. Polymerisation temperature for hot rubber is typically 25-50 °C and that for cold rubber is 5-25 °C. Today most of the E-SBR is of the latter type, but some high-gel rubber is made for a special purpose. It may be made either at a higher temperature or carrying the polymerisation to a higher conversion at a lower temperature.

S-SBR comes in two distinctly different subgroups, one made by an anionic initiator and the other by, for example, free radical initiators. The anionic rubbers have a very narrow MW distribution, sometimes called 'monodispersed'; the expression is only symbolic and not accurate. This molecular feature results in a unique mixing behaviour. The rubber has no branches or gels unless specifically designed to have them. The MW distribution can also be broadened by design. The microstructure of butadiene portion is for example, 33% *cis*-1,4, 54% *trans*-1,4 and 13% vinyl.

However, a high vinyl rubber is also made. The styrene content may be varied widely. The chain-end may be modified to improve affinity to carbon black, resulting in a better dispersion of the filler. These variations in molecular architecture were developed for satisfying the requirements of automotive tyres for a low energy loss and a high skid resistance. The anionic polymerisation provides a flexibility in designing molecular architecture; such a flexibility is unavailable for the current practice of other polymerisation systems.

S-SBR made from initiators other than anionic has a broader MW distribution, which depends upon the polymerisation conditions. The branching probability is much less than that in the emulsion polymerisation primarily because of the lower local concentration of polymer. The mechanisms of the long branch-formation are different for different initiator (catalyst) systems. This aspect will be discussed with butadiene (BR) polymerisation.

1.1.3 Polybutadiene

BR is made with similar polymerisation systems as SBR. The molecular architecture of the anionic BR is essentially the same as that described for the anionic SBR. The microstructure is also the same and some high vinyl BR is also made. This system gives well-defined polymers, for example 'monodispersed' linear and equal-arm star molecules. The equal arm star molecule is a branched polymer with equal branch-lengths. These samples have been extensively investigated to obtain scientific information.

BR made by emulsion polymerisation with a free radical initiator is used as the rubber component of a high impact polystyrene and acrylonitrile-butadiene-styrene (ABS) resins. No discussion will be given on the molecular structure of this rubber. For those, who are interested in the relationship between molecular architecture and mixing behaviour, this is discussed in Section 1.1.2 on E-SBR.

Cis-1,4-BR is one of the rubbers widely used for the automotive tyres. It has a high *cis*-content (greater than 90%), and the remainder is vinyl. Because of its unique microstructure it must be regarded as a polymer, which is chemically different from other BRs. Use of the same symbol, BR, for all rubbers polymerised from butadiene, may be misleading.

Cis-1,4-BR is polymerised with a catalyst, a metal-coordination complex, where the metal may be cobalt, neodymium, nickel or titanium and the rest consists of organic moieties having coordination bonding with the metal. A co-catalyst may also be used. The polymerisation mechanism is distinctly different from that in the free-radical system.

In the latter the growing end is the free radical, where the monomer reacts and keeps the chain growing. In the metal-complex system the growing polymer is attached to the metal and a monomer is inserted between the metal and the growing chain. The polymer chain is pushed out as it grows, in a similar way to the growth of a hair.

Because the growth mechanisms are different between the free-radical and the metal-complex systems, mechanisms of branch formation and resulting branch patterns are also quite different. The free radical of the growing-end, abstracts the hydrogen atom from other polymer-chain and thus terminates its growth. The other polymer chain, where hydrogen was abstracted, now has a radical at the site, which starts growing a new polymer branch. As explained using E-SBR as an example in Section 1.1.2, the branched chain becomes more branched and the branched-branches are the pattern. The extensive formation of branches results in gigantic molecules, called gels. The mechanism of branch-formation in the metal-complex system is insertion; instead of the monomer being inserted, a grown polymer chain becomes inserted, i.e., a macromer insertion. Because the vinyl group in *cis*-BR is more reactive than the double-bond along the main chain, the vinyl is the most likely group to be inserted. There is a trend that when the vinyl content is higher in the rubber, there are more long branches. Because the macromer is more difficult to insert than the monomer, the branch-formation is not frequent. Once branching occurs an additional branch-formation becomes less likely because of the steric effect. Therefore, not only the branch pattern is different from that in the free-radical systems, but also there is no gel formation. The degree and length of branching depend upon the availability of the macromer and the nature of the catalyst site. For example, cobalt-based *cis*-1,4-BR shows significant branching with increased conversion [4] and the presence of chain insertion to aluminium alkyl during polymerisation was suggested for the neodymium catalyst system [5]. It has also been shown that the degree of branching can be controlled by a use of a highly reactive catalyst and co-catalyst [6].

1.1.4 Nitrile rubber

NBR is made as an emulsion with a free radical initiator. Therefore, the mechanisms of polymerisation and branch (gel) formation are very similar to those of E-SBR. Polymers are made with an acrylonitrile (AN) content of, for example, 28, 33 or 40 weight percent, depending upon the required oil resistance. The copolymerisation is described as 'random' but the reactivity ratio is such that it is biased towards an alternating sequence. Because of this and because AN is the minor component, it is used up early and polymer formation at a later stage of polymerisation becomes butadiene rich [7]. In order to have a uniform composition among polymer chains, the monomer mixture of the prescribed ratio is 'metered in' with the progress of polymerisation.

A special grade contains as much as 70% gel, which is a 'tree-like' branched molecule. Another special grade is made with a 'crosslinking termonomer', a difunctional monomer. This makes a microscopic network of the emulsion polymer, a 'micro ping pong ball'. This is also called a gel, but has a different molecular architecture. In order to differentiate these two types, the former has been called a 'macro-gel' and the latter 'microgel'. The above terms originated from the work-place and became accepted widely but only within rubber technology. Concerning the microgel there are two different usages even within the field. With rubbers made by methods other than emulsion polymerisation, micro ping pong balls are not made. With these rubbers, the term 'microgel' is sometimes used for a smaller sized tree-like molecule. In this case the difference between macro and micro is only a difference in degree. On the other hand with the emulsion polymerised rubbers there is a distinct difference between micro- and macro-gel in structure and in processability.

1.1.5 Ethylene-propylene terpolymer

EPM and EPDM are made using a metal coordination complex. Although there are minor variations, it is generally called 'Ziegler-Natta' polymerisation. MW distribution varies and not 'monodispersed' like that in the anionic polymerisation. EPMs are linear. EPDM contains a difunctional comonomer, either ethylidene-norbornene (ENB) or dicyclopentadiene (DCPD). These comonomers are there to provide crosslinking sites for vulcanisation. However, some crosslinking occurs during polymerisation, resulting in long branch formation. The branch pattern may lead to a branched-branch and to a gel formation. Here also, the degree of long branching and that of gel are very important to the processability.

1.1.6 Polyethylacrylate

This rubber is made by the emulsion polymerisation with a free radical initiator. Therefore, the mechanisms of polymerisation and the long-branch (gel) formation are the same as those of SBR and NBR. However, there are some significant differences in the nature of the chain:

(i) it has a large pendent group, which forms 73% of its MW so that it is a fat and short chain for a given MW.

(ii) it is a polar polymer, having a polar group on every other carbon atom along the chain.

(iii) it has a saturated chain so that a cure-site comonomer is copolymerised for providing crosslinking sites. It is called a 'homopolymer' commercially. The 'copolymer' contains a third monomer in the chain.

1.1.7 Polydimethyl siloxane

MQ is usually made by a condensation polymerisation, which gives a theoretically dictated 'equilibrium' molecular-weight-distribution. This means there is significant amount of the low MW fraction. The extremely low MW fraction is removed prior to finish manufacturing. However, the intermediate low MW fraction weakens the crosslinked product, because the free-ends do not contribute to the strength. The condensation mechanism does not create a very high MW tail, which is often found with other rubbers. The polymer may also be made with an anionic system. In this case the MW distribution is very narrow and it does not contain a low MW fraction.

1.1.8 Masterbatches

Some gum rubbers come with preblended oil or preblended carbon black. They are called 'oil-masterbatch' or 'carbon black masterbatch', respectively. The oil is called 'extending oil' and is either aliphatic, naphthenic or an aromatic fraction of petroleum. Some standard grades of E-SBR oil masterbatch contain 37.5-50 parts oil by parts per hundred by weight of rubber (phr). However, the oil masterbatch does not give an oily surface and it is not easy to distinguish it from non-oil extended rubber. Gum rubber used to prepare the oil masterbatch usually has a very high MW and long branches. Without the preblended oil, it may be difficult to mill. Because of these molecular features, the products made from the masterbatch have good strength in spite of the presence of large amount of oil.

Oil masterbatches are among the standard grades in E-SBRs, *cis*-1,4-BRs and EPDMs. The carbon black masterbatches are also among the standard grades in E-SBR and *cis*-1,4-BR. The amount of carbon black is typically 50 or 100 phr. With a use of a masterbatch a better dispersion of carbon black may be obtained.

1.2 What is rubber?

In this book the word 'rubber' means uncrosslinked raw material unless stated otherwise. By posing the question 'what is rubber?' we are concerned with fundamental but very common sense meaning of the term.

The word, rubber usually indicates such substances as NR, SBR and so on. But, this does not lead to the definition of rubber. The definition is actually based on a very simple experience:

(i) A rubber material allows a large deformation without break; it stretches easily several times and even more than fifteen times in some case.

(ii) The deformation recovers almost 100% instantly.

The substances usually called rubber, exhibit the above behaviour at ambient conditions. However, the same substance called rubber loses the behaviour (i) at low temperatures, becoming a glass. When a rubber is heated to a high temperature, it becomes a viscous fluid, losing the behaviour described in (ii).

Here the word, rubber, is used in two different ways; one is referring to specific substances such as natural rubber and SBR. The other is an expression of mechanical behaviour for material at a specific temperature range.

In the rest of the book the former will be termed as gum rubber and the latter as the rubbery state or rubbery behaviour.

Among the substances encountered daily, there are many which exhibit behaviour (i) such as hot candies and bread dough; but they do not exhibit behaviour (ii). On the other hand most solids behave as (ii) but break without giving large deformation (i). The rubber is the only substance which satisfies both conditions (i) and (ii). Stated differently, any substance which shows both (i) and (ii) behaviour is a rubber, regardless of its chemical nature. Namely, the definition of rubber is based on purely physical behaviour. This is in contrast to chemically based definitions of substances such as carbohydrates, alcohols and hydrocarbons.

A substance exhibiting rubbery behaviour may become glassy if a very high rate of deformation is imposed. This is rather difficult to demonstrate, because extremely high rates are required. On the other hand, if the rate is very low, it deforms permanently, i.e., flows. This is also difficult to demonstrate, but is observable with relatively low MW rubber. When bales of such a rubber are stuck on top of the others, the bottom bale may show a 'cold flow' over a long period of time.

Because a high rate of deformation corresponds to a short time, we can see that the rubbery behaviour is manifested only within a certain time-frame. It is manifested within a certain temperature-frame also. Putting the time and temperature frames together, it is called the 'time-temperature window'. Only when a polymer is within this window, does it exhibit rubbery behaviour. Outside of the window at the higher rates (shorter times) or

at a lower temperature, it is glassy. At the lower rates (longer time) or the higher temperature, it is a high viscosity fluid.

Even though the definition of rubber is based on physical aspects only, there must be structural features which provide rubbery behaviour. In fact, there are three structural requirements for a given substance to be a rubber.

First, rubber is made up of a polymer chain, linear or branched. Second, the chain is flexible. And, third, the chain is longer than a certain threshold length. The last is called 'entanglement coupling distance' [8], *Xe* and in terms of the corresponding MW, M_e. The entanglement is a coupling of adjacent chains to form a three-dimensional network, giving rubber the appearance of a solid, albeit a 'soft solid'. This network and the flexibility of the chain are the reasons why rubber behaves as defined earlier in (i) and (ii).

The concept of entanglement is indispensable for explaining rubber behaviour. Yet, nobody has observed the entanglement as such. The concept is a result of rationalisation that because polymer chains are long, they must entangle. Spaghetti and worms are often cited as models. However, these models are not proof. From a similarity in behaviour of a crosslinked rubber-network and an uncrosslinked rubber, the latter is assumed to have a 'network' made up of the entanglements. Those who are interested in a more critical discussion, are referred to Ferry [8].

In this book the term 'entanglement' is used without specifying the nature of the interactions among polymer chains. However, understanding of *behaviour* as a manifestation of the entanglement is indispensable for interpreting processing of rubber.

Even though the rubbery behaviour is defined by time as well as temperature, the various gum rubbers are usually classified according to their temperature dependence alone. This is probably because the temperature dependence is more obvious. For convenience the temperature at which the rubber becomes glassy is selected as a representative parameter and designated as glass transition temperature (T_g). Because there is a temperature range where rubbery behaviour changes to glassy, exactly which temperature in the glass-rubber transition to be assigned as T_g must be decided. Also, the transition behaviour depends upon the time-scale (or frequency) of measurements and the cooling rate. Therefore, the data of T_g are those measured with mutually agreed procedures. For more detailed discussion the readers are referred to Ferry [8]. Table 1.2 lists T_gs, for representative commercial rubbers [8].

A more flexible chain tends to have a lower T_g as can be seen with *cis*-1,4-BR. The pendent group and its size tends to increase the T_g as can be seen in IR against *cis*-1,4-BR and SBR against NR. The presence of polar groups in NBR and ACM raises T_g.

Table 1.2 Glass-Rubber Transition Temperature, T_g, of Representative Rubbers		
Rubber	**Tg, °C**	**Remarks**
NR	–73	
SBR	–63	23.5% styrene
BR	–112	*Cis*-1,4
	–68	*Cis*, *trans*, vinyl
NBR	–58	20% AN
	–24	40% AN
CR	–50 ~ –45	
EPM	–31	E/P=16/84 by mole
	–57	E/P=56/44 by mole
EPDM	–60 ~ –40	
IIR	–70	
MQ	–123	
ACM	–14	
E/P: Ethylene:Propylene ratio		

In addition to low temperature limit, T_g, the ceiling temperature for the rubbery behaviour is important, because the gum rubber changes into a high viscosity fluid. A very low T_g rubber tends to have the low ceiling temperature, but the T_g alone does not have an exact relation to the temperature of rubber-to-flow transition.

As the ceiling temperature is approached, some rubber loses chemical stability. The initial reaction is crosslinking, creating long-branches. When the reaction is extensive both chain-scission and crosslinking occur. Such a reaction may be intensified by the mechanical action like milling and by the presence of oxygen or peroxide.

1.3 Formulation

Rubber is seldom used alone. Almost always a number of additives are used [9]. Table 1.3 gives an example of a passenger tyre formulation [10], which is also called a 'recipe'.

Table 1.3 Example of a Rubber Formulation for a Passenger Car Tyre	
	phr
SBR 1712	96.25 (70.0 rubber, 26.25 oil)
Cis-1,4 BR	30.0
Zinc oxide	3.0
Stearic acid	2.0
Carbon black (N-330)	85.0
Aromatic oil	20.0
Anti-oxidant	1.0
Accelerator	1.2
Sulphur	1.5
Total	**239.95**
Rubber %	41.7

SBR 1712 is an E-SBR extended with 37.5 phr of aromatic oil. Zinc oxide shortens the cure-time and stearic acid promotes the efficiency of the accelerator in vulcanisation. Examples of typical formulations for specific applications are given in handbooks [11].

Even though there are many additives most of the attention in this book will be given on mixing of rubber and reinforcing fillers. This is because mixing of these is most difficult and when it is done satisfactorily, other ingredients are usually well mixed. Some additives cause specific effects on mixing; for example, a premature crosslinking reaction during mixing will be discussed in Chapter 12.

1.4 Mixing equipment

There are essentially two types of mixing equipment, a roll-mill and an internal mixer. Examples are shown in Figures 1.1 and 1.2 . With the roll-mill an operator performs part of mixing operation whereas with the internal mixer, only charging and discharging are done by the operator.

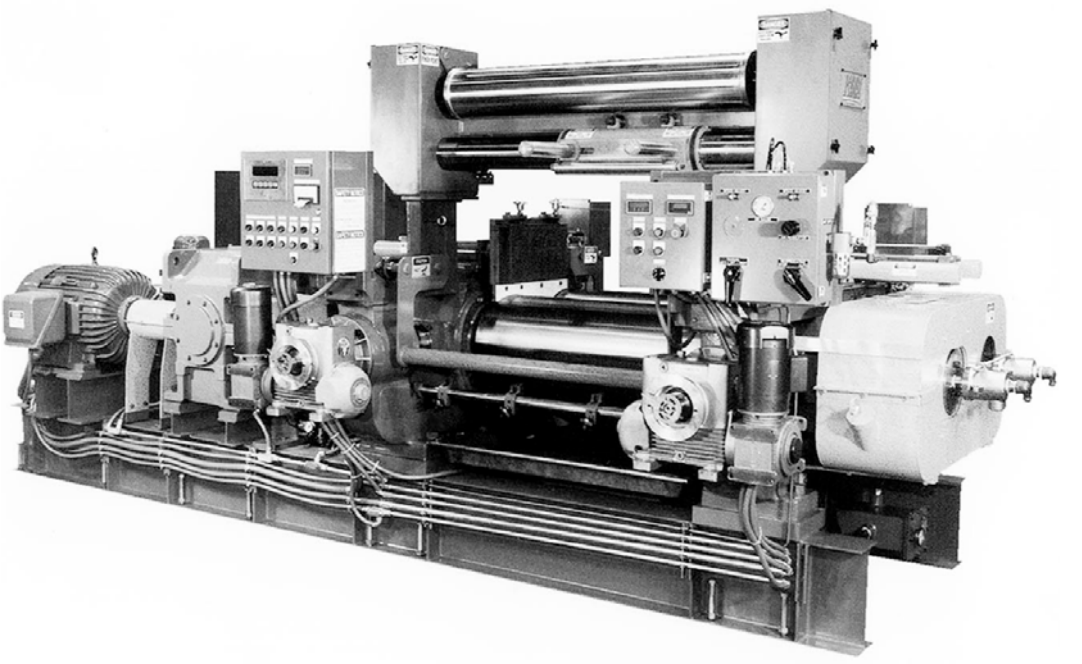

Figure 1.1 Roll Mill.

Reproduced by kind permission of Kobelco Stewart Bolling, Inc.

The rolls in a roll-mill are rotated at constant speeds, 15-20 rpm, with the back roll running a little faster. A gap between the rolls is adjustable. The rolls may be heated or cooled with a liquid circulating inside. The entire mixing operation is performed through repeated charging and discharging of rubber. The additives are charged while the rubber is banded onto a roll.

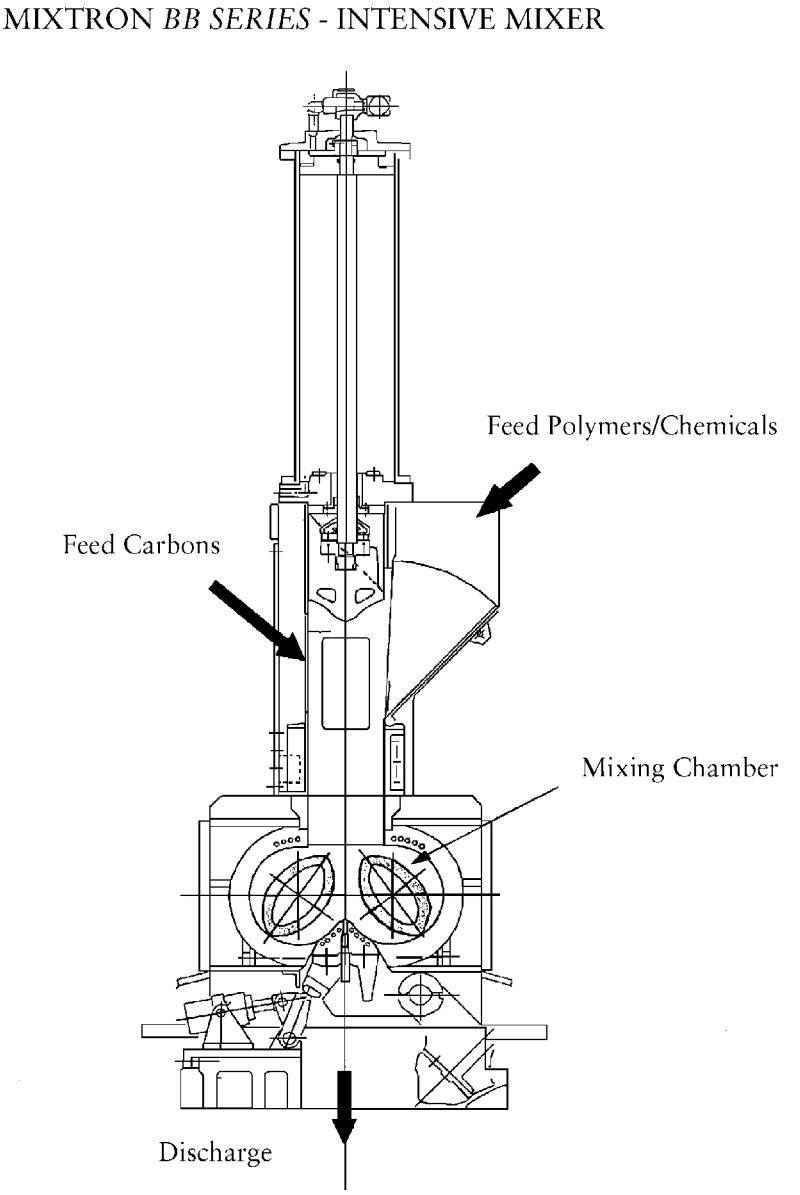

Figure 1.2a Internal Mixer.

Reproduced by kind permission of Kobelco Stewart Bolling, Inc.

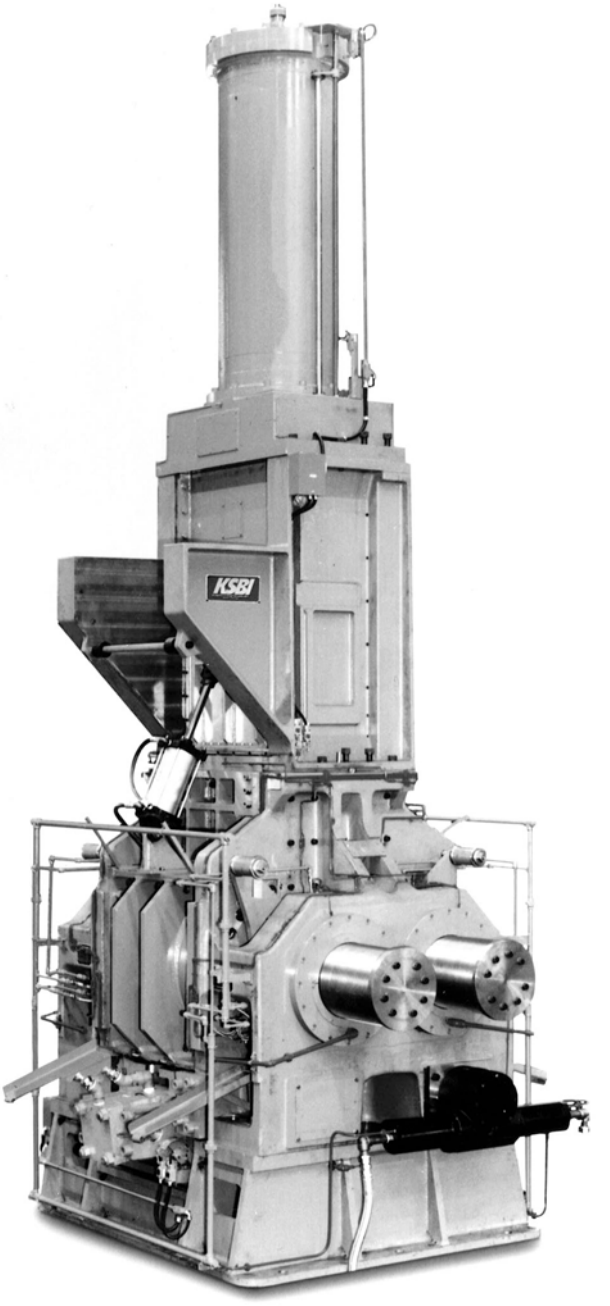

Figure 1.2b Internal Mixer.

Reproduced by kind permission of Kobelco Stewart Bolling, Inc.

Mixing with the internal mixer is performed with two rotors, which are confined within a chamber (see Figures 1.2a, 1.2b and 1.3). Unless specially modified, the rotor speeds are fixed and there may be a small difference in the speed of two rotors. Both the chamber wall and rotors may be heated or cooled with a circulating liquid. Usually, it is cooled with water.

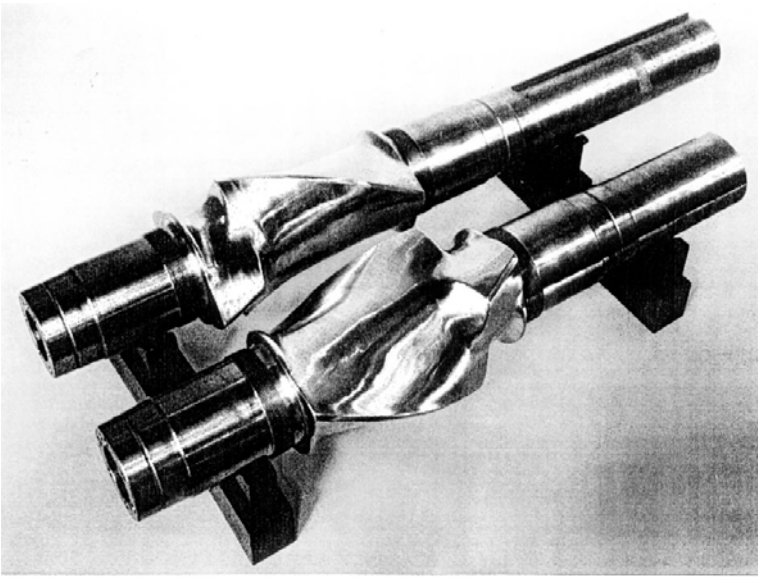

Figure 1.3 Rotors for an internal mixer.

Reproduced by kind permission of Kobelco Stewart Bolling, Inc.

The internal mixers are made in two types, one is tangential and the other is intermeshing [12]. Most widely used in mixing rubber are Banbury mixers (see Figures 1.4a and 1.4b), which are tangential. An intermeshing type is shown in Figure 1.4c.

In the tangential mixer, there is a gap between two rotors. The mixing action is primarily between the rotor tip and the chamber wall, the milling zone. The rest of the space is used to circulate material.

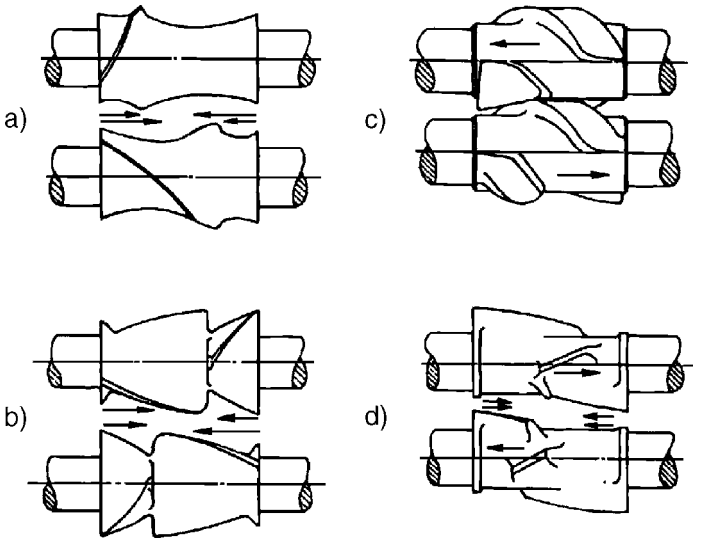

Figure 1.4 Examples of rotor designs (arrows indicate pumping action of wings).
a) Banbury two-wing, wings pumping from ends to centre section
b) Banbury four-wing, wings pumping from ends to centre section
c) Shaw intermix three-wing, the large wings on each rotor pump to opposite ends, while the small ones do not contribute very much to axial flow
d) Werner & Pfleiderer four-wing, the two large wings on each rotor pumping from ends to centre section, while the two small ones operate to give a reversing action.

Figure 1.5 illustrates these actions schematically [13]. The descriptions such as longitudinal cut-back, kneading and lateral overlap are derived from the behaviour of rubber on the mill. The longitudinal cut-back is slicing the band of rubber on the mill and laying sidewise to form a double layer. The lateral overlap is making layers of rubber by rolling a sheet of rubber off the mill and recharging. Kneading is the action of the rubber above the mill rolls prior to entering into the mill gap. Similar behaviour is assumed to occur in the internal mixer also, but the content of the mixer may not always behave in this manner because each rubber behaves differently. With the intermeshing rotors the milling zone is between the rotors as well as between the rotor and chamber wall.

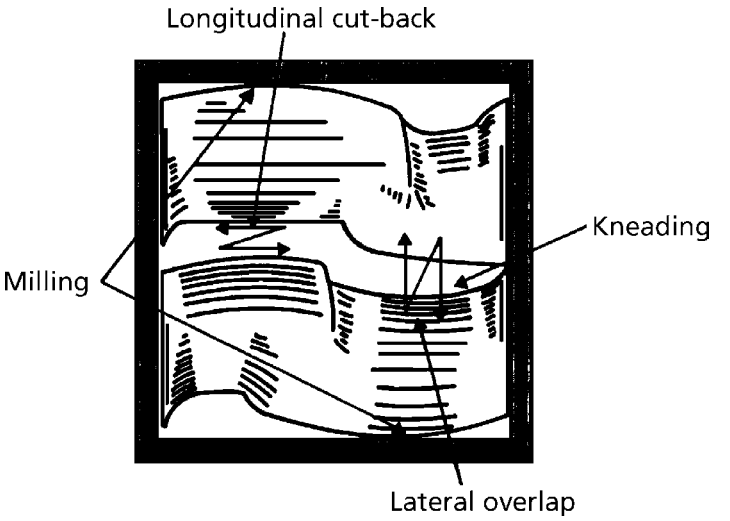

Figure 1.5 Behaviour of compound in the internal mixer.

Reprinted with permission from Understanding the Banbury Mixer, The Farrel Company. Copyright 1968, The Farrel Company.

Choice of a mixer depends upon technical as well as economic requirements. Roll-mill is more labour intensive and often used for research and development. However, in many production lines the mixing is started in an internal mixer and finished in a roll-mill as the two types of mixers are installed in tandem.

References

1 *Kirk-Othmer Encyclopedia of Chemical Technology*, 4th Edn., Wiley, New York, 1997, **8**, 905 and **9**, 1.

2 Rubber Chemistry and Technology, Annual Reviews:
Emulsion Technology:
a) J. Ugelstad and F. K. Hansen, *Rubber Chemistry and Technology*, 1976, **49**, 3, 536.
b) C. A. Uraneck, *Rubber Chemistry and Technology*, 1976, **49**, 3, 610.
Anionic Polymerisation:
c) M. Morton and L. J. Fetters, *Rubber Chemistry and Technology*, 1975, **48**, 3, 359.
d) B. J. Bauer and L. J. Fetters, *Rubber Chemistry and Technology*, 1978, **51**, 3, 406.
e) A. F. Halasa, *Rubber Chemistry and Technology*, 1981, **54**, 3, 627.

3 Y. Tanaka, H. Sato, K. Hatada, Y. Terawaki and H. Okuda, *Rubber Chemistry and Technology*, 1978, **51**, 2, 168.

4 L. J. Kuzma and W. J. Kelly in *Kirk-Othmer Encyclopedia of Chemical Technology*, 3rd Edn., Wiley, New York, 1978, **8**, 555.

5 H. L. Hsieh and H. C. Yen, *Rubber Chemistry and Technology*, 1985, **58**, 1, 117.

6 H. Fries and B. Stollfuss, Presented at the 134th Meeting of the ACS Rubber Division, Cincinnati, OH, Fall 1988, Paper No.8.

7 A. H. Jorgensen, L. A. Chandler and E. A. Collins, *Rubber Chemistry and Technology*, 1973, **46**, 4, 1087.

8 J. D. Ferry, *Viscoelastic Properties of Polymers*, 3rd Edn., John Wiley and Sons, New York, 1980, 241 and 280.

9 *Kirk-Othmer Encyclopedia of Chemical Technology*, 4th Edn., Wiley, New York, 1996, **21**, 460.

10 *JSR Handbook*, JSR Ltd., Tokyo, Japan, p.45.

11 *The Vanderbilt Rubber Handbook*, R. T. Vanderbilt Co., Inc., Norwalk, CT, 1990.

12 H. Palmgren, *Rubber Chemistry and Technology*, 1975, **48**, 3, 462.

13 *Understanding the Banbury Mixer*, The Farrel Company, Ansonia, CT, 1968, p.8.

2 Mill Processability

2.1 Mastication and mill processability

Mixing of rubber is often preceded by kneading the gum rubber to soften it, a process called mastication. What happens to the rubber in this process may be observed in a mill. During World War II when synthetic rubbers were being developed difficulty in milling was one of the problems that needed to be overcome. In the later years with the introduction of a variety of synthetic rubbers, each rubber was found to show a unique behaviour on the mill. Through experience mill operators learned that there are certain patterns in mill behaviour. Accordingly, they adjusted milling conditions to ease the milling difficulties.

Subsequently, the milling patterns were classified by Tokita and White [1] into four regions of mill processability [1], see Figure 2.1.

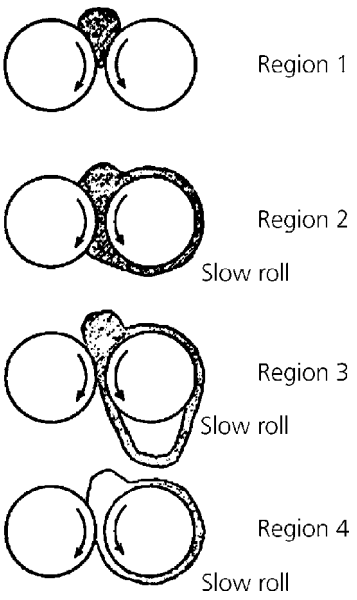

Figure 2.1 Regions of mill behaviour of rubber.

Reprinted with permission from N. Tokita and J. L. White, Journal of Applied Polymer Science, 1968, 12, 7, 1589. Copyright 1968, John Wiley & Sons, Inc.

When a piece of rubber is charged into a mill, if the rubber is too stiff, it slips on the roll and does not go into the mill-gap. If the rubber is forced into the gap, it breaks into pieces, falling down underneath instead of banding around the roll; this is Region I. When the rubber is soft enough it enters the mill-gap easily and forms a band around the roll. When the banded rubber is elastic enough and acts as if squeezing the roll, this is Region II. When the rubber is even softer, it enters the mill-gap, forming a band, but the band does not have the elastic tension; it tends to sag and tear, Region III. Further softening of rubber is accompanied by development of tack, whereby the rubber bands on the roll, however, there is no elastic tension, Region IV. Similar observations have been reported on the behaviour of rubber in the internal mixer [2].

When the behaviour of rubber is in Region I, the operator must scoop up the broken pieces of rubber and recharge them into the mill. This makes the milling operation cumbersome; therefore, the operator makes the mill-gap wide enough so that the rubber goes through without breaking or with a minimum break. The gap is gradually narrowed, while the rubber is passed through the gap repeatedly. Meanwhile the rubber becomes warmer and as a result its behaviour changes to that of Region II. The rubber behaviour in Region II is preferable, not only for mastication, but also for incorporation and dispersion of the reinforcing filler, such as carbon black or silica. In Region III, the operator sometimes pushes rubber against the roll in an attempt to establish a tight band but it is often ineffective. Moreover, the rubber sometimes adheres to the back roll, which is rotating at a somewhat higher speed. There are times when only a part of the rubber goes into the back roll and the rest remains on the front roll.

All in all the handling of rubber is very difficult. The operator tries to avoid Region III behaviour as much as possible. In Region IV there is no problem in the incorporation of the filler but the dispersion is not effective, because the stress transmitted from the machine to the filler agglomerate is not high enough to break it. The tack of the rubber also makes handling difficult.

When the internal mixer is used, the rubber behaviour is not directly observable. However, if the rubber behaviour is in Region I, the rubber breaks down to many pieces. If the filler is added before the rubber is massed, the incorporation becomes difficult. The mixing either takes too long or results in unsatisfactory dispersion. Region II is also the most preferred behaviour with the internal mixer. When the rubber is expected to behave in Region III or IV, the usual practice is to charge the filler first, followed by rubber, i.e., upside-down mixing. In this way a good dispersion of filler may be achieved.

Sometimes rubber and additives are charged together into the internal mixer without masticating the rubber. This is done with relatively soft rubber or with the aid of a ‘process oil’. During mastication, NR chains break, resulting in a substantial decrease of

molecular weight. With synthetic rubbers only a small number of the chains usually break. However, some chain breaking does occur, resulting in the generation of free radicals. The free radicals react with other polymer chains to form long branch chains.

NR, in general, has a very high MW and mastication is used to bring its molecular weight down to a more easily processible range. Traditionally, the MW level expressed as a Mooney index of 50 was considered to be the easiest processing level. This is the reason why the standard grade, E-SBR 1500 (copolymer of styrene and butadiene prepared by emulsion polymerisation) was made to a Mooney index of 50. The E-SBR, as is well-known, was the first synthetic rubber designed to be a substitute for NR.

2.2 Interpretation of mill processability

In section 2.1 the behaviour of rubber on the mill was explained with respect to four typical behaviours, i.e., four regions of processability. With some rubbers, milling starts from Region I, finishing at Region II, and other rubbers remain at Region II throughout milling. Starting from Region II, sometimes rubbers go to Region III or Region IV. Nevertheless, the four regions of behaviour are common to all rubbers; therefore, it provides a means of systematic classification. The scientific explanation for the four regions of processability behaviour is as follows.

In Region I, the rubber is too stiff which means that the modulus is too high. If the rubber is forced into the mill-gap, it breaks into pieces because the strain at break is not large. In Region II, rubber has an ideal softness; that is, the modulus is lower than that in Region I. The rubber does not break and makes a tight band around the roll because its strain at break is large. In both Regions I and II the elasticity is the controlling factor.

But, what is elasticity in this context? The high elasticity does not necessarily mean a high modulus. It is related to the extensibility and more importantly to the ability of the rubber to recover from deformation. Although elasticity controls Region I and II, the temperature of the rubber increases as the milling continues. This is due to the internal friction, which is the viscous contribution. Therefore, both viscosity and elasticity are recognised to be the contributing factors. Thus, the subject of viscoelasticity is introduced into mixing of rubber.

When a certain amount of mechanical energy is imparted to rubber a part of the energy is stored as elastic energy and other part is dissipated as heat. A part of the energy converted to heat is lost. Only the elastic energy is effective for recovering from deformation. When the elasticity is controlling Region I and Region II behaviour, it means the ratio of stored energy to dissipated energy is high.

In Region IV, the modulus is lower than in Region II; the elasticity becomes low, giving a large permanent deformation. It is a fluid state, which is manifested as tackiness. In Region IV viscosity is the controlling factor.

Region III is the border between Region II and IV where elasticity and viscosity compete with each other for the control of the overall behaviour. Rubber on the mill is not uniform; when it is taken out as a sheet, it is wavy and has non-uniform thickness. In Region III the overall behaviour comes from Region II in some areas and Region IV in other areas. Region II and IV co-exist like a mosaic pattern. The areas where viscosity dominates lack tension and therefore, the rubber sags. The areas of high elasticity pull apart the viscous, weak areas, which deform permanently and tear.

Summarising the discussion up to this point, the state of rubber during roll-milling may be classified using modulus, strain at break and a ratio of elastic to viscous energy. The modulus and the viscoelastic ratio are subjects concerning deformation and flow, i.e., rheology. The strain at break is related to a large deformation and failure. Thus, a bridge is built between the hands-on experience of roll-milling and scientific methodology.

The increase of the temperature resulting from the milling of rubber tends to change the behaviour of rubber in the direction from Region I towards Region IV. Instead of the viscous heat generation, the machine or rubber may be externally heated to bring about the same change. This indicates that temperature is an important (dynamic) state variable.

When a rubber has a milling problem in Region I, the mill-gap is made wider in the beginning and gradually the gap is made narrower. When the roll speed is kept constant, a wider gap makes the deformation rate lower. The wider gap also gives a smaller deformation. However, the rubber behaviour needs to be considered from a dynamic (time-dependent) view point; therefore, deformation rate is selected rather than deformation itself as a variable. In general, when the gap is made wider, the rubber behaviour changes in a direction from Region I towards Region II; the reverse change can also occur. Therefore, the deformation rate is also a dynamic-state variable. Increasing temperature and decreasing deformation rate changes the rubber behaviour in the same direction: that is, there is a correspondence between temperature and deformation rate. Under the lower deformation rate, deformation takes a longer time. Therefore, the above correspondence may also be called time-temperature correspondence. However, at this stage of the discussion the correspondence principle remains to be qualitative. It must be differentiated from the quantitative definition of viscoelasticity [3].

When the mill processability is in Region II, it is within the time-temperature window, which defines the rubbery state. The Region I is the border (transition) between the

rubbery and glassy state. The Region IV is the flow state outside of the window. The Region III is at the border between rubbery and flow state.

Although most of mixing of rubber has been done with a tangential mixer, some rubbers like EPDM may be more advantageously mixed with an intermeshing mixer. If a relatively stiff rubber such as E-SBR or NBR is charged into an intermeshing mixer, the rubber tends to behave like Region I in the mill because the gap is narrow. The problem may be overcome by prewarming the rotors. EPDM softens easily and is not likely to give the behaviour of Region I. The basic difference between EPM and NBR in viscoelastic characteristics is described in Chapter 6.

So far the discussion has covered traditional rubber processing for making tyres, belts, and other industrial products. However, the recent trend of using new materials such as thermoplastic elastomers and polymer blends should also be noted. Also, non-traditional formulations have been developed, for example, for rollers in office printers and belts for money changers. Sound-proofing and vibration-damping are another area, which bring new formulations. For these new areas, the criteria of the mill processability may or may not be valid. When polymers of widely varied glass transition temperature (T_g) are blended, grafted or block-polymerised, the time-temperature correspondence discussed earlier, becomes very complicated. Therefore, interpretations of the mill behaviour must be properly modified. Even when the four regions of the mill processability appear applicable, subsequent handling of material may require fresh thinking. More discussion on this topic will be given in Chapter 14.

2.3 Science of mill processability

When the mill behaviour can be related to the fundamental properties of rubber, the mill-operator's experience can be interpreted in a scientific manner. When a piece of rubber is subjected to tensile testing, its modulus and the strain at break can be evaluated. The test may be performed at different temperatures and with different deformation rates, in order to include all ranges of temperature and deformation rates encountered in the mixer. An example of tensile stress-strain data is shown in Figure 2.2 for a sample of NBR [4].

A high speed tensile tester was used to match the deformation rates in the internal mixer.

This type of experiment has been a subject of scientific investigation for some time. The failure behaviour is presented as a locus of breaking strength and the breaking strain, i.e., failure envelope [5]. Examples of the failure envelopes are shown in Figure 2.3a for four different grades of NBR [4].

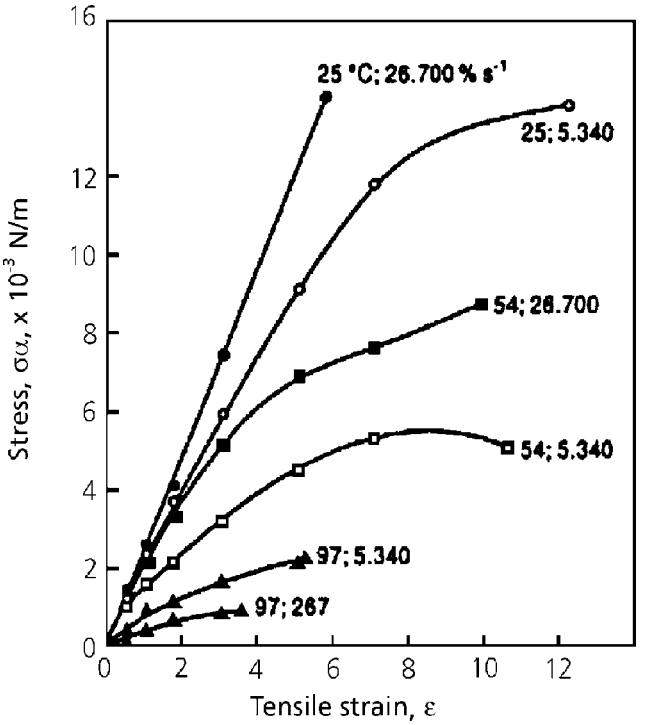

Figure 2.2 Tensile stress-strain data of NBR.

Reprinted with permission from N. Nakajima, E. A. Collins and H. H. Bowerman, Rubber Chemistry and Technology, 1974, 47, 2, 318. Copyright 1974, Rubber Division of the ACS.

The stress, σ, based on the undeformed cross-section is converted to that based on the deformed cross-section with a use of the extension ratio, α. The value plotted in the figure, σ_{α} is therefore the true stress.

As mentioned in section 2.2, the characteristic mill behaviour can be defined on the basis of modulus and strain at break. Therefore, a new failure envelope is proposed as a locus of the modulus at break and the strain at break [4], see Figure 2.3b.

The upper part of the figure corresponds to the lower temperature or a higher rate of deformation; the modulus is high and the breaking strain is small, Region I. Either by increasing temperature or decreasing the rate of deformation, the behaviour moves downward in the figure, showing the lower modulus and the larger strain at break, Region II. Passing downward through this region in the figure, the strain at break becomes smaller, Region III. The bottom part of the figure represents Region IV, where the temperature is even higher or the deformation rate is lower. Whether the breaking strain becomes larger or not, cannot be ascertained, because at Region IV the specimen tends to elongate non-uniformly.

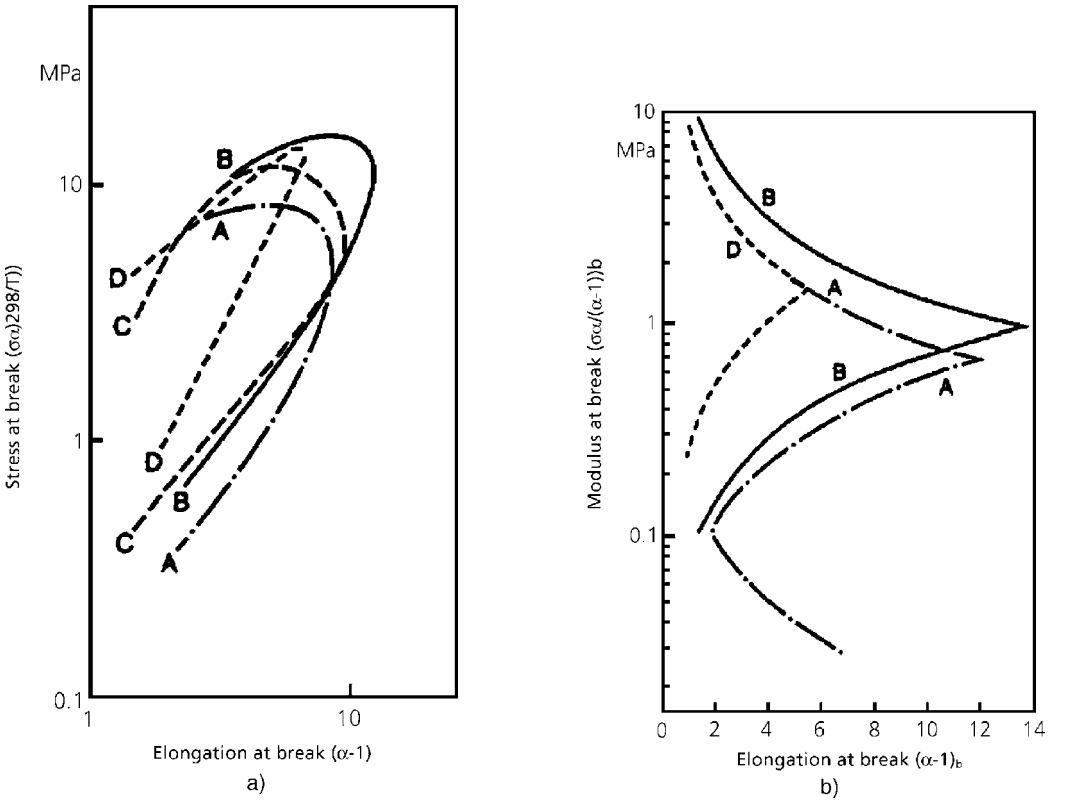

Figure 2.3 Failure envelopes of butadiene-acrylonitrile copolymer, samples A, B, C and D.
a) locus of breaking strength and breaking strain
b) locus of modulus at break and elongation at break

In this figure, samples A and B show Region II behaviour, indicated here with large strain at break; these are easy to mill. Sample D does not deform as much as samples A and B. Also, at the maximum strain at break, the modulus is high. Sample D tends to give Region I behaviour. Although not shown in Figure 2.3b, the behaviour of sample C is similar to those of A and B.

Because the mill behaviour and the results of the tensile test are shown to be related, the tensile test results may be used for the characterisation of processability for a given rubber. This aspect will be expanded in Chapter 6.

Mixing in a mill or an internal mixer involves both small and large deformations. The modulus at break is only one point in the large deformation. Therefore, the evaluation of modulus over the range from small to large deformation is required in order to fully explain the mixing behaviour.

Samples A and B are 'gel-free' grades and sometimes called easy processing grades. Method of the gel determination is given in ASTM D3616-95 [6] and sometimes as much as a few percent of gel may be found by this method without giving processing difficulty. A difference between A and B is their MW level. A lower MW rubber, A, was made using a MW modifier, which also suppressed the branch formation.

Sample D was made in such a way that it contained approximately 70% of macrogel. Although this material presents mixing difficulties, it is made for special applications. For example, it accepts a higher amount of reinforcing filler, e.g., carbon black, compared to samples A and B. It also provides a higher 'green-strength' (resistance to sagging), when a sheet of uncrosslinked compound is held up. When high gel-content latex is coagulated, dried and compressed into a bale, the multi-branched gels appear to form a complex network of entanglement. This entanglement is different from that formed by linear molecules. The entangled gel-network makes the bale appear as if it were permanently crosslinked. This type of gel is sometimes called a 'macrogel', because of its appearance. In reality, however, each gel molecule is microscopic in size, because it was formed in an emulsion particle.

The macrogel is different from crosslinked latex particles prepared with use of a difunctional comonomer; the latter is sometimes called, 'microgel', which contains crosslinked network chains and some branches. The rubber containing a significant amount of macrogel tends to behave as Region I at the beginning of milling. In the open mill an operator can make an adjustment of mill gap and thereby the milling operation may be controlled. With an internal mixer, however, the behaviour of rubber is not directly observable. Therefore, it is important to know the characteristics of a rubber before mixing. Otherwise, the results of mixing may be unsatisfactory and the compound may have to be remilled. How much macrogel is allowed in a gum rubber in order to avoid the mixing problem, depends upon the mixing conditions and formulation. For example, the mixer may be prewarmed or a process oil may be added.

Sample C contains 50% of microgel, and the other 50% is the same as sample B. Its mill behaviour is very similar to samples A and B. All grades of NBR exhibit either Region I or Region II of mill behaviour except for a specially made grade having a very low MW, which may show Region III or IV behaviour. The E-SBRs behave in a similar way.

On the other hand rubbers made through anionic polymerisation tend to go into Region III and IV. These rubbers have a very narrow MW distribution and no branches unless

the rubber is manufactured to have them by design. The reason for the mill behaviour is the absence of the high MW tail of the distribution. If the distribution is not extended to the high MW tail, even though the distribution is not necessarily narrow, the rubbers still tend to go into Region III and IV. This trend is accentuated if the average MW is low or there are no longer branches.

ACM is made through emulsion polymerisation, in much the same way as NBR is. There is a chain transfer mechanism, resulting in long branches and macrogel. Yet, this rubber tends to go to Region III or IV. The reason lies in its chain structure. The 73% of its MW is in the pendent group and therefore, it is a fat and short chain. Even when the MW is high, it acts like an equivalent of the low MW NBR.

Cis-1,4-butadiene rubbers (*cis*-1,4-BR) tend to go into Regions III and IV, even though they are very long and thin molecules, 100% of their MW being in the main chain. This is because their T_g, is very low, -112 ~ -120 °C. The normal milling temperature lies at the upper border of the time-temperature window.

In general the question of which region of mill processability a given rubber goes into, is related to its time-temperature window. Temperature-wise it is the processing temperature range compared to the T_g of a given rubber. Time-wise it is related to a 'mobility' of a given molecular segment at the shorter times and the mobility of the whole molecule at the longer times. The shorter-time border of the window is independent of the MW and the longer-time border is dependent. In the latter, therefore, the higher the MW the wider the window time-wise. Instead of the term 'mobility', the term 'relaxation-time' is used in science and its definition is given in Chapter 6.

The low MW tail of the molecular weight distribution is usually not a concern in rubber processing. The rubber is manufactured not to have this fraction, because it weakens the finished products.

MQ made through a condensation reaction is an exception. Because of the inherent nature of the reaction, there are low MW fractions, as discussed in Chapter 1.

References

1. N. Tokita and J. L. White, *Journal of Applied Polymer Science,* 1966, **10**, 7, 1011.

2. A. Morikawa, K. Min and J. L. White, *International Polymer Processing*, 1989, **4**, 1, 23.

3. J. D. Ferry, *Viscoelastic Properties of Polymers*, 3rd Edition, John Wiley, New York, 1980.

4. N. Nakajima, *International Polymer Processing*, 1996, **11**, 1, 1.

5. T. L. Smith, in *Strength and Extensibility of Elastomers in Rheology*, Vol.5, Ed., F. R. Eirich, Academic Press, New York, 1969, p.127.

6. ASTM D3616-95
Standard Test Method for Rubber, Raw-Determination of Gel, Swelling Index, and Dilute Solution Viscosity.

3 Overview of Mixing of Rubber

3.1 Unit processes

Mixing of rubber involves several additives, such as reinforcing fillers, non-reinforcing fillers, oils, vulcanisation chemicals, stabilisers and so on. However, discussion will be limited to rubbers and reinforcing fillers because upon satisfactory mixing of these, other additives are usually well mixed. Often more than one rubber is blended; also more than one kind of reinforcing filler may be used. However, for simplicity, mixing of one rubber and one reinforcing filler, primarily carbon black, will be considered. Use of an internal mixer is the primary interest, although the mill-mixing may be interpreted similarly.

Mixing of mutually soluble substances, such as alcohol and water occurs in one step. Therefore, it is a one unit process. Mixing of rubber and carbon black is not done by one step. In general, four unit processes are involved, each requiring separate consideration; they are mastication, incorporation, dispersion and distribution. Mastication has already been discussed in Chapter 2. Incorporation is a process where the filler particles become included inside the rubber. Dispersion is a process where carbon black pellets and their fragments, agglomerates, are broken down to the primary units called aggregates. Distribution corresponds to mixing in the usual sense except that it is homogenisation on the macro-scale.

If a rubber is in Region I of mill processability, incorporation is difficult because rubber and carbon black tend to stay separate; sometimes it is described as, 'a rubber is too dry'. In Region II the rubber is a soft, stretchable solid.

Dizon and Papazian [1] removed the contents of an internal mixer at an early stage of incorporation, see Figure 3.1. It consisted of 1,800 identifiable pieces classified into 9 kinds. As incorporation progresses the pieces stick together, becoming compacted to form one piece. This process is sometimes called 'massing'. How easily and quickly the compaction occurs, depends upon the nature of rubber. When the rubber is in Region IV the massing is easier because the rubber is tacky to begin with. The importance of compaction is obvious, because when compaction is insufficient, the compound becomes very difficult to handle. In addition the transmission of stress becomes ineffective such that dispersion becomes ineffective. Difficulty in compaction tends to occur with a high loading of fillers.

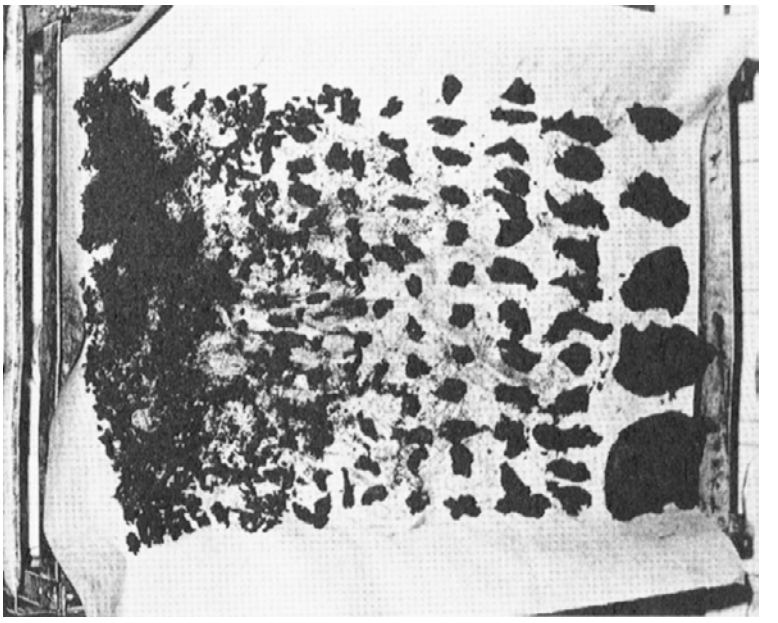

Figure 3.1 Batch appearance of low-energy (200 MJ/m^3) mix.

Reprinted with permission from E. S. Dizon and L. A. Papazian, Rubber Chemistry and Technology, 1977, 50, 4, 765. Copyright 1977, Rubber Division of the ACS.

The dispersion process requires transmission of stress from the mixing machine to the carbon black through the medium of rubber and rubber containing already dispersed carbon black. The higher the modulus the more effective is the transmission of stress; therefore, the lower temperature is preferred as long as the rubber stays in Region II. Towards the end of mixing the temperature of compound goes up and if it is excessive the dispersion becomes ineffective, because the modulus becomes low.

The distribution depends greatly upon how the compound as a whole moves around in the chamber of the internal mixer. Uniform movement without a partial stagnation is the key. If the mixing chamber is 100% filled, the compound cannot move easily. In an extreme case, the rubber mixture may be separated into one part which passes under the rotor tips repeatedly and another part which does not. The latter will have a higher modulus, because of the poorer dispersion. It is less likely to have a higher modulus fraction passing under the rotor tips than a lower modulus fraction.

3.2 Interpretation of the mixing process

In Chapter 2 the mill processability was related to the viscoelastic characteristics of a given rubber. This establishes a rational basis of interpreting the mixing behaviour of rubber. However, the phenomenon concerns only mastication and the initial stage of mixing. It does not extend to incorporation and dispersion.

To consider the mixing of rubber from a scientific viewpoint, questions must be asked about the scientific treatment of mixing. An approach was proposed, which begins with definitions of the initial and final state of mixing [2]. These states are relatively easy to define; and then, the intermediate state of mixing can be examined, which is much more complex. In the beginning a gum rubber and a filler are present separately, assuming only one rubber and one filler is involved. The viscoelastic characteristics of the rubber can be defined as explained already. An additional parameter of importance is the size of the rubber block. The filler may be characterised with respect to structure, surface area and friability.

The final state of mixing may be defined by the morphology of the mixed compound; a number of years ago Hess presented many photographs, one of which is reproduced in Figure 3.2 [3]. It is assumed that the equipment used is an internal mixer and that the filler is a carbon black. As in Figure 3.2 the rubber phase is a continuous matrix. However, as a model the rubber may be regarded as domains surrounded with carbon black. The domain-size is in the order of 1 μm. The border of the domain has a pattern, indicating that one domain may consist of many rubber particles of the order of 0.1 μm.

A block of rubber charged into the internal mixer has a dimension of several cm or larger. During mixing the size is gradually reduced to the domain size of about 1 μm. The torn and fractured surfaces of the rubber either attach to the surfaces of the carbon black or to that of other pieces of rubber. Considering the process of fracture and attaching, the ultimate domain may be regarded as consisting of many rubber particles of approximately 0.1 μm size. The mechanism of gradual decrease of the rubber particle-size is called comminution [4].

In a recent observation, NR was breaking down to small pieces in the initial stage of milling [5]. In general, with a fracture of a body, new surfaces are created and simultaneously the broken pieces are separated. However, in comminution, only the creation of new surfaces occurs. The fresh surfaces are immediately attached to the surface of carbon black or that of rubber. Therefore, direct observation of comminution is difficult. However, during roll milling lumps are seen; they become smaller with the progress of milling, implying the comminution mechanism.

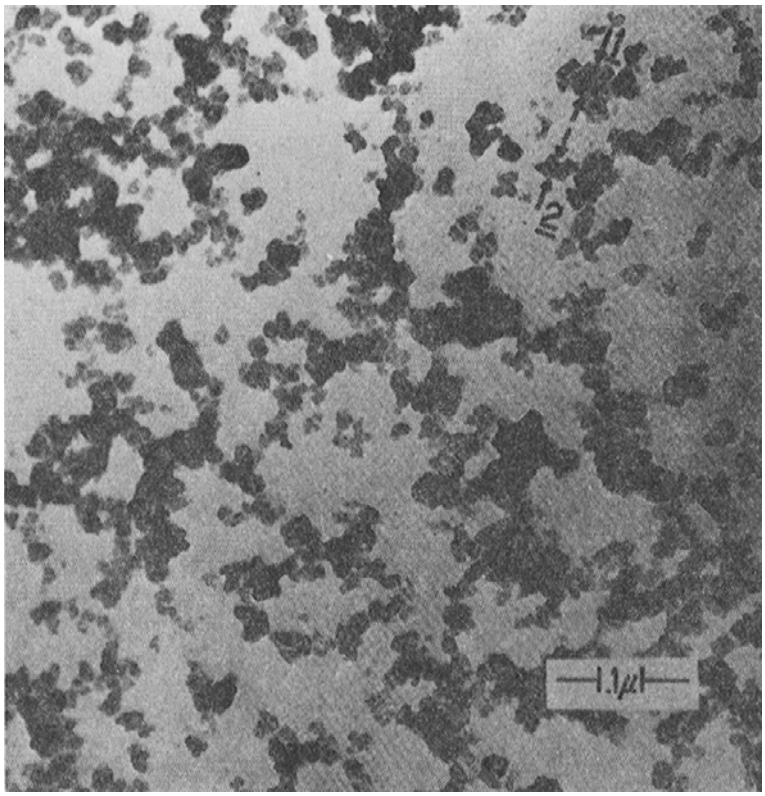

Figure 3.2 Elastomer domains and well-dispersed carbon black aggregates.

Reprinted with permission from W. M. Hess in Reinforcement of Elastomers, Ed., G. Kraus, John Wiley, New York, 1965, Chapter 6. Copyright 1965, John Wiley.

Carbon black is supplied as pellets, which have a size somewhat smaller than 1 mm. At the completion of mixing, the size of the aggregates are in the range of 100 to 10 nm. At the beginning of mixing the pellets break into pieces, agglomerates, in the size range of 100 to 10 μm, but thereafter, the break-down mechanism is not comminution. A microscopic observation by Shiga and Furuta [6] revealed that the aggregates peel off from the surface of the agglomerates in the manner of peeling onion, i.e., the onion model, see Figure 3.3.

So far the behaviour of rubber and carbon black has been described separately, but the way in which these components mix with each other has not yet been considered. Usually the rubber is masticated before the mixing starts. The behaviour of rubber at this stage has been discussed already. The mixing process usually consists of incorporation and dispersion. In the incorporation stage, carbon black present on the outside of rubber blocks becomes included inside the rubber. In order to accept a large number and a large

bulk of carbon black particles, the rubber must provide a large surface area. This may be accomplished either with a large deformation (flattening) of the rubber or with generation of small particles [4]. In the former mechanism, carbon black becomes sandwiched between two sheets of rubber; called the 'lamination mechanism'. The latter mechanism corresponds to the early stage of comminution, see Figure 3.4. Although the lamination and comminution are idealised models, the portions corresponding to these mechanisms appear in the microscopic observation, see Figure 3.5 [6].

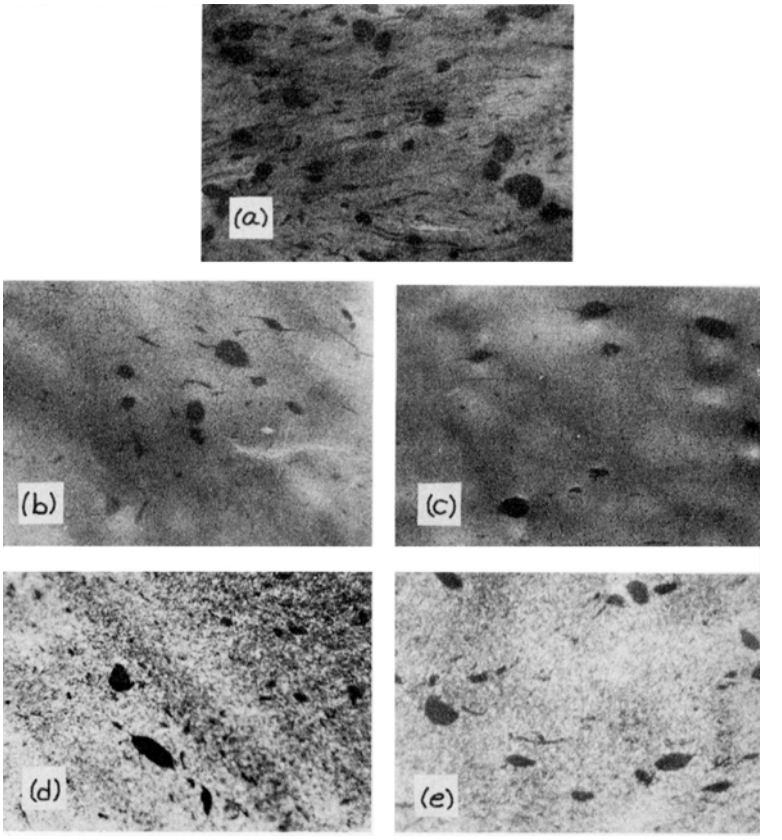

Figure 3.3 Photomicrographs of EPDM compound. Photomicrographs a, b and c: EPDM 100, N330 10, oil 10, ZnO 5, stearic acid 1 (all phr); a) after two minutes, b) after 4 minutes, and c) after 6 minutes mixing.
Photomicrograph d: EPDM 100, N550 10, oil 10, ZnO 5 and stearic acid 1 (all phr)
Photomicrograph e: EPDM 100, N550 20, oil 20, ZnO 5 and stearic acid 1 (all phr)

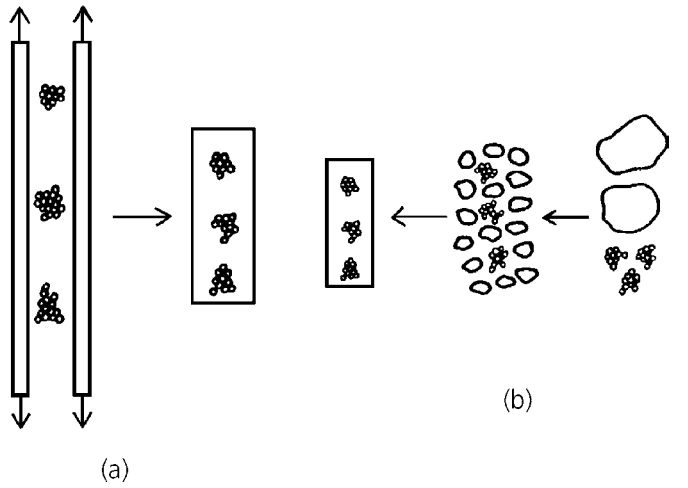

Figure 3.4 Schematic illustration of mechanisms incorporating carbon black into elastomer, a) lamination, b) comminution.

Reprinted with permission from N. Nakajima, Rubber Chemistry and Technology, 1982, 55, 3, 931. Copyright 1982, Rubber Division of the ACS.

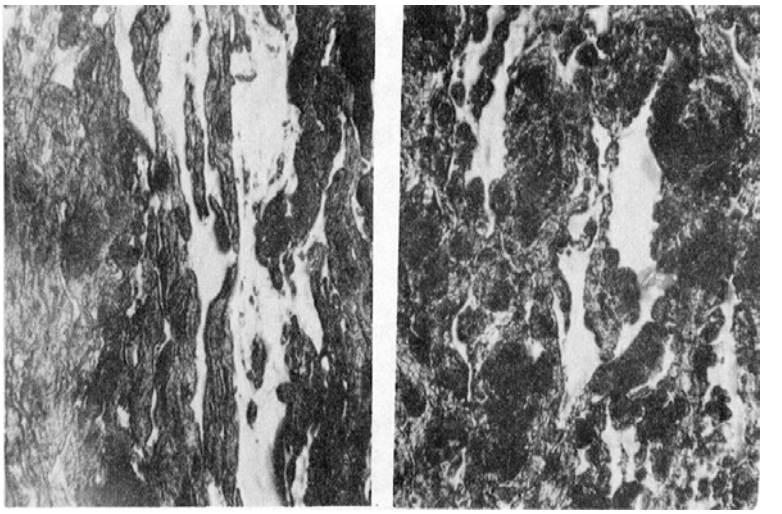

(a) (b)

Figure 3.5 Incorporation of carbon black into elastomer; photomicrographs of EPDM compound with a mixing time of a) 30 seconds and b) 45 seconds.

Reprinted with permission from S. Shiga and M. Furuta, Journal of the Society of the Rubber Industry, Japan, 1982, 55, 491. Copyright 1982, Journal of the Society of the Rubber Industry, Japan.

Once incorporation is accomplished, carbon black agglomerates break into aggregates via the onion model mechanism. When agglomerates practically disappear and disintegrate into aggregates, the mixing is considered to be complete. However, every portion of the compound must have the same composition; namely distributive mixing is also important and must occur simultaneously with dispersion.

So far we have discussed the behaviour of rubber, that of carbon black and the rubber-carbon black interaction. Next the interaction between a machine and material will be considered. At the beginning of the mixing the internal mixer contains a large bulk of material, which is compressed with a ram. The ram pressure indirectly contributes to incorporation. The question is whether static pressure would directly aid mixing or not. Comparing the beginning and the end of incorporation, a difference is not only where carbon black is present, from outside to inside of rubber, but also the feel of the rubber surface. In the beginning the rubber surface is dry, but at the end it becomes tacky. This change occurs within about one minute of the incorporation stage. The change is brought about neither with the ram pressure nor with the pressure generated between the rotor and the chamber wall. It is a result of tearing and bringing out fresh surfaces of rubber [7]. This finding has an importance in understanding of mixing of rubber and therefore, the experimental detail will be presented later in a separate section. A reason for the fresh surface being tacky is the result of the pulling out of polymer chains, whose chain-ends become concentrated on the fractured surface. When the compound is aged, the chain-end distribution equalises between surface and bulk, thereby the surface loses the tackiness.

The interaction between machine and material is manifested in the temperature-rise, the torque-time curve and the cumulative energy input. Here, we will discuss the torque-time curve, see Figure 3.6 [1].

There are two different interpretations of this curve; one says that the part leading to the second peak corresponds to incorporation and thereafter is dispersion, see Figure 3.7 [8]. However, this interpretation is only approximate.

The other interpretation [1] is based on the actual sampling at different stages of mixing. The detailed examination of the state of mixing reveals that except for the very beginning, incorporation and dispersion are occurring simultaneously. In the earlier period incorporation is dominant and in the later period dispersion is dominant. This observation also tells us that the contents of an internal mixer are not uniform.

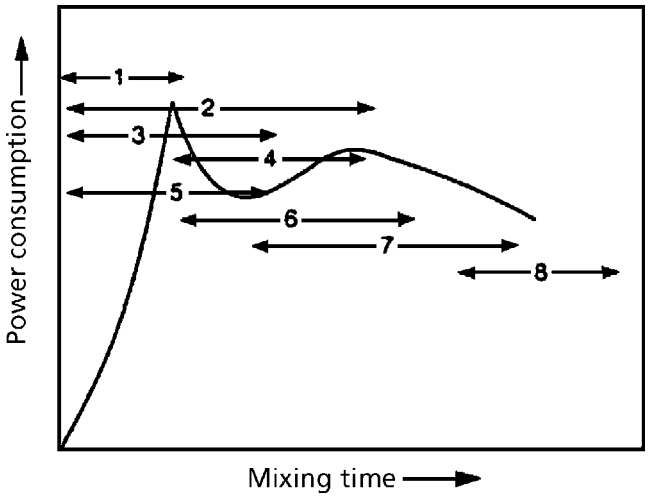

Figure 3.6 Material transformation process in rubber processing:
1: fragment rubber
2: distribute powders and liquids
3: incorporate powder and liquids
4: fuse fragments
5: break down carbon black
6: disperse carbon black
7: break down rubber and black-polymer interaction
8: shape compound

In the operation of a roll-mill the rubber compound is cut, sheeted out of the mill, rolled up and recharged. This process is then repeated. Therefore, the entire compound receives uniform treatment. In the internal mixer, (i) a part of the content is slowly transported in the wide space between two rotors, (ii) another part passes quickly through the narrow gap between the rotor and chamber wall, (iii) yet another part may stagnate, and (iv) some part is stretched. In the course of mixing the compound does not uniformly receive these four treatments. At the end of mixing the compound consists of parts having a non-uniform mechanical history. The extent of the non-uniformity depends upon the characteristics of gum rubber and the specific formulation used. The extent of the uniformity of the compound has an important bearing on the downstream processability. The characteristics of a compound depends on not only its chemical composition but also the mechanical history of mixing.

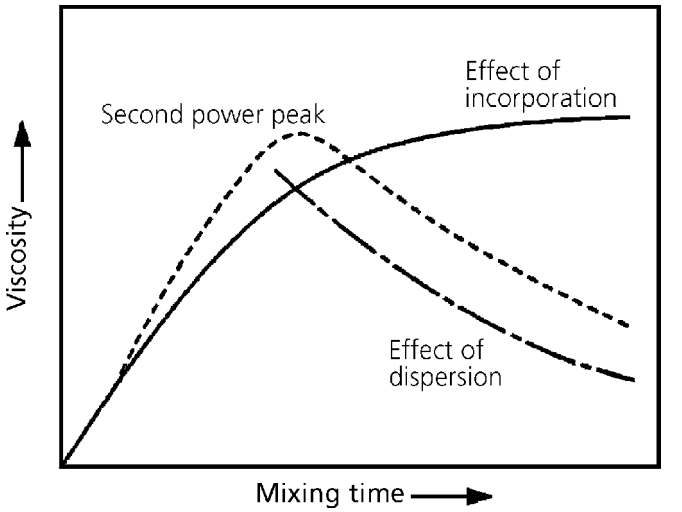

Figure 3.7 Effect of incorporation and dispersion processes on viscosity.

Reprinted with permission from G. R. Cotten, Rubber Chemistry and Technology, 1984, 57, 1, 118. Copyright 1984, Rubber Division of the ACS.

The causes of non-uniformity stated above concern the distributive mixing. They also affect non-uniformity in incorporation and dispersion, because at any time during mixing a part of the rubber compound is receiving a mechanical treatment different from the other part. Because the non-uniformity in the internal mixer has been well-recognised, the development of the Banbury mixer, for example, follows from a two-wing rotor to four-wing rotor. A more recent development is an improved four-wing design, which provides more uniform movement of the contents. This is discussed in Chapter 11.

Because incorporation and dispersion are different unit processes, having different requirements, design of the internal mixer optimised for one of the processes may not be the optimum for the other. Therefore, in some production lines only incorporation is done with the internal mixer and the contents are dumped onto a mill or fed into a transfer mixer to complete dispersion. Also, the mixing is not always done in one step from the raw material-charge to dump. The charging of the rubber and additives may be done in two or three steps.

3.3 Compaction as a part of the mechanism in incorporating carbon black into an elastomer [9]

3.3.1 Introduction

Incorporation requires both breaking of the elastomer into smaller pieces and stretching of the elastomer to provide large surface areas. Viscoelastic behaviour and failure characteristics of a given elastomer obviously play important roles.

In addition to these two mechanisms, a mixture of elastomer and carbon black have to be compacted. Compaction is the elimination of free spaces between carbon black particles and elastomer domains by an externally applied force. The importance of the compaction step may be illustrated by the following example.

A recent development of an efficient cooling design for an internal mixer, allowed the use of warm water cooling instead of the traditional cold water. This resulted in a significant saving of mixing time and energy (this depends upon the choice of elastomer and formulation, of course), [4]. A major saving was found to be in the time period required for ram seating [10], i.e., the compaction. Implied here is a temperature deformation-rate relationship, which dictates an optimum condition for the compaction process.

The nature of physical and chemical interactions between the elastomer and the surface of carbon black has been a subject of interest for many years. A prerequisite to such surface interactions is the wetting of the surface with elastomer molecules. However, the elastomer molecules do not spontaneously flow to the surface of carbon black. The elastomer domains must be deformed to conform with the topology of the carbon black and made to relax in the deformed state. This mechanism may constitute the essence of the theory of compaction, which is examined in this study.

In order to develop the details of the theory, a model experiment was carried out. A preblend of powdered rubber and carbon black was loaded into a rheometer and compacted. The bulk compression and relaxation behaviour were characterised to gain insight into the time-temperature relationship.

3.3.2 Experiment-I

- *Samples*

Usually, the mixing of an elastomer is started by charging a slab of elastomer into a mixing machine. At the onset of mixing there are grossly different sizes of rubber. The

distribution of carbon black is also very non-uniform. Such inhomogeneity is difficult to treat theoretically. Therefore, this problem is left for future research. Instead, a preblend of powdered rubber and carbon black was used. Therefore, the sample was macroscopically uniform from the beginning. The powdered rubber was a butadiene-acrylonitrile copolymer with a Mooney index (ASTM D1646-72, [11]) of about 80 and the average particle diameter was approximately 250 μm. The compound formulation is given in Table 3.1. The powder was preblended with a high-intensity Henschel mixer.

Table 3.1 Compound Formulation

Rubber	100[a]
Zinc oxide	5
Stearic Acid	1
N550 Carbon black	65
DOP	10

[a] All quantities in phr. DOP: dioctyl phthalate

A Rheometrics mechanical spectrometer was used with the 25 mm diameter parallel plates assembly to which a moulding ring was affixed.

Loading of the sample was done carefully to level the powder, so that it would result in uniform compaction. The top plate was then lowered until the normal force registered about 5 g. This magnitude of normal force indicated that the top plate was pressing the sample very slightly. Under this force, the top plate was rotated slowly in order to pack the powdered sample uniformly. Then, approximately 10 minutes were allowed for the sample to equilibrate to a specific temperature. At this point, the gap between the two plates was measured with a dial gauge. The gaps between the molding ring and the plates were closed with shims (thin pieces of metal) to prevent leakage of material when pressure was applied.

The bulk compression was started by quickly lowering the top plate until the normal force reached 9 kg, (nine-tenths of the maximum available load). Then, this load was maintained for 12 minutes by manually lowering the top plate. During this process, the thickness of the sample was recorded as a function of time, using readings from a dial gauge. At the end of 12 minutes, the position of the top plate was fixed and relaxation of the normal force was recorded against time for a specified period of time. Subsequently,

the sample was removed and left to cool to room temperature. The effectiveness of compaction was evaluated qualitatively by visual inspection of the friability of the moulded piece. The measurements were performed at 100, 150 and 175 °C. The temperature, 100 °C, was selected because the compound temperature at the completion of incorporation (just before dusting) was about 100 °C [12]. The measurements at 150 and 175 °C were made to accelerate the compaction process, because it proceeded very slowly at 100 °C and also, to obtain the temperature-dependence of the process. In addition to the above measurements with the compound, a similar measurement was made for the powdered rubber alone.

3.3.3 Results-I

- *Morphology of powdered rubber compound*

Figure 3.8 shows photographs of the powdered rubber and the compound, taken at a low magnification with a scanning electron microscope, AMR Model 1400.

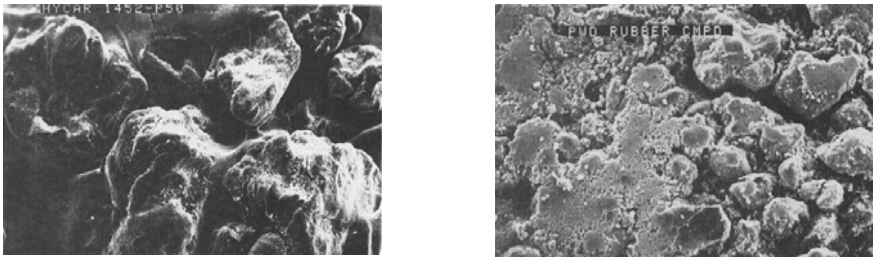

Figure 3.8 Scanning electron micrograph of the powdered rubber (40X) and powdered rubber compound (17X).

Reprinted with permission from N. Nakajima and E. R. Harrell, Rubber Chemistry and Technology, 1983, 56, 1, 197. Copyright 1983, Rubber Division of the ACS.

In both photographs, particles of rubber are clearly observed. In the compound, the rubber particles are coated with fine particles as shown at high magnification in Figure 3.9. The fine particles were identified as carbon black.

- *Compression measurements*

Figure 3.10 is a result of the compression measurement at 150 °C under a 9 kg load.

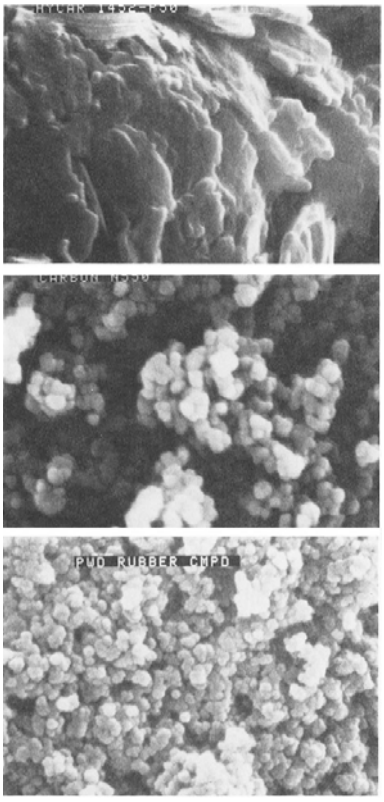

Figure 3.9 Scanning electron micrograph (14,000X) of powdered rubber, carbon black and powdered rubber compound (top to bottom).

Reprinted with permission from N. Nakajima and E. R. Harrell, Rubber Chemistry and Technology, 1983, 56, 1, 197. Copyright 1983, Rubber Division of the ACS.

The change of the thickness of the sample is shown over 12 minutes of time. Before the 9 kg load was applied, the sample thickness was 4.652 mm at the 5 g load, but as soon as the 9 kg load was applied, the thickness decreased to very close to 3.4 mm. Because the thickness change was very rapid initially, the first thickness reading was taken after 30 seconds. It was not possible to record the initial thickness under the 9 kg load.

Under the same conditions, the compaction of powdered rubber alone or that plus non-carbon black additives was complete within less than ten seconds. Therefore, the behaviour presented in Figure 3.10 is the compaction of rubber onto the complex topology of carbon black, exclusive of the compaction of rubber particles onto themselves.

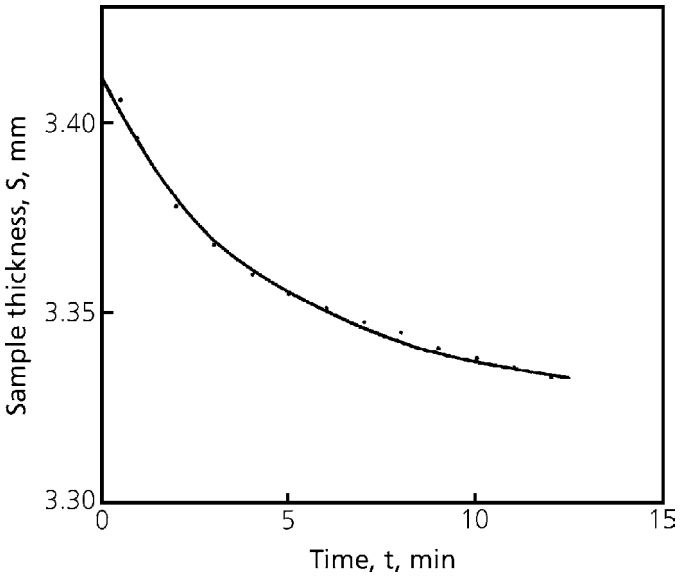

Figure 3.10 Compression data at 150 °C expressed as change of sample thickness with time.

Reprinted with permission from N. Nakajima and E. R. Harrell, Rubber Chemistry and Technology, 1983, 56, 1, 197. Copyright 1983, Rubber Division of the ACS.

Although neither initial thickness, S_o, nor ultimate thickness S_∞, is obvious from these data, the thickness, S at corresponding time, t may be represented by the following expression:

$$(S - S_\infty) / (S_o - S_\infty) = e^{-kt} \tag{3.1}$$

where k is a rate constant. The fitted curve is shown with the solid line in Figure 3.10. Equation (3.1) was found to fit the results obtained at 100 °C and 175 °C. The deviations of the observed data from the fitted curve were less than 0.004 mm, therefore, the curve-fitting was considered to be satisfactory.

The 9 kg load corresponds to the pressure of 0.18 MPa, which is the same order of magnitude as the ram pressure. For example, during the mixing of the powdered rubber compound, the ram pressure was maintained at 0.24 MPa [2]. The pressure exerted by the rotating blade is an order of magnitude higher, e.g., 3.5 MPa. The lower pressure level is explored next and the latter pressure level later.

The information desired from the compression measurements is a quantitative measure of how closely the rubber particles have become compacted onto the carbon black. The data treatment for this purpose will be done in two ways. One is a degree of packing,

and the other is a degree of penetration into the void volume. The degree of packing, *PAC*, is defined as

$$PAC = (v_p + v_c) / V \tag{3.2}$$

where v_p and v_c are volume of polymer (plus non-carbon black additives) and volume of carbon black, respectively.

The observed sample volume V is related to the sample thickness, S, by

$$V = S(\pi r^2) \tag{3.3}$$

where r is the radius of the rheometer plate.

The volumes, v_p and v_c, are related to the mass of polymer (plus non-carbon black additives) w_p, and the mass of carbon black, w_c, by

$$v_p = w_p / \rho_p \tag{3.4}$$

and

$$v_c = w_c / \rho_c \tag{3.5}$$

where ρ_p and ρ_c are the densities of polymer and carbon black, respectively.

The value of ρ_c is taken as the density of amorphous carbon.

The degree of penetration, *PEN*, into the void volume, v_v is expressed as the percentage of void volume occupied by the volume of penetrated rubber, v_n:

$$PEN = v_n / v_v \tag{3.6}$$

The void volume may be calculated as a difference between apparent volume of carbon black under a given pressure, v_a, and its true volume, v_c

$$v_v = v_a - v_c \tag{3.7}$$

The volume of penetrated rubber is

$$v_n = (v_p + v_a) - V \tag{3.8}$$

Information on the amount of sample and the corresponding volumes, v_p, v_c, v_a, and v_v, and the densities are listed in Table 3.2. The bulk compression of elastomer itself is very small and negligible for the purpose of the above calculation [13].

The data on degree of packing and degree of penetration of elastomer into void volume are summarised in Table 3.3.

Table 3.2 Compression Experiment, Material Parameters

Experiment No	7	3	5	2
Temperature, °C	100	150	150	175
Sample compound, g	1.36	1.35	1.36	1.33
Rubber and additives, g	0.885	0.878	0.885	0.865
Density of rubber, g/cm^3 [a]	0.9690	0.9645	0.9645	0.9580
Volume of rubber, v_p, cm^3	0.913	0.910	0.917	0.903
Carbon black, g	0.475	0.472	0.475	0.465
True density of carbon black[b], ρ_c, g/cm^3	1.88	1.88	1.88	1.88
True volume of carbon black, v_c, cm^3	0.253	0.251	0.253	0.246
Apparent specific volume[c] of carbon black under 0.18 MPa pressure, cm^3/g	2.07	2.07	2.07	2.07
Apparent volume of carbon black under 0.18 MPa, v_a, cm^3	0.983	0.977	0.983	0.963
True volume of sample, $v_p + v_c$, cm^3	1.166	1.161	1.170	1.149
Apparent volume of sample, $v_p + v_a$, cm^3	1.896	1.887	1.900	1.866
Void volume, $v_v = v_a - v_c$	0.730	0.726	0.730	0.717

[a] Temperature dependence of specific volume as given in Reference [14]
[b] Density of gas carbon, see Reference [15]
[c] Extrapolated to 0.18 MPa from the data given in Reference [16]

When the sample is loaded but not compressed, i.e., under 5 g load, the material occupies about 50% of the available space; this indicates a loose packing of the powder-compound. As soon as the 9 kg load is applied, the degree of packing increases to about 70%, indicating a tight packing of the powders. The degree of penetration by the elastomer into the void space of carbon black is about 25-30% in the beginning, increasing to 30-35% at the end of 12 minutes of compression. The 30-35% penetration is also the maximum attainable penetration under 0.18 MPa.

Table 3.3 Compression Experiment, Degree of Packing and Degree of Penetration Into Void Volume				
Experiment No.	**7**	**3**	**5**	**2**
Temperature, °C	100	150	150	175
Sample thickness, cm				
5 g load	0.4770	0.4652	0.4796	0.4957
9 kg load				
S_o	0.3468	0.3412	0.3422	0.3423
S_∞	0.3400	0.3330	0.3334	0.3324
Sample volume, cm^3				
5 g load	2.342	2.284	2.355	2.433
9 kg Load				
v_o	1.702	1.675	1.680	1.680
v_∞	1.669	1.635	1.637	1.632
v at 12 min	1.669	1.636	1.638	1.633
Degree of packing, %				
5 g load	49.8	50.8	49.7	47.2
9 kg load				
PAC_o	68.2	69.3	69.6	68.4
PAC_∞	69.5	71.0	71.5	70.4
PAC at 12 min	69.5	71.0	71.4	70.4
Degree of penetration into void volume, %				
PEN_o	26.6	29.2	30.1	25.9
PEN_∞	31.1	34.7	36.8	32.6
PEN at 12 min	31.1	34.6	35.9	32.5

- *Compressive stress relaxation*

The compressive stress relaxation experiment followed immediately after compression measurements under 9 kg of a constant load. In the compressive stress relaxation, the behaviour was recorded as the decrease of the load from the initial 9 kg to about 1 kg. The results of measurements at 150 °C and 175 °C (Experiments 2, 3 and 5) are shown in Figure 3.11 with solid curves.

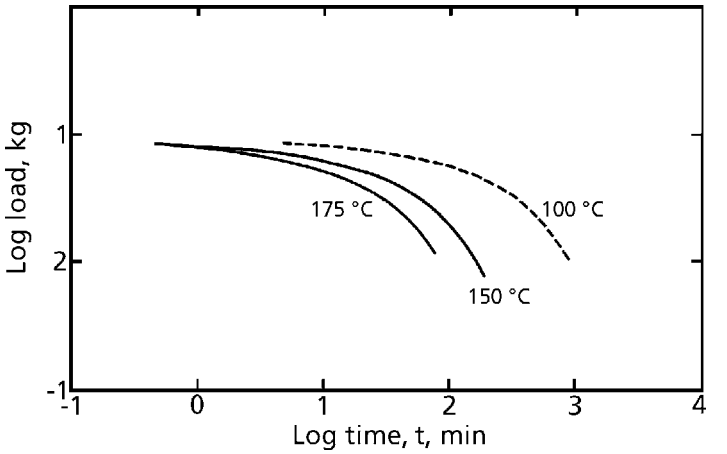

Figure 3.11 Compressive stress relaxation, expressed as relaxation of load with time.

Reprinted with permission from N. Nakajima and E. R. Harrell, Rubber Chemistry and Technology, 1983, 56, 1, 197. Copyright 1983, Rubber Division of the ACS.

The 150 °C results were obtained in duplicate, which were in good agreement with each other. The time-temperature correspondence in the viscoelastic behaviour of elastomers may be represented with the WLF equation [17]. For the present elastomer, i.e., butadiene-acrylonitrile copolymer having 33% acrylonitrile, the temperature time shift factor, a_T was previously given by [18]

$$-\log a_T = 5.95(T - T_o)(109 + T - T_o) \tag{3.9}$$

Because the T_g of this polymer is about -24 °C, Equation (3.9) is not necessarily expected to apply to the data at 150 °C and 175 °C, which are far removed from the T_g.

Nevertheless, the calculated shift factor, 1.86, was found to be exactly the same as the time-shift between the observed data of 150 °C to 175 °C. Subsequently, the 175 °C data were shifted by the calculated shift factor of 10.3 to predict the 100 °C data as shown in Figure 3.11 by the broken curve. The prediction indicates that it will take 15 hours for the load to relax down to 1 kg. At present, this is too long for precise measurement, but an approximate measurement indicated that the prediction is very close.

The previous arguments assume that the magnitudes of strain were the same at all three temperatures. Because the vertical axis is the load and not the relaxation modulus, there should be some vertical shift required to compensate for the differences in strain. Since the preceding compression was done at a constant load for a constant period of time, the lower temperature results in a smaller strain. A precise estimate of relative difference of

strain at different temperatures is possible from the present relaxation measurements and it will be pursued in the future.

After the relaxation experiment was terminated, the sample was removed from the rheometer. Although it was very friable, the sample was nevertheless compacted into one piece. If an order of magnitude higher pressure had been applied, it would have compacted much better.

3.3.4 Discussion-I

The compaction process may be defined as a process whereby the elastomer comes in contact with the topological surface of carbon black. The question is how to express the degree of compaction quantitatively. If carbon black were a porous material, whose pores were as depicted in Figure 3.12a, the degree of compaction might be expressed as a percentage of pore-volume occupied with rubber.

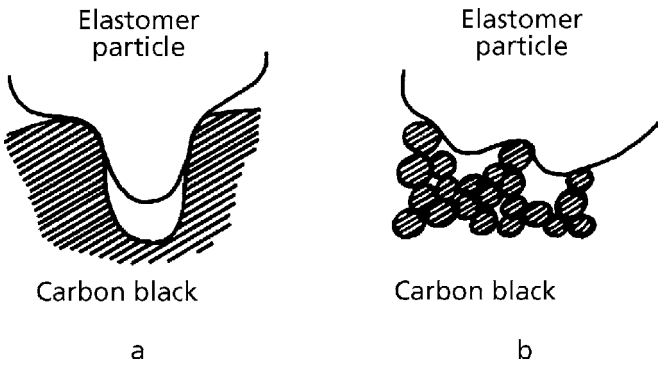

Figure 3.12 Schematic illustrations of penetration of elastomer into hypothetical pore of carbon black (a) and into void volume of carbon black (b).

In reality, the topology of carbon black is more like Figure 3.12b, so that it is difficult to define the pore volume. For this reason, a void volume is used for a volume to be penetrated by elastomer. The void volume defined here is the difference between the apparent volume under a given pressure and the real volume of carbon black. An advantage of using void volume is that it can be measured quantitatively [15]. It is highly pressure-dependent, which may be expected because some of the void spaces are more easily accessible than others.

The question arises of how to define the total void volume, which is independent of the applied pressure. This is not an easy task, because the apparent specific volume of carbon black is linearly dependent on the logarithm of pressure, so that extrapolation to zero pressure cannot be made.

Therefore, a somewhat arbitrary reference pressure must be chosen for defining the total volume. The void volume of carbon black at a pressure of 0.18 MPa was chosen to be the reference in this case. This level for the reference pressure has a practical significance in that it is lower by one order of magnitude than the pressure exerted by the rotor blade of an internal mixer. Accepting this definition of void volume, the degree of penetration into the void volume, *PEN*, in Table 3.3, becomes a good measure of the degree of compaction. Under the present set of experimental conditions 30-35% of the void volume was penetrated by the elastomer.

The degree of packing, *PAC*, in Table 3.3, also increases with the progress of compaction. Therefore, it serves as a measure of compaction. However, the difference in the degree of compaction is more magnified in *PEN* than in *PAC*.

- *Rate of compaction*

The rate of compression is expressed by the change of thickness of the sample in Equation (3.1):

$$(S - S_\infty) / (S_o - S_\infty) = e^{-kt} \tag{3.1}$$

where k is the constant. If the importance of relaxation in the compaction process is ignored for the moment, the rate of compression may be taken to mean the rate of compaction. The observed values of k are given in Table 3.4

Table 3.4 Rate Constant of Compression

Experiment No.	**7**	**3**	**5**	**2**
Temperature, °C	100	150	150	175
Rate Constant, k, s^{-1}	0.00526	0.00399	0.00437	0.00386
Degree of Penetration, *PEN*, %	31.1	34.7	36.8	32.6

An inspection of the rate constants at 100 °C and 150 °C reveals that at the lower temperature, the rate is faster. Actually, this is probably a misleading statement. The elastomer has a higher modulus at the lower temperature so that the maximum attainable degree of penetration is smaller than that at the higher temperature (*PEN*

% values). For this reason, the penetration process is completed sooner at the lower temperature than at the higher temperature. The rate constant at 175 °C is not very different from that at 150 °C. This is probably because the polymer is not entirely stable at 175 °C and slight chemical crosslinking has probably occurred during the compression experiment. The ultimate degree of penetration, PEN_{∞}, at 175 °C is also smaller than that at 150 °C probably because of the crosslinking.

- *Compressive stress relaxation*

In the compression experiments, if the pressure is released immediately after termination of the compression, the elastomer recovers from the deformation to some degree. Consequently, the degree of compaction decreases upon release of the pressure. Instead, in this experiment the compressive deformation was held constant and the relaxation of stress was observed. Although the bulk deformation was held constant, the deformation of each elastomer particle might not have remained constant, because it can rearrange its shape within the available void space. Although the details of the relaxation mechanism are a subject of future study, the following point may be emphasised. Our primary interest is the deformation of elastomer particles, and not the bulk deformation of elastomer-carbon black mixture. The change in shape of the elastomer particles to conform to the topology of carbon black is a complex deformation but is a combination of shear and elongation. It is not a compressive deformation. Consequently, the relaxation behaviour is interpreted in terms of viscoelastic behaviour of the elastomer. The temperature dependence of the relaxation is described by the Williams-Landel-Ferry (WLF) relationship of this elastomer. Considering the behaviour of elastomer particles, the compression stage corresponds to creep behaviour in a complex combination of shear and elongational deformation. Then the relaxation follows. This type of relaxation is different from that following instantaneous deformation; such a complex relaxation behaviour is the subject of a separate study [19]. The results from this study will be used to interpret the details of the compaction mechanisms in the future.

- *Comparison of the present experiments with an actual mixing operation*

The time spent for the present experiment is unrealistically long. For example, 12 minutes was spent for the compression experiment, when in the actual mixing the incorporation process is finished in 40 seconds [12]. However, the experiments were deliberately made slower in order to provide a better definition of the material behaviour.

The pressure of this experiment was also low. It was 0.18 MPa, whereas in the actual mixing, the pressure exerted by the rotor blade of the internal mixer is more than

one order of magnitude higher, e.g., 3.5 MPa [2]. This higher pressure will undoubtedly expedite the compaction process. It is also expected to increase the degree of penetration from the present 30-35% to a higher percentage.

- *Energy required for compaction*

An approximate estimate of the energy of compaction may be calculated from the compression data. With the pressure of 0.18 MPa, this energy is only about 0.2 J/g. In the actual mixing with an internal mixer, the pressure created by the rotor blade is, for example, 3.5 MPa. The energy of compaction for the pressure may be estimated from the present data; this is done by extrapolating the specific volume-logarithm of pressure data to 3.5 MPa as shown in Figure 3.13. The estimated energy of compaction is 3.4 J/g.

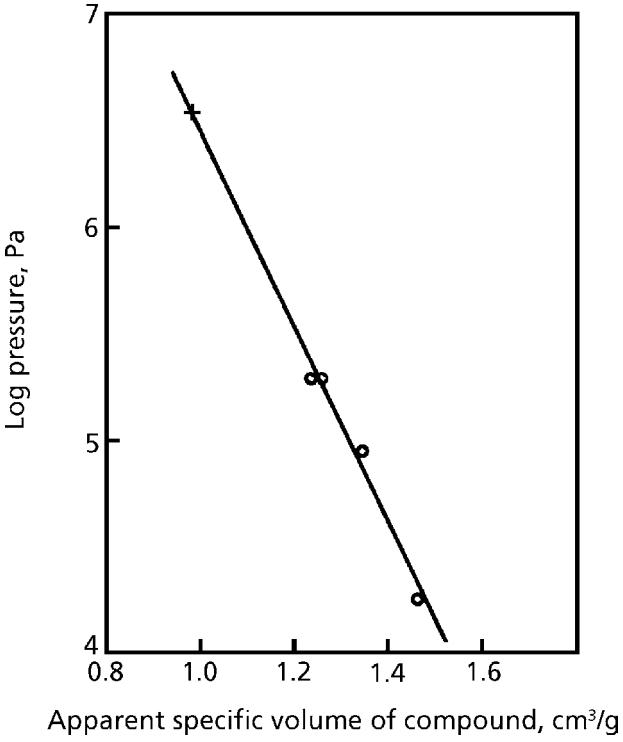

Figure 3.13 Apparent specific volume of compound as a function of pressure; observed (○), and extrapolated (X).

Reprinted with permission from N. Nakajima and E. R. Harrell, Rubber Chemistry and Technology, 1983, 56, 1, 197. Copyright 1983, Rubber Division of the ACS.

In the mixing experiment performed previously, 1,400 g of the powdered rubber compound was charged [2]. For this amount, the estimated energy of compaction according to the present work is about 5 kJ. On the other hand, the total energy for the incorporation process was estimated to be 80 kJ [2]. This large discrepancy needs to be explained. In addition to the energy of compaction, other contributions are the energy required to increase the surface area of elastomer particles and energy loss by the viscous dissipation. Part of the viscous energy is required for raising the temperature of the material in order to facilitate the incorporation process, and the other part is an inevitable loss accompanying any deformational process of elastomers. More detail of the deformational mechanisms of elastomers and compounds will be described in Chapter 4.

3.3.5 Experiment-II

- *Instruments and operation*

A Sieglaff-McKelvey capillary rheometer (Tinius-Olsen Testing Machine Company) was used for compression with the barrel plugged and for shear with an appropriate capillary. This rheometer is driven with nitrogen gas pressure applied to a piston, which exerts pressure on the material in the barrel. A barrel of 6.35 mm radius was chosen for this experiment. A predetermined amount of sample was charged and preheated in the barrel for 5 minutes before pressure was applied. Measurements were made at 100 °C and 150 °C.

Also, a Rheometrics mechanical spectrometer was used with 25 mm diameter parallel plates. Both the flat plates and serrated plates were used. The test geometry consisted of the cavity formed by the parallel plates and a molding ring. A shim was inserted between the bottom plate and the moulding ring in order to prevent leakage of the sample. A constant pressure was maintained by manually adjusting (pressing down) the top plate, while the top plate was rotated at a rotational speed of 0.1 rad/s. This experiment was used to separate the effect of shear from that of pressure on compaction at relatively low pressure levels. Measurements were made at 100 °C.

3.3.6 Results-II

- *Effect of pressure on compaction (capillary rheometer)*

The time-dependent compression data at 100 °C with 4 g charges in the capillary rheometer are shown in Figure 3.14 for the five levels of pressure in the range of 0.2-4.0 MPa. This temperature is chosen because at the end of the incorporation step, where the compound

is compacted, the temperature of the compound is about 100 °C [12]. The lowest pressure, 0.2 MPa, was chosen to compare the compaction data of this work and the previous one, where a different instrument, the Rheometrics mechanical spectrometer, was used. The higher pressure, 1-4 MPa, corresponds to the pressure generated in a commercial internal mixer by the rotor blade working on the compound against the chamber wall [20, 21].

The reproducibility of the data is reasonably good as indicated for the experiment at 2.0 MPa pressure. A general pattern in this result is that at the lowest pressure, the compound quickly comes to an equilibrium. At the higher pressure, there is a transient period, where the volume continues to decrease, eventually reaching equilibrium. This transient period is shortened as the pressure level is increased.

The specific volume at equilibrium was plotted against pressure in Figure 3.15.

It is called an apparent specific volume because it includes void volume. The data of this work labelled as S-MK are compared to those of the previous work, RH. Obviously, there is a large disagreement between the two sets of data; this will be discussed later in this section.

The time-dependent compression data at 150 °C with 4 g charges are shown in Figure 3.16 for the pressure range of 0.2-2.0 MPa.

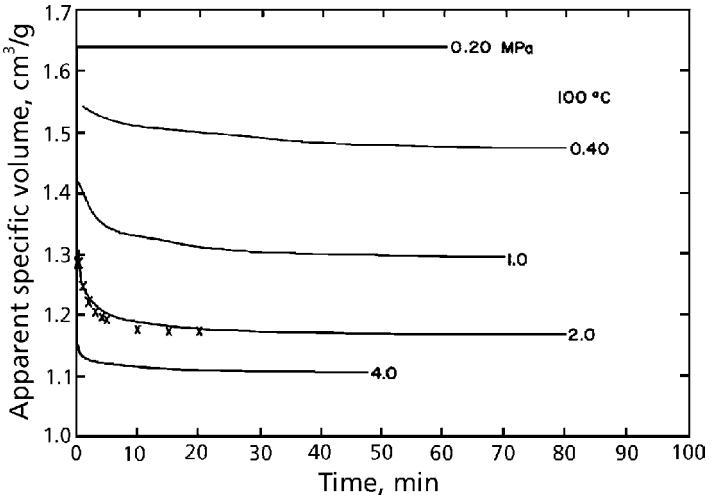

Figure 3.14 Time-dependent compression curves of a powdered rubber-carbon black mixture at 100 °C; measurements with a Sieglaff-McKelvey rheometer.

Reprinted with permission from N. Nakajima, P. R. Kumler and E. R. Harrell, Rubber Chemistry and Technology, 1985, 58, 2, 392. Copyright 1985, Rubber Division of the ACS.

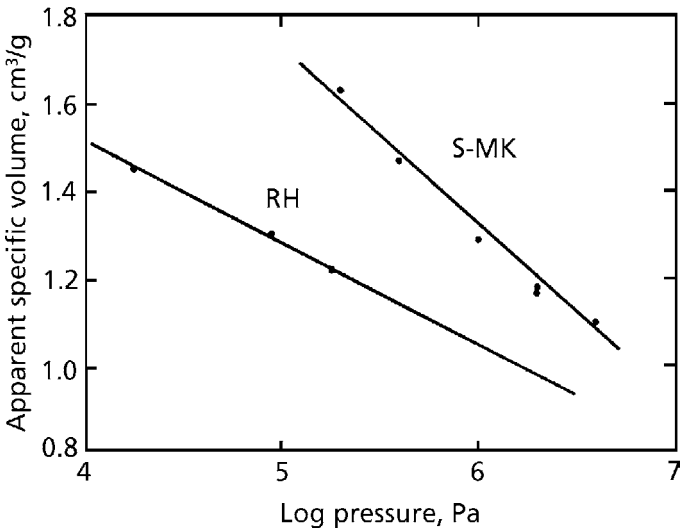

Figure 3.15 Apparent specific volume of a powdered rubber-carbon black mixture observed with two different instruments, Rheometrics mechanical spectrometer, RH and Sieglaff-McKelvey capillary rheometer, S-MK, at 100 °C.

Reprinted with permission from N. Nakajima, P. R. Kumler and E. R. Harrell, Rubber Chemistry and Technology, 1985, 58, 2, 392. Copyright 1985, Rubber Division of the ACS.

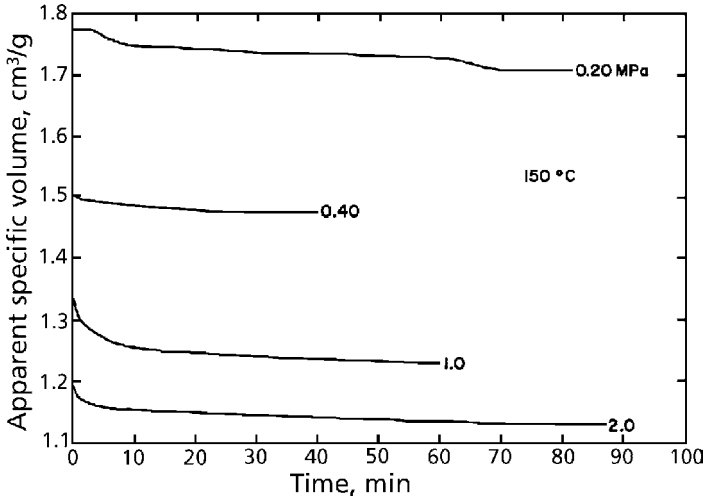

Figure 3.16 Time-dependent compression curves of a powdered rubber-carbon black mixture at 150 °C; measurements with a Sieglaff-McKelvey rheometer.

Reprinted with permission from N. Nakajima, P. R. Kumler and E. R. Harrell, Rubber Chemistry and Technology, 1985, 58, 2, 392. Copyright 1985, Rubber Division of the ACS.

Except for the irregular pattern at 0.2 MPa, a trend similar to that in Figure 3.14 was observed in regard to the transient period of decreasing volume and subsequent near-equilibrium period. The equilibrium data of the apparent specific volume were added to the data of Figure 3.15 and are presented in Figure 3.17.

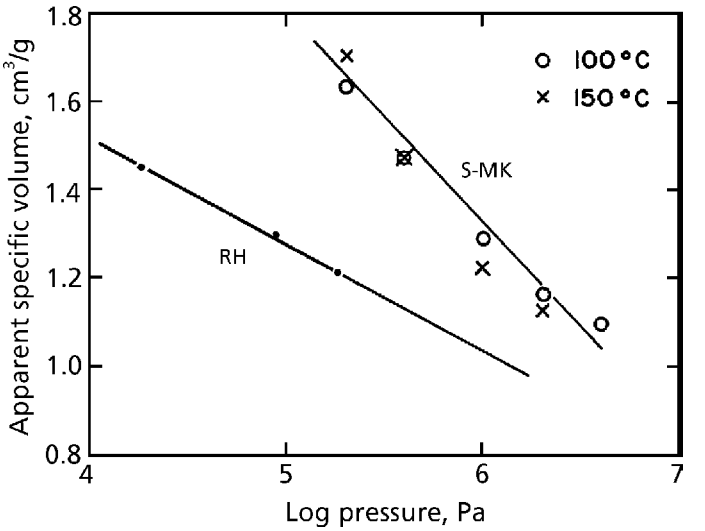

Figure 3.17 Apparent specific volume of a powdered rubber-carbon black mixture at 100 °C and 150 °C.

Reprinted with permission from N. Nakajima, P. R. Kumler and E. R. Harrell, Rubber Chemistry and Technology, 1985, 58, 2, 392. Copyright 1985, Rubber Division of the ACS.

The data obtained at 150 °C are in general agreement with those obtained at 100 °C except that the scattering of the data increased somewhat. The degree of penetration of elastomer into the void space is apparently not temperature-dependent. This has also been indicated in previous work at 0.18 MPa. The moduli of this type of elastomer had been shown to be approximately temperature-independent over this temperature range [22].

The compression of the powdered rubber has also been examined in the absence of carbon black. A sample of 8 g was charged and compressed at 100 °C for 4.5 minutes under 4.0 MPa pressure and then, for 10 minutes under 0.20 MPa. The compression behaviour of the powdered rubber itself was found to be very different from that of the mixture with carbon black. The volume equilibrated immediately after the application of pressure and stayed constant for the stated time periods. There was difficulty in maintaining a strictly

constant pressure at the lower pressure level, i.e., 0.17-0.21 MPa, and the volume fluctuated accordingly, but within 1%. The observed specific volume data are presented in Table 3.5.

Table 3.5 The Specific Volume of Powdered Rubber, using Butadiene-Acrylonitrile Copolymer

Specific volume, cm^3/g				
Pressure, MPa	Atmospheric	0.17	0.2	4.0
Observed	—-	1.030	1.022	0.987
Calculated	1.032	1.031	1.031	1.011

The calculated data are those of butadiene-styrene copolymer; the handbook values of the specific volume at the ambient condition, thermal expansion data, and compressibility data were used [13]. The observed and calculated data are in good agreement within the error of this work, which is about ±1%.

This sequence of experiments demonstrated that the Sieglaff-McKelvey rheometer was providing reliable pressure-volume relationships. However, a few facts suggested that the true equilibrium compression data for the elastomer-carbon black mixture were not being obtained. One fact is that, whereas the rubber alone equilibrates immediately, the mixture goes through a transient volume decrease over 10-20 minutes. Even after this period, the volume is very slowly but perceptibly decreasing. A more dramatic indication of the experiment not reaching its true equilibrium is the top curve in Figure 3.16, where the volume decrease is taking place in steps. The pseudoequilibrium is followed by the decrease of volume, leading to another pseudoequilibrium; the process is repeated with successive pseudoequilibria lasting a longer and longer time.

As shown before, the powdered rubber is coated with carbon black particles. When the mixture is charged in the barrel and compressed, it sets a 'bridging' structure. At first, the pressure equilibrates with the weakest structure, which soon yields. Then, the pressure equilibrates with the weakest of the remaining structure, which takes a little longer to yield. And this process is repeated. Because the psuedoequilibrium period increases significantly after each step, it is impossible to ascertain whether the true equilibrium is attained or not.

Re-examining the raw data presented in Figures 3.14 and 3.16, many examples of the pseudoequilibrium and stepwise compression are seen. However, it is not always obvious, when the data are presented in the linear plot of time. Figure 3.18 shows examples of apparent specific volume plotted against the logarithm of time.

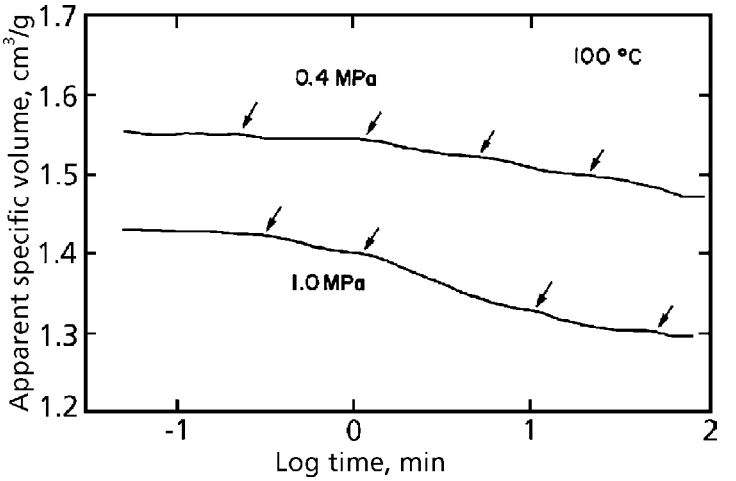

Figure 3.18 Time-dependent compression curves of a powdered rubber-carbon black mixture, indicating yielding of structures with the arrows.

Reprinted with permission from N. Nakajima, P. R. Kumler and E. R. Harrell, Rubber Chemistry and Technology, 1985, 58, 2, 392. Copyright 1985, Rubber Division of the ACS.

This plot emphasises the earlier pseudoequilibrium, which corresponds to a weaker structure. The yielding of the structure is indicated by the arrow. The pattern of pseudoequilibrium and yielding is not always clear, even in the log-time plot. Moreover, it is not reproducible. Therefore, it is suspected that the pattern is influenced by the way the powder in the barrel packs. The 4 g charge produced, depending upon the pressure, a 36-53 mm compressed height in the barrel of 6.35 mm radius. It is very difficult to charge powder uniformly in the deep 'well', rheometer barrel. The previous experiment with the Rheometrics mechanical spectrometer was performed with a disc shaped sample of 25 mm diameter and about 3 mm thickness.

With the above considerations, a new set of compressive experiments were performed with a decreased charge of 1.5 g. The time-dependent compression data were obtained at 100 °C at the pressures of 0.35, 0.88, and 1.98 MPa. Although the pattern of pseudoequilibrium-yielding was not eliminated, the specific volume was significantly smaller than that with a 4 g charge; the 'equilibrium' values estimated at 50 minutes or longer are shown in Figure 3.19.

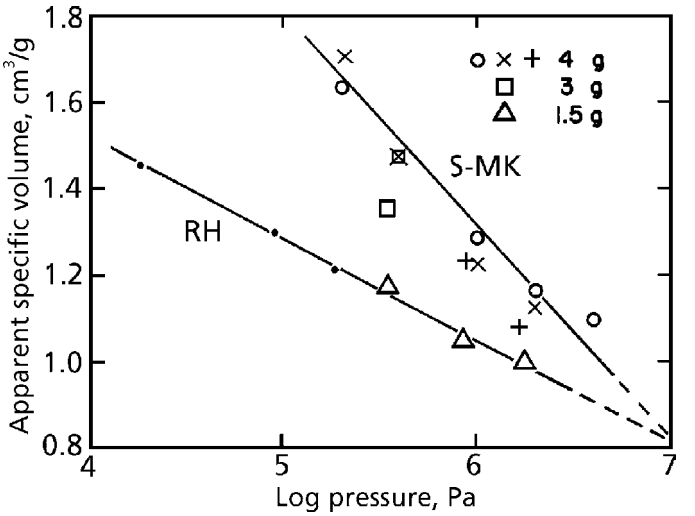

Figure 3.19 Apparent specific volume of a powdered rubber-carbon black mixture; the dependence on the sample thickness indicating a presence of a 'bridging' structure.
RH: this graph was obtained using a Rheometrics Mechanical Spectrometer.
S-MK: this graph was obtained using a Sieglaff-Mckelvey capillary rheometer.

Reprinted with permission from N. Nakajima, P. R. Kumler and E. R. Harrell, Rubber Chemistry and Technology, 1985, 58, 2, 392. Copyright 1985, Rubber Division of the ACS.

The three new data points line up well with the extension of the previous data with the Rheometrics mechanical spectrometer. However, the agreement of the data obtained from two different instruments does not necessarily mean that the true equilibrium is reached. For example, if the compression measurements had been continued for several hours instead of less than 2 hours, it is quite possible that even lower values of the specific volume would have been observed. However, such a long time measurement has no practical significance for the mixing behaviour. Rather, an important discovery is that the thickness of material is one of the important controlling variables on the deficiency of compaction. In the internal mixer at the space one-quarter of the circumference in front of the rotor tip, a significant level of pressure is maintained during mixing [20]. However, the gap between the rotor and chamber wall is wide except at the rotor tip. The implication is that until a compound passes through the narrowest gap, the compaction is not really effected. In our mixing experiments with a laboratory size mixer, this gap was 2.4 mm [2]. This is similar to the thickness used for our compaction experiments. Therefore, these data are valid for interpreting the mixing results.

Along with the measurements with 1.5 g charges, a few more measurements were made with 3 and 4 g charges. These data are also shown in Figure 3.19. Although the data with a 3 g charge lies between the two lines, so do some of the data with 4 g charges. This indicates the difficulty of reproducing the compaction behaviour with a thick charge in the deep well (barrel).

The degree of compaction was calculated at 100 °C per 1 g of compound from RH and S-MK lines of Figure 3.18 and presented in Table 3.6. The quantities, v_p, v_c and v_a are independent of the pressure.

Table 3.6 Degree of Compaction

Pressure, MPa	**0.02**	**0.1**	**0.2**	**0.4**	**1.0**	**2.0**	**4.0**
RH Line							
V, cm^3	1.45	1.28	1.22	1.14	1.05	0.98	0.92
v_p+v_c, cm^3 0.857							
PAC, %	59	67	70	75	82	87	93
v_p+v_a, cm^3 1.395							
v_n, cm^3	–0.055	0.115	0.175	0.255	0.345	0.415	0.475
v_v, cm^3, 0.538							
PEN, %	0	21	32	47	64	77	88
S-MK Line							
V, cm^3	—-	—-	1.66	1.51	1.31	1.16	1.02
v_p+v_c, cm^3 0.857							
PAC, %	—-	—-	52	57	65	74	84
v_p+v_a, cm^3 1.395							
v_n, cm^3	—-	—-	–0.265	–0.115	0.085	0.235	0.375
v_v, cm^3, 0.538							
PEN, %	—-	—-	0	0	16	44	70

The degree of compaction evaluated from the RH line of Figure 3.19 is the highest degree of compaction attained in the present study. It also represents the compacted thickness of about 3 mm, which corresponds to the gap between the rotor tip and the chamber wall of the internal mixer.

The degree of compaction estimated from the S-MK line represents the less effective compaction, when more material (an increased thickness) was to be compacted. The structure, resulting from the carbon black bridges, hinders an effective compaction as previously discussed. This situation may correspond to the compaction at the zone in front of the rotor tip in the internal mixer. In the above interpretation, the effect of shear on the compaction has not yet been considered. This subject will be discussed in the next section.

The degree of packing (PAC%) indicates a macroscopic picture of the extent of compaction, as it expresses percent of volume occupied by the real volume of carbon black and polymer. The degree of penetration (PEN%) gives an insight into the microscopic picture of the extent of compaction, as it represents a relative measure of how close the rubber particles come in contact with the topology of carbon black.

At the pressure level comparable to that generated by the blade tip and the chamber wall of the internal mixer, i.e., 1-4 MPa, and with the material thickness corresponding to the gap between the blade-tip and the chamber wall, the compaction was shown to occur very effectively, with a PAC of 82-93% and a PEN of 64-88%. However, it took 5-10 minutes to reach these values.

In the mixing operation, the time available for compaction of the material is only a fraction of a second. The present compaction study does not provide such short time results. It indicates that within such a short time, the compaction does not progress very much (see Figures 3.14, 3.15, and 3.16). Therefore, it is necessary to find out what effect shear has in accelerating compaction.

- *Effect of shear on compaction*

The experiments previously described, show that the compaction can be achieved with static pressure alone, i.e., without application of shear. However, the time required to achieve compaction was approximately 5-10 minutes, which is orders of magnitude longer than the action of the blade tip on the material against the chamber wall of the internal mixer, i.e., a fraction of a second.

The shearing action must have a significant effect on the rate of compaction; this was explored by applying a shear at different levels of static pressure. For the higher pressure levels, the Sieglaff-McKelvey capillary rheometer was used. For the lower pressure levels, the Rheometrics mechanical spectrometer was used. As will be shown next, the capillary experiments were not successful, but the work with both instruments will be described.

Capillary rheometer - Because the material experiences both pressure and shear in the capillary extrusion, the compaction by extrusion is expected to be more effective than

that by pressure alone. We have attempted to see if the capillary extrusion results in an additional decrease in the specific volume of the compound. The dimensions of dies and the operating pressure are given in Table 3.7.

Table 3.7 Die Dimensions and Operating Pressure

Die No.	Radius mm	Length mm	Precompaction		Extrusion Pressure MPa
			Pressure MPa	Time min	
1	0.89	25.40	0.88	78	14.0 35.0
2	0.79	0.79	1.76	78	6.9 14.0
3	3.15	25.96	3.5	75	3.5

The barrel size was 6.35 mm radius. Dies No. 1 and 3 have 90 degree entrance angles; die No. 2 is very short and the entrance geometry from the barrel to the die is 'wine glass' shaped.

The measurements were performed at 100 °C. The sample was precompacted in a barrel with the die-end closed to form a plug under the pressure and time given in Table 3.7. The plug was removed and recharged after the respective die was attached to the barrel. Then, the compound to be extruded was at the pressure equal to the precompaction pressure to see if the extrusion resulted in the further decrease of specific volume. However, with dies No. 1 and No. 2, a pressure much higher than the precompaction pressure was required to produce 'flow'. Therefore, any decrease of specific volume could be the result of the applied shear or that of the higher pressure. These two effects could not be separated. Also, the pressure levels required for extrusion were an order of magnitude higher than the highest pressure encountered in the internal mixer. Therefore, the extrusions with these dies were found to lack practical significance.

Subsequently, die No. 3, which has a large diameter, 6.3 mm, was used so that the extrusion could be achieved at a pressure comparable to that in the internal mixer. Also, the radius of this die, 3.15 mm, is similar to the gap between the rotor tip and the chamber wall, 2.4 mm.

As shown in Table 3.7, the extrusion could be achieved at the pressure of precompaction. However, no significant decrease was found in the specific volume; it was 1.112 ± 0.007 cm^3/g before and 1.116 cm^3/g after the extrusion. Perhaps, the shear rate of the extrusion was too low, 0.03-0.05 s^{-1}, to demonstrate the effect of shear on compaction.

Mechanical spectrometer -With the top plate rotating, the compound leaked out of the fixture when a 9 kg load was applied. This fact indicates that the force was transmitted more effectively when shear was applied. Also, the bridge structure was effectively destroyed by shear. However, the quantitative measurement on the compaction rate could not be made when the compound was leaking. With a 4.5 kg load (90 kPa pressure), the compound did not leak. Figure 3.20 shows the compaction curve without the plate rotating (curve 1) and curves with the plate rotating (curves 2 and 3).

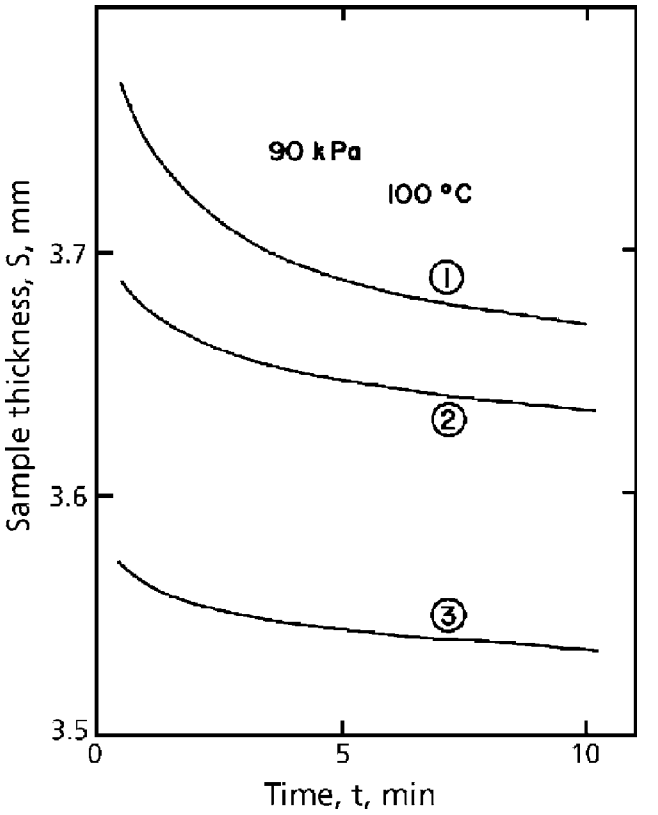

Figure 3.20 Time-dependent compression curves of a powdered rubber-carbon black mixture at 100 °C under 90 kPa; measurements with a Rheometrics Mechanical Spectrometer. Curve 1 without shear; curves 2 and 3 with shear.

The latter indicate the extent of reproducibility; the shape of curve reproduced very well, although the level of the compaction disagreed by 0.1 mm, approximately 3%. The disagreement arises from the difficulty of charging the powder compound in a reproducible

manner. Therefore, the differences in the level of the compaction curves cannot be attributed to the effect of shear. However, with the application of shear, the compaction proceeds faster in the beginning, for example, at a time of less than one minute.

With the serrated plates, the compound leaked out even at 90 kPa when the top plate was rotated. This indicates that the transmission of force and breaking of structure were more effective with the serrated plates. Only with a 0.9 kg load (18 kPa pressure) could the leakage be avoided. In Figure 3.21 curves 1 and 2 were obtained with the flat plates and curve 3 with the serrated plates. Curve 1 is without the top plate rotating and curves 2 and 3 with the rotation. The trend shown by curves 1 and 2 is the same as the case with 90 kPa pressure, that with the application of shear, the compaction occurs faster in the beginning.

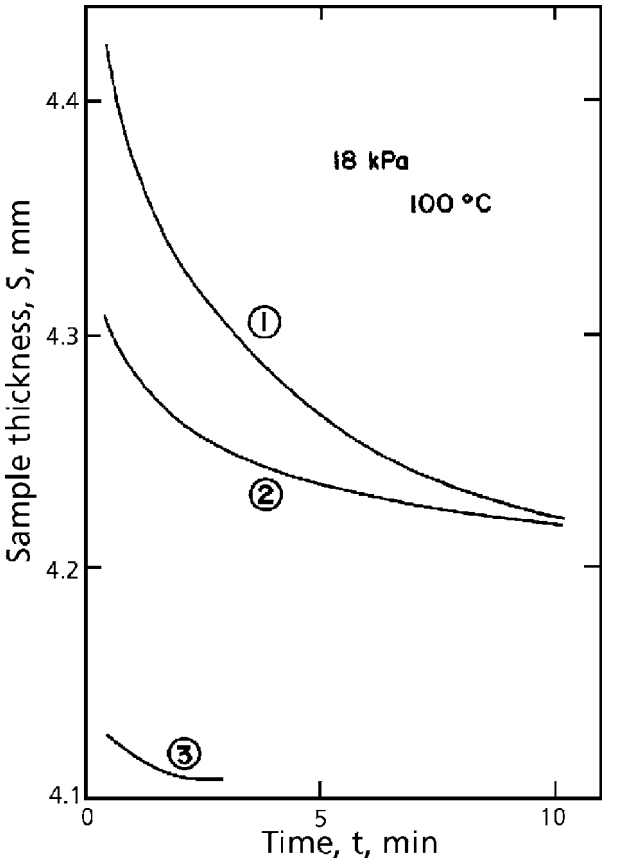

Figure 3.21 Time dependent compression curves at 100 °C under 18 kPa. Curves 1 and 2 with flat plates; curve 3 with serrated plates; curve 1 without shear; curves 2 and 3 with shear.

Curve 3 shows that with the serrated plates, the effect of shear is even more dramatic. Almost immediately after the application of the load, the volume reached the ultimate value, which is in agreement with the apparent specific volume of RH line, Figure 3.19. In addition, the thickness of the compound fluctuated as shown in Figure 3.22. This behaviour is very different from the smooth curves obtained with the flat plates.

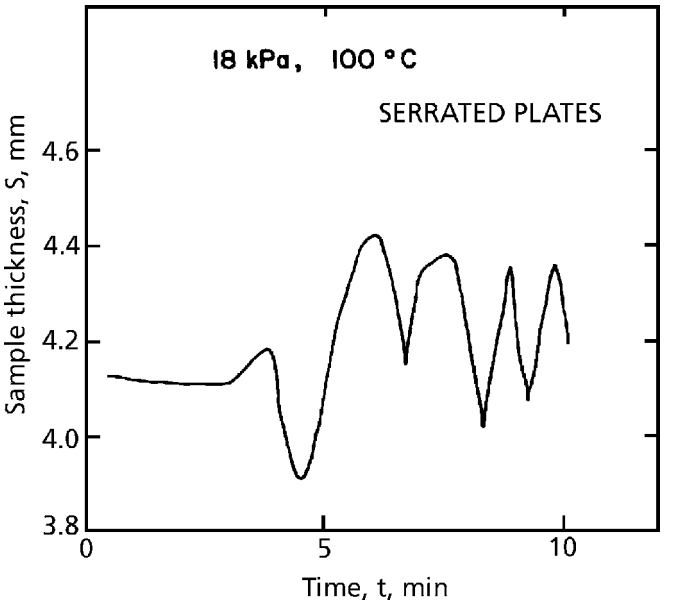

Figure 3.22 The fluctuation of volume under shearing condition.

Reprinted with permission from N. Nakajima, P. R. Kumler and E. R. Harrell, Rubber Chemistry and Technology, 1985, 58, 2, 392. Copyright 1985, Rubber Division of the ACS.

Subsequently, a number of differences in material behaviour were found between the cases with the flat plates and those with the serrated plates. After the compaction experiment was over and the top flat plate was lifted, the compound surface was shiny, indicating that the plate was slipping at the surface. With the serrated plates, there was no slipping at the plate-compound interface. With the flat plates, the compacted material was still friable. With the serrated plates, the rubber particles were 'fused' together and no longer friable.

When the top plate was lifted, the flat plate cleanly separated at the plate-compound interface. This also implies that there was slipping. When the serrated plate was lifted, the sample broke in the middle. The fractured surface showed that the rubber particles were stretched and torn. The behaviour observed with the serrate plates is very significant, and it will be discussed in section 3.3.7.

3.3.7 Discussion-II

The significant points deduced from the observation with the serrated plates are as follows:

- When the compound does not slip at the interface with the plates, shear is very effective in stretching the rubber particles.
- The resulting large deformation can lead to a fracture of the rubber.
- The carbon black probably aids the fracture process as it acts like sandpaper.
- The newly created surfaces readily adhere to the surface of carbon black.
- The newly created surfaces attach by cohesion to other rubber particles to 'fuse' with each other.
- Carbon black agglomerates disintegrate, while the rubber particles are deformed and fractured. This aspect has been discussed in section 3.2.
- The compaction of the mixture of carbon black and powdered rubber proceeds primarily through a large deformation and fracture of rubber particles. The static pressure required is rather small: it is two orders of magnitude smaller than the pressure generated by the action of the rotor blade against the chamber wall and one order of magnitude smaller than the ram pressure.
- When the large deformation is imposed on the particle-packed systems, there is a tendency for dilatation to occur in order to make a way for the particles to pass each other, [23]. This is indicated by the increase of the thickness of the sample from 4.1 mm to 4.4 mm (see Figure 3.22). The magnitude of the increase is approximately the size of the rubber particles, the average being 0.25 mm in diameter. The thickness decreases to about 4.1 mm as the particles rearrange themselves to new positions.
- The relaxation of rubber domains occurs as a result of fracture and rearrangement of particles. This explains why the relaxation occurs almost instantaneously during mixing. If the relaxation were through viscoelastic relaxation of the long chain molecules, it would have taken orders of magnitude longer.
- The previous observation was made with the pressure held constant. If the volume had been kept constant, it would have resulted in the fluctuation of pressure. In the internal mixer, neither pressure nor volume is held constant. However, certain volumetric constraints exist so that the pressure fluctuation occurs [20].

- During the mixing in the internal mixer the torque fluctuates. This is another observation of the same phenomenon. The end-point of mixing is considered to be the time, when the magnitude of the fluctuation becomes sufficiently small and no longer decreasing. It is proposed here that the magnitude of the fluctuation is related to the rubber-domain size.

From the time of loading to the end of incorporation a significant change takes place under the pressure of the ram and by the action of the rotor blades. What might be taking place with rubber and carbon black has been examined through simulated experiments with laboratory instruments. The most important finding is the contribution of the deformation and fracture of rubber and not just pressure on compaction (massing). The blades of rotors are made with a smooth surface. The present study indicates that a serrated surface is more effective for mixing. Because of the well-known wear of the blades, the serrated surface may not be practical but it may lead to an improvement of the mixing machine, if the way was found to minimise the wear.

References

1. E. S. Dizon and L. A. Papazian, *Rubber Chemistry and Technology*, 1977, **50**, 4, 765.

2. N. Nakajima, *Rubber Chemistry and Technology*, 1981, **54**, 2, 266.

3. W. M. Hess, in *Reinforcement of Elastomers*, Ed., G. Kraus, 1965, John Wiley & Sons, New York, Chapter 6.

4. N. Nakajima, *Rubber Chemistry and Technology*, 1982, **55**, 3, 931.

5. S. Hashizume, *Journal of the Society of the Rubber Industry, Japan*, 1990, **63**, 2, 71.

6. S. Shiga, and M. Furuta, *Rubber Chemistry and Technology*, 1985, **58**, 1, 1.

7. N. Nakajima, P. R. Kumler and E. R. Harrell, *Rubber Chemistry and Technology*, 1985, **58**, 2, 392.

8. G. R. Cotten, *Rubber Chemistry and Technology*, 1984, **57**, 1, 118.

9. N. Nakajima and E. R. Harrell, *Rubber Chemistry and Technology*, 1983, **56**, 1, 197.

10. K. Nakagawa and I. Amano, *Journal of the Society of the Rubber Industry, Japan*, 1980, **53**, 9, 550.

11. ASTM D 1646 - 96a
Test Methods for Rubber - Viscosity, Stress Relaxation and Pre-vulcanization Characteristics (Mooney Viscometer).

12. N. Nakajima, E. R. Harrell and D. A. Seil, *Rubber Chemistry and Technology*, 1982, **55**, 2, 456.

13. *Polymer Handbook*, 4th Edn., Eds., J. Brandrup, E. H. Immergut and E. A. Grulke, John Wiley & Sons, New York, 1999.

14. R. F. Robbins, Y. Ohori and D. H. Weitzel, *Rubber Chemistry and Technology*, 1964, **37**, 1, 154.

15. *Handbook of Chemistry and Physics*, 31st Edn., Chemical Rubber Publishing Company, Cleveland, Ohio, 1949, 1715.

16. J-B. Donnet and A. Voet, *Carbon Black, Physics, Chemistry and Elastomer Reinforcement*, Marcel Dekker, Inc., New York, 1976, 204.

17. J. D. Ferry, *Viscoelastic Properties of Polymers*, 2nd Edn., John Wiley, New York, 1970, 303.

18. N. Nakajima, H. H. Bowerman and E. A. Collins, *Rubber Chemistry and Technology*, 1973, **46**, 2, 417.

19. N. Nakajima and E. R. Harrell, *Journal of Rheology*, 1983, **27**, 3, 241.

20. S. Toki, M. Takeshita, Y. Morimoto and M. Okuyama, Presented at the 124th Meeting of the ACS Rubber Division, Fall 1983, Houston, TX, Paper No.37.

21. P. K. Freakley and W. Y. Wan Idris, *Rubber Chemistry and Technology*, 1979, **52**, 1, 134.

22. N. Nakajima, E. A. Collins and P. R. Kumler, *Rubber Chemistry and Technology,* 1974, **47**, 4, 778.

23. N. Nakajima, *Journal of Non-Newtonian Fluid Mechanics*, 1983, **12**, 349.

4 Viscoelasticity and Fracture

4.1 Introduction to viscoelasticity

Following the manner of presentation in the previous sections, the subject of viscoelasticity will be explained by reference to experiments familiar to the practitioner of rubber technology. This is a rather unorthodox approach and different from the usual one, which begins with an introduction of the theory. The experiment is tensile stress-strain measurement. In the rubber industry tensile measurements are routinely performed with crosslinked specimens. Here, we are concerned with gum-rubber behaviour. Therefore, we must perform the measurements with uncrosslinked specimens. First, compression-moulded specimens must be prepared; they require special attention, which will be described next.

When a gum rubber is compression-moulded for preparing a flat sheet a few millimetres thick, the surface is often uneven, retaining the memory of the sizes and shapes of the pieces of rubber charged to the press. Even when the surface is flat and smooth, the sheet may become wrinkled while in storage. In order to minimise the elastic memory, rubber can be charged as small pieces, evenly spaced, and preheated before applying pressures and/or the pressure may be applied gradually. Even with these precautions, some rubber does not produce a satisfactory sheet. In this case, after compression-moulding, the sheet of rubber is kept in a picture-frame mould with a weight on it and maintained at room temperature for a sufficient time to relax-out the memory. Sometimes this may take more than a week.

In general, the higher temperature and the longer time of pressing yield a flat sheet more easily. But it may introduce crosslinks, which alter the viscoelastic properties, thereby, the characteristics of original rubber become obscured. Usually there is a ceiling temperature below which crosslinking does not occur. A typical pressing condition for many commercial rubbers is 160 °C for 20 minutes. Even in this case, the gel-content (insoluble) of the pressed sheet must be checked against that of the rubber before pressing in order to ensure that no significant crosslinking has taken place [1].

Figure 2.2 shows the tensile stress-strain curves of the NBR [2], where the measurements were made with three (high) speeds and at the three temperatures. The same data are replotted in Figure 4.1 as the modulus-strain curves. This conversion is made because the modulus is the material property and the stress is only the manifestation of the property. The

modulus is observed to decrease with the increase in strain, i.e., strain-softening. The modulus-strain relationship is different for different temperature and different strain-rate. At the lower temperature or at the higher strain rate, the modulus is higher and at the reverse conditions the modulus is lower. Data like these can be obtained for the temperature and the strain-rate range corresponding to those during mixing of a rubber.

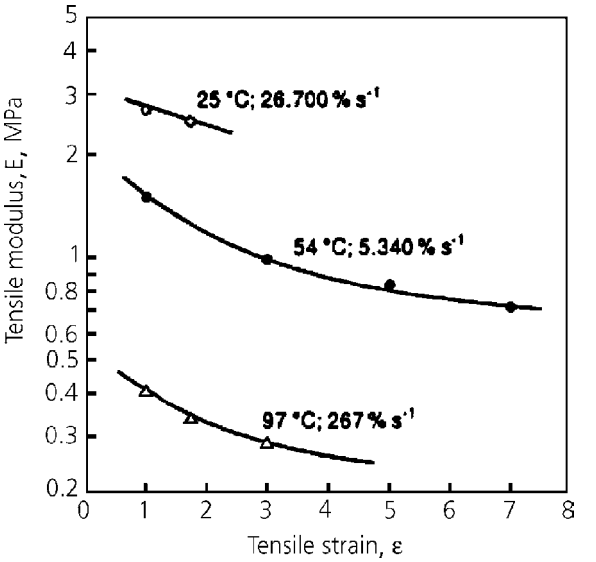

Figure 4.1 Tensile modulus-strain curves of NBR sample B.

Reprinted with permission from N. Nakajima, International Polymer Processing, 1996, 11, 1, 3. Copyright 1996, Hanser Publishers, Munich.

The data of Figure 4.1 can be converted into modulus-time (t) curves; in the tensile measurements, the strain-rate, $\dot{\varepsilon}$ is fixed. Therefore, t may be calculated from the strain-rate and a magnitude of strain, ε:

$$t = \varepsilon / \dot{\varepsilon} \tag{4.1}$$

As shown in Figure 4.2a the data obtained at the lower temperature lie in the shorter time range and those at the higher temperature lie in the longer time range. The next step is the application of the time-temperature correspondence principle [3] to the data at different temperatures, thereby reducing the data to those at 100 °C (Equation 3.9); in this calculation the observed time, t, at a given temperature, T, is changed to the corresponding time, t/a_T, at the reference temperature, T_0, (100 °C in this case) with the use of the factor, a_T (see Figure 4.2b). Then, the time axis is modified further by multiplying with the extension ratio, α, to make it $\alpha t/a_T$. As shown in Figure 4.2c, a master curve is formed from separate curves in Figure 4.2b.

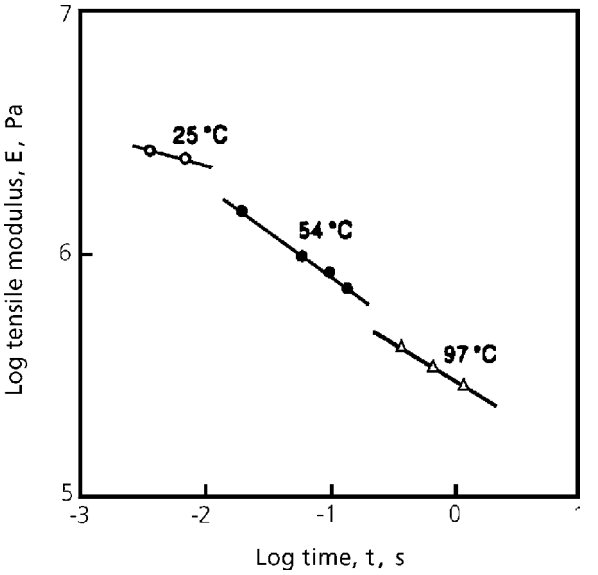

Figure 4.2a Tensile modulus-time curves at 25, 54, and 97 °C.

Reprinted with permission from N. Nakajima, International Polymer Processing, 1996, 11, 1, 3. Copyright 1996, Hanser Publishers, Munich.

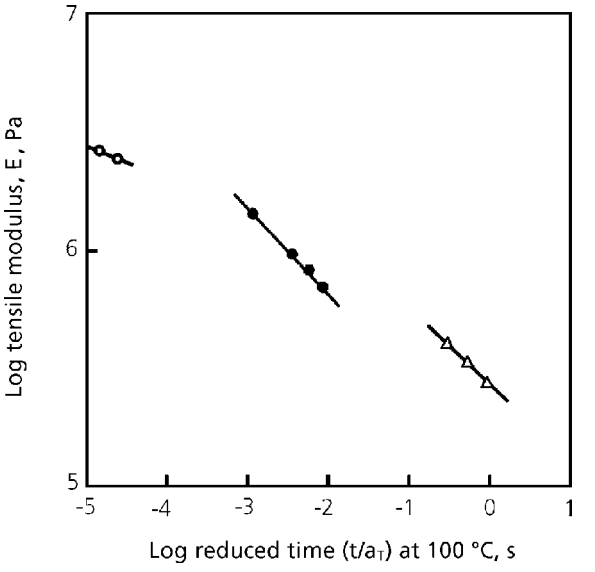

Figure 4.2b Tensile modulus-time curves, reduced to 100 °C.

Reprinted with permission from N. Nakajima, International Polymer Processing, 1996, 11, 1, 3. Copyright 1996, Hanser Publishers, Munich.

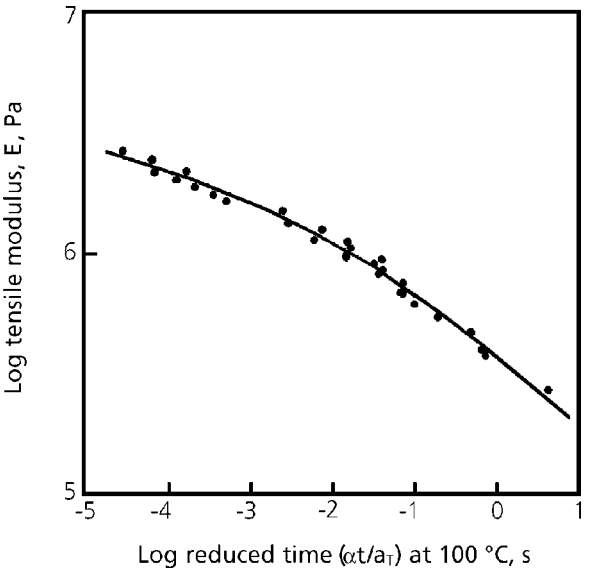

Figure 4.2c Tensile modulus-reduced time curve at 100 °C after application of strain-time correspondence.

Reprinted with permission from N. Nakajima, International Polymer Processing, 1996, 11, 1, 3. Copyright 1996, Hanser Publishers, Munich.

Among many rubber samples, some of them do not yield a master curve with this treatment. This will be discussed later in this section. In general, the modulus, E, is a function of temperature, T, time, t, and strain, ε or α. At a fixed temperature, E is a function of t and ε(or α). In the above example, E takes a specific form of the dependencies on a time and strain set as αt. This is the same form as the temperature dependence, t/a_T. However, a_T is species-dependent and requires the experimental determination. On the other hand, α is species-independent, a 'universal parameter.'

If the temperature dependence of a_T is known, the value of the tensile modulus may be calculated from the master curve for any temperature, time, and strain. The implication is that the modulus may be estimated for a rubber in the internal mixer at a specified location and at a specified time, provided that its thermal-mechanical history is known.

Modulus-strain curves of another sample of NBR are shown in Figure 4.3 [2]. The shapes of the curves are different from that in Figure 4.1. In Figure 4.3, the modulus is shown to increase with the increase of strain, i.e., strain-hardening.

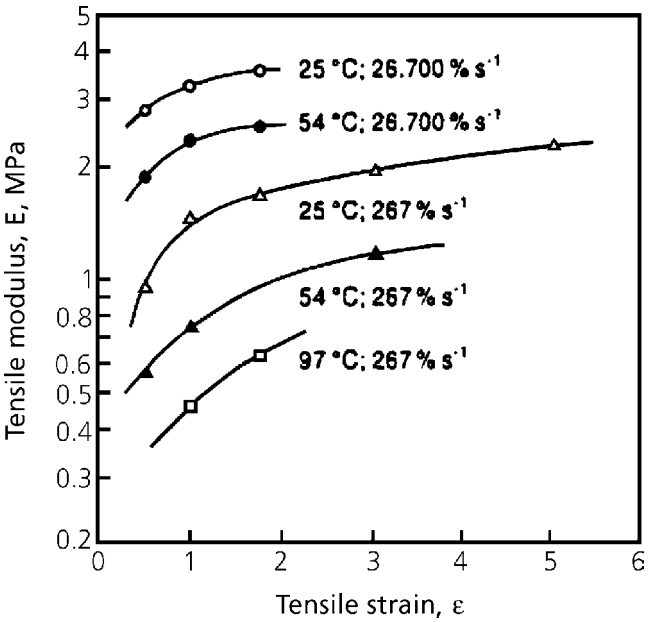

Figure 4.3 Tensile modulus-strain curves of NBR sample D.

Reprinted with permission from N. Nakajima, International Polymer Processing, 1996, 11, 1, 3. Copyright 1996, Hanser Publishers, Munich.

In this case, the use of reduced time, αt, does not give a master curve, Figure 4.4a. Dividing modulus, E, with a factor, Γ, a master curve is formed as $E/\Gamma \sim \alpha t$, Figure 4.4b. The factor, Γ, is an increasing function of α and represents a degree of strain-hardening. With this sample of NBR, Γ takes the following form:

$$\Gamma = \alpha^n \tag{4.2}$$

with n being a positive number. The master curve generated according to the above two methods represents the viscoelastic behaviour of a given gum rubber. Further analyses of the viscoelastic behaviour may be made by the use of these master curves according to the methods given by Ferry [3].

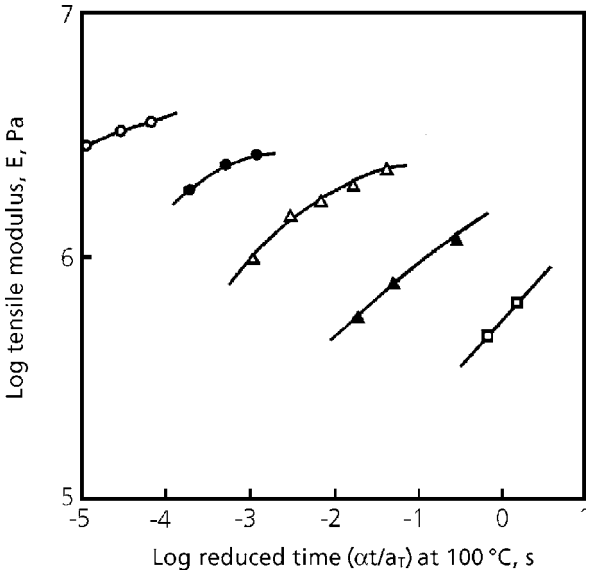

Figure 4.4a Tensile modulus-reduced time a_T at 100 °C after application of strain-time correspondence.

Reprinted with permission from N. Nakajima, International Polymer Processing, 1996, 11, 1, 3. Copyright 1996, Hanser Publishers, Munich.

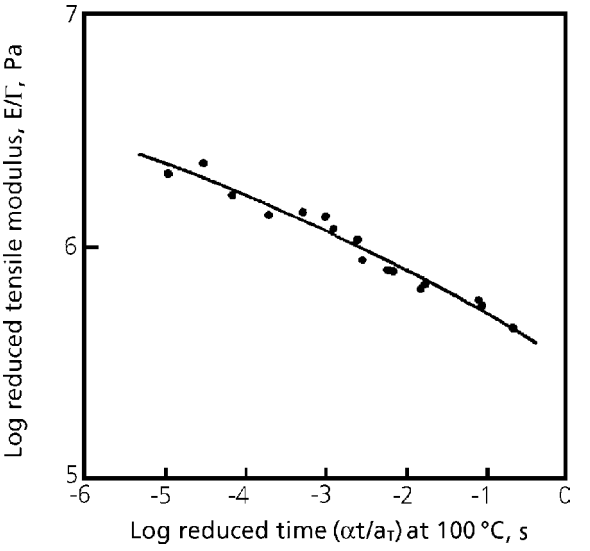

Figure 4.4b Tensile modulus divided by strain hardening factor, Γ, plotted against reduced time at 100 °C.

Reprinted with permission from N. Nakajima, International Polymer Processing, 1996, 11, 1, 3. Copyright 1996, Hanser Publishers, Munich.

4.2 Viscoelasticity for characterisation

Through hands on experience, a mill operator knows that each gum rubber exhibits a characteristic behaviour. The mill behaviour of gum rubbers is systematically categorised into the four regions of processability [4] in such a way that the behaviour of a given rubber falls in one category or more during milling while temperature of the rubber rises. These four regions obviously describe deformational behaviour, which is shown to correspond to the modulus and the strain at the break [5].

The important point is that the deformational measurements and observations of fracture provide methods for characterising gum rubber. Because the characterisation results must be related to the processability, the above method is most suitable for the purpose.

Examples are presented in Section 4.1 of the characterisation of two samples of NBR using tensile stress-strain measurements. The presentation concerns deformational behaviour only, and the failure behaviour will be discussed in Section 4.4.

The master curves obtained are related to the MW, its distribution, long branching and gels. This molecular architecture is, in turn, related to the polymerisation conditions. In general, for the polymer characterisation, the standard procedure involves the measurements of MW, its distribution, and branching. With gum rubbers these techniques are often either meaningless or misleading because of the presence of gel, i.e., insoluble fraction. Even small amounts of gel may influence the processability of gum rubber. Therefore, a characterisation method without dissolution of sample is required. The viscoelastic method is suitable for this purpose, although only indirect information is available on the variation of the molecular architecture. Furthermore, there are two types of gels, which require differentiation: one type is a result of the extensive long-branch formation, macrogel; and the other is crosslinked latex particles, microgel. For the samples of unknown origin, the only method available for differentiating macro- and micro-gels is the tensile stress-strain (large deformation) measurements. When the macrogel is present in a significant amount, the rubber exhibits strain-hardening as described in Section 4.1. The exponent n of Equation (4.2), is, therefore, an approximate measure of the macrogel content [6]. When the MW is sufficiently high, the macrogel-containing rubber tends to give a region I behaviour, presenting a difficulty in milling. The relative level of MW may be assessed by comparing master curves of the two samples. Also, the relative degree in the spread of MW distribution is indicated by the shape of the master curve. However, these will be discussed in Chapter 6.

4.3 Viscoelastic behaviour of rubber in an internal mixer

There have been many attempts for describing the behaviour of rubber in internal mixers. Practically all treat rubber as a viscous, inelastic liquid. If the behaviour corresponds to that in Region IV of mill processability [4], it is a viscous fluid but it still has an elastic contribution. As a first step the behaviour of viscous-inelastic fluid and viscoelastic fluid will be compared. A rotational rheometer such as cup-and-bob, cone-plate, or parallel-plates, is switched on at time, $t = 0$ to start a steady rotation, see Figure 4.5.

With a viscous-inelastic fluid, the torque instantly reaches a steady value. With a viscoelastic fluid, it takes a finite time to reach a steady torque. Starting from zero, the torque gradually rises to a constant level for a low rotational speed; it goes over a peak and decreases to a constant value for a high rotational speed, see Figure 4.5. This is called stress overshoot.

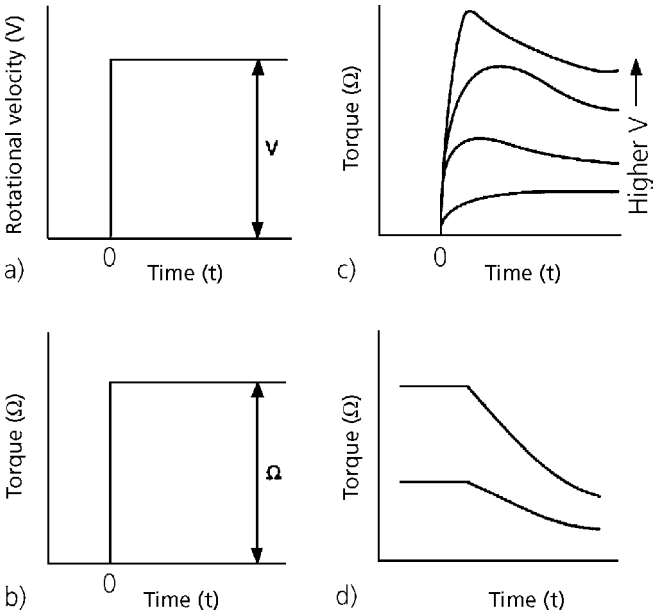

Figure 4.5 Operation of rotational rheometers.
a: steady rotation
b: response of viscous liquid
c: response of viscoelastic body
d: viscoelastic relaxation from steady state

When the torque reaches a constant value, the flow is in the steady state; the time period before reaching the steady state is called the transient state. The behaviour in Figure 4.5c is commonly observed with plastic melts and also with gum rubbers [7]. The transient state exists not only when the rotation is started, but also when the rotational speed is changed. When the speed is increased, the torque curve takes the shape shown in Figure 4.5c. When the speed is decreased, the shape is that of the relaxation curve shown in Figure 4.5d. The above behaviour has been described as a relationship between the rotational speed and the responding torque. Taking account of the geometry of the rheometer, the rotational speed may be converted to the shear rate and the torque to the shear stress.

In the internal mixer, rubber is present between the chamber wall and a rotor or between two rotors. Using the knowledge of the geometry of the mixer and the relative speed, the shear rate may be calculated for any part of the mixer at a given instant. The key is to recognise that the passageway for rubber is changing all the time; the rubber goes through a wide gap and then a narrow gap. Therefore, the deformation rate is always changing. For viscous-inelastic fluid, the material reaches the steady state instantaneously, but for viscoelastic material it always remains in the transient state.

As explained in Chapter 2 the most desirable behaviour of rubber in the mixing process is described by Region II of mill processability [4]. Rubber in this state is elastic and gives a large deformation without break.

The torque-time curves recorded at various rotational speed of a rheometer are shown in Figure 4.6 for a sample of gum rubber.

The general behaviour is similar to that for the plastic melts shown in Figure 4.5, except that for rubber the torque-level is higher and the stress-over-shoot appears at a relatively lower shear rate [7]. In the on-going discussion it will be assumed that the rubber behaviour in the internal mixer corresponds to Region II of mill processability.

Because the rubber in Region II is an elastic material, it deforms and recovers from deformation but it does not flow. Then, the rubber in the internal mixer does not flow but moves to change its position with accompanying deformation and recovery. Is this picture correct? When a rubber is milled in a roll, it deforms initially but gradually takes on the appearance of flow. When the behaviour changes from Region II to Region IV, it starts flowing because Region IV represents viscoelastic fluid. However, even when the rubber behaviour remains in Region II, it gradually assumes an appearance of flow. What is the explanation for this transformation? This question has existed for many years going back at least to the 1940s. When an NR is masticated, polymer chains break, resulting in the significant decrease of MW. The chain scission also occurs with synthetic rubbers but it is usually so slight that it does not noticeably alter the viscoelastic properties

(synthetic polyisoprene is an exception which degrades like NR). In summary, the chain scission is not an explanation for the appearance of flow.

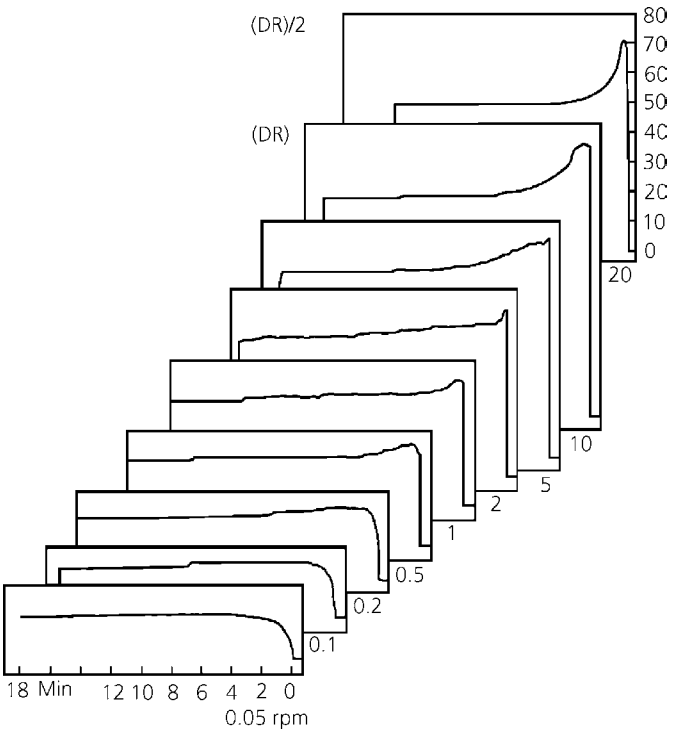

Figure 4.6 Recorder traces of variable speed Mooney rheometer with SBR 1500 at 100 °C. DR is the dial reading of the Mooney rheometer.

As an explanation, Mooney proposed a generation of super-molecular flow unit [8]. When a matter flows, adjacent molecules present across the velocity gradient changes the mutual position permanently. With an elastic body, the change of the mutual position is not permanent, but recoverable to the original position. However, even with an elastic body, if the strain imposed by the velocity gradient exceeds a limit, it breaks. Between the adjacent broken pieces the mutual position changes permanently. Such broken pieces are much larger than the size of polymer molecules; they are called super-molecular flow units.

Mooney used a parallel plate rheometer with a piece of rubber, with one surface which was dyed. As the rotation continued, the colour of the dye was observed to spread in the direction of thickness of the specimen. The fractured rubber particles, as they rotated under the shear field, carried the dye like an ink-roll. This process imprinted the dye from the surface down to the successive layers of the rubber particles. On the basis of this model Mooney calculated the size of the rubber particles, i.e., the flow unit to be of the order of 10 μm [9]. Mooney's model on the generation of super-molecular flow units is one of models used as the basis for proposing the comminution model for mixing of rubber with fillers [10].

Thus far the behaviour of rubber in an internal mixer has been explained in terms of shear deformation and fracture to create super-molecular flow units. However, elongational deformation and subsequent fracture is equally important, because wherever the passageway changes its cross-sectional area, the elongational deformation is present. In this case elongational deformation is not limited to pulling. When rubber is squeezed between rotor-tip and the chamber-wall, the deformation is equivalent to elongation. In order to consider the viscoelastic behaviour, therefore, both shear and elongational deformation must be considered. The bulk compression need not be considered because gum rubber is essentially incompressive.

4.4 Mechanism of fracture of gum rubber

For a long time it was thought that gum rubber was fractured to smaller and smaller pieces during milling and mixing with carbon black. However, the mechanisms of the fracture of gum rubber had not been examined scientifically. When a given body is deformed gradually to a certain limit, it fractures. This limit is when the stored energy resulting from the deformation becomes equal to the energy required for fracture. With an idealised elastic body, fracture occurs as the elastic stored energy becomes equal to the energy required for creating new fractured surfaces [11].

It is very important to recognise that fracture is inseparable from deformation. Yet, deformation and fracture are distinctly different phenomena. In general, for characterising deformation, the test piece is deformed uniformly. Otherwise, the stress-strain relationship becomes too complex to describe. Even for the treatment of a complex non-uniform deformation, it is sub-divided into small elements, which are assumed to deform uniformly. On the other hand, fracture originates from microscopic flaw, which is an extreme case of non-uniformity. Under the driving force of the stored mechanical energy, the flaw grows to become the fracture surface.

In general, unintended or inherent flaw lacks reproducibility, which results in the scatter of the fracture data. In order to improve reproducibility sometimes a prescribed cut is

made in the specimen to cause stress-concentration. A typical example is the trouser-tear test for rubber [12]. The results of the experiment revealed that the energy required for tear is more than 100 times that for creating new surfaces. Obviously, a large amount of energy is consumed for purposes other than creating new surfaces. The consumption of the energy is attributable to viscoelastic energy-loss in the vicinity of the crack.

It is important to explore the mechanism of the viscoelastic loss. Observing the advance of the crack, the vicinity of the crack front is highly deformed. How the crack grows through the highly deformed area is modelled in Figure 4.7.

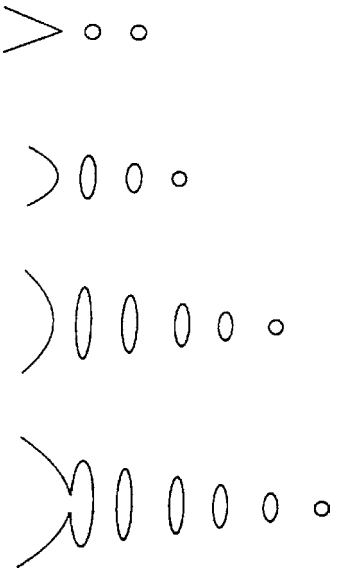

Figure 4.7 Birth of a vacuole, pull-out of molecular bundle and growth of crack.

According to this model the first step is the generation of a vacuole, which becomes deformed in the direction of stress. The wall between the crack and the deformed vacuole becomes thinner and thinner, eventually breaking into molecular bundles. This is a typical model but the reality may be quite different, depending upon whether the material is in the glassy state, glass-rubber transition, rubbery state or fluid state.

For example, in the glassy state the material cannot contract in transverse to the stretch direction; therefore, tensile stress causes dilatation and generates a vacuole. Shear stresses would not generate vacuoles.

In the rubber state, shear stress may become the equivalent of tensile stress if the axis may be freely rotated (Figure 4.8) [13].

For uniaxial extension, there is no vacuole generation, because the volume remains unchanged. However, if the stress is biaxial, the vacuole may form. In the fluid state, local unbalance of the principal stresses becomes shear and there is no vacuole formation.

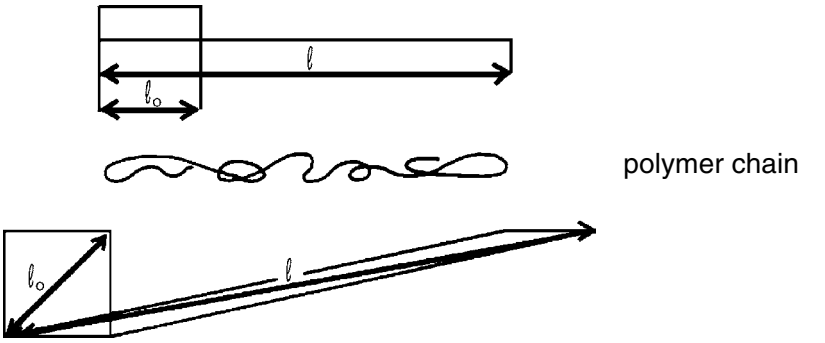

Figure 4.8 Equivalence of shear and elongational strain, where ℓ_o is the original length and ℓ is the increase in length.

Reprinted with permission from N. Nakajima, Rubber Chemistry and Technology, 1980, 53, 5, 1088. Copyright 1980, Rubber Division of the ACS.

In the process of rubber mixing, which may be either in glass-rubber transition, rubbery state or fluid state, the fracture mechanisms vary. However, a common feature is the pulling out of bundles of polymer chains in the process of creating new surfaces. This must involve disentanglement of chains. Furthermore, the disentanglement must occur through slipping of chain ends. Therefore, the layer close to the fracture surface must have a higher concentration of the chain ends, compared to the interior of the material. Because the chain ends are less constricted by entanglement, they are more fluid compared to the entangled portion of the chain. This explains the fact that rubber becomes tacky as mixing progresses [14].

The next subject is the initiation of the fracture of the rubber during mixing. In the presence of carbon black, sharp corners of the filler may act like sand paper, initiating the tear. Before the addition of the filler, stress concentration is generated when rubber is forced into the narrow gap of a roll-mill or an internal mixer. The flaw initiating the tear must be the molecular heterogeneity of a kind, which gives easier slipping through entanglements. Where the deformation of gum rubber is concerned, the entanglement is assumed to be uniformly distributed. On the other hand, the fracture starts from a microscopic flaw, which is a localised non-uniformity. The presence of the localised non-

uniformity of entanglement is plausible when we consider the process of polymerisation, where molecules of different size and shapes are generated. They may be different in MW, branching and even in chemical composition, if copolymerisation is involved. The perfect molecular homogenisation probably does not occur, because the resulting entropy-gain is very small. Therefore, at the microscale, there must be regions where entanglements slip easily and other regions where entanglements resist slipping. An extreme example is a rubber containing a microgel, which is made by crosslinking the latex particle with a difunctional comonomer in the emulsion polymerisation.

The crosslinked particle is smaller than 100 nm. A rubber containing 50% microgel requires a shorter mixing time compared to the matrix rubber alone without microgels [15]. The microgel introduces the heterogeneity, which facilitates the initiation of fracture. It might also be considered that the microgel constitutes the broken down particles in the comminution mechanism.

The pull-out of molecular bundle in fracture of gum rubber is difficult to demonstrate, because the bundle is in a fluid state such that it tends to flatten out. The retraction due to elasticity may also obscure the evidence of the pull-out.

When the retraction is slowed, the pull-out in the fracture surface is observed, see Figure 4.9.

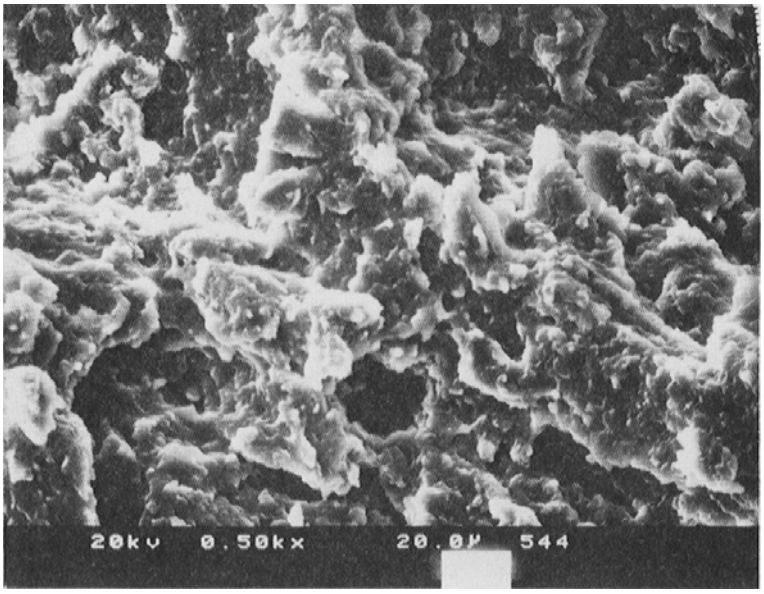

Figure 4.9 High magnifications of the fracture sample of PVC-NBR (gel-freeblend) at 0.15 s^{-1} strain rate.

Adapted, by permission, from N. Nakajima and J. L. Liu, Polymer Network Blends, 1993, 3, 2, 93. Copyright 1993, ChemTec Publishing.

The sample was a 50/50 by weight mixture of NBR and polyvinyl chloride (PVC). The NBR contains 33% acrylonitrile and was miscible with PVC. The presence of stiffer PVC chains presumably slowed retraction of the molecular bundle. The fracture was a result of the elongation at room temperature at 0.15 s^{-1} strain rate.

In the previous sections, the fracture of rubber in the mixing process was thought to be different from general behaviour of fracture. The latter involves creation of new surfaces and separation of broken pieces. In the former, the broken pieces do not separate but adhere to the filler surface or to the other piece of rubber. When the adhesion occurs between two pieces of rubber, the healing of the interface is the subject of autohesion [16]. When the surfaces of two pieces of the rubber are contacted for certain period of time and then torn apart at the interface, the force of detachment becomes larger with a longer contact time. This indicates the extent of healing with time by re-establishment of entanglement across the interface. When the force of detachment becomes equal to the force required to create the fresh surfaces in a single piece of specimen of the double thickness, the healing is complete and the interface disappeared completely. Even after 96 hours contact time, a slow peeling indicated that the interface did not heal completely. This means that full reforming of entanglement across the interface takes a long time.

References

1. N. Nakajima, R. A. Miller and E. R. Harrell, *International Polymer Processing*, 1987, **2**, 2, 88.

2. N. Nakajima, *International Polymer Processing*, 1996, **11**, 1, 3.

3. J. D. Ferry, *Viscoelastic Properties of Polymers*, John Wiley & Sons, New York, 1980.

4. N. Tokita and J. L. White, *Journal of Applied Polymer Science*, 1966, **10**, 7, 1011.

5. N. Nakajima and E. A. Collins, *Rubber Chemistry and Technology*, 1976, **49**, 1, 52.

6. N. Nakajima, *Journal of Applied Polymer Science: Applied Polymer Symposia*, 1992, **50**, 79.

7. N. Nakajima and E. A. Collins, *Rubber Chemistry and Technology*, 1974, **47**, 2, 333.

8. M. Mooney and W. E. Wolstenholme, *Journal of Applied Physics*, 1954, **25**, 9, 1098.

9. M. Mooney, *Journal of Applied Physics*, 1956, **27**, 7, 691.

10. N. Nakajima, *Rubber Chemistry and Technology*, 1982, **55**, 3, 931.

11. A. A. Griffith, *Philosophical Transactions of the Royal Society*, 1921, **221**, 163.

12. R. S. Rivlin and A. G. Thomas, *Journal of Polymer Science*, 1953, **10**, 3, 291.

13. R. S. Rivlin, in *Rheology*, Vol. 1, Ed., E. R. Erich, Academic Press, New York, 1956, Chapter 10.

14. N. Nakajima, P. R. Kumler and E. R. Harrell, *Rubber Chemistry and Technology*, 1985, **58**, 2, 392.

15. M. E. Woods and W. H. Whittington, Presented at the 103rd Meeting of the ACS Rubber Division, Detroit, MI, Spring 1973, Paper No.47.

16. G. R. Hamed and C-H. Shieh, *Rubber Chemistry and Technology*, 1985, **58**, 5, 1038.

5 Characterisation of Gum Rubber Using Dilute Solution Methods

5.1 Introduction

The purpose of characterisation may be stated as, in the most general terms, elucidation of a structure-property relationship. The structural characteristics include MW, its distribution, branch patterns and gel types. Microstructure is also included in this category. In addition there are compositional differences among copolymers and blends. The term, property, implies static characteristics such as density and specific heat, although sometimes, dynamic characteristics such as viscoelastic behaviour, are called viscoelastic properties. In order to be all-inclusive the structure-property relationship may be restated as the relationship between the structure/composition and property/behaviour.

Why do we need to elucidate such a relationship? This question is seldom asked because the answer may be presumed to be obvious. In the industrial context, the answer lies in the relationship shown in the following sequence:

Manufacturing
|
Characterisation
|
Processability
|
Product Properties

Specific gum rubber is manufactured to meet the requirements of a finished product having certain properties. This also requires the gum rubber to be processable with the available equipment. Therefore, the characterisation activity is a valuable and often indispensable link in the above relationship. When a problem arises because of an unsatisfactory property in the product or unsatisfactory processability, the final answer must be sought on how to alter the manufacturing process to produce a gum rubber with acceptable properties. In short, we need to establish the above relationship as the background knowledge needed for a day-to-day operation of the manufacturing process as well as for problem solving.

Table 5.1 Grades of NBR Manufactured by the BFGoodrich Company

Type	DTA T_g (°C)	Nominal % Acrylo-nitrile	Specific Gravity	Average Mooney Viscosity	Anti-Oxidant	Special Properties	Potential Uses
VT455	–18	40	1.00	55	Non-staining	High oil resistance. Low foul. Easy processing	Fuel hose, rolls, gaskets, packings, oil seals, food grade applications.
VT480	–18	40	1.00	80	Non-staining	High oil resistance. Low foul, easy processing	Fuel hose, rolls, gaskets, packings, oil seals, food grade applications.
VT330	–30	30	0.99	30	Non-staining	Good oil resistance, good water resistance, low foul, easy processing	Adhesives, moulding, extruding, calendering, non-corrosive to metal.
VT355	–30	30	0.98	55	Non-staining	Good oil resistance, good water resistance, low foul, easy processing	Print rolls, sheeting, gaskets, resin modification, blends of SBR, Hydrin®, PVC.
VT380	–30	30	0.98	80	Non-staining	Good oil resistance, good water resistance, low foul, easy processing	Hose, tubing and other extruded goods. Also adhesives and solution coatings.
1000 x 132	–12	51	1.02	55	Slightly staining	Very high acrylonitrile polymer; unusually good oil and fuel resistance	For better oil, fuel, and solvent resistance than with standard high acrylonitrile Hycar® rubbers: transformer gaskets, fuel lines, et. Hycar® 1000x88 makes outstanding adhesives in blends with thermosetting resins.
1000 x 88		43	1.00	95	Slightly staining	High acrylonitrile	
101CG	–18	41	1.00	85	Slightly staining	Excellent oil and fuel resistance, controlled cement viscosity	Hycar® 1001CG, excellent for high strength adhesives. Available in several cement viscosity ranges and with non-staining antioxidants. Oil well parts, fuel cell liners, fuel hose, other uses requiring resistance to aromatic fuels, oils, solvents. Rolls, lathe-cut gaskets, packings, oil seals, O-rings, phenolic resin modification.

Table 5.1 Grades of NBR Manufactured by the BFGoodrich Company (continued)							
Type	**DTA T_g (°C)**	**Nominal % Acrylo-nitrile**	**Specific Gravity**	**Average Mooney Viscosity**	**Anti-Oxidant**	**Special Properties**	**Potential Uses**
1002	–31	33	0.98	95	Slightly staining	The original medium-high acrylonitrile copolymer	Compounds of Hycar® 1002 have very good water resistance during prolonged service.
1022	–29	33	0.98	50	Non-staining	Low Mooney viscosity, directly soluble, cement grade polymer. FDA applications	Adhesives. Moulded, calendered, extruded goods requiring relatively low moduli. Low heavy metal ion content.
1042x82		33	0.98	85	Non-staining	Nerve-free Hycar® 1042, non-soluble. Crosslinked	Gives minimum die swell in extrusion. Excellent calendering stock with low shrinkage. Recommended for tubing, sheet goods and print plates.
1014	–61 –39	21	0.95	80	Slightly staining	Easy processing polymer	Applications in which excellent low-temperature properties are critical.
1034-60	–30.5 –62.0	21	0.95	55	Slightly staining	Corrosion resistance and easy processing	Applications in which excellent low-temperature properties are critical.
1094-80	–43	21	0.95	80	Non-staining	Low nitrile with outstanding physical properties	Applications in which excellent low-temperature properties are critical.
1095-80	–52.5	–	0.98	80	Non-staining	Very low nitrile	Specialised low temperature applications.

The characterisation activity may be divided into three kinds. The first is that requiring chemical analysis to find compositional differences. This activity is not dealt with in this book. The second is to find differences among gum rubbers having essentially the same chemical composition but different properties/behaviour. The third is an extreme case of the second; that is, in every respect two gum rubbers are supposed to be the same but either process differently or the properties of the finished products are different. This book deals with the second and the third, where the difference in the processability is the primary focus. Statements on the finished products are also included when they are important.

The commercial gum rubbers are made in different grades to satisfy the needs of different applications. The preceding is an example of the grades of NBRs manufactured around 1985 at the BFGoodrich Company, Table 5.1.

Among the 15 grades there are compositional differences as well as the differences in structure. Four representative samples, A, B, C, and D, are described in Chapters 2 and 4 with respect to their molecular structure and mill processability. Comparison between the different grades is the first and the second kind of characterisation mentioned earlier. Processability problems may arise within a given grade, if, for example, the processing latitude is very narrow. Matching a competitor's gum rubber with the same grade may not always work. Handling of these problems requires the third kind of characterisation activity.

The dilute solution methods have been used for characterising polymers since day one of polymer science. Measurements of dilute solution viscosity, osmotic pressure and light scattering have been well-established in theory as well as in practice. They are described practically in every textbook and in many review articles. More than 30 years have passed since the introduction of size exclusion chromatography (or gel permeation chromatography; GPC), which provides fractionation data very conveniently. This chapter is not intended to be a review of these methods. It is directed to examining how useful these methods are with respect to sensitivity, reproducibility, and reliability. Stated differently, the question is whether or not differences in processability can be explained on the basis of information available from the dilute solution methods.

5.2 Gel determination

As described in Chapters 1, 2 and 4, gels are present in many gum rubbers, exerting a critical influence on their processability. For gel-containing rubbers, the dilute solution methods are not applicable, because gels are removed by filtration. Therefore, the determination of gel content is the first order of the business in the characterisation of gum rubbers.

ASTM D3616-95 [1] describes a method for determining of gel, swelling index and dilute solution viscosity (DSV). The method has been developed for E-SBR and NBR, and toluene and methyl ethyl ketone, respectively, are used as solvents. The method is for the determination of macrogel content but it may also be used for microgel, a particle of a crosslinked network.

A sample is taken from a bale without milling. Approximately 0.4 g of weighed sample is placed on a 50 mesh screen having 300 μm opening, and soaked in 100 ml of solvent for 16-20 hours at 25 °C without stirring. During this period the soluble fraction is extracted. When the gel-content is high such as 50% or more the sample sitting on the screen is visible to the eyes. The reason why the solution is not stirred is because better reproducibility is obtained. Gels originate in emulsion droplets of less than 0.1 μm diameter and, if stirring breaks up the gels, some of them would go through the screen of 300 μm opening.

The gel content is determined indirectly from the amount of soluble fraction and directly by weighing the dried gel. Examples of the reproducibility of the data by round-robin tests are given for two SBR copolymers and three NBRs of 0 to 85% gel content. For the 'zero' sample the standard deviation is as high as ± 100% indicating that a very small amount of gel may be distributed non-uniformly. The standard deviations for 50-85% gel samples are at most ± a few per cent.

The swelling index indicates a denseness of the branch point; the denser it is, the lower the swelling. The DSV of the soluble fraction is a measure of MW, but only an approximate one, because some molecules may have branches. For the selected samples mentioned previously, the soluble fraction of the higher gel-containing sample had a lower MW. This conforms with the mechanisms of generating branches and gels in free radical polymerisation, which were explained by Flory many years ago, [2]. Because the measured gel content depends upon the pore size of a filter, generally more gel is found with a gel permeation chromatography (GPC) filter having 0.1 - 0.2 μm opening compared to the result from the ASTM screen having a 300 μm opening.

The ASTM test is intended to give a pragmatic definition of gel content in such a way that if a sample is gel-free according to this analysis, the effect of gel on the processability is usually negligible. Strictly speaking, this statement may not be acceptable in some cases. For each processability requirement, the assumptions involved in the gel determination need to be examined. Also, the method is only for E-SBRs and NBRs. With ACM gum rubbers, the results from using the 300 μm screen were not useful and the gel-content results obtained with 20 μm opening of a filter paper agreed well with the results from various viscoelastic measurements [3].

Sometimes a gel is generated in the post-polymerisation process; it may come from hung up material somewhere in the reactor, dryer or in the passage-way. They may be hard or soft. They may appear sporadically and are difficult to catch.

5.3 Dilute solution method

For gel-containing rubbers the dilute solution properties of the soluble fraction obviously do not represent the gum rubber.

On the other hand for completely soluble rubbers such as *cis*-1,4-BR and ethylene-propylene copolymer (EPM), useful information may be obtained. EPDM tends to have some fraction, which is filtered out with 0.1~0.2 μm filter. The osmotic pressure and light scattering methods give absolute MW, the number-average $\overline{M_n}$ and the mass-average $\overline{M_w}$, respectively. These values alone cannot be used to determine whether a polymer has branches or not. On the other hand, DSV depends upon the degree of branching, because a branched polymer gives a lower viscosity for a given MW. A degree of branching is defined as a ratio of the DSV of a linear sample and that of a branched sample at the same MW.

Scientific treatment of DSV is to use the intrinsic viscosity, which is the value extrapolated to zero concentration. For a reason of convenience a DSV at a fixed concentration, for example, 0.2 g/100 ml, is more frequently used in industry. Just which average MW should be used for this comparison may be a problem, if there is a large difference in the MW distribution. Usually a 'viscosity-average' MW is used. However, the averaging requires a prior knowledge of the degree of branching, which affects the exponent of Mark-Houwink-Sakurada equation. Original works in developing the method used narrow distribution samples such as a $\overline{M_w}/\overline{M_n}$ ratio which was close to one. For finding a difference between samples of the same grade, the method may not be sensitive enough.

Because determination of osmotic pressure and light scattering requires special instrumentation and skill to operate, they are usually used for fundamental research only. Because of the convenience, DSV and GPC are more frequently used. GPC provides a fractionation curve, not just mass-average and number-average. DSV is usually just used to obtain a bench-mark of MW, without questioning a presence or absence of branching. The following discussion covers the reliability of information obtainable from GPC with processability in mind.

GPC is often described as a method for determining MW and its distribution. This is not true - it is a method for fractionation according to the hydrodynamic size of the swollen polymer coil. The fractionation uses columns packed with porous material; usually it is

porous polystyrene beads crosslinked to make them insoluble. Because commercial rubbers often have very broad MW distribution, as many as four columns are used in series, each having different pore size designation. A dilute solution of a sample polymer is injected to a solvent-stream, which is flowing slowly through the columns. Because smaller polymer-chains can diffuse into the pores, it resides in the columns for a longer time. Therefore, the larger molecules are eluted first. The concentration of polymer at any instant of elution is measured by the difference between the refractive index of the solution and that of the solvent. Because the elution time is the measure of the swollen size of the polymer chain, the elution time must be calibrated for the swollen size of polymer chain; then it must be converted to MW. For convenience, usually fractions of known MW of unbranched polystyrene are used for the calibration. If a sample in question is a linear polystyrene, this calibration is satisfactory. For branched polystyrenes the calibration samples must also be branched, because the branched polymer has a smaller hydrodynamic size than the linear one for the same MW. If the branch pattern is different, for example, an equal arm star against a comb-type, the hydrodynamic size is different. For evaluating the MW of a branched polymer by GPC, calibration samples having exactly the same branch pattern are required.

When the branch pattern of a sample in question is not known, there is no way to calibrate. The question of calibration is often ignored. The data of MW and MW distribution reported in the literature are often only relative values, based on the linear polystyrene standards. This may still be useful if a sample in question is unbranched. For branched polymers, such data does not have a precise meaning.

Some elaborate methods have been developed for obtaining information about the degree of branching from GPC data. It requires a rather tedious procedure. Moreover, degree of branching ignores the difference of branch patterns. Therefore, it has only a very limited use.

There are other problems concerning the calibration. The elution time is also a measure of elution volume. The rate of elution must be controlled so that it is constant all times. Earlier GPC instruments were deficient in this regard, contributing to the reproducibility problem. In the later models a satisfactory pumping system giving a steady flow-rate, is installed.

The advanced models of GPC are equipped to measure the MW of the eluting polymer with a low angle laser light scattering device (LALLS). This enables the calibration problem to be eliminated. A special attachment to measure the viscosity of the eluting solution is also available. From the above two measurements a degree of branching may be estimated. The information on the branch pattern is not obtainable, however.

Because the LALLS was not available for the earlier work and even at present it is not always used, the following discussion is given on the use of calibration curves.

Because a very high MW polymer and a very small gel accumulate in the columns, the column performance changes with time. This requires a frequent re-calibration or a running a reference sample. When columns lose satisfactory performance or eventually even plug up, the columns must be repacked and re-calibrated. For this reason a sample solution is carefully filtered through a 0.1-0.2 mm filter. If a very high MW fraction is removed by filtration, the resulting elution curve does not represent the sample in question.

This is a serious problem when we consider that the processability is often affected by the presence of a small amount of very high MW fraction. Most annoying is when it is not known whether the higher MW fraction is removed by filtration or not. Figure 5.1 is an example of the calibration curve [4].

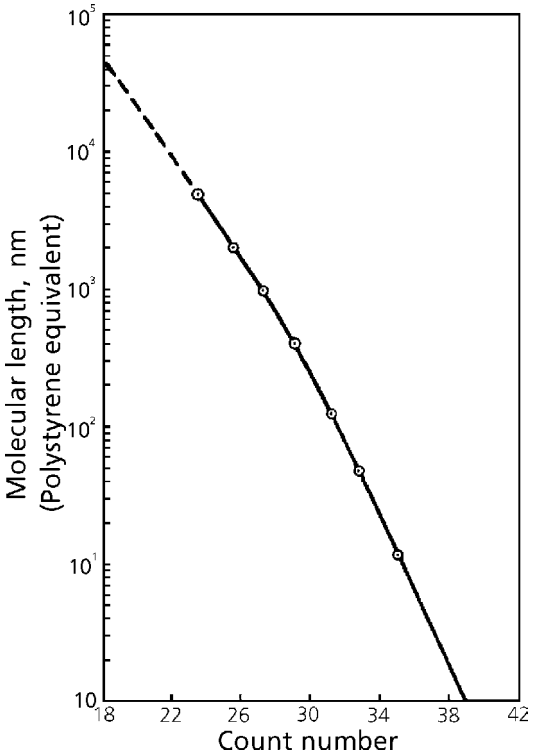

Figure 5.1 Calibration curve obtained using polystyrene standards.

Reprinted with permission from N. Nakajima, Advances in Chemistry Series, 1973, 125, 98. Copyright 1973, The ACS.

Because the calibration curve is a semi-log relationship, a small error in the elution volume is magnified at the MW scale. Another problem is a lack of the calibration standard at the very high MW. The significance of this is shown in Figure 5.2 [5].

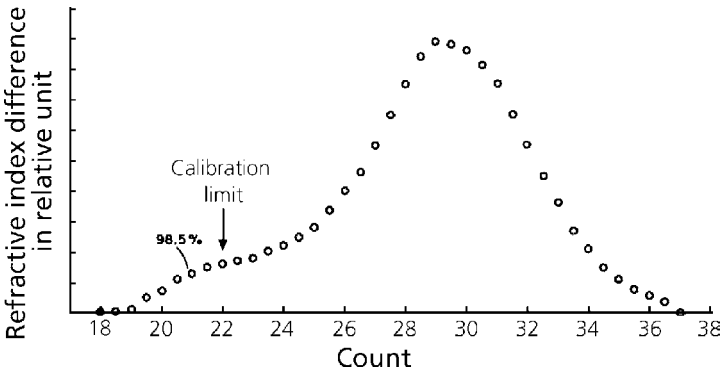

Figure 5.2 A typical 4 column GPC chromatogram of linear polyethylene. Solvent: trichlorobenzene. Temperature: 137 °C. Columns: 7 x 10^6, 3 x 10^6, 10^5, and 10^3 Å. Solution concentrate: 0.5%. Injection time 130 s. Flow rate: 2 cm^3/min. Refractive index difference in relative unit.

Reprinted from N. Nakajima, Separation Science, 1971, 6, 2, 277, Figure 1, by courtesy of Marcel Dekker, Inc.

It is evident that below count no. 22, there is no calibration. Assuming the extrapolated part of the calibration curve, is correct, the mathematical moments of the MW distribution were calculated according to Equations (5.1)-(5.5), where Q_i's are zeroth to fourth moments, A_i is the relative MW based on the polystyrene standard and W_i is the mass fraction of polymer having MW, A_i. The corresponding curves for the area-integration are shown in Figures 5.3a-e [5].

$$Q_0 = \int 1/A_i \left(dW_i/dA_i\right) dA_i = \int \left(dW_i/dA_i\right) d \ln A_i \qquad (5.1)$$

(Curve a)

$$Q_1 = \int \left(dW_i/dA_i\right) dA_i = \int A_i \left(dW_i/dA_i\right) d \ln A_i \qquad (5.2)$$

(Curve b)

$$Q_2 = \int A_i \left(dW_i/dA_i\right) dA_i = \int A_i^2 \left(dW_i/dA_i\right) d \ln A_i \qquad (5.3)$$

(Curve c)

$$Q_3 = \int A_i^2 \left(dW_i/dA_i\right) dA_i = \int A_i^3 \left(dW_i/dA_i\right) d \ln A_i \qquad (5.4)$$

(Curve d)

$$Q_4 = \int A_i^3 \left(dW_i/dA_i\right) dA_i = \int A_i^4 \left(dW_i/dA_i\right) d \ln A_i \qquad (5.5)$$

(Curve e)

$\overline{A}_n = Q_1 / Q_0$ *or* $1/Q_0$ (number average) (5.6)

$\overline{A}_w = Q_2 / Q_1$ *or* Q_2 (weight average) (5.7)

$\overline{A}_z = Q_3 / Q_2$ (z average) (5.8)

$\overline{A}_{z+1} = Q_4 / Q_3$ (z + 1 average) (5.9)

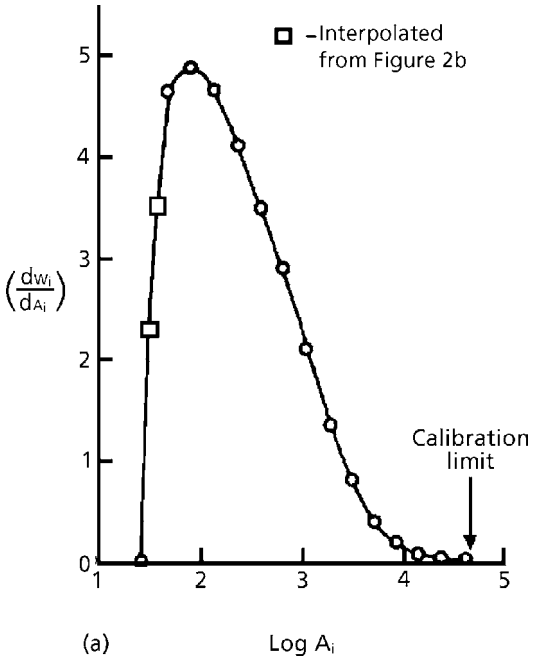

Figure 5.3a is based on Equation (5.1).

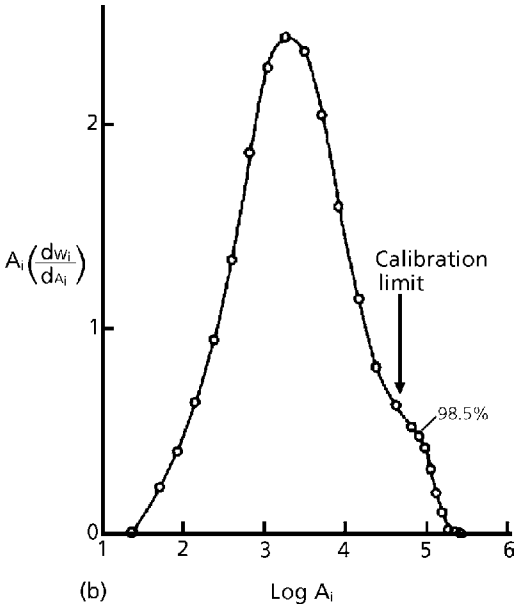

Figure 5.3b is based on Equation (5.2).

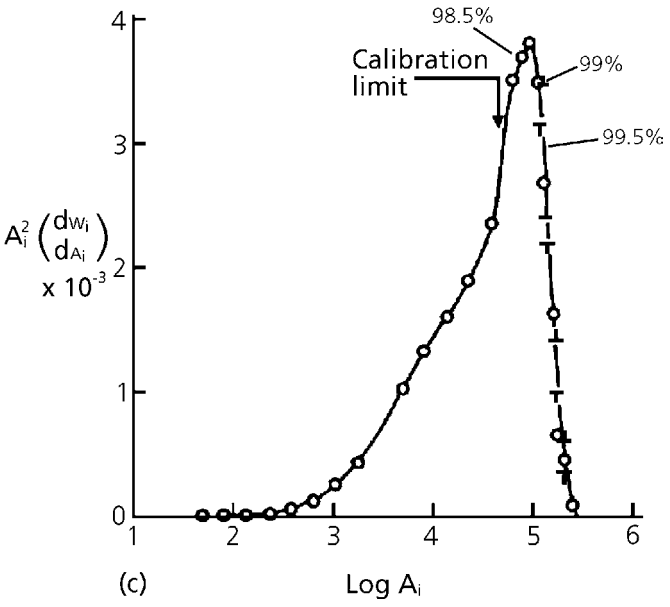

Figure 5.3c Based on Equation (5.3).

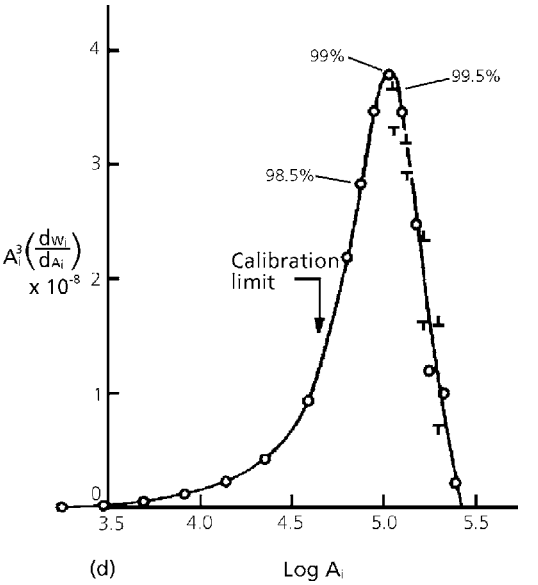

Figure 5.3d is based on Equation (5.4).

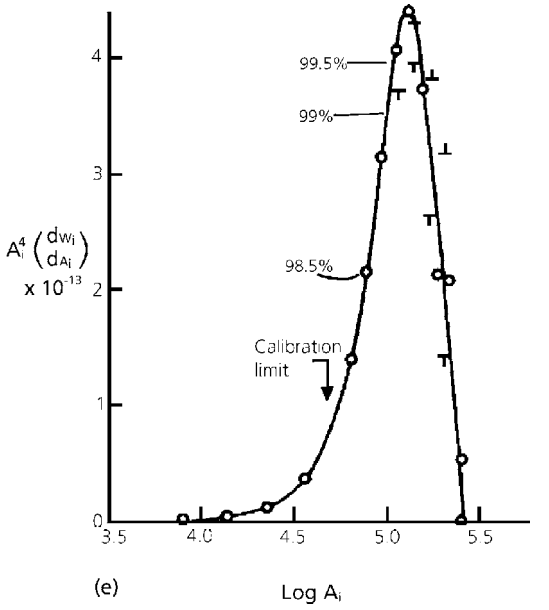

Figure 5.3e is based on Equation (5.5).

Figure 5.3 Moments, percentages shown are cumulative weight fractions.

Reprinted from N. Nakajima, Separation Science, 1971, 6, 2, 279, Figures 2a, 2b, 2c, 2d and 2e, by courtesy of Marcel Dekker, Inc.

Table 5.2 Moments and Average Chain Length		
Quantity	**Computer integration**	**Possible range of values resulting from baseline error (hand calculation)**
Q_0	1.59×10^{-3}	Negligible
Q_1	1.01	Negligible
Q_2	8.95×10^{3}	Negligible
Q_3	4.77×10^{8}	$4.52\text{-}4.85 \times 10^{8}$
Q_4	4.82×10^{13}	$4.32\text{-}5.30 \times 10^{13}$
$\overline{A}_n$	6.3×10^{2}	Negligible
$\overline{A}_w$	8.9×10^{3}	Negligible
$\overline{A}_z$	5.3×10^{4}	$5.05\text{-}5.4 \times 10^{4}$
$\overline{A}_{z+1}$	1.01×10^{5}	$0.96\text{-}1.09 \times 10^{5}$

Integrating for Q_0, (see Figure 5.3a), the entire area falls within the calibration limit and for Q_1, (see Figure 5.3b), almost whole area is calibrated. Therefore, the number average MW, $\overline{A}_n$, given by Equation (5.6), is approximately correct. For Q_2 (see Figure 5.3c), only one-half of the area falls within the calibration limit and therefore, the weight average MW, $\overline{A}_w$, Equation (5.7) is not very reliable.

For the Q_3 and Q_4 integration almost entire areas are not calibrated. Therefore, Z average $\overline{A}_z$ and Z +1 average $\overline{A_{z+1}}$, Equations (5.8) and (5.9), are creations of the arbitrary calibration curve. Because the computer provides a neat printout of $\overline{M_w}$, $\overline{M}_z$ and $\overline{M}_{z+1}$, the values are often accepted without scrutinising whether they are the creation of the software or not.

One more problem with GPC is a possible lack of the resolution at the high molecular tail. In Figure 5.2 the elution appears to start at about count number 19. Is this because the MW distribution has a cut-off or is it the limit of the resolution of the column?

5.4 Relationship between dilute solution properties and processability

Because of the calibration problems, the information obtained from GPC is at best the relative values of MW and its distribution. The higher averages such as $\overline{M}_z$ and $\overline{M}_{z+1}$

are often meaningless. When the branching is involved, the credibility is reduced further. For example, when two samples have a difference in the apparent values of T_g, we are not sure whether there is a difference in the true $\overline{M}_n$ or if one sample has more branches than the other.

There is a well-established relationship for polymer melts between the low shear Newtonian viscosity and MW, $\eta_0 = k \overline{M}_w^n$ (Equation 5.6), where K is a constant and n is 3.4 or a very similar number [6].

Very high MW dependence, i.e., 3.4 power, comes from extensive entanglements of polymer chains, which are slipping through each of the other chains at low shear rate conditions.

The low shear Newtonian viscosity is sometimes called zero-shear viscosity. Strictly speaking the two are different. The zero-shear viscosity is a viscosity extrapolated to zero shear rate and the value depends upon the method of extrapolation. This is particularly true for a polymer having a very high MW tail or a polymer with long branches. On the other hand, the low shear Newtonian viscosity is an observed value. The relationship in Equation (5.6) was established with series of samples having different MWs and a very narrow MW distribution. In order to observe the relationship, a given gum rubber must be in the flow state. This often requires a temperature where degradation sets in, or it takes a very long time so as to be impractical. The exception to this is rubbers prepared via anionic polymerisation and polydimethyl siloxane (PDMS); in these rubbers the high MW tail of distribution is not extending very much.

In general, a gum rubber has a very high MW fraction, long branches or both. In the processing condition it is usually not in the flow state but it is in the rubbery state. In the latter state a rubber, having apparently a higher MW may have a lower modulus, if it has long branches. Likewise, a lower Mooney index does not necessarily mean a given rubber having lower MW. Instead, it may have more branches.

When there are large differences in the pattern of the MW distribution among the samples, GPC may provide information such as shown in Figure 5.4 [7].

A caution is that even in this case the fractionation curve of E-SBR does not represent MW distribution, because there are branches and probably gels in the sample.

The main purpose of this chapter is to caution the reader against over-reliance on the dilute solution properties, particularly on GPC. The methods are good for detecting relatively large differences. They often lack sensitivity required for problem solving in processability. Much time may be wasted in trying to interpret data and trying to obtain information, which is not really there.

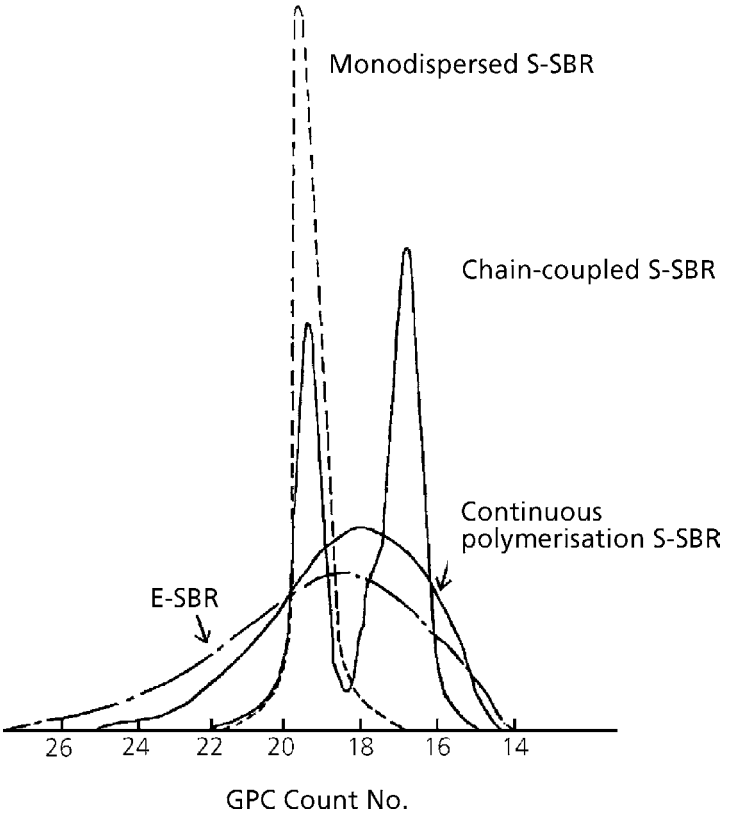

Figure 5.4 Examples of MW distribution of SBRs.

References

1. ASTM D3616-95.
Standard Test Method for Rubber, Raw - Determination of Gel, Swelling Index, and Dilute Solution Viscosity.

2. P. J. Flory, *Principles of Polymer Chemistry*, Cornell University Press, Ithaca, New York, 1953, 347.

3. N. Nakajima and S. K. Sundarapandian, *Rubber World*, 1995, **212**, 3, 33.

4. N. Nakajima, *Advances in Chemistry Series*, 1973, **125**, 98.

5. N. Nakajima, *Separation Science*, 1971, **6**, 2, 275.

6. J. D. Ferry, *Viscoelastic Properties of Polymers*, 3rd Edition, John Wiley & Sons, Inc., New York, 1980, p.509.

7. A. Saito, *Journal of the Society of the Rubber Industry, Japan*, 1998, **71**, 6, 315.

6 Viscoelastic Characterisation of Gum Rubber

6.1 Introduction

In the previous chapters the processability of gum rubber was related to its behaviour at large deformation and fracture. A given rubber has a unique deformational behaviour, which may be characterised by its viscoelastic properties. The latter is, in turn, related to the molecular architecture. Therefore, viscoelastic properties play a central role in relating polymerisation conditions to processability of gum rubber. The viscoelastic characterisation has particular importance for gum rubbers, because many of them contain an insoluble fraction called 'gel', which makes solution-based characterisation inapplicable.

In this chapter, a development of the viscoelastic characterisation method is described. It begins with methods of describing deformation behaviour, subsequently a treatment of non-linear viscoelasticity is presented. Finally, by using the viscoelastic characterisation method, the processability of gum rubber is related to its molecular architecture.

6.2 Methods of describing deformation

When the subject of deformation of rubber is considered, a conventional approach such as shear or elongation is accepted. The definition of steady state viscosity is an example of the former and that of tensile testing is an example of the latter. However, the deformation of rubber during mixing is not completely shear nor elongation. Therefore, the way to describe this deformation needs to be examined. The bulk compression need not be considered, because rubber is practically incompressible.

For simplicity, consider an elastic body which is in isolation. The deformation of this body may be described by the stress tensor σ_{ij} and the deformation tensor ε_{ij} as:

$$\sigma_{ij} = \Sigma a_{ij} \varepsilon_{ij} \tag{6.1}$$

where the subscripts i and j are for the 1, 2, and 3 directions, in orthogonal co-ordinate systems and $a_{ij}s$ are moduli, [1]. Equation 6.1 represents nine equations and is very

complex. Rubber being an isotropic and amorphous body, the relationship may be simplified to only simple shear, σ_{12}, and normal stress components σ_{11}, σ_{22}, and σ_{33}. For an infinitesimal deformation, the shear modulus G and elongational modulus E are related as:

$$G = \frac{E}{2(1+\nu)} \tag{6.2}$$

where ν is Poisson's ratio and equal to 0.5 for rubber:

$$E = 3G \tag{6.3}$$

When Equation 6.3 holds, either shear or elongational measurements need to be performed to adequately describe the rubber behaviour. However, this is limited to infinitesimal deformation.

For describing a finite deformation, a concept of strain energy function is introduced instead of stress, because energy is the basic quantity and stress is the phenomenological expression for the energy change resulting from deformation. The expression for strain takes a strain invariant form. This is based on the understanding that strain should not depend upon a particular choice of coordinate system. Also, the coordinate axis may be rotated from that before deformation to that after deformation. This enables any deformation to be described with strains in three principal axes only. In order for this to be possible, the body must be isotropic and uniform. Therefore, it is not applicable to compounds containing filler. Also, for the rotation of the axis not to alter the magnitude of strain, the body must be isolated. For interconnected elements in finite element analysis, the rotation of the axis may affect the strain in the neighbouring elements. The final derivation of the above theory [2] is presented in the following form for strain energy U:

$$U = \sum_{i=0,\, j=0} C_{ij} \left(I_1 - 3\right)^i \left(I_2 - 3\right)^j \tag{6.4}$$

where C_{ij} is a material constant, I_1 and I_2 are strain invariants. In this case $I_3 = 1$ because rubber is practically incompressible. When Equation 6.4 is applied to extensional deformation, the following equation is often used:

$$U = C_1(I_1 - 3) + C_2(I_2 - 3) \tag{6.5}$$

This equation is called the Mooney [3] or Mooney-Rivlin equation.

Although Equation 6.5 is derived through rigorous logic, it is based on a number of premises. Therefore, before applying it to the system of interest, we need to examine if a given case is in conformity with the premises. The equation assumes an equilibrium, and therefore it applies to a crosslinked network only. As gum rubbers are uncrosslinked, they do not attain equilibrium because of the slipping of entanglements. Even with a network, the large deformation data progressively deviate from the form given by the equation.

There is another approach which uses the concept of strain energy and principal strains only; it is called the Valanis-Landel equation [4]. It assumes that the total strain energy may be subdivided into those corresponding to each of three principal strains:

$$u(\lambda_1,\lambda_2,\lambda_3) = u(\lambda_1)+u(\lambda_2)+u(\lambda_3) \tag{6.6}$$

Where λ_1, λ_2, and λ_3 are strains expressed as the elongational ratios in the direction of the principal axes. This equation assumes that $u(\lambda_1)$, $u(\lambda_2)$, and $u(\lambda_3)$ may in general take different values; this means the coordinate axes are fixed and are not free to be chosen. This is more like the usual shear and elongational measurements where the magnitude of strain is tied to a specific coordinate system. The concept of strain invariance is not used.

Ogden's equation [5] may be regarded as a specific form of Equation 6.6:

$$u(\lambda_i) = (\mu_i / \alpha_i)(\lambda_i^{\alpha i} - 1) \tag{6.7}$$

where $i = 1$, 2, and 3. This equation has six material constants, μ_i and α_i.

The approaches described so far employ a specific form of the equation for relating stress and strain (constitutive equation). The equation contains a number of material constants, which must be determined through fitting the equations to the experimental data. Heretofore, there has been no attempt to relate these material constants to the molecular architecture of gum rubbers.

Next, an approach commonly used for the viscoelastic treatment, which involves non-equilibrium is presented. The following example relates to elongational measurement. Because gum rubber is amorphous, isotropic and incompressible:

$$\lambda_1 = 1 / \lambda_2\lambda_3 \tag{6.8}$$

and

$$\lambda_2 = \lambda_3 = \sqrt{\lambda_1} \tag{6.9}$$

Therefore, λ_1 is the only independent variable of strain and the elongational stress σ_{11} is a function of λ_1 only:

$$\sigma_{11} = f(\lambda_1) = f'(\varepsilon_1) \tag{6.10}$$

where

$$\lambda_1 = \varepsilon_1 + 1 \tag{6.11}$$

Equation 6.10 may be expressed in terms of tensile modulus with the recognition of time-dependence as

$$E = \sigma/\varepsilon = f''(\dot{\varepsilon}, \varepsilon) \tag{6.12}$$

where $\dot{\varepsilon}$ is the rate of elongation. Also, the subscript is dropped because it is no longer necessary.

When the rate of elongation is constant, time t is given by

$$t = \varepsilon / \dot{\varepsilon} \tag{6.13}$$

and

$$E = f'''(t, \varepsilon) \tag{6.14}$$

The constitutive equation is

$$\sigma = E(t, \varepsilon)\varepsilon \tag{6.15}$$

where the stress and strain are related through the material function $E(t, \varepsilon)$ instead of the material constants. The use of material functions for describing the mechanical behaviour of polymers is the general method in the field of viscoelasticity [6] and this paper follows the convention.

6.3 Non-linear viscoelasticity

When the magnitude of response of a material is proportional to the strength of the imposed field, a linear relationship exists. Typical examples in the field of rheology are Hooke's law:

$$\sigma = E\varepsilon \tag{6.16}$$

and the Newtonian flow equation

$$\tau = \eta\dot{\gamma} \tag{6.17}$$

where τ is the steady state shear stress and $\dot{\gamma}$ is the steady state shear rate. In this case, E and η are material constants.

In the field of viscoelasticity, the definition of linearity is modified to

$$\sigma = E(t)\varepsilon \tag{6.18}$$

where $E(t)$ is a function of time, i.e., a material function. The material functions may be the storage modulus G′(ω) and the loss modulus G″(ω) of shear dynamic measurements, the relaxation modulus, $G(t)$ and creep compliance $J(t)$. For linear viscoelasticity the material functions are functions of the 'time scale' only. The time scale includes the observed time as well as the frequency ν (Hz) or the angular frequency ω (rad/s). However, the steady state non-Newtonian flow equation

$$\tau = \eta(\dot{\gamma})\dot{\gamma} \tag{6.19}$$

is understood to be non-linear [6].

Gum rubbers in general exhibit linear behaviour at small deformations. For studying mixing of rubber, we must treat large deformations. In this case, modulus is not only a function of time, but also of strain; the relationship is called non-linear. An example with elongational measurements is already stated in Equation 6.15

$$\sigma = E(t,\varepsilon)\varepsilon$$

When the material behaviour is linearly viscoelastic for a sample (Equation 6.18), $E(t)$ plotted against t forms a curve, which is unique for a given sample; usually a log $E(t)$ versus log t plot is used. When the material behaviour is non-linear, as in Equation (6.15), it requires both the t-axis and ε-axis to present the sample characteristics as a curved surface.

Where two different samples are concerned, the two curved surfaces must be compared and the process is rather cumbersome. In addition, many measurements are required to construct the characteristic surface.

There have been various attempts to simplify the situation; they are, in general, attempts to 'linearise' the non-linear behaviour. The linearisation is possible in some cases and not

possible in others. In general, it is possible when the 'separability of time and strain' holds.

The separability may be explained by the following example

$$E(t, \varepsilon) = F(t)\phi(\varepsilon) \tag{6.20}$$

At the limit, $\varepsilon \rightarrow 0$, it gives $\phi(\varepsilon) \rightarrow 1$ and therefore

$$E(t, \underset{\varepsilon \rightarrow 0}{\varepsilon}) = F(t) \tag{6.21}$$

This gives a linear relationship at infinitesimal strain [7]. When equation (6.20) is written as

$$E(t,\varepsilon) \,/\, \phi(\varepsilon) = F(t) \tag{6.22}$$

the modulus is linearised through the modification with $\phi(\varepsilon)$. Although these expressions for linearisation, i.e., equations (6.20-6.22), are often cited, the physical meaning of the function $\phi(\varepsilon)$ has not been examined.

The linear behaviour at small deformations may be interpreted as follows. The elongational modulus E is independent of the magnitude of strain, equation (6.16), a fact which means that the internal structure of the material is unaffected by the deformation. Stated the other way around, if the internal structure is altered as a result of the deformation, E must change. Therefore $\phi(\varepsilon)$ is a measure corresponding to the change of the internal structure which is affected by strain ε.

In general, the internal structure is expected to change upon deformation, and non-linear behaviour is the rule at a finite deformation.

However, the gum rubber chain segments, which are shorter than the entanglement coupling distance, are in liquid motion. Therefore, any change in the structure may immediately be relaxed. This may explain the apparent linear behaviour exhibited by many gum rubbers at finite but relatively small deformations.

When rubber crystallises upon stretching, e.g., NR, obviously there is structure change and non-linear behaviour is expected. Even with non-crystallising gum rubbers, non-linear behaviour is observed at large deformations. With the form given in equations (6.20-6.22), the internal structure is affected by strain but is independent of strain rate. The internal structure of rubber is affected by the motion of chain segments and their relaxation times. Therefore, non-linearity should appear in both time-dependence and

strain-dependence. With consideration of both dependences, Schapery gave a general form for the separability of time and strain [8]. His theory is presented [1] for the non-linear creep compliance, $J_u(t)$, and for the non-linear stress relaxation modulus, $G_n(t)$:

$$J_u(t) = \frac{e(t)}{\sigma} = g_0 J_u + g_1 g_2 \Delta J(t \,/\, a_\sigma) \tag{6.23}$$

$$G_n(t) = \frac{\sigma(t)}{e} = h_e G_r + h_1 h_2 \Delta G(t \,/\, a_e) \tag{6.24}$$

where σ is the stress and e is the strain, J_u is the unrelaxed compliance, i.e., glassy compliance, and

$$\Delta J(t) = J(t) - J_u \tag{6.25}$$

The symbols g_0, g_1, g_2, and a_σ are functions of stress and represent the extent of non-linearity. At the limiting condition, $\sigma \rightarrow 0$, these functions approach one, and represent linearity.

Referring to equation 6.24, G_r is the relaxed modulus, which has a constant value for crosslinked rubber but otherwise is zero:

$$\Delta G(t) = G(t) - G_r \tag{6.26}$$

The symbols h_e, h_1, h_2, and a_e are functions of strain and represent the extent of non-linearity. At the limiting condition, $e \rightarrow 0$, all these approach one.

According to the interpretation of this chapter, g_0, g_1, g_2, and h_e, h_1, h_2, reflect the changes of internal structure upon application of stress in the former and strain in the latter case, respectively.

The functions a_σ and a_e represent the effect of stress and strain, respectively, on the time scale. This may be explained as follows. When a body is deformed, the corresponding amount of mechanical energy is imparted to the body. This energy brings about a certain degree of excitation. This is analogous to the excitation resulting from thermal energy input. In the latter case, the excitation takes the form of time-temperature correspondence with many polymer melts and rubbers. The extent of temperature effect on time scale is the 'shift' factor', a_T, which is a function of temperature. Likewise, the mechanical excitation is expected to have an influence on time scale [9]. In this case, a_σ and a_e are similar to a_T. The material functions g_0, g_1, g_2, a_σ and h_e, h_1, h_2, a_e must be determined

experimentally. Once they are known, linearisation becomes possible for non-linear behaviour.

With many gum rubbers a very simple form of linearisation is possible [10, 11]. In terms of Schapery's theory, it corresponds to $h_e = 0$, $h_1 = 1$, $h_2 = 1$, and $a_e = 1 / \alpha$ for the elongation data:

$$\sigma = E(\alpha t)\varepsilon \tag{6.27}$$

Because α is the extension ratio, it is a 'universal parameter', which does not require experimental determination.

There are gum rubbers which do not obey the relationship given by equation 6.27. One case is rubber exhibiting strain-hardening. The linearisation in this case is in terms of Schapery's theory, $h_e = 0$, $h_1 = 1$, $h_2 = 1 / \Gamma(\alpha)$, and $a_e = 1 / \alpha$. $\Gamma(\alpha)$ represents the extent of strain-hardening and must be determined from experimental measurements:

$$\sigma = [F(\alpha t)\Gamma(\alpha)]\varepsilon \tag{6.28}$$

where

$$F(\alpha t) = E(\varepsilon,t) / \Gamma(\alpha) \tag{6.29}$$

A phenomenological explanation has been given for equations 6.27-6.29 by this author [12] without reference to Schapery's theory. It is a rational analysis of the relationship between macroscopic deformation and the deformation in the segmental level of polymer chains. An increase of free volume resulting from deformation in the dynamic state is the explanation for the strain-time correspondence.

6.4 Conventional methods of characterisation

For a given type of gum rubber, if the compositional aspects such as the comonomer ratio, microstructure and their distributions are known, characterisation becomes centered around the determination of MW, its distribution, and the degree of branching.

For expediency, the DSV (see Chapter 5) is often used as a measure of MW. For the determination of absolute MWs, osmotic pressure measurement is used for number-average and light scattering for weight average. A relative spread of MW distribution is expressed by the ratio of the weight-average to the number-average MW. With the advent of size exclusion chromatography, much more detail of the MW distribution is obtained quickly. The raw data are processed to yield various MW averages, $\overline{M}_n$, $\overline{M}_w$, $\overline{M}_z$, and $\overline{M}_{z+1}$. For the dilute solution methods of characterisation the theoretical background has been well developed [13]. On the other hand, the information derived from these

methods is often inadequate or even misleading when related to the processability of gum rubbers. There are a number of reasons for this:

(i) the sample size is so small that it may not be representative of a large commercial lot

(ii) the solution is so dilute that the response signal may be weak for the part of the information relevant to processability

(iii) the high MW chains may associate

(iv) the ultra-high MW fraction may be filtered off

(v) the gel, i.e., insoluble fraction, is removed by the filters

(vi) there may be no adequate resolution for the very high MW range

(vii) there are no calibration standards for the ultrahigh MWs in GPC.

Items (iii), (iv), and (v) give much uncertainty in interpreting results, because of the presence or absence of molecular association, ultra-high MW and gel usually remains unknown. The high MW fraction and gel often have significant effects on processability even though the amount is small.

In production control, GPC data are sometimes collected routinely along with measurements of the Mooney index [14]. When these two sets of data are compared for hundreds of production lots, in only about 50% of cases may a correlation be found. This is partly because the Mooney index is a very crude measure of rubber property, but the uncertainties described above on GPC data are also responsible.

The Mooney index is often called 'Mooney viscosity' but there is no rationale that the index represents viscosity. It is an expression of some aspect of viscoelasticity in that there may be some relationship to the processability. The method uses an instrument with a particular design, which provides a simple operation and a quick result. Compared to the dilute solution method, the sample size required is much larger so that it is more representative of the commercial lot. The Mooney index has been used worldwide as a specification for gum rubbers.

However, there is no firm theoretical basis for this index. It is only a very crude method of differentiation between samples; for the same value of the index, the processability of two gum rubbers may be different. In other cases, with rather wide differences in the value of the Mooney index, two rubbers may process almost equally well.

There have been attempts to interpret the meaning of the Mooney index. Often it is assumed that the measurement concerns steady state viscosity at a prescribed temperature.

The standard procedure [14] requires 1 minute of preheating before the rotation is started. Because the temperature is set at for example, 100 °C, the sample is not even in temperature equilibrium. The procedure is obviously a compromise for obtaining the data quickly. The rotational speed being 2 rpm, most of the rubber at 100 °C shows stress-over-shoot (see section 4.3) [6]. The torque value is recorded after 4 minutes of rotation and expressed as the Mooney unit. At 4 minutes, the torque is usually past the peak and in the relaxation part of the curve but not in the steady state. This is shown in Figure 6.1, for somewhat exaggerated examples, which gave the same Mooney index but vary in viscoelastic behaviour.

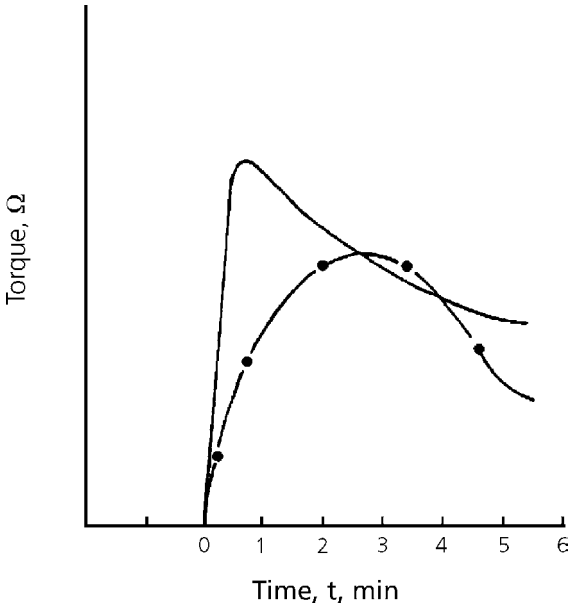

Figure 6.1 Typical Mooney curves; very different viscoelastic properties for the same Mooney indices.

If sufficient time is given for preheating, more than several minutes, and the rotation is continued, a steady state torque may be observed, [15].

The steady torque is not necessarily the result of the flow, but quite often a result of the fracture of the rubber and the generation of supermolecular flow units [16]. Nevertheless, it is sometimes assumed to be the steady state flow and the steady state viscosity is calculated as a function of shear rate. Such a calculation is quite involved, because of the geometry of

the instrument and non-uniform distribution of shear rates [17]. More useful is the torque rise part of the curve, the transient behaviour from which a complex property may be calculated. Being a complex property, it may be resolved into elastic and viscous contributions. However, 2 rpm is too fast to obtain accurate data of the torque rise. As slow a rate as possible, e.g., 0.05 rpm, is recommended both for reasons of accuracy and for covering a wide range of time scales.

As described in Chapters 4 and 5, an adequate description of gum rubber processability requires a scientific approach; it requires observation of non-linear viscoelasticity and fracture behaviour over a range of temperatures and time. The non-linear viscoelastic data are represented by a curved surface as mentioned earlier in section 6.3 and the fracture behaviour is summarised in a failure envelope. Quite often, numbers (indices) are preferred to graphs and figures for representing a sample; a minimum number of the indices necessary for adequately describing a given gum rubber was determined to be 12, a '12 point characterisation' [18]. If values are known for some of the indices, or if they do not vary among the samples of interest, the number of determinations may be considerably reduced.

The method this author prefers is the use of curves. The surface, representing non-linear viscoelasticity, may be converted to a curve, through the linearisation scheme described in section 6.3. The fracture behaviour is expressed as a failure envelope of the modulus and the strain at break.

6.5 Characterisation based on viscoelasticity

Characterisation of a gum rubber requires determination of the amount of gel fraction, unless it is known to be gel-free. The most direct means of determining gel content is the filtration of the solution. However, the absolute value of gel content is difficult to assess, because the value depends upon the pore size of the filter. Also, the gel is not necessarily distributed uniformly throughout a given lot so that the data are only approximate measures. The viscoelastic method is relative but more reproducible than filtration because the sample size is larger. For a critical examination of the presence of gel, the viscoelastic method provides a better comparison among samples; the filtration results may be used as supplementary information.

The generation of a macrogel, a highly branched insoluble molecule, begins with the formation of long branches. At present, there is no clear knowledge about how many long branches per molecule must form before it becomes insoluble. Because our present interest is in processability and not in solubility, long branches and gel may be considered to be of the same kind but differing in degree. The following method may be used for evaluating the relative degree of long branching or gel content. Firstly, shear dynamic measurements are preformed to obtain storage modulus $G'(\omega)$ and loss modulus $G''(\omega)$. Then, G' and G'' are

taken at the same value of ω, and plotted as log G˝ versus log G′. Examples are shown in Figure 6.2 for the samples of NBR which are listed in Table 6.1 [19].

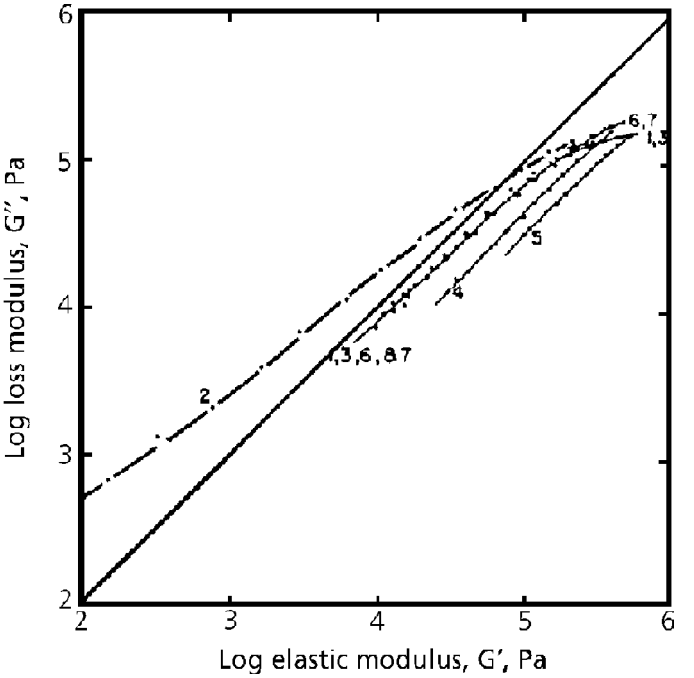

Figure 6.2 Log G˝ - log G′ curves of NBR samples 1-7 (see Table 6.1).

Reprinted from N. Nakajima, Polymer International, 1995, 36, 2, 105. Copyright 1995, SCI. Reproduced with permission.

Table 6.1. Characteristics of butadiene-acrylonitrile copolymer samples

Sample	Mooney[b] index ML-4-100	Acrylonitrile content of polymer (%)	Gel[a] (%)
1	71	43.7	0.9
2	22	41.2	0.1
3	121	39.4	0.1
4	103	40.3	54.7
5	88	40.9	71.7
6	52	33.8	0
7	56	28.4	5.11

[a]ASTM D 3616-95 [20], only an approximate measure
[b]ASTM D 1646-96a [14]

Samples 1, 6, and 7 are so-called 'gel-free', commercial polymers, containing acrylonitrile of 44, 34, and 28%, respectively. The gel determination is based on ASTM D 3616-95 [20], which requires a screen having a 300 μm opening. If a GPC filter with 0.1 ~ 0.2 μm opening is used, a significant amount of gel may be found in the 'gel-free' polymer. The ASTM test is intended to give a pragmatic definition of gel content in such a way that if a sample is gel-free according to this analysis, the effect of gel on the processability is negligible. Strictly speaking, the above statement may not be acceptable in some cases. Therefore, for each polymer type and for each processability requirement, the assumptions involved in the gel determination need to be examined.

Returning to Samples 1, 6, and 7, the log G˝ versus log G′ curves of these polymers are the same; this fact indicates that these polymers have the same degree of long branching and are 'gel-free'.

Next, Samples 1, 2, and 3 are compared. Samples 2 and 3 were made in a pilot plant under the same polymerisation conditions (except for MW) as that of the commercial product, Sample 1. Sample 2 is made to a lower MW with the use of a modifier, which also suppresses the long branch formation. Sample 3 is made to have a higher MW. Samples 4 and 5 contain significant amounts of gel.

In Figure 6.2, the curves of the seven samples form four groups. Sample 2 containing the least long branches lies on the left; the 'gel-free' samples, 1, 3, 6 and 7, are in the middle; Sample 4 containing 55% gel is on the right; and Sample 5 containing 70% gel is on the far right. This figure illustrates that from the position of log G˝ versus log G′ plots, the degree of long branching or the gel content may be assessed.

The 45° line in the figure represents G˝ = G′. The curve of Sample 2 is above this line, G˝ > G′. The data of this sample are in the flow region. The curves of all other samples are in the state G′ > G˝, indicating the dominance of elastic behaviour over viscous behaviour. In the earlier chapters, the mill processability of gum rubber was interpreted on the basis of whether elasticity or viscous loss dominates. Although the mill processability involves large deformation and the data of Figure 6.2 are limited to small deformations, an approximate relationship between Figure 6.2 and the mill processability may be found. Only one exception to this relationship, but a very important one, is gum rubber containing microgel. The microgel is a particle containing a crosslinked network, which may be formed during emulsion polymerisation with difunctional co-monomer [21]. The response of microgel to processability is entirely different from that of macrogel, and yet in Figure 6.2 only gel content may be assessed but not the difference between macrogel and microgel.

In order to differentiate between gel types, large deformation measurements must be performed and the strain-time correspondence must be used for linearisation. The elongation measurements performed at a constant temperature and various elongation rates are expressed

as the elongational modulus $E(\alpha t)$. With some gum rubbers, $E(\alpha t)$ becomes a master curve, which is independent of the elongation rates, and with others it is rate dependent. The former type is either gel-free or contains a small amount of macrogel and any amount of microgel. The latter type shows strain-hardening and contains a significant amount of macrogel. Typical examples are shown in Chapter 4, but additional examples are now given.

Instead of using elongational modulus, the equivalent of complex viscosity may be used:

$$\eta_T = E(\alpha t)\alpha t \tag{6.30}$$

In this case, η_T is expressed as a function of the reduced rate, $1/\alpha t$. If linearisation holds, $1/\alpha t$ is numerically equal to ω. Further, for a Poisson's ratio of 0.5, η_T is related to shear complex viscosity $|\eta^*|$ as

$$\eta_T = 3\,|\eta^*| \tag{6.31}$$

In this manner large deformation elongational data may be compared with small deformation shear data. A number of examples are presented below in the form of equation (6.31).

Figure 6.3 shows the data for sample C of NBR with 33% acrylonitrile containing about 50% of microgel.

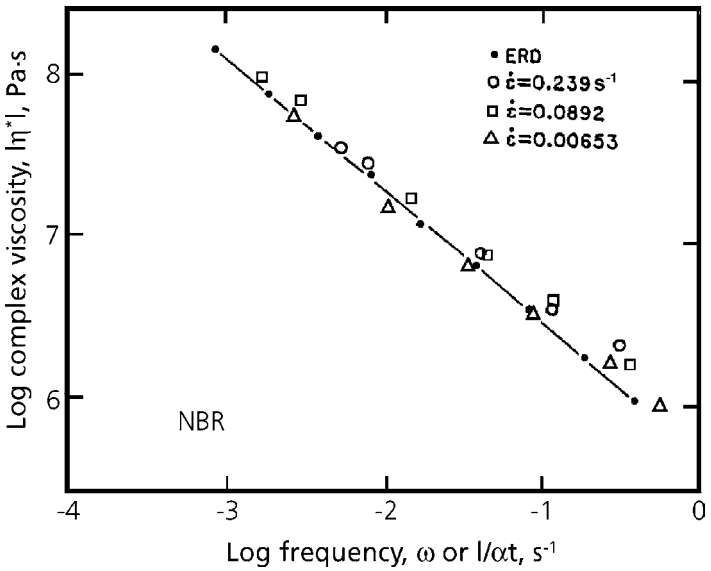

Figure 6.3 Comparison of viscosities calculated from tensile measurements with dynamic shear viscosities for sample C of NBR with 33% acrylonitrile and about 50% microgel. Shear viscosities, ERD; elongation rate, $\dot{\varepsilon}$.

There is some scatter in data points but the data at three different elongation rates form a master curve, which is also in agreement with the shear data as per equation (6.31). Figures 6.4 and 6.5 are for a sample of SBR 1502, and a sample of SBR 1712, respectively, both being gel-free. SBR 1712 is an oil-extended gum rubber. A sample of polyisobutylene is shown in Figure 6.6. All three samples, even though chemical compositions are quite different, obey the strain-time correspondence. The elongational and the shear data are in good agreement, equation (6.31).

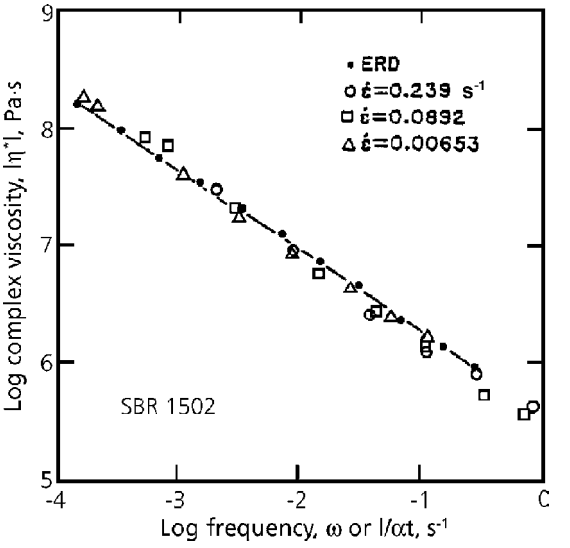

Figure 6.4 Comparison of viscosities calculated from tensile measurements with dynamic shear viscosities for a sample of SBR 1502. Shear viscosity, ERD; elongation rate, $\dot{\varepsilon}$.

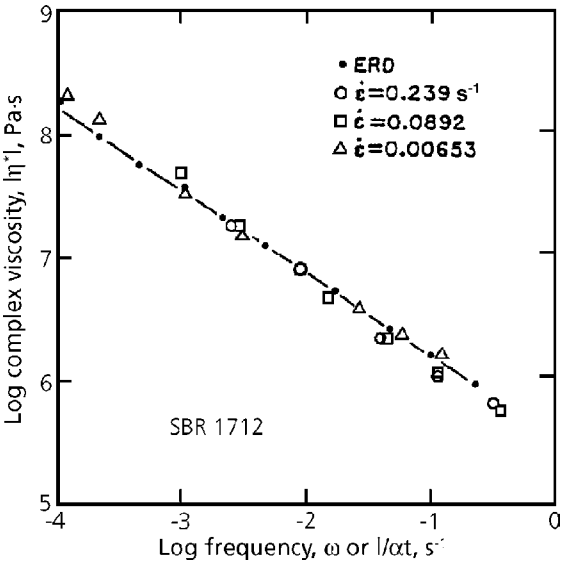

Figure 6.5 Comparison of viscosities calculated from tensile measurements with dynamic shear viscosities for a sample of SBR 1712. Shear viscosity, ERD; elongation rate, $\dot{\varepsilon}$.

Reprinted from N. Nakajima, Polymer International, 1995, 36, 2, 105. Copyright 1995, SCI. Reproduced with permission.

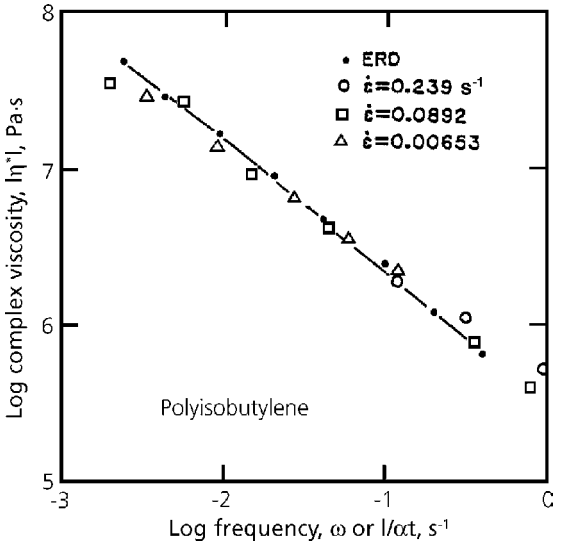

Figure 6.6 Comparison of viscosities calculated from tensile measurements with dynamic shear viscosities for a sample of polyisobutylene. Shear viscosity, eccentric rotating disk (ERD); elongation rate, $\dot{\varepsilon}$.

Reprinted from N. Nakajima, Polymer International, 1995, 36, 2, 105. Copyright 1995, SCI. Reproduced with permission.

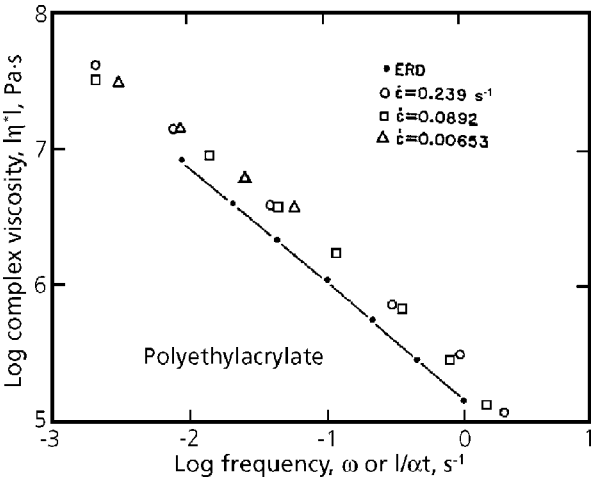

Figure 6.7 Comparison of viscosities calculated from tensile measurements with dynamic shear viscosities for a sample of polyethylacrylate. Shear viscosity, ERD; elongation rate, $\dot{\varepsilon}$.

Reprinted from N. Nakajima, Polymer International, 1995, 36, 2, 105. Copyright 1995, SCI. Reproduced with permission.

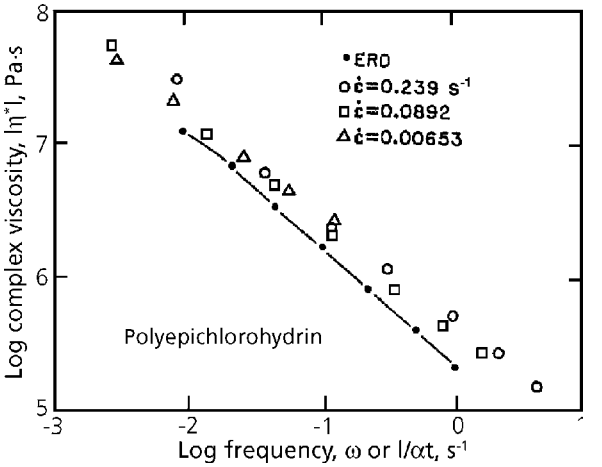

Figure 6.8 Comparison of viscosities calculated from tensile measurements with dynamic shear viscosities for a sample of polyepichlorohydrin. Shear viscosity, ERD elongation rate, $\dot{\varepsilon}$.

Reprinted from N. Nakajima, Polymer International, 1995, 36, 2, 105. Copyright 1995, SCI. Reproduced with permission.

Examples of polyethylacrylate and polyepichlorohydrin, are shown in Figures 6.7 and 6.8, respectively.

These polymers consist of polar monomeric units. They are very different from diene rubbers and polyisobutylene. The elongational data of these polymers obey the strain-time correspondence and form master curves. But the elongational and shear data do not agree:

$$\eta_T > 3\,|\eta^*| \tag{6.32}$$

This behaviour may be attributable to intermolecular polar association, which may be weak at small deformations but becomes significant at large deformations, somewhat analogous to strain-induced crystallisation. With NBR having a high polar content, i.e., above 40% acrylonitrile, a similar observation was made about polar association [22]. One note of caution is the effect of humidity on the viscoelastic properties of rubber containing polar groups [23]. The absorbed moisture may prevent the polar association. This can happen in humid climates or when the gum rubber is not completely dried. This aspect warrants further investigation.

Gum rubber is not a crosslinked network, but for some reason if a network is formed, the elongational data are as shown in Figure 6.9.

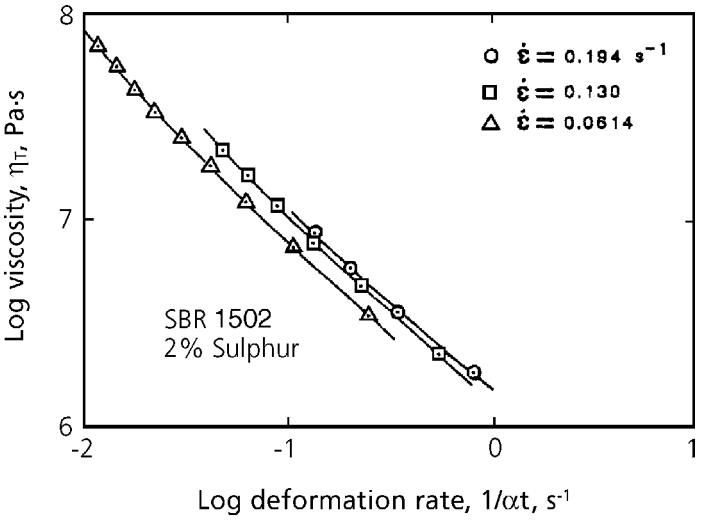

Figure 6.9 Application of strain-line correspondence principle to the tensile stress-strain data of SBR 1502 crosslinked with 2 phr of sulphur.

Reprinted from N. Nakajima, Polymer International, 1995, 36, 2, 105. Copyright 1995, SCI. As Figure 6.1.

The data at different elongation rates do not obey strain-time correspondence but form different curves, which have an upturn indicating limited extensibility [22].

Some gum rubbers obey strain-time correspondence. Other rubbers do not obey the principle, because of strain-hardening. There is yet another type which does not obey strain-time correspondence, because it exhibits linear behaviour even at rather large deformations. In general this type of rubber is soft, and it may be difficult to obtain accurate elongational data. By using a rotational rheometer operated at very low speeds in order to avoid slip, it is possible to obtain accurate data at large shear strains [24].

For shear stress τ and shear strain γ the shear modulus G is

$$G = \tau/\gamma \tag{6.33}$$

Because shear strain rate $\dot{\gamma}$ is constant, the time t is

$$t = \gamma/\dot{\gamma} \tag{6.34}$$

For linear behaviour, viscosity η is

$$\eta = \tau/\dot{\gamma} = \mathrm{G\ t} \tag{6.35}$$

and at equal values of ω and 1/t

$$\eta = |\eta^*| \tag{6.36}$$

the viscosity η has an equal value to that of the complex viscosity.

For non-linear behaviour which obeys strain-time correspondence, viscosities η and $|\eta^*|$ are equal at equal values of ω and $1/\alpha$t. Instead of equation (6.35), viscosity has the form

$$\eta = \mathrm{G}\ \alpha\mathrm{t} \tag{6.37}$$

or

$$\eta = (\tau/\dot{\gamma})\alpha = |\eta^*| \tag{6.38}$$

The relationship between shear strain and the extension ratio is given as [15]:

$$\gamma = \alpha - (1/\alpha) \tag{6.39}$$

An example with an ethylene-propylene rubber of Mooney index 40, is shown in Figures 6.10a and 6.10b.

The points in the figures represent η and the lines $|\eta^*|$. Figure 6.10a shows that the linear form, equation (6.35), holds, and Figure 6.10b shows that the non-linear, strain-time correspondence, equation (6.37), does not hold.

On the other hand, an NBR with a Mooney index of 35 and acrylonitrile content of 33% does not obey equation (6.35), see Figure 6.11a, but obeys the non-linear equation (6.37), see Figure 6.11b.

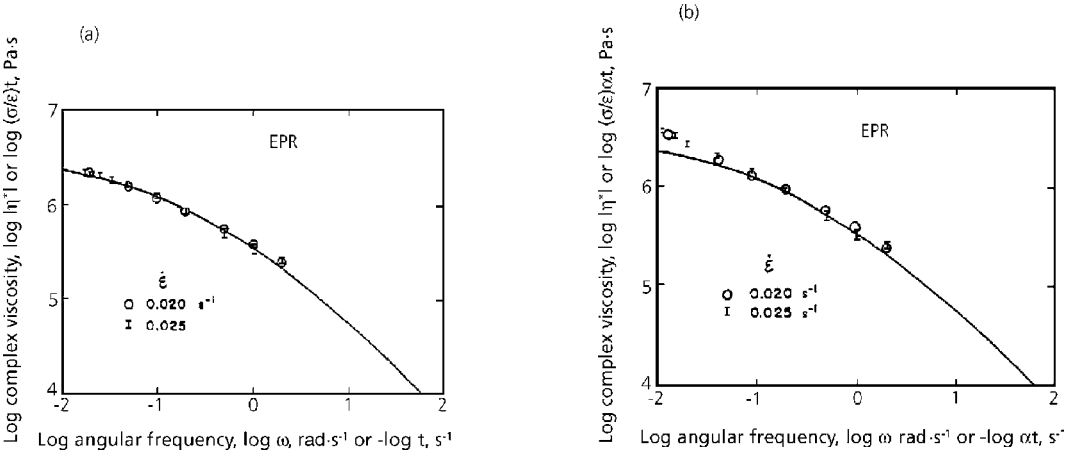

Figure 6.10 (a) Complex viscosity of ethylene-propylene rubber (EPR) at 30 °C. The line represents the observed data and the markings are the data calculated from the stress rise at a constant deformation rate. The calculation is based on linear viscoelasticity. The stress rise measurements at $\varepsilon = 0.025$ s^{-1} were performed in triplicate. The figure shows agreement between calculated and observed data. (b) The same data as in (a), except that the calculation is based on the non-linear relation, the strain-time correspondence. This figure shows disagreement between calculated and observed data.

The rubber exhibiting linear behaviour, Figure 6.10a, tends to go to the flow state where viscous contribution dominates over the elastic contribution. This type of rubber has a relatively low MW and no significant long branching. On the other hand, a rubber exhibiting non-linear behaviour, Figure 6.11b may have a high MW, some long branching, and even a small amount of macrogel. The Mooney values of these two rubbers are very similar, but the viscoelastic behaviour of these rubbers is very different.

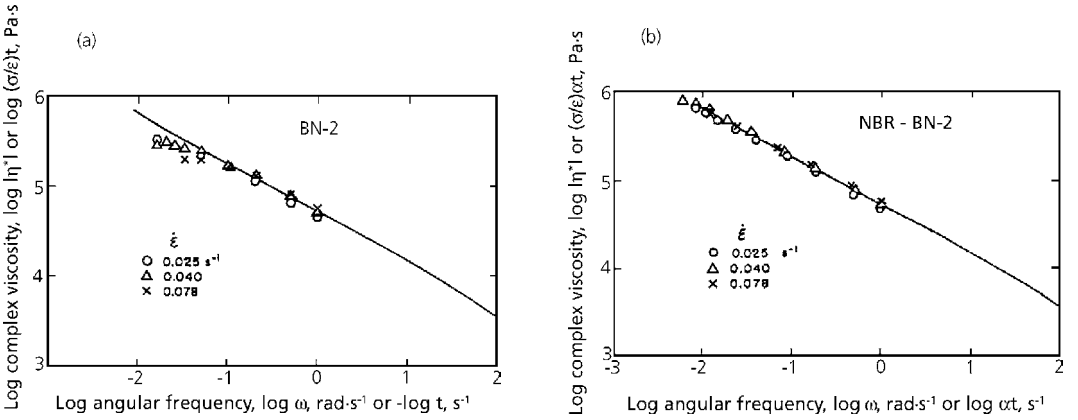

Figure 6.11(a) Complex viscosity of NBR sample BN-2 at 100 °C. The line represents the observed data and the markings are the data calculated from the stress rise at constant deformation rates. Three different rates were used. The calculation is based on linear viscoelasticity. This figure shows disagreement between calculated and observed data. (b) The same data as in (a), except that the calculation is based on the non-linear expression, the strain-time correspondence. This figure shows agreement between calculated and observed data.

Reprinted from N. Nakajima, Polymer International, 1995, 36, 2, 105. Copyright 1995, SCI. Reproduced with permission.

As stated before, the presence or absence of gel is the first and a most important aspect of gum rubber characterisation. When gel is present, the concept of MW loses practical meaning, because the MW of gel is extremely high and cannot be measured. Nevertheless, when two gum rubbers are compared, the question may arise as to which has the higher MW. In such a case, because the comparison of MWs has no real meaning, the question may be redirected to the level of the viscoelastic properties.

The Mooney index is usually used for this comparison. However, this practice may be misleading because in some cases, a higher gel content gives a lower Mooney index [21]. What is needed here is some measure of viscoelastic property, which gives a higher value for a higher gel content. If gel is absent, the same property should give a higher value for a higher MW. For this purpose the dynamic complex viscosity at low frequencies may be used. Figure 6.12 shows gel-free EPM. At low frequencies, samples of a higher weight-average MW $\overline{M}_w$ have a higher $|\eta^*|$ [25].

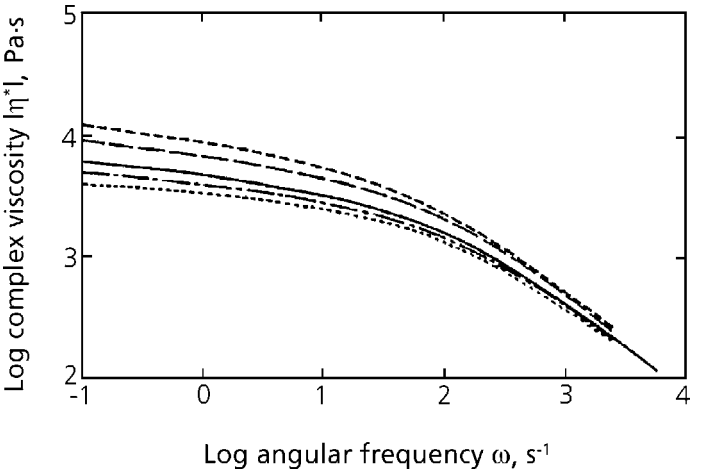

Figure 6.12 Effect of variation in $\overline{M}_w$ on the complex viscosity curves at 230°C: (.....) A, 1.13 x 10^5; (_. _) B, 1.35 x 10^5; (_ _) C, 1.56 x 10^5; (___) D, 1.70 x 10^5; (__) XL-0, 1.16 x 10^5.

Reprinted from N. Nakajima, Polymer International, 1995, 36, 2, 105. Copyright 1995, SCI. Reproduced with permission.

When the EPM is milled in presence of a peroxide, long branches and gel are generated. As shown in Table 6.2 the different amounts of peroxide do not give a systematic relationship with GPC data nor with DSV.

Table 6.2. GPC measurements of EPMs with differing amounts of long branches[a]

Sample Designation	Dicumyl Peroxide (phr)	(10^4)	(10^5)	(10^5)		(10^5)	DSV[b]
XL-0	0.0	5.37	1.16	2.87	2.16	1.04	1.45
XL-1	0.05	4.96	1.04	2.31	2.10	0.94	1.40
XL-2	0.1	4.34	0.96	2.34	2.22	0.86	1.33
XL-3	0.2	4.52	1.18	4.33	2.61	1.02	1.38
XL-4	0.4	4.53	2.37	41.57	5.23	1.64	1.67

a Symbols $\overline{M}_n$, $\overline{M}_w$, $\overline{M}_z$, describe relative hydrodynamic size, i.e., MW averages are not corrected for branching

b DSV determined with a concentration of 0.1 g/ml in toluene at 25 °C

$\overline{M}_v$: viscosity average MW

Unknown amounts of gel must have been removed by filtration. On the other hand, $|\eta^*|$ values at low frequencies in Figure 6.13 are higher for larger amounts of peroxide, clearly indicating the generation of more long branches and gel.

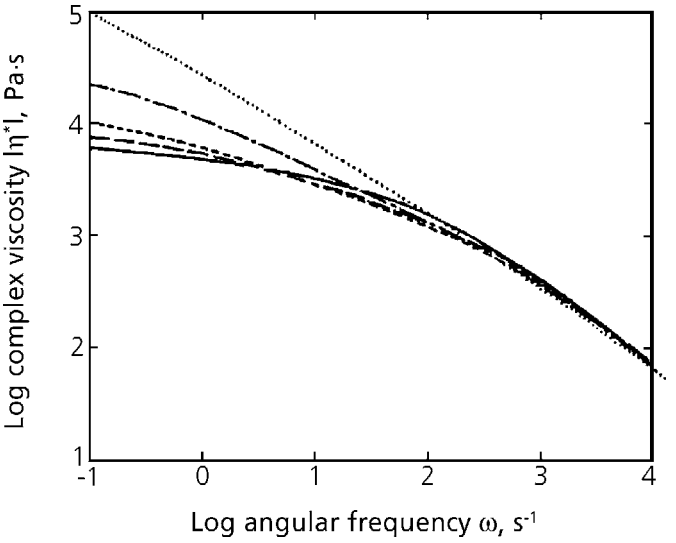

6.13 Effect of increasing long branching (XL-0 - XL-4) on the complex viscosity master curves at 230 °C: (__) XL-0; (_ _) XL-1; (___) XL-2; (_. _) XL-3; (.....) XL-4.

A summary of the viscoelastic characteristics of gum rubber is given below.

1. Relative but quantitative method for the degree of long branching and gel content. Preparation of log G˝ versus log G′ plot. For a higher degree of long branching and higher gel content the curve is placed to the right. With reference to the line G˝ = G′, the position of the curve shows whether viscous behaviour or elastic behaviour dominates.

2. Differentiating macrogel and microgel. Perform elongation measurements with different rates of elongation and test the applicability of strain-time correspondence. Those rubbers obeying the principle are either linear molecules, molecules with long branching but gel-free (ASTM D3616-95) [20], those containing microgel, or in some cases containing a small amount (<10%) of macrogel. Those containing macrogel, e.g., more than approximately 10%, tend to give strain-hardening.

Linearisation requires shifts in both time axis by α and modulus axis by $\Gamma(\alpha)$. The latter represents a relative degree of macrogel content.

3. Rubbers exhibiting linear viscoelastic behaviour. These have either a low MW, a linear molecule, a few long branches, or all of these. The MW distribution is narrow in the sense that there is no excessive spread towards high MWs. Of course, they are gel-free.

4. Differentiating macrogel from microgel when the former is less than 10%. Compare the elongational data with the shear data according to the method given earlier equation (6.27), i.e., without applying the modulus shift. In the presence of macrogel, the elongational modulus divided by a factor of three is higher than the shear modulus.

5. In method 4, there is a case where shear modulus is higher than the elongational modulus (after dividing by three). Examples are triblock copolymers; in small strain shear measurements the physical crosslinks remain intact, but in large strain elongational measurements the crosslinks are destroyed, thus softening the rubber [26].

6. With rubbers having many polar groups, e.g., polyethylacrylate, polyepichlorohydrin, and NBR with 40% acrylonitrile, elongational modulus (divided by three) is higher than shear modulus even in the absence of macrogel. A molecular association similar to strain-induced crystallisation appears to occur at high elongation.

7. In the presence of absorbed moisture, the molecular association may not occur.

8. Complex viscosity at low frequency is a good measure of the 'MW' of a rubber regardless of the presence or absence of gel.

6.6 Processability and molecular structure

Certain specific samples of gum rubber are said to have a good processability or poor processability. These statements have no real meaning unless the processing conditions are specified. For example, the presence of long branching may improve processability or harm it. Therefore, a generalised relationship does not exist between processability and molecular structure. With a full understanding of this difficulty, a discussion is given here on the subject; however, the relationships given are not without exceptions.

During the Second World War, in the early days of the emulsion polymerisation of synthetic rubbers, macrogels were generated which caused difficulty in the milling process. If the

polymerisation temperature was too high, 'hot rubber' was produced. The 'cold rubber' process was developed later, producing easy processing rubber. Macrogel is also produced at high conversion; therefore, the degree of conversion (of monomer to polymer) is limited to a certain percentage. Even with 'gel-free' rubber according to ASTM D3616-95 [20] gel may be detected by the use of a GPC filter. The implication is that below a certain size, or at less than a certain gel content, the macrogel has no adverse effect on mill processability.

In some cases the presence of macrogel is preferred. When a large amount of reinforcing filler must be compounded, the compound tends to become crumbly and breaks into pieces, i.e., 'dry'. In this case, dispersion of carbon black is not achieved and the compound cannot be formed into a shape. The presence of large amounts of macrogel can overcome this problem.

Macrogel-containing rubber may be oil-extended to alleviate the milling problem. Sometimes oil-extended rubber has a superior strength as a vulcanisate compared with the gel-free, non-oil-extended counterpart.

Without oil extension, macrogel-containing rubber has a low tensile strength as a vulcanisate compared with gel-free rubber. This is because branch points increase the crosslink density, thereby limiting the elongation to break.

When green strength is needed for the mixed compound, long branches and even, to some extent, the presence of gel are appreciated. The green strength is the resistance to drape of the sheet made of the uncrosslinked compound.

The presence of long branches and gel generates more free ends in vulcanisates compared with linear molecules. Such free ends increase heat build-up of finished products under repeated stressing.

Mill processability also depends upon the additives in the formulation. Oils, plasticisers and even small amounts of powder [27] affect the mill performance. However, the present discussion will be confined to gum rubbers only.

The most significant difference is found among different types of rubber; *cis*-1,4-polybutadienes being polymerised in solution, the MW distribution is less spread out at the high MW end compared with emulsion polymerised SBR. For this reason and because of the low T_g, some grades of this rubber may tend to go into Region III of mill processability [28] causing mixing problems. The presence of long branches imparts long relaxation times (see section 6.8) and the mixing problem may be overcome. More discussion of this will be given in section 6.7.1.

Even with emulsion polymerisation, polyethylacrylate rubber tends to go into Region IV of mill processability, i.e., the flow region. This is because the rubber has 73% of its MW as the pendent group. It is a fat and short molecule compared with diene rubber. The presence of some long branches may help mill processability. However, when the tendency for Region IV behaviour is known, upside-down mixing, i.e., charging carbon black first into an internal mixer and then the rubber, is the usual practice.

Microgel is a crosslinked latex particle. Rubber containing a large amount of microgel breaks down easily on milling, hence decreasing time and energy of mixing [29]. However, the strength of vulcanisate is somewhat inferior because it gives a lower elongation to break. The microgel-containing compounds tend to give a smoother extrudate. Extrudate swelling is reduced and the degree of swelling is independent of the extrusion rate. The spread of MW distribution towards lower MW has no detrimental effect on processability. The mechanical strength is decreased and the heat build-up is increased in the finished product.

Although much knowledge has been systematically accumulated on the linear viscoelastic behaviour of gum rubber, attempts to relate the linear behaviour to processability may result in misleading or even wrong conclusions. Gum rubber processing involves non-linear behaviour and fracture, which may not be predictable from linear behaviour.

6.7 Processability and viscoelastic characteristics

6.7.1 Cis-1,4-polybutadiene

Bearing the cost-benefit relationship in mind, an important question is what is the minimum activity required for obtaining sufficient information on the characteristics of a given gum rubber. Section 6.6 showed that at least two types of measurement are required; one is the dynamic mechanical measurements over the temperature and the frequency region covering processing conditions. The other is the tensile stress-strain measurements at room temperature with at least three and preferably four strain rates. In this section examples are presented to show how this characterisation scheme is used to determine structure-processability relationships.

The first example uses *cis*-1,4-BR. A major application of *cis*-1,4-BR is for tyres. The rubber improves wear resistance, rolling resistance, and flexibility at low temperature. It is usually blended with other rubbers, such as NR or SBR because it does not have a good processability, flex-crack resistance and green strength. Because the rubber has a very low T_g of -112 °C, it tends to fall in Region III or IV of the mill processability.

In order to overcome the problems associated with milling, long branching is considered to be one of the variables to manipulate. Questions are how much and how long the long

branch should be. In addition *cis*-1,4-BR is known to give a strain-induced crystallisation under favourable conditions. Does the strain-induced crystallisation occur during mill-mixing and if so, what effect does it have? Another question is the effect of addition of crystalline particles on the mill processability and strain-induced crystallisation.

The mechanism of branch formation is discussed in Section 1.1.3. In the free radical polymerisation, the chain-transfer mechanism is responsible and the branched molecule becomes more branched leading to gel-formation. In the metal-coordinated catalyst systems used for *cis*-1,4-BR polymerisation, branches are formed by insertion of macromers. Once insertion occurs, the probability of another insertion is considerably decreased because of the steric effect. Therefore, no gel is formed. Not only are fewer branches present but also the branch pattern is different from those in the free-radical polymerised rubbers.

- *Experiment - I* [30]
- *Samples*

The samples were four commercial polybutadienes produced by Bayer AG, see Table 6.3.

Table 6.3 Properties of *cis*-1,4-butadiene samples[a]

Sample	BUNA CB11[b]	BUNA CB22[b]	BUNA CB23[b]	BUNA CB24[b]
Catalyst	Ti	Nd	Nd	Nd
Cis-1,4-(%)	93	98	98	98
1,2-vinyl (%)	4	1	1	1
$\overline{M}_w$ x 10^{-4} [c]	51	53	51.5	66.5
$\overline{M}_n$ x 10^{-4} [c]	12	20.5	15	12
$\overline{M}_w/\overline{M}_n$ [c]	4.3	2.6	3.4	5.5
MV [d]	47	63	51	44
T_g (°C)	–105	–109	–109	–109
Degree of branching (%)[e]	10	5	5	3

a: All data supplied by the manufacturer
b: Registered Trade mark of Bayer AG
c: Data obtained by GPC; MW are not absolute but relative values based on the hydrodynamically equivalent volume of polystyrene standards
d: Mooney Index
e: Calibrated with star-branched polymers
$\overline{M}_w$: mass-average MW $\overline{M}_n$: number-average MW MV: Mooney Viscosity

The sheets of gum rubbers were prepared by pressing at 140 °C for 10 minutes. After removal from the press, the sheets were cut in quarters, piled in four layers, and pressed again under the same conditions to completely remove bubbles. After the second pressing the sheets were placed between two steel plates at room temperature with heavy weights placed on top. The sheets were allowed to rest at least 2 days under the heavy weights to prevent wrinkling when removed.

Oscillatory shear specimens were cut from the sheets as discs 25 mm in diameter and tensile specimens were cut using the dumbbell die C described in ASTM D412 [31].

The gel contents of the sheets were measured by dissolving about 0.4 g of rubber in 100 ml of *n*-heptane for 48 h. The solution was filtered through a Whatman No. 4 filter paper. The filter paper was weighed before and after filtration to estimate the amount of gel removed from the solution. The filtered solution was evaporated in an oven at 110 °C and the amount of dissolved polymer was measured. No gel was found in these samples.

- *Instruments*

The oscillatory shear measurements were performed with a Rheometrics mechanical spectrometer (RMS 800) with parallel plates. The angular frequency range was from 10^{-2} to 10^{2} rad/s. The samples were tested at 30, 60, 120, and 150 °C. In addition to the calibration specified by the instrument manufacturer, a standard silicone rubber (SE30; General Electric Company) was used every time to double-check the calibration. The frequency sweep was made from the lowest to the highest and then reversed to the lowest frequency. The data at the lowest frequency should be reproducible if there is no degradation during the measurements.

Tensile tests were performed with a Monsanto Tensometer 500. The strip chart recorder recorded force against time. The force was measured with a 0.45 kg load cell. The extent of deformation was measured by recording with a video camera. An extensometer was not used because the samples were not strong enough to hold it. The samples were held with plastic grips having relatively loose springs in order to prevent breaking at the grips. The tests were performed at room temperature with strain rates of 0.004, 0.017, 0.057, 0.118, and 0.250 s^{-1}.

- *Results and discussion*

- *Oscillatory shear measurements*

Time-temperature superposition was performed in the following sequence: first, tan δ data were plotted against log ω. The superposition involves the log ω axis only, because any modulus-shift in G′ and G″ cancels out. From this procedure the time-shift factor, a_T, was evaluated. Next, log |G*| data were plotted against log ωa_T. From these plots

the modulus-shift factor, β_T, was evaluated. The results of superposition are shown in Figures 6.14-6.17, where all the data were reduced to 30 °C.

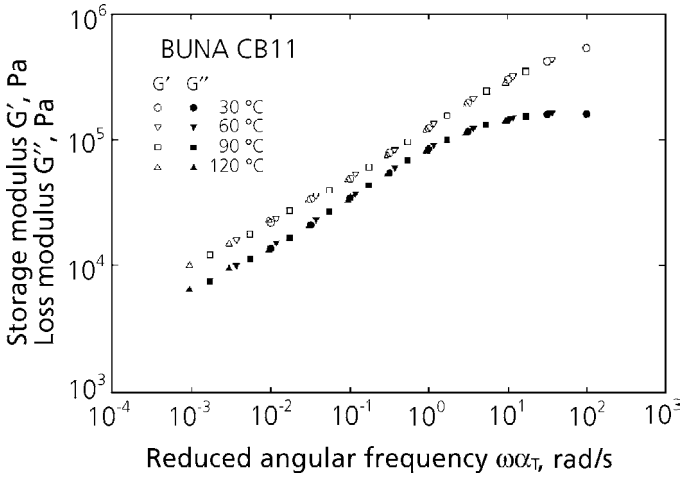

Figure 6.14 Master curves of storage and loss modulus of Buna CB11 (Reference temperature 30 °C).

Reprinted from N. Nakajima and Y. Yamaguchi, Journal of Applied Polymer Science, 1996, 61, 9, 1525. Copyright 1996, reprinted by permission of John Wiley and Sons, Inc.

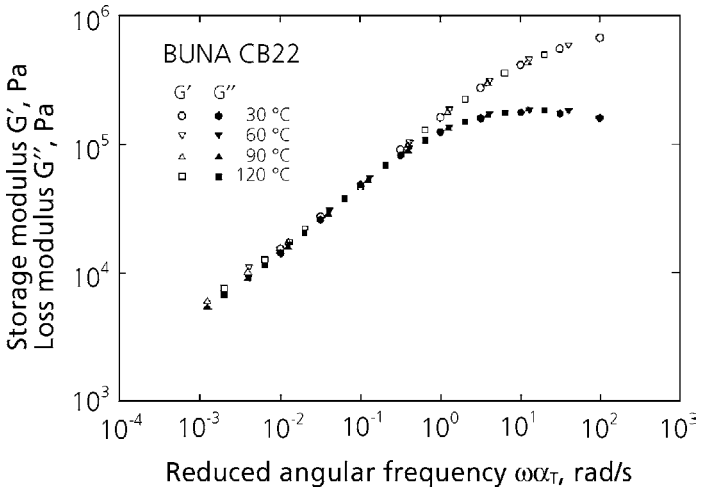

Figure 6.15 Master curves of storage and loss modulus of Buna CB22 (Reference temperature 30 °C).

Reprinted from N. Nakajima and Y. Yamaguchi, Journal of Applied Polymer Science, 1996, 61, 9, 1525. Copyright 1996, reprinted by permission of John Wiley and Sons, Inc.

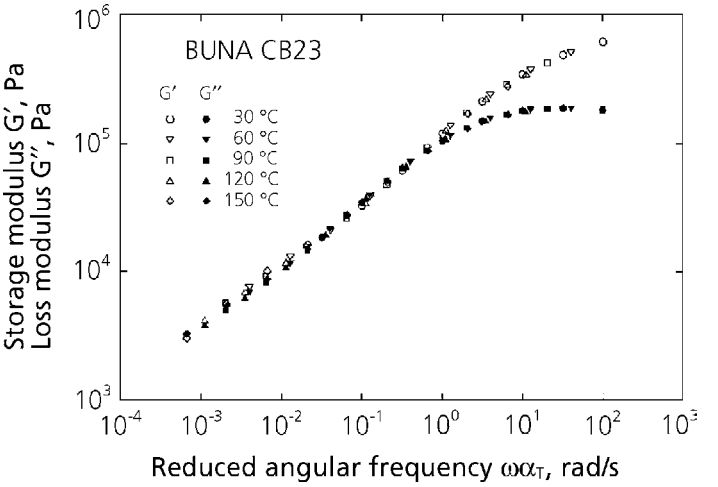

Figure 6.16 Master curves of storage and loss modulus of Buna CB23 (Reference temperature 30 °C).

Reprinted from N. Nakajima and Y. Yamaguchi, Journal of Applied Polymer Science, 1996, 61, 9, 1525. Copyright 1996, reprinted by permission of John Wiley and Sons, Inc.

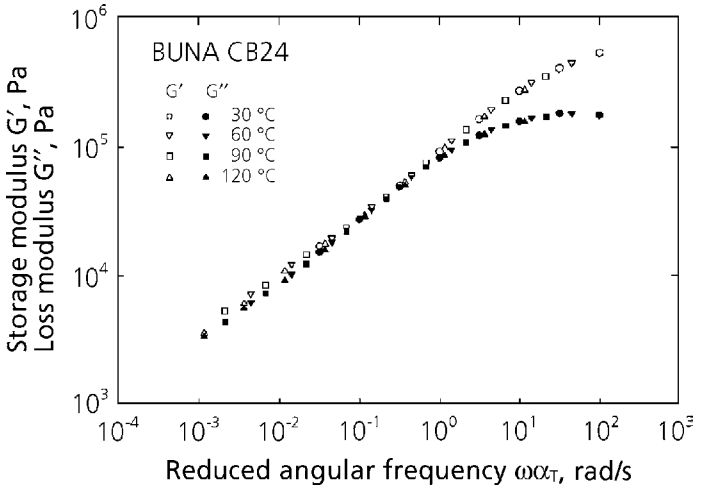

Figure 6.17 Master curves of storage and loss modulus of Buna CB24 (Reference temperature 30 °C).

Reprinted from N. Nakajima and Y. Yamaguchi, Journal of Applied Polymer Science, 1996, 61, 9, 1525. Copyright 1996, reprinted by permission of John Wiley and Sons, Inc.

The extent of time-shift was rather small; for the data obtained at 30-120 °C, the frequency range was extended only about one decade to lower frequencies. This is because the glass-transition temperature of *cis*-1,4-BR is very low, -110 °C. All master curves approach the plateau region at the higher frequencies. The lower frequency region is the transition from the plateau towards terminal region. However, these curves do not show a cross-over of G´ and G´´. They are almost parallel to each other. This indicates that all these samples have some branching. In Figure 6.18, G´ curves of four samples are compared.

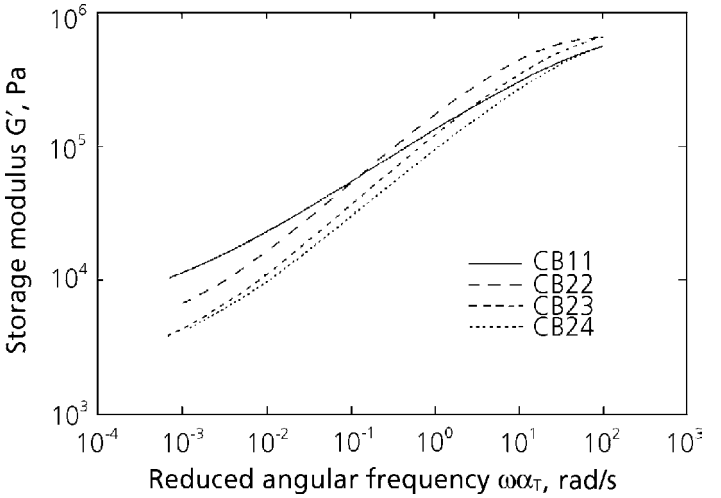

Figure 6.18 Compression of master curves of storage modulus of various Buna samples. (Reference temperature 30 °C).

The curve of CB11 shows a smaller slope and higher G´ than those of the other samples at low frequencies. This indicates that CB11 contains a structure having a longer relaxation time compared, for example, to CB24. This cannot be explained from the differences in MW and its distribution because CB24 has a higher MW and broader MW distribution than CB11, see Table 6.3. Therefore, this must be the effect of more extensive branching in CB11 than in the others. The differences among CB22, CB3, and CB24 are related to their MW distribution, and G´ is higher for the higher $\overline{M}_n$. This indicates the effect of the low MW fraction on G´.

Figure 6.19 shows log G´´ versus log G´ plot for the four samples. The curve of CB11 lies at the right side of those of the others [25].

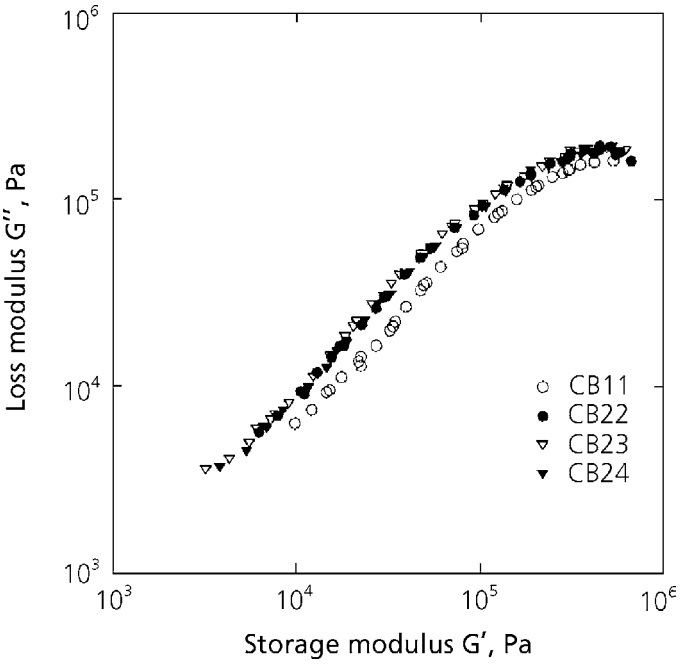

Figure 6.19 Comparison of log G˝ versus log G´ curves.

Reprinted from N. Nakajima and Y. Yamaguchi, Journal of Applied Polymer Science, 1996, 61, 9, 1525. Copyright 1996, reprinted by permission of John Wiley and Sons, Inc.

The values of the shift factors, a_T and β_T are given in Table 6.4. The a_Ts are sample-dependent and CB11, which has the highest degree of branching, shows the highest temperature dependence. At the lower temperature CB24 shows a lower temperature dependence than CB22 and CB23. However, the differences diminish at the higher temperature. The fact that the differences of a_T diminish at the higher temperature indicates that the constraints introduced by the branching become less effective at the higher temperature. The observed β_T values, Table 6.4, are comparable to the values of $\rho_0 T_0/\rho T$.

No further significant information was obtained from β_T. From the results mentioned above, (see Figure 6.19 and Table 6.3), the order of degree of branching is CB11>CB22=CB23>CB24. Figure 6.20 shows the absolute values of complex viscosity $|\eta^*|$ of the samples at 30 °C.

As observed in many commercial rubbers, these do not show the Newtonian region within the observed time scale because of their high MW, broad MW distribution, and branching. At low frequencies, they show the viscosity enhancement resulting from branching, which is longer than the critical length [25]. The sample of CB11, in spite of having the same $\overline{M}_w$ as those of CB22 and CB23, shows the highest degree of the viscosity enhancement at low frequencies and viscosity reduction at high frequencies; that is the curve of CB11 crosses over the other curves. This also indicates that CB11 has more extensive branching compared to other samples [25]. For CB22, CB23 and CB24 the magnitude of $|\eta^*|$ is in the order of number average MW, $\overline{M}_n$, see Table 6.3.

Table 6.4 Shift Factors, a_T and β_T

Temperature (°C) Sample	**30**	**60**	**90**	**120**	**150**
a_T					
CB11	1	0.368	0.171	0.094	0.052*
CB22	1	0.409	0.202	0.124	0.071*
CB23	1	0.400	0.202	0.111	0.066
CB24	1	0.449	0.215	0.117	0.067*
β_T					
CB11	1	0.934	0.834	0.794	–
CB22	1	0.910	0.803	0.753	–
CB23	1	0.893	0.844	0.734	0.660
CB24	1	0.938	0.828	0.726	–
$\rho_0 T_0/\rho T$	1	0.910	0.835	0.771	0.716
*Slight degradation was noticed.					

- *Tensile stress-strain measurements*

Figures 6.21 and 6.22 show tensile stress-strain curves of CB11 and CB24 at various deformation rates. The filled circles show the data at break. Reproducibility shown in the figures is less than ± 15%. The modulus increases with increasing deformation rates.

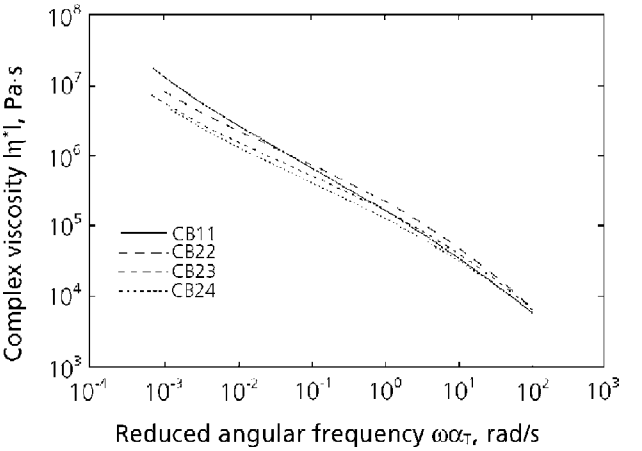

Figure 6.20 Comparison of master curves of complex viscosity of BUNA samples (reference temperature 30 °C).

Reprinted from N. Nakajima and Y. Yamaguchi, Journal of Applied Polymer Science, 1996, 61, 9, 1525. Copyright 1996, reprinted by permission of John Wiley and Sons, Inc.

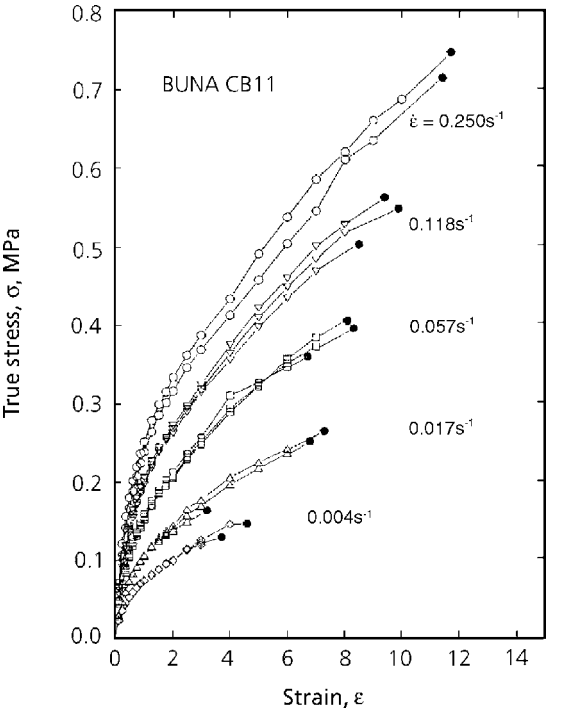

Figure 6.21 Tensile stress-strain curves of BUNA CB11.

Reprinted from N. Nakajima and Y. Yamaguchi, Journal of Applied Polymer Science, 1996, 61, 9, 1525. Copyright 1996, reprinted by permission of John Wiley and Sons, Inc.

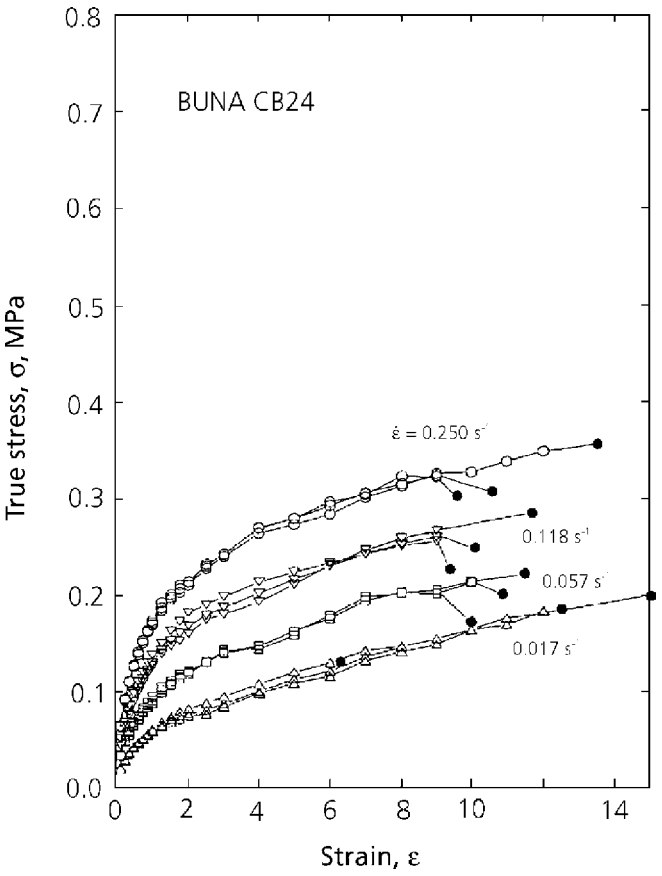

Figure 6.22 Tensile stress-strain curves of BUNA CB24.

Reprinted from N. Nakajima and Y. Yamaguchi, Journal of Applied Polymer Science, 1996, 61, 9, 1525. Copyright 1996, reprinted by permission of John Wiley and Sons, Inc.

Figure 6.23 shows the plots of tensile modulus, $E(t)$, against time, t, at various deformation rates for CB24. The data obtained at different deformation rates do not give a master curve, because the behaviour is not linearly viscoelastic [7].

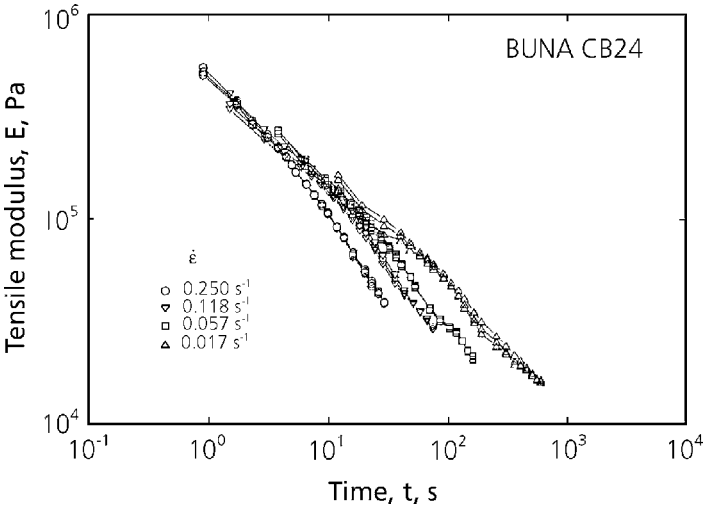

Figure 6.23 Tensile modulus as a function of time for BUNA CB24.

Reprinted from N. Nakajima and Y. Yamaguchi, Journal of Applied Polymer Science, 1996, 61, 9, 1525. Copyright 1996, reprinted by permission of John Wiley and Sons, Inc.

Figures 6.24-6.26 show the plots of tensile modulus, E(αt), against reduced time, αt, as given by Equation 6.27.

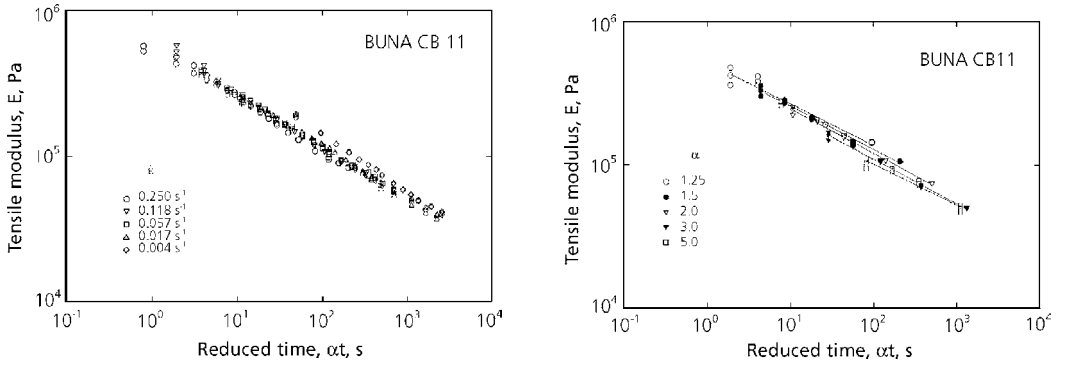

Figure 6.24 a) Tensile modulus as a function of reduced time at fixed rates for BUNA CB11. b) Tensile modulus as a function of reduced time at fixed extension ratios for BUNA CB11.

Reprinted from N. Nakajima and Y. Yamaguchi, Journal of Applied Polymer Science, 1996, 61, 9, 1525. Copyright 1996, reprinted by permission of John Wiley and Sons, Inc.

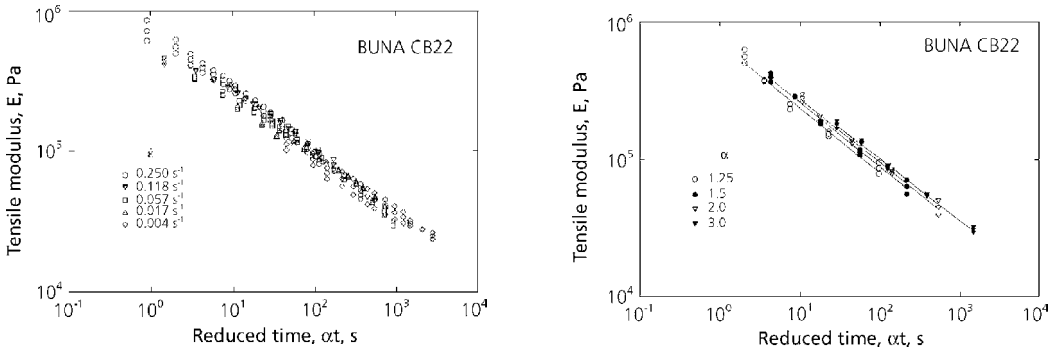

Figure 6.25 a) Tensile modulus as a function of reduced time at fixed rates for BUNA CB22. b) Tensile modulus as a function of reduced time at fixed extension ratios for BUNA CB22.

Reprinted from N. Nakajima and Y. Yamaguchi, Journal of Applied Polymer Science, 1996, 61, 9, 1525. Copyright 1996, reprinted by permission of John Wiley and Sons, Inc.

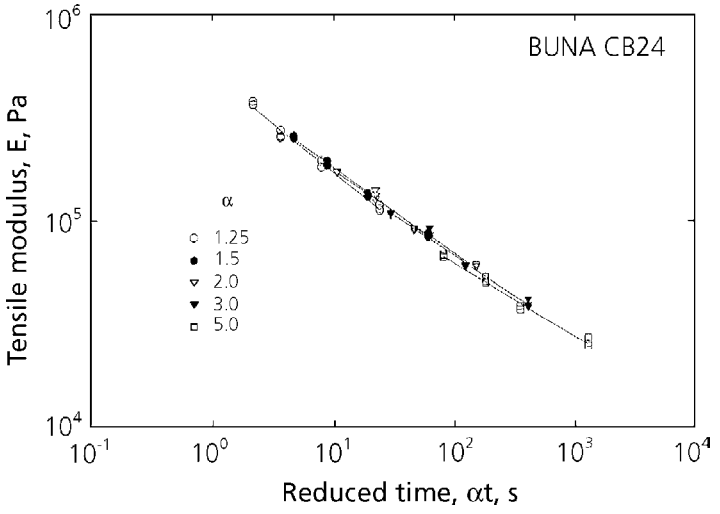

Figure 6.26 Tensile modulus as a function of reduced time at fixed extension ratios for BUNA CB24.

Reprinted from N. Nakajima and Y. Yamaguchi, Journal of Applied Polymer Science, 1996, 61, 9, 1525. Copyright 1996, reprinted by permission of John Wiley and Sons, Inc.

In Figures 6.24 (a) and 6.25 (a) the data are plotted for each strain rate, and in Figures 6.24 (b), 6.25 (b) and 6.26 the lines are for constant values of α. CB11 and CB22 show a systematic relationship with α, while CB24 gives a master curve which is independent of α. With CB11 the deviation is in the direction of strain-softening and for CB22 and CB23 it is strain-hardening. Among CB22, CB23, and CB24 the extent of the strain-hardening relates to the amount of branching given in Table 6.3. Even though CB11 has the highest amount of branching, it shows strain-softening behaviour. It should be noted that CB11 is made with a catalyst system different from that used for the other systems, see Table 6.3. Evidently, the branches of the polymer are not long enough to provide the constrained entanglement upon stretching.

When the modulus shift [32], Equation 6.28, is applied, master curves are formed for CB11, CB22, and CB23. Figure 6.27 shows the result for CB22.

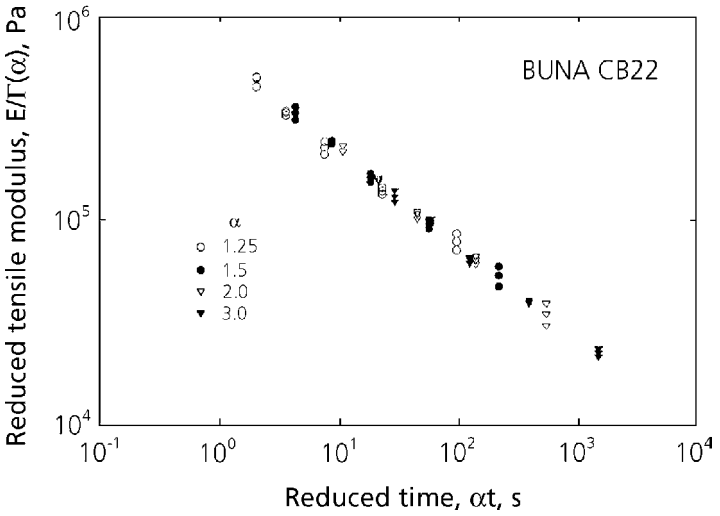

Figure 6.27 Reduced tensile modulus as a function of reduced time for BUNA CB22.

Reprinted from N. Nakajima and Y. Yamaguchi, Journal of Applied Polymer Science, 1996, 61, 9, 1525. Copyright 1996, reprinted by permission of John Wiley and Sons, Inc.

With the emulsion-polymerised rubbers, the modulus shift is required only when an extensive amount of macrogel is present [22]. However, there is no gel in the samples referred to in this work. This is the only time when strain hardening was observed for the sample containing no gel. It implies that the long branches in these BRs are very long.

Figure 6.28 shows the modulus shift, $\Gamma(\alpha)$, for the samples of CB11, CB22 and CB23 as a function of extension ratio.

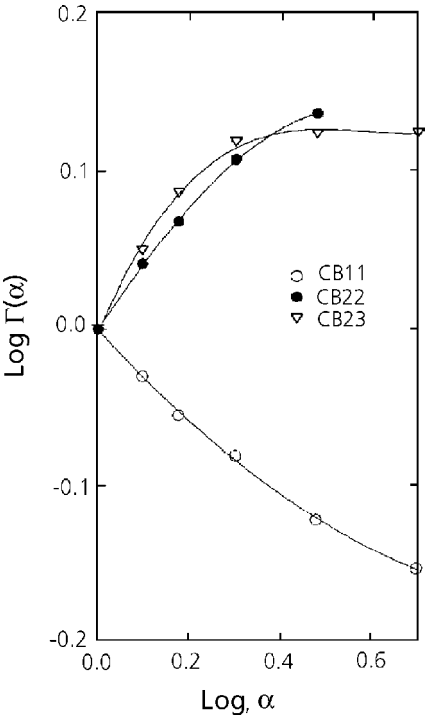

Figure 6.28 Modulus shift factor as a function of extension ratio.

In this figure, no data for CB24 are shown. Although CB24 has long branching, it shows neither strain-hardening nor strain-softening. This indicates that it has the critical length of branching bordering strain-hardening and strain-softening. At this critical branch-length, branches no longer contribute to such behaviour as strain-hardening or strain-softening.

Figures 6.29-6.32 show the comparison between the complex viscosity, $|\eta^*|$, and the equivalent shear viscosity, η_T calculated from the tensile stress-strain data.

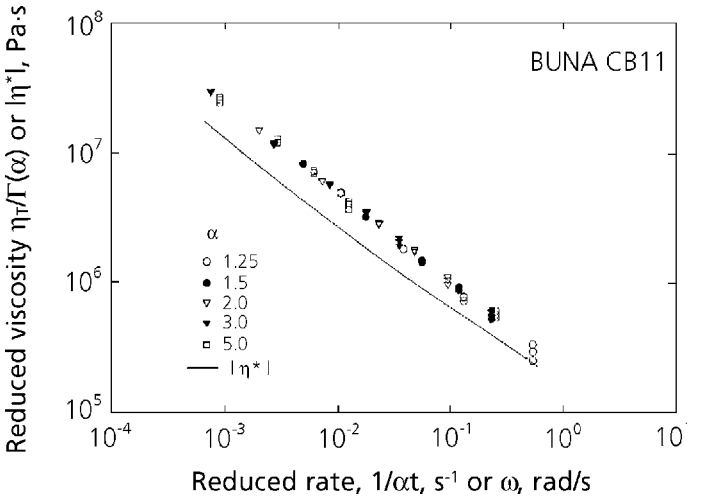

Figure 6.29 Comparison of complex shear viscosity with corresponding viscosity calculated from tensile data for BUNA CB11.

Reprinted from N. Nakajima and Y. Yamaguchi, Journal of Applied Polymer Science, 1996, 61, 9, 1525. Copyright 1996, reprinted by permission of John Wiley and Sons, Inc.

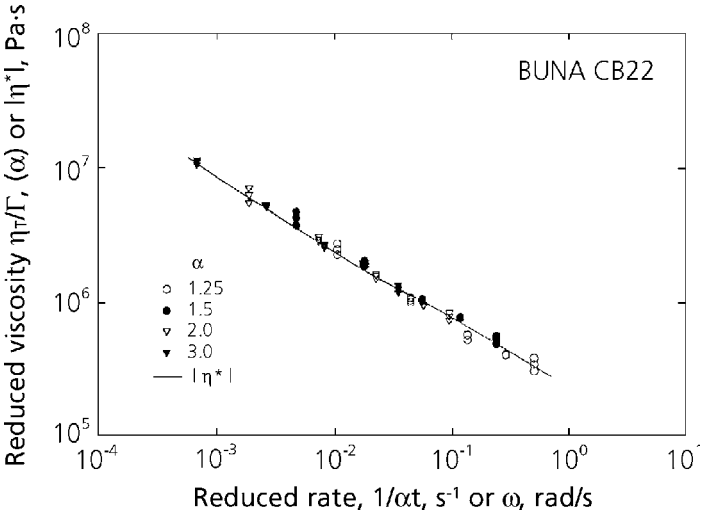

Figure 6.30 Comparison of complex shear viscosity with corresponding viscosity calculated from tensile data for BUNA CB22.

Reprinted from N. Nakajima and Y. Yamaguchi, Journal of Applied Polymer Science, 1996, 61, 9, 1525. Copyright 1996, reprinted by permission of John Wiley and Sons, Inc.

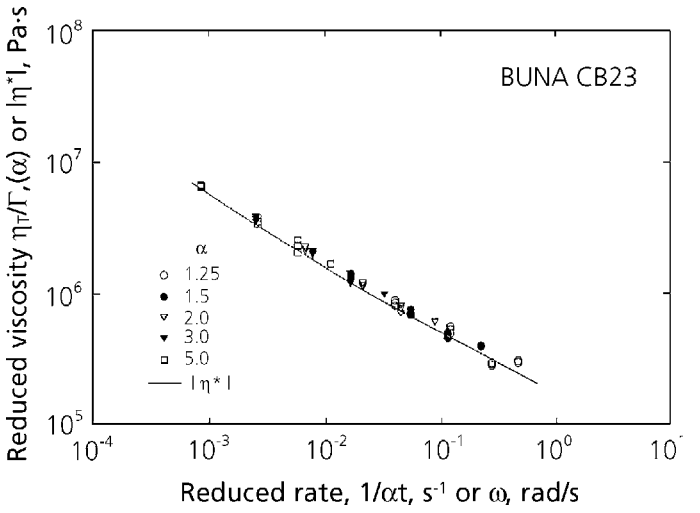

Figure 6.31 Comparison of complex shear viscosity with corresponding viscosity calculated from tensile data for BUNA CB23.

Reprinted from N. Nakajima and Y. Yamaguchi, Journal of Applied Polymer Science, 1996, 61, 9, 1525. Copyright 1996, reprinted by permission of John Wiley and Sons, Inc.

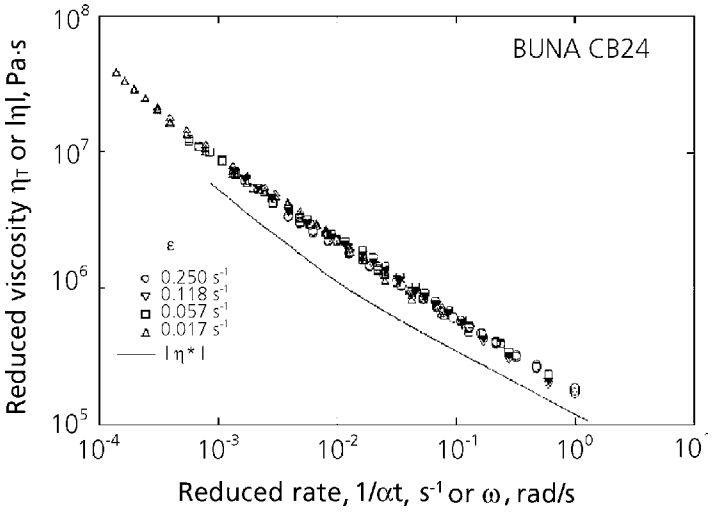

Figure 6.32 Comparison of complex shear viscosity with corresponding viscosity calculated from tensile data for BUNA CB24.

Reprinted from N. Nakajima and Y. Yamaguchi, Journal of Applied Polymer Science, 1996, 61, 9, 1525. Copyright 1996, reprinted by permission of John Wiley and Sons, Inc.

The calculation of η_T for CB11, CB 22, and CB23 includes the modulus shift. The values of η_T are higher than those of $|\eta^*|$ for CB11 and CB24. These results indicate that the deformational modes are different for shear and extension. The η_T for CB11 and CB24 tends to converge with $|\eta^*|$ at the higher reduced rate, ie., at smaller deformation. With CB22 and CB23, the values of η_T agree with $|\eta^*|$. The above disagreement between η_T and $|\eta^*|$ indicates strain-induced crystallisation at the larger deformation. The rubber, CB11, was previously shown to give the strain-softening, and CB 24 neither softening nor hardening. The implication is that easily stretchable rubbers crystallise more easily upon straining. At present we do not know why strain-induced crystallisation does not appear as strain-hardening. The results of this work show that the effect of branching and that of strain-induced crystallisation are observable separately, the fact which is an obvious advantage in analysing the behaviour.

- *Experiment-II* [33]

- *Samples*

The samples used were four commercial polybutadienes, UBEPOL-VCR, produced by UBE Industries, see Table 6.5.

Table 6.5 Properties of UBEPOL-VCR Polybutadienes

Sample	**VCR309**[a]	**VCR412**[a]	**VCR617**[a]	**VCR512**[a]
Catalyst	Co	Co	Co	Co
$\overline{M}_w\ 10^{-4}$ [b]	45.9	45.1	46.2	44.2
$\overline{M}_n\ 10^{-4}$ [b]	17.1	18.4	17.6	15.5
$\overline{M}_w/\overline{M}_n$ [b]	2.7	2.5	2.6	2.9
SPB [c] (wt%)	9	12	17	12
MV [d]	39	45	63	43

Data supplied by the manufacturer
a: Registered trademark of UBE Industries
b: Data obtained by GPC; MW are not absolute but relative values based on the hydrodynamically equivalent volume of PS standards. The data represent the matrix polymer only.
c: The amount of syndiotactic 1,2-polybutadiene crystalline particles
d: Mooney Viscosity

These rubbers contain crystalline particles of syndiotactic 1,2-polybutadiene in the matrix polymer of *cis*-1,4-BR. The crystalline particle is composed of block copolymers of *cis*-1,4 butadiene/1,2-vinyl butadiene [34]. It has 80% crystallinity in the 1,2-polybutadiene domain and a melting point of 204 °C. The rubbers of VCR309, VCR412, and VCR617 have different amount of crystalline particles in the same matrix polymer. Although not shown in Table 6.5, VCR512 has a different matrix polymer that is more branched than the matrix polymer of other samples.

- *Results and discussion*

- *Oscillatory shear measurements*

The results of time-temperature superposition are shown in Figures 6.33 to 6.36, where all the data were reduced to 30 °C. All curves approach the plateau region at the higher frequencies.

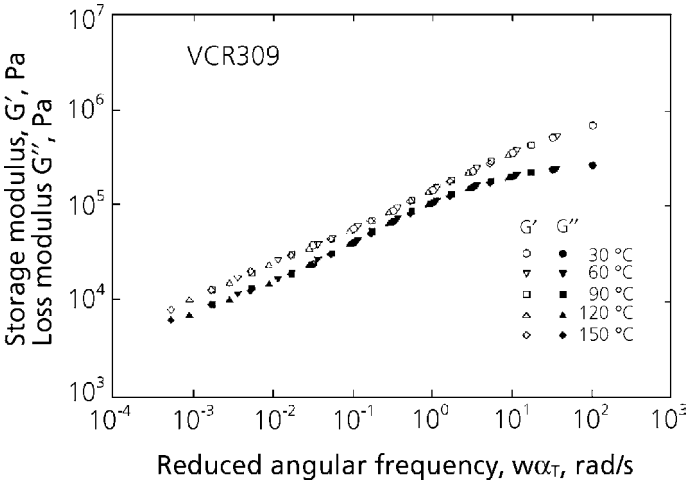

Figure 6.33 Master curves of storage and loss modulus of VCR309 (reference temperature is 30 °C).

Reprinted from N. Nakajima and Y. Yamaguchi, Journal of Applied Polymer Science, 1996, 62, 13, 2329. Copyright 1996, reprinted by permission of John Wiley and Sons, Inc.

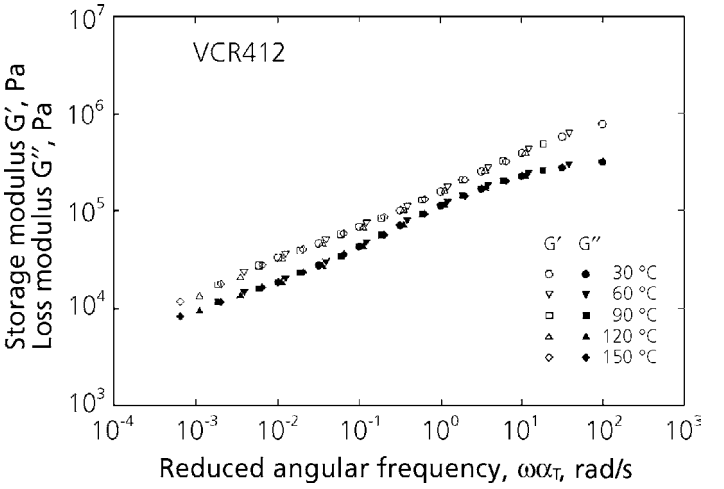

Figure 6.34 Master curves of storage and loss modulus of VCR412 (reference temperature is 30 °C).

Reprinted from N. Nakajima and Y. Yamaguchi, Journal of Applied Polymer Science, 1996, 62, 13, 2329. Copyright 1996, reprinted by permission of John Wiley and Sons, Inc.

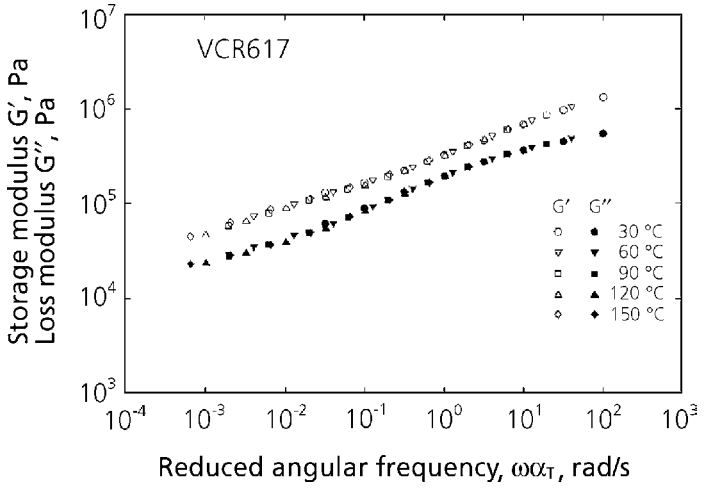

Figure 6.35 Master curves of storage and loss modulus of VCR617 (reference temperature is 30 °C).

Reprinted from N. Nakajima and Y. Yamaguchi, Journal of Applied Polymer Science, 1996, 62, 13, 2329. Copyright 1996, reprinted by permission of John Wiley and Sons, Inc.

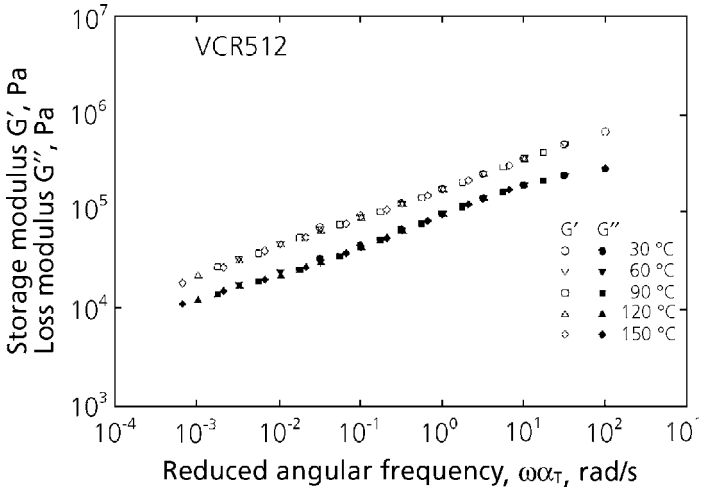

Figure 6.36 Master curves of storage and loss modulus of VCR512 (reference temperature is 30 °C).

Reprinted from N. Nakajima and Y. Yamaguchi, Journal of Applied Polymer Science, 1996, 62, 13, 2329. Copyright 1996, reprinted by permission of John Wiley and Sons, Inc.

However, these curves do not show the cross over of G´ and G´´. They are almost parallel to each other. This is because of the presence of the crystalline particles and branching in the matrix polymer.

Figure 6.37 shows log G´´ versus log G´ plot for all four rubbers.

The curves shift to the right with an increasing amount of crystalline particles. This indicates that the rubber becomes more elastic in the presence of the particles. The curve of VCR512 lies at the right side of that of VCR412 because the matrix polymer of the former is more branched than the matrix of the latter. The values of the shift factors, a_T and β_T are given in Table 6.6.

The a_Ts are sample dependent, and VCR309, which has the least amount of the crystalline particles, shows the highest temperature dependence among the rubber having the same matrix polymer. The rubber with a more branched matrix, VCR512, shows somewhat higher temperature dependence than that of VCR412. However, the differences of a_T diminish at the higher temperature. The observed values of β_T, see Table 6.6, are comparable to the values of $\rho_0 T_0/\rho T$. The temperature dependence of β_T decreases with the increasing particle content, and it almost disappears for VCR 617 between 30 and 90 °C. This may be the result of the difference in the thermal expansion coefficients of the matrix rubber and the crystalline particle.

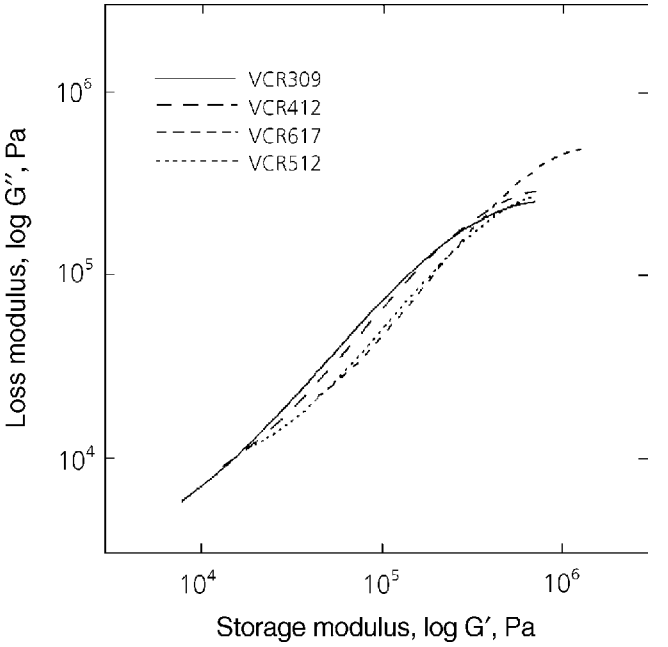

Figure 6.37 Comparison of log G˝ versus log G′ curves.

Reprinted from N. Nakajima and Y. Yamaguchi, Journal of Applied Polymer Science, 1996, 62, 13, 2329. Copyright 1996, reprinted by permission of John Wiley and Sons, Inc.

Table 6.6 Shift Factors, a_T and β_T

Temperature (°C) Sample	30	60	90	120	150
a_T					
VCR309	1	0.360	0.171	0.089	0.052
VCR412	1	0.388	0.186	0.111	0.064
VCR617	1	0.404	0.195	0.102	0.065
VCR512	1	0.325	0.178	0.104	0.067
β_T					
VCR309	1	0.906	0.830	0.731	0.665
VCR412	1	0.971	0.889	0.839	0.793
VCR617	1	1.000	1.000	0.879	0.855
VCR512	1	0.859	0.849	0.774	0.714
$\rho_0 T_0/\rho T$	1	0.910	0.835	0.771	0.716

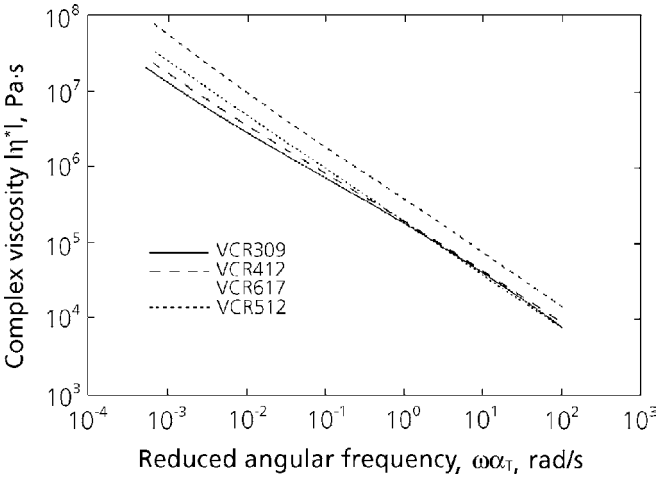

Figure 6.38 Comparison of master curves of complex viscosity VCR412 (reference temperature is 30 °C).

Reprinted from N. Nakajima and Y. Yamaguchi, Journal of Applied Polymer Science, 1996, 62, 13, 2329. Copyright 1996, reprinted by permission of John Wiley and Sons, Inc.

Figure 6.38 shows the absolute values of complex viscosity $|\eta^*|$ of the rubber at 30 °C. As observed in many commercial rubbers, these do not show the Newtonian region within the observed time scale because of their high MW, broad MW distribution, branching and the presence of the particles. Among VCR309, VCR412, and VCR617, the value of $|\eta^*|$ is higher for larger amount of the crystalline particles. At low frequencies, viscosity enhancement increases with increasing amount of crystalline particles. This is similar to the effect of the dispersed particles on viscosity. At low frequencies, the viscosity of VCR512 is higher than that of VCR412. As the frequency is increased, the curve of VCR512 crosses over the curve of VCR412. This is the result of VCR512 having more extensive branching than VCR412.

- *Tensile stress-strain measurements*

Figures 6.39 and 6.40 show tensile stress-strain curves of VCR412 and VCR617 at various deformation rates.

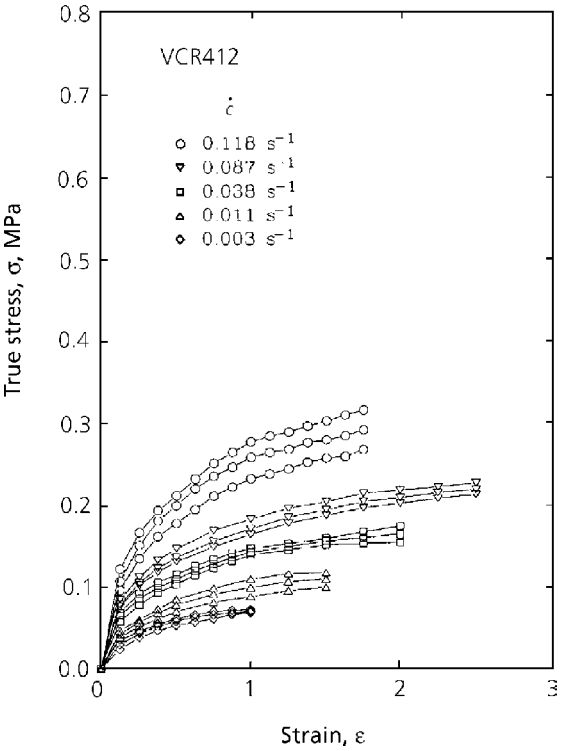

Figure 6.39 Tensile stress-strain curves of VCR412.

Reprinted from N. Nakajima and Y. Yamaguchi, Journal of Applied Polymer Science, 1996, 62, 13, 2329. Copyright 1996, reprinted by permission of John Wiley and Sons, Inc.

The stress σ is the true stress based on the deformed cross-section. Reproducibility shown in the figures is less than ±15%. The modulus increases with increasing deformation rates. It is higher for the higher amount of the crystalline particles. The stress-strain curves of the other samples are similar to those shown in Figures 6.39 and 6.40.

Figure 6.41 shows the plots of tensile modulus E(αt) against reduced time αt for VCR412, as given by Equation 6.27.

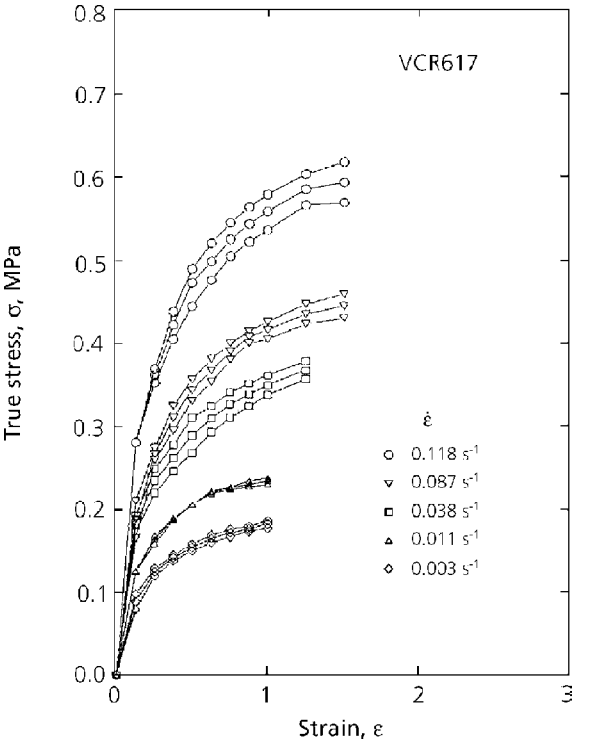

Figure 6.40 Tensile stress-strain curves of VCR617.

Reprinted from N. Nakajima and Y. Yamaguchi, Journal of Applied Polymer Science, 1996, 62, 13, 2329. Copyright 1996, reprinted by permission of John Wiley and Sons, Inc.

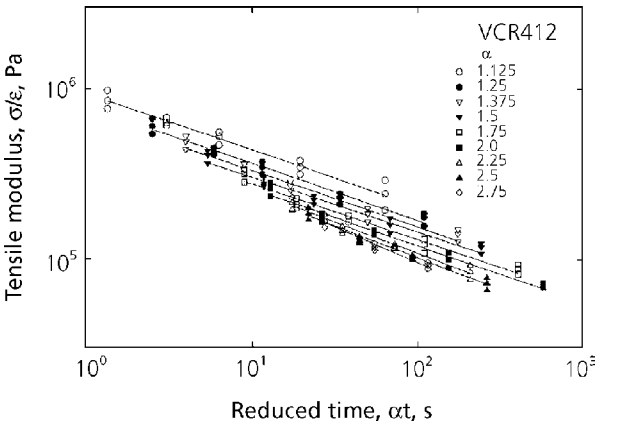

Figure 6.41 Tensile modulus as a function of reduced time at fixed extension ratios for VCR412.

Reprinted from N. Nakajima and Y. Yamaguchi, Journal of Applied Polymer Science, 1996, 62, 13, 2329. Copyright 1996, reprinted by permission of John Wiley and Sons, Inc.

In this figure, the lines connect the data at a constant value of α. Instead of forming a master curve, the data systematically change with α. The deviation is in the direction of strain-softening.

When the modulus shift, Equation 6.29 is applied, and master curves are formed for all rubbers, as in Figure 6.42 for VCR412.

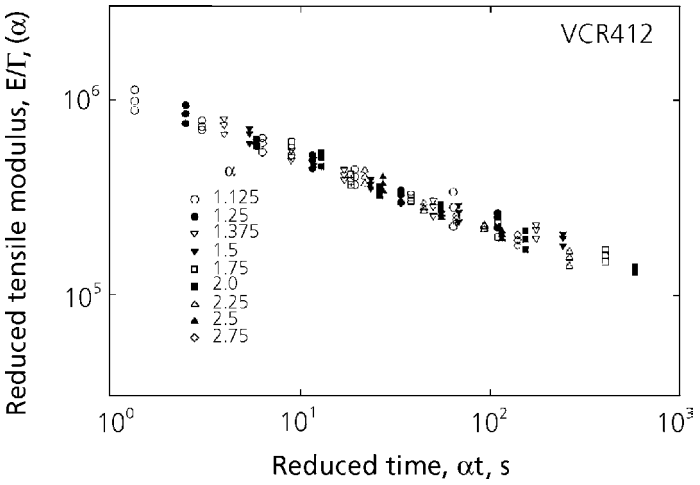

Figure 6.42 Reduced tensile modulus as a function of reduced time for VCR412.

Reprinted from N. Nakajima and Y. Yamaguchi, Journal of Applied Polymer Science, 1996, 62, 13, 2329. Copyright 1996, reprinted by permission of John Wiley and Sons, Inc.

Figure 6.43 shows the modulus shift $\Gamma(\alpha)$ as a function of the extension ratio.

The degree of the strain-softening increases with the increasing amount of the crystalline particles. As mentioned before, the crystalline particles consists of a block copolymer of *cis*-1,4-BR and 1,2-BR, the latter providing a crystalline morphology. The *cis*-1,4 chains presumably cover the surface of the particles, compatibilising the particles with the matrix rubber. A diffused boundary between the particle and the matrix was observed with transmission electron microscopy (TEM) for an ultrathin section [34]. Therefore, the *cis*-1,4 chains are like branches spreading out of the surface of the particles. When the branches are not long enough to give the entanglement constraints, they facilitated stretching by lubrication. Because the crystalline particles confer strain-softening, the branches on the particles are not long enough to give the entanglement constraints. This

is also evident since more particles give more strain-softening. Although VCR512 and VCR412 contain the same amount of the crystalline particles, the latter gives more strain softening than the former. The matrix polymer of VCR512 has longer branches than that of VCR412 such that the branching in the former is giving a constrained entanglement. The consequent strain-hardening tendency somewhat offsets the overall degree of the strain-softening from the crystalline particles.

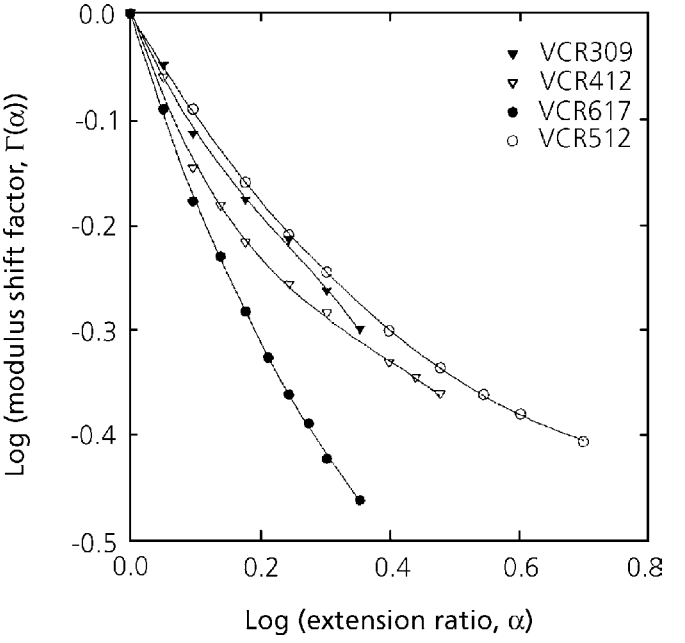

Figure 6.43 Modulus shift factor as a function of extension ratio.

Reprinted from N. Nakajima and Y. Yamaguchi, Journal of Applied Polymer Science, 1996, 62, 13, 2329. Copyright 1996, reprinted by permission of John Wiley and Sons, Inc.

Figures 6.44 to 6.47 show comparisons between the complex viscosity $|\eta^*|$ and the equivalent of shear viscosity η_T, calculated from the tensile stress-strain data.

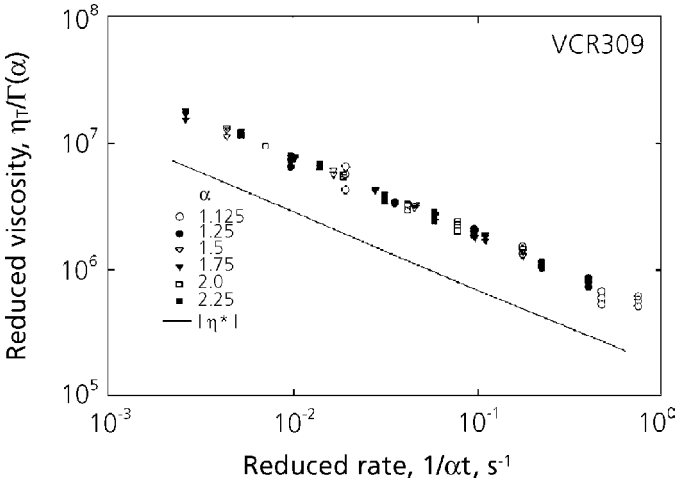

Figure 6.44 Comparison of shear complex viscosity with corresponding viscosity calculated from tensile data for VCR309.

Reprinted from N. Nakajima and Y. Yamaguchi, Journal of Applied Polymer Science, 1996, 62, 13, 2329. Copyright 1996, reprinted by permission of John Wiley and Sons, Inc.

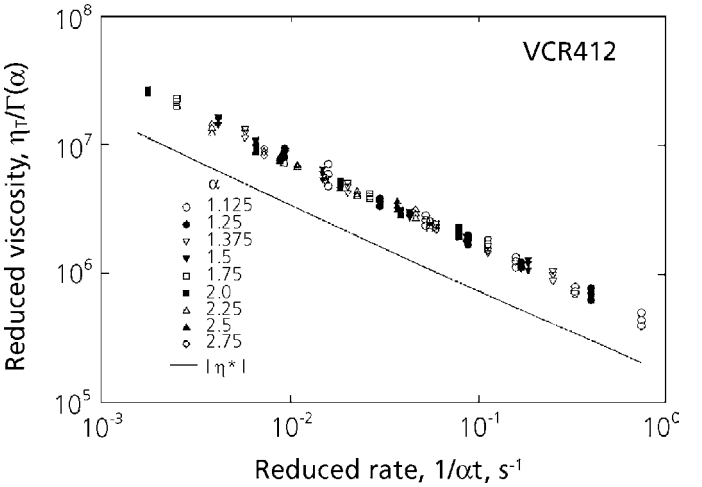

Figure 6.45 Comparison of shear complex viscosity with corresponding viscosity calculated from tensile data for VCR412.

Reprinted from N. Nakajima and Y. Yamaguchi, Journal of Applied Polymer Science, 1996, 62, 13, 2329. Copyright 1996, reprinted by permission of John Wiley and Sons, Inc.

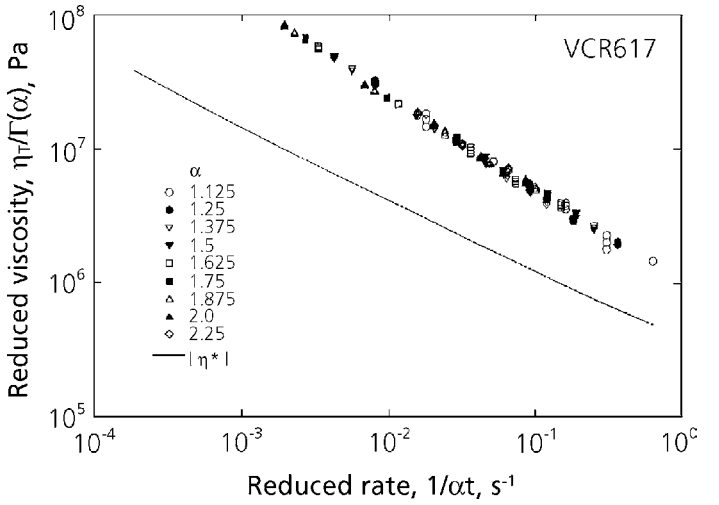

Figure 6.46 Comparison of shear complex viscosity with corresponding viscosity calculated from tensile data for VCR617.

Reprinted from N. Nakajima and Y. Yamaguchi, Journal of Applied Polymer Science, 1996, 62, 13, 2329. Copyright 1996, reprinted by permission of John Wiley and Sons, Inc.

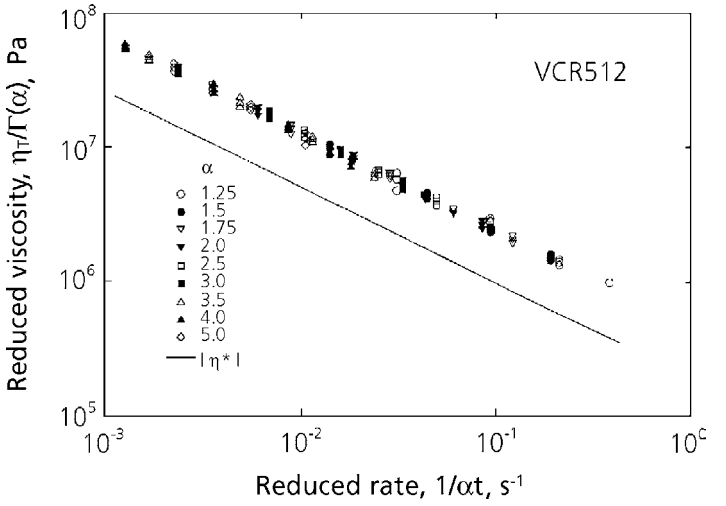

Figure 6.47 Comparison of shear complex viscosity with corresponding viscosity calculated from tensile data for VCR512.

Reprinted from N. Nakajima and Y. Yamaguchi, Journal of Applied Polymer Science, 1996, 62, 13, 2329. Copyright 1996, reprinted by permission of John Wiley and Sons, Inc.

The calculation of η_T includes the modulus shift. The curve of η_T is higher than the curves of $|\eta^*|$ for all rubbers. This indicates the strain-induced crystallisation of the matrix polymer at the large elongational deformation. The curves of η_T and $|\eta^*|$ for VCR309, VCR412, and VCR512 are almost parallel to each other. The curves for VCR617 are not parallel, and the difference becomes larger toward lower frequencies. This is because higher crystalline-particle content introduces higher strain-induced crystallisation, and the crystallisation is more significant at the large deformation, which corresponds to the lower frequency in this presentation. In Experiment I as well as this study, the strain-softening was found to facilitate the strain-induced crystallisation. This is contrary to what might be expected from the constraint against elongation, forcing the orientation of the chains, and thus enhancing the crystallisation. The exact mechanism of strain-induced crystallisation requires further study.

- *Experiment-III* [35]

- *Samples*

The gum rubber samples used are listed in Tables 6.3 and 6.5. They may be classified into three groups:

1. Titanium-polymerised rubber, CB11, is the most branched. However, the branches are relatively short. The rubber gives strain-softening and strain-induced crystallisation upon stretching [30].

2. Neodymium-polymerised rubbers, CB22, CB23 and CB24, have low degrees of branching compared to CB11. However, the branches are longer; long enough to give a 'constrained' entanglement. It results in strain-hardening when the degree of branching is relatively high, i.e., CB22 and CB23. They do not give strain-induced crystallisation. The least branched rubber, CB24, gave neither softening nor hardening [30], but gave strain-induced crystallisation.

3. Cobalt-polymerised rubbers, VCR309, VCR412, VCR617 and VCR512, contain dispersed crystalline particles of 1,2-polybutadiene [34]. The first three have different amounts of particles in the same matrix rubber. The matrix rubber of VCR512 has more long branches than that of VCR412. The crystalline particles are made up of a block copolymer of *cis*-1,4 and 1,2-butadiene [34]. The crystalline particles cause strain softening. The extent of strain-softening is lessened in VCR512 because the branching of the matrix is long enough to give the 'constrained' entanglement resulting in strain-hardening. All VCRs gave strain-induced crystallisation [33].

The compounds were made from these rubbers with the addition of 50 phr N330 carbon black from Cabot.

- *Mixing and milling*

A Banbury-type internal mixer with a 250 ml capacity was used for mixing the compounds. The fill factor was 0.7 and the rotor speed was 100 rpm. After mastication of the rubber for 1 minute, carbon black was added over a period of 1 minute. After an additional 2 minutes, the compound was dumped. All dumped compounds were crumbly and a small amount of the free filler remained. After dumping, the compounds were immediately milled with a 6-inch two-roll mill in order to develop further mixing and to observe mill processability. Photographs (see Figures 6.48-6.57) of the rubber on the mill were taken after milling for 2 minutes. The speed of the fast roll was 28 rpm and the friction ratio was 1:1.26.

- *Results*

When CB11 gum was loaded on the mill, it broke into many pieces, which required recharging. The process was repeated several times until a band was formed. The band was loose and sagging as shown in Figure 6.48(a). After taking the photograph, the band was pushed up against the roll in an attempt to make a tight band. The band sagged again if not pushed up and tore at many places as shown in Figure 6.48(b). The CB11 compound did not make a band and crumbled after passing through mill; therefore, no photograph is shown. With CB22, CB23, and CB24, the gum rubbers formed bands immediately after loading. The bands are as shown in Figures 6.49-6.51. The surface of CB22 had a rough texture, that of CB24 was smooth, and that of CB23 was intermediate. The stickiness was observed with all three, but observed least with CB22, more with CB23, and the most with CB24. When the band was cut and the sheet was pulled, CB22 was the most elastic, giving a large mill-shrinkage. The elasticity decreased in the order from CB22 through CB23 to CB24. The CB22, CB23, and CB24 compounds made smooth bands, which were loose on the mill and sagging somewhat, see Figure 6.52.

VCR309, VCR412, and VRC617 made smooth bands immediately after charging as shown in Figures 6.53-6.55. For VCR512, although it did not break into pieces, the band sagged. When it was pushed against the roll, the band was torn, see Figure 6.56, but the tearing was not as extensive as that in the case of CB11. The bands were not sticky; when the sheet was cut and pulled out, there was no appreciable elastic tension. The VCR309, VCR412, VCR617, and VCR512 compounds made tight bands, of which VCR412 and VCR617 had a slight tear, see Figure 6.57.

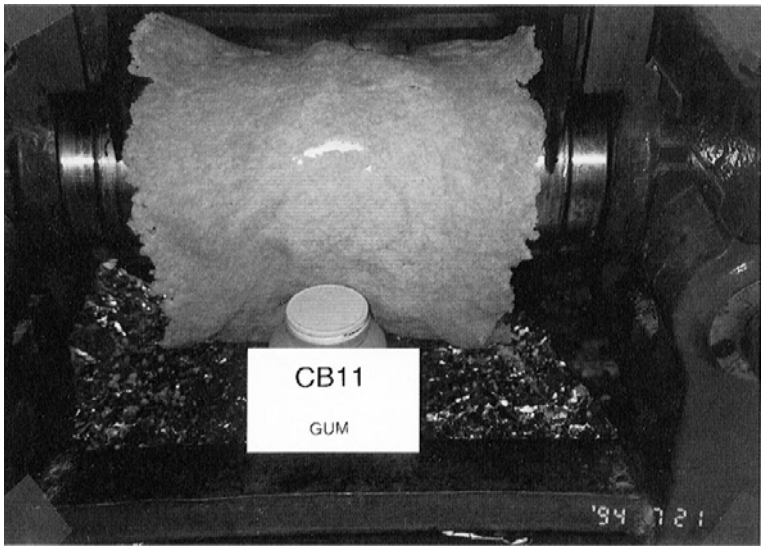

Figure 6.48 a) Photograph of CB11 gum rubber on the mill.

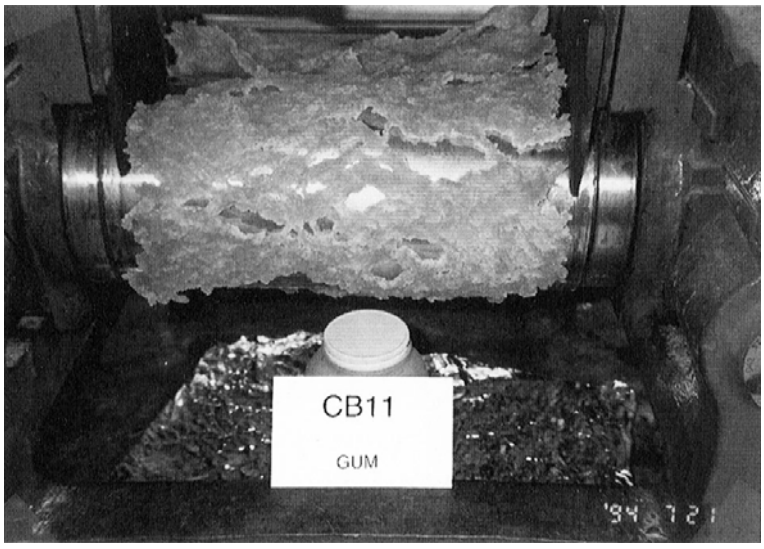

Figure 6.48 b) Photograph of CB11 gum rubber on the mill.

Figure 6.49 Photograph of CB22 gum rubber on the mill.

Reprinted from N. Nakajima and Y. Yamaguchi, Journal of Applied Polymer Science, 1997, 65, 10, 1995. Copyright 1997, reprinted by permission of John Wiley & Sons, Inc.

Figure 6.50 Photograph of CB23 gum rubber on the mill.

Reprinted from N. Nakajima and Y. Yamaguchi, Journal of Applied Polymer Science, 1997, 65, 10, 1995. Copyright 1997, reprinted by permission of John Wiley & Sons, Inc.

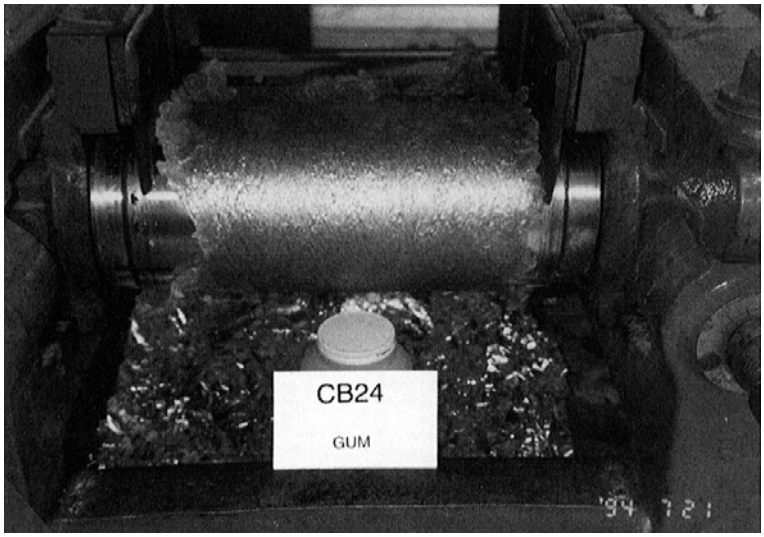

Figure 6.51 Photograph of CB24 gum rubber on the mill.

Reprinted from N. Nakajima and Y. Yamaguchi, Journal of Applied Polymer Science, 1997, 65, 10, 1995. Copyright 1997, reprinted by permission of John Wiley & Sons, Inc.

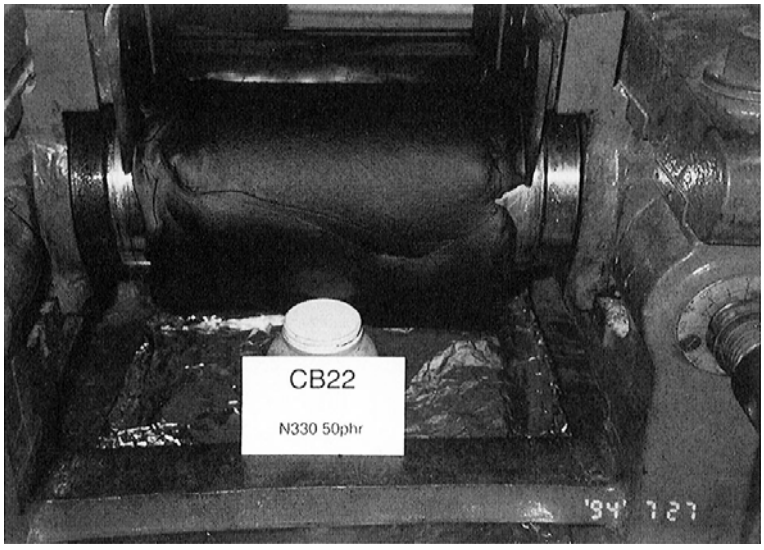

Figure 6.52 Photograph of CB22 carbon black-filled compound on the mill.

Reprinted from N. Nakajima and Y. Yamaguchi, Journal of Applied Polymer Science, 1997, 65, 10, 1995. Copyright 1997, reprinted by permission of John Wiley & Sons, Inc.

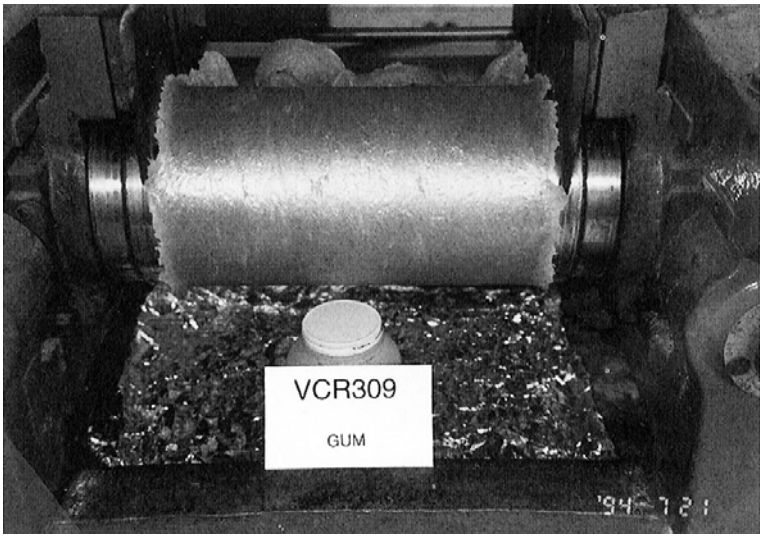

Figure 6.53 Photograph of VCR309 gum rubber on the mill.

Reprinted from N. Nakajima and Y. Yamaguchi, Journal of Applied Polymer Science, 1997, 65, 10, 1995. Copyright 1997, reprinted by permission of John Wiley & Sons, Inc.

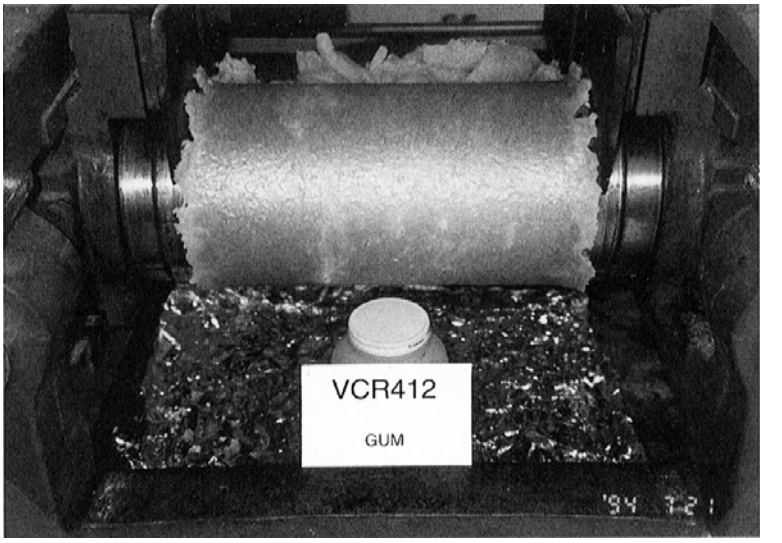

Figure 6.54 Photograph of VCR412 gum rubber on the mill.

Reprinted from N. Nakajima and Y. Yamaguchi, Journal of Applied Polymer Science, 1997, 65, 10, 1995. Copyright 1997, reprinted by permission of John Wiley & Sons, Inc.

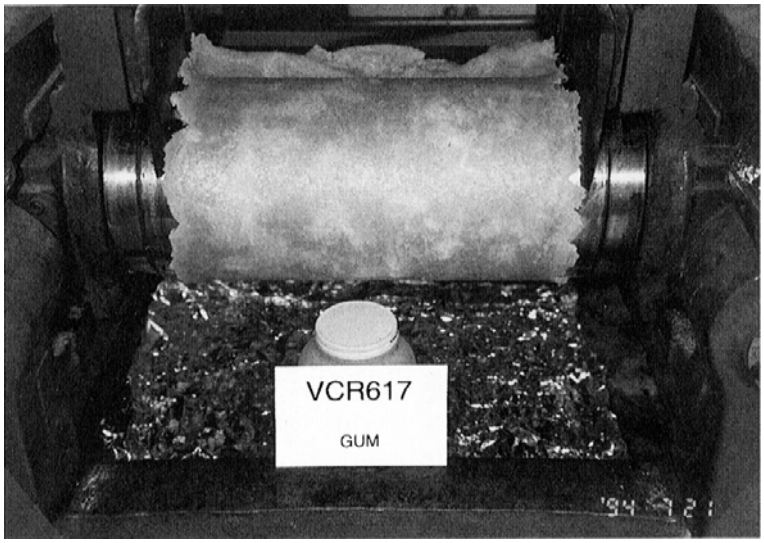

Figure 6.55 Photograph of VCR617 gum rubber on the mill.

Reprinted from N. Nakajima and Y. Yamaguchi, Journal of Applied Polymer Science, 1997, 65, 10, 1995. Copyright 1997, reprinted by permission of John Wiley & Sons, Inc.

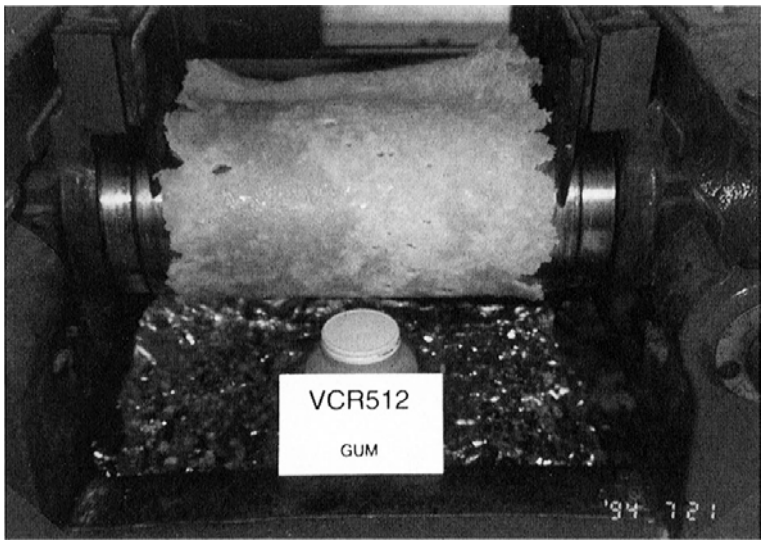

Figure 6.56 Photograph of VCR512 gum rubber on the mill.

Reprinted from N. Nakajima and Y. Yamaguchi, Journal of Applied Polymer Science, 1997, 65, 10, 1995. Copyright 1997, reprinted by permission of John Wiley & Sons, Inc.

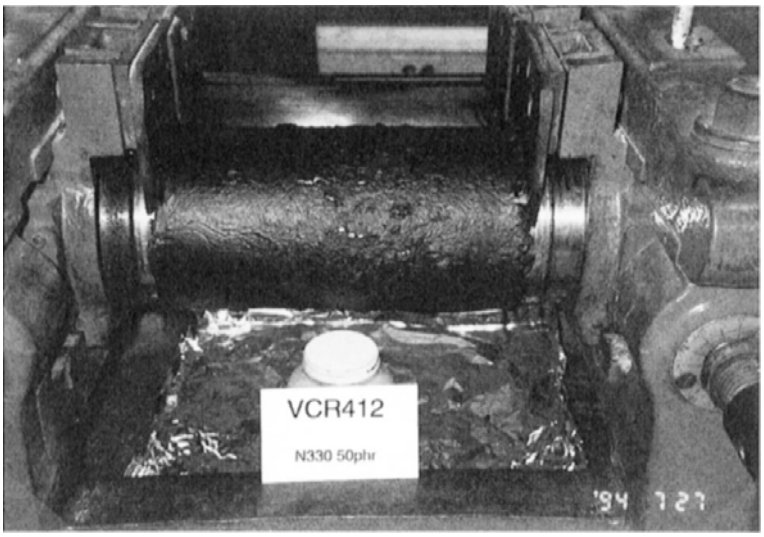

Figure 6.57 Photograph of VCR412 carbon black-filled compound on the mill.

Reprinted from N. Nakajima and Y. Yamaguchi, Journal of Applied Polymer Science, 1997, 65, 10, 1995. Copyright 1997, reprinted by permission of John Wiley & Sons, Inc.

- *Discussion*

Although CB11 gum broke into many pieces on charging, it is not likely to be processing in Region I, because the rubber is not stiff, and when the band was eventually formed, it behaved more as in processing Region III. If it had been in Region I, it would have moved to Region II eventually. As shown in Figure 6.58, CB11 gum has a rather high rate-dependence (for other CB rubbers, refer to the original articles [30]). From the principle of time-temperature correspondence, we also expect a relatively high temperature dependence. This was already observed in the dynamic measurements [30], where this rubber had highest values of the temperature shift factor, a_T. When the rate decreased, the strain at break decreased significantly, meaning that when the temperature increases, the strain at break also decreases, going into Region III. The high-temperature dependence comes from the high degree of branching. The nature of the difficulties in milling of CB11 gum rubber and its compound are from the same origin. Although CB11 gum rubber gave strain-induced crystallisation in tensile tests, it did not help the processability. When the rubber is in Region III, there is insufficient tension to cause the crystallisation.

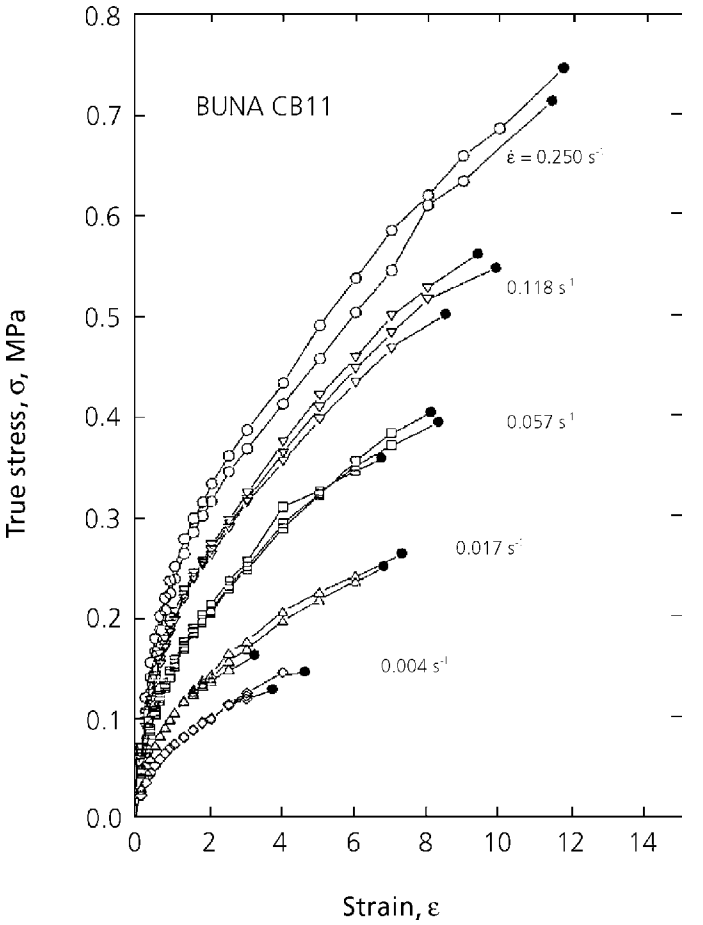

Figure 6.58 Tensile stress-strain curves of CB11 gum rubber.

Reprinted from N. Nakajima and Y. Yamaguchi, Journal of Applied Polymer Science, 1997, 65, 10, 1995. Copyright 1997, reprinted by permission of John Wiley & Sons, Inc.

The stickiness of gum rubbers CB22, CB23, and CB24, indicates that they were in Region IV on the mill. When the carbon black was added, stickiness was no longer observed. Because the stickiness was the reason for forming the band in Region IV, the compound became loose from the surface of the roll. Also, in Region IV, there is insufficient tension to cause strain-induced crystallisation for CB24, which crystallises in a tensile test. With VCR309, VCR412, VCR617 and VCR512, the gum rubbers were in Region II, bordering toward Region III, exhibiting slight sagging and tearing in some cases but not sticky. Consequently, the compounds made tight bands, but showed slight tearing. VCR512 gum showed a relatively large rate-dependence in the stress-strain measurement compared to those of other VCRs. This is similar to the behaviour of CB11 as compared to the

other CB rubbers. It implies the higher-temperature dependence as well. This explains the fact that VCR512 tends to move toward Region III as the rubber becomes warmer on the mill. This is seen as a slight sagging and a slight tearing, see Figure 6.56, whereas no sagging or tearing occurred with other VCRs. In contrasting three types of gum rubbers, which are represented by CB11, CB22, and VCR412, a clear-cut differentiation may be made about their mill behaviour. CB11 was in Region III, CB22 type was in Region IV and VCR412 type was in Region II. This ordering is related to the modulus level at the very low frequency region in the dynamic shear measurements [30, 33]. The lower-frequency region of the data represent the higher temperature behaviour, which is encountered in milling. Evidently, the added crystalline particles are most effective in raising the modulus at the low frequency as shown with VCR rubbers. A degree of branching is more effective than is a relative length of branching with respect to the modulus level, CB11 versus CB22. However, if a sticky band, Region IV, is preferred over a sagging band, Region III, CB22 is said to be easier for milling than is CB11.

Among the three neodymium-polymerised rubbers, CB22 had the highest degree of branching, followed by CB23, and CB24 was the least branched. Because branching makes rubber more elastic, it explains the roughest texture and least stickiness of CB22 among the three. CB22 was most elastic when pulled from the mill and showed a large mill shrinkage. The difference in CB23 and CB24 may be explained similarly on the basis of the difference of the degree of branching.

Concerning VCR309, VCR412, and VCR617, there was no significant difference in mill behaviour among these gum rubbers and also among their compounds, meaning that, within the present variation in the amount of the crystalline particles, no difference was detected in the milling. In detail, however, a significant number of white spots appeared in the band of VCR617, a little in that of VCR412, and none in that of VCR309, see Figures 6.53-6.55. The white spots gradually disappeared when the sheets were removed from the mill and left to relax. The white spots appear to be the strain-induced crystalline domains.

Previously, it was noticed with the matrix rubber [33] that in the presence of the larger amount of the crystalline particles there was an indication of more strain-induced crystallisation. Among the samples that we examined, the three rubbers of the VCR series were the only ones, which gave an indication of strain-induced crystallisation in milling. This means that in order for the gum rubber and the compound to have strain-induced crystallisation during milling the material must be under sufficient tension, i.e., Region II.

The mill behaviour of the compounds with respect to the four regions of processability was readily explained from the mill behaviour of the matrix rubber. Within the

structural variables investigated in this study, both gum rubbers and the corresponding compounds were in the same region of mill processability.

6.7.2 Polyethylacrylate

The next example is ACM, which has a rather high T_g of –14 °C, but it tends to fall in the Region III or IV of mill processability, because it is a relatively short and fat molecule. This polymer is made via emulsion polymerisation with a free radical initiator. Therefore, the presence of macrogel is one of the concerns. In one of the samples a difunctional co-monomer was used for providing a cure site. It presents a possibility of forming microgels. Effects of these structural variables on the viscoelastic behaviour and processability are examined.

It is a common occurrence in industry that two elastomers, overall very similar, behave differently on the mill. Sometimes, they are the same grade of material made for the same specification. Other times they are similar but made with some known difference. In either case it is necessary to relate the observed difference in processability with the difference in the molecular architecture of the polymers. Further, such a molecular difference must be related to the difference in the manufacturing process. This work is an example of such an activity, where the rheological analyses have played key roles. Two commercial ACMs, one having an epoxide (EP) crosslinking site and the other ethylidene norbornene (ENB), were used for this study. The dynamic shear oscillation measurements at very small strain were used to characterise the viscoelastic properties. The tensile stress-strain measurements at several different deformation rates were used to characterise the large deformation behaviour. These data were systematically analysed to explain the difference in mill processability. They were also used to pin-point major differences in long branching and gel structure, which impart a dominant influence on rheology and hence, processability. The gel determination was made by filtration in order to support the rheological findings. The dilute solution techniques were not used, because such results would only pertain to the soluble fraction of the polymer.

- *Experimental*
- *Samples*

The samples were two commercial ACMs having a Mooney index of about 50 [14]. The carbon black used for the mill processability was a standard N330 [37]; 50 parts per 100 parts of rubber by weight was used.

The sheets of gum elastomers were prepared in a picture frame between two polished stainless steel plates. The pressing was done at 160 °C for 20 minutes. A mould release agent was used. The sheets were cooled in the press. After removing from the press, the sheets were placed between two steel plates with 10.5 kg weight placed on top. The sheets were allowed to rest for 3 days under the weight to prevent wrinkling. Tensile specimens were cut from the sheets using ASTM D412 dumbbell die C [31].

The gel content of each sample was determined by dissolving about 0.4 g of material in 100 ml of methyl ethyl ketone, and stirring on a magnetic stirrer for 24 hours. The solution was filtered through a Whatman No. 4 filter paper. The filtered paper was weighed before and after filtering to determine the amount of gel removed from the solution. The filtered solution was evaporated and the amount of dissolved polymer was determined. The gel contents before and after pressing are given in Table 6.7.

Table 6.7 Samples and Gel Content

Sample	Before pressing (% Gel)	After pressing (% Gel)
EP	9.4	15.9
ENB	71.4	66.6

- *Instruments*

- *Viscoelastic measurement*

The viscoelastic properties were measured with a Rheometrics mechanical spectrometer in the oscillation mode. The frequency range was from 10^{-2} to 10^{2} rad/s. Samples were tested at 25, 60, 100 and 150 °C.

- *Tensile stress-strain measurement*

Tensile tests were performed on a Monsanto Tensometer 500. The practical upper limit of crosshead speed was 0.847 cm/s and the lower limit was 0.0359 cm/s. The speed was calibrated by measuring with a stopwatch the time required for the crosshead to travel a set distance measured with a measuring tape. This was double checked by measuring the time required to elongate the specimen an additional 100% as measured by the strip chart recorder. A Monsanto extensometer designed for use with the Tensometer 500 was

used to record the strain directly as a percentage. The strip chart recorder was equipped with an area compensator so that all stress data were recorded as force per unit original cross-sectional area of the sample. The force was measured by a 45 kg load cell. The samples were held by roller grips. The tensile test was performed at 25 °C and ambient humidity conditions using strain rates of 0.177, 0.0872, 0.0441 and 0.00775 s^{-1}. These strain rates encompass the practical operating conditions of the tester.

- *Mill processability*

A Stewart-Bolling laboratory mill of 152 mm diameter and 305 mm width, was used to evaluate the mill processability. The speed of the fast roll was 29 rpm and the friction ratio was 1:1.25. The mill rolls were cooled by circulating city water.

- *Results*

Figure 6.59 is the comparison of viscoelastic properties of the two polymers at 25 °C. Both storage modulus, G′ and loss modulus, G″ are very similar for the two samples, except at the higher frequency the moduli of the ENB polymer are lower than those of the EP polymer. From this limited data no significant information on the molecular structure can be extracted.

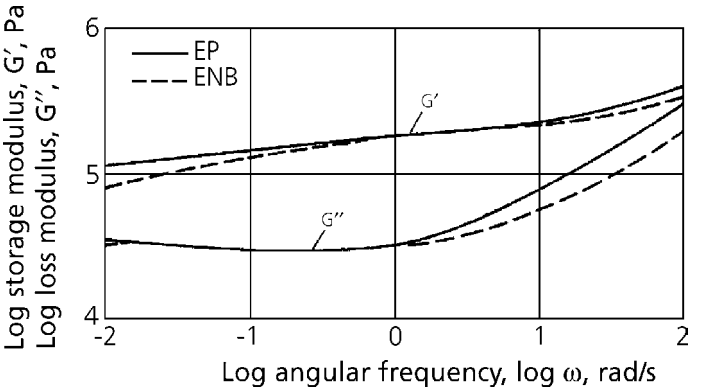

Figure 6.59 Storage and loss modulus of EP and ENB ACM at 25 °C.

Reprinted with permission from N. Nakajima, R. A. Miller and E. R. Harrell, International Polymer Processing, 1987, 2, 2, 87. Copyright 1987, Hanser Publishers.

Figures 6.60 and 6.61 are G´ and G´´ curves which are extended to lower frequencies with the aid of the temperature reduction scheme [6] using the data obtained at 60, 100 and 150 °C. At the reduced frequency, lower than 10^{-3} rad/s, there are significant differences in the behaviour of two samples. The G´ and G´´ curves of the EP polymer

begins to turn downward and assume a slope higher than those of the ENB polymer. This indicates that there are differences in the size and amount of the largest species contained in the samples. Here, the term, species, is used instead of MW in order to include gels. Another important difference is that the G′ and G″ curves of the EP polymer cross over, G′ becoming lower than G″ at $\omega<10^{-5}$ rad/s. However, with the ENB polymer the G′ is above G″ and the two curves are almost parallel to each other. This behaviour indicates that the ENB polymer contains much more gel than the EP polymer. The gel-content data in Table 6.7 support this finding. Figure 6.62 shows log G″ versus log G′ plots of the EP and ENB polymers. The curve of the ENB polymer lies at the right side of that of EP polymer; this indicates that ENB polymer contains more gel than the EP polymer.

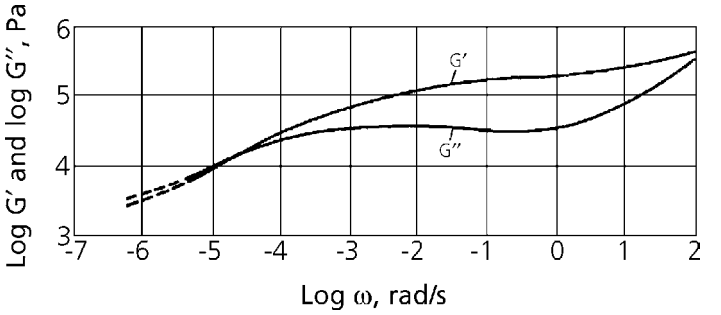

Figure 6.60 Storage and loss modulus as functions of angular frequency. EP ACM data reduced to 25 °C.

Reprinted with permission from N. Nakajima, R. A. Miller and E. R. Harrell, International Polymer Processing, 1987, 2, 2, 87. Copyright 1987, Hanser Publishers.

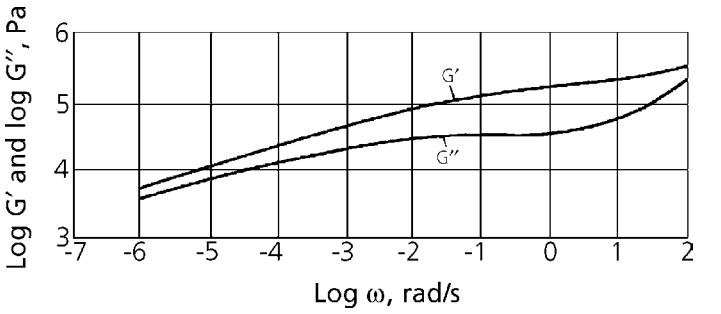

Figure 6.61 Storage and loss modulus as functions of angular frequency. ENB ACM data reduced to 25 °C.

Reprinted with permission from N. Nakajima, R. A. Miller and E. R. Harrell, International Polymer Processing, 1987, 2, 2, 87. Copyright 1987, Hanser Publishers.

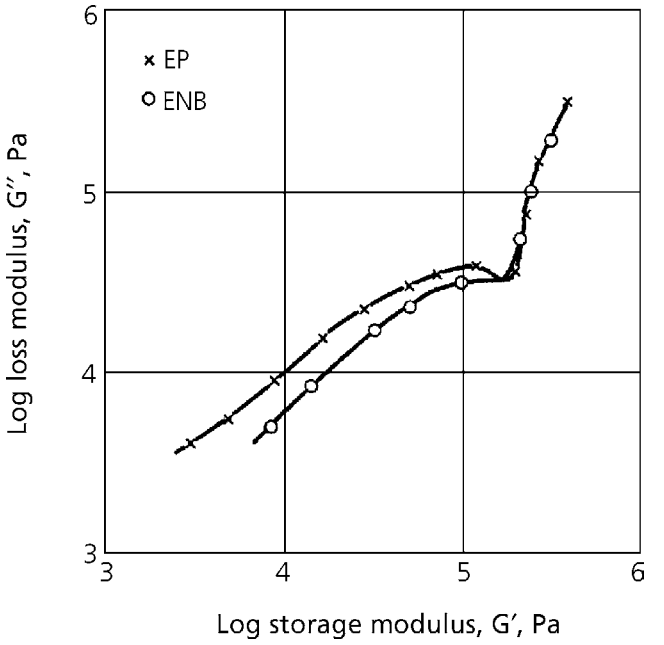

Figure 6.62 Modified Cole-Cole plots of EP and ENB ACM.

Reprinted with permission from N. Nakajima, R. A. Miller and E. R. Harrell, International Polymer Processing, 1987, 2, 2, 87. Copyright 1987, Hanser Publishers.

The tensile stress-strain data obtained at the previously mentioned four deformation rates have been converted to viscosity as a function of $(1/\alpha t)$. The data are presented in Figures 6.63 and 6.64, as $(\eta_T/3)$. The data points do not fall on one curve for the EP polymer, except for the shorter time range, at the right hand side of the figure. The deviations are systematic in that a higher deformation rate gives a higher viscosity. The difference appears to increase for the longer time, at the left hand side of the figure.

With the ENB polymer the data points fall on one curve, although some deviation of points similar to that of the EP polymer occurs. It can be concluded that the strain-time correspondence principle applies approximately to this sample. From the preceding argument, the gel particles in the ENB polymer must be microgels. On the other hand the EP polymer appears to contain long branching and macrogel.

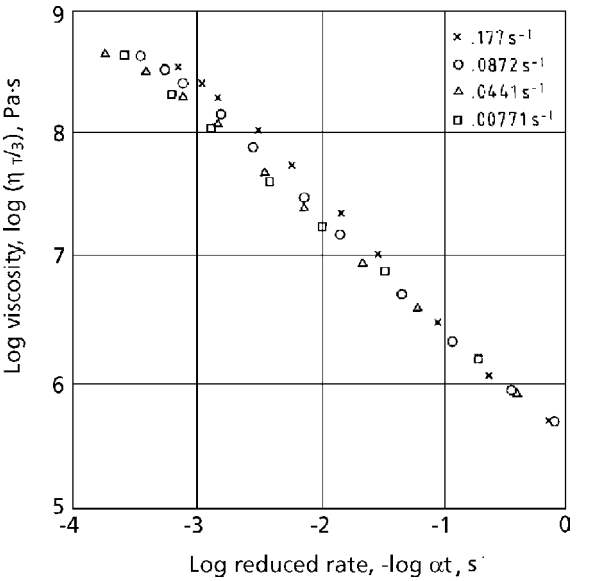

Figure 6.63 Viscosity evaluated from tensile stress-strain measurements; no formation of master curve, showing inapplicability of strain-time correspondence principle, EP ACM.

Reprinted with permission from N. Nakajima, R. A. Miller and E. R. Harrell, International Polymer Processing, 1987, 2, 2, 87. Copyright 1987, Hanser Publishers.

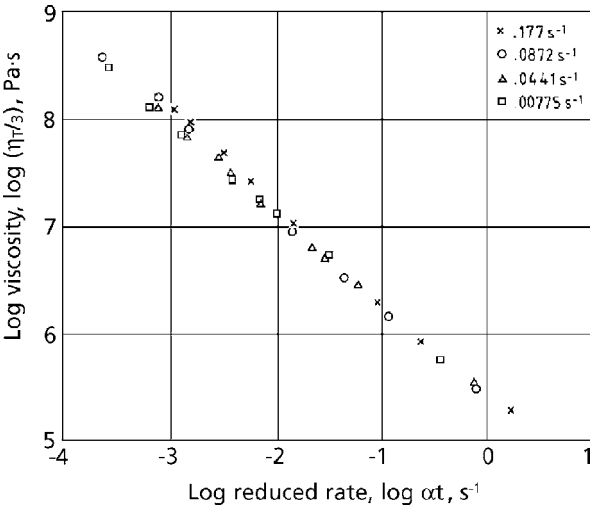

Figure 6.64 Viscosity evaluated from tensile stress-strain measurements; formation of master curve through application of strain-time correspondence principle, ENB ACM.

Reprinted with permission from N. Nakajima, R. A. Miller and E. R. Harrell, International Polymer Processing, 1987, 2, 2, 87. Copyright 1987, Hanser Publishers.

In Figure 6.65 the data of Figure 6.63 and 6.64 are plotted as modulus-reduced time ($1/\alpha t$) curves. The data had been interpolated at fixed extension ratios of $\alpha = 2$, 4, and 6. With the EP polymer the modulus data do not fall on one curve so that the strain-time correspondence does not apply. The modulus tends to be higher at the higher extension ratio, indicating strain-hardening. Therefore, the EP sample contains long branching and macrogel. On the other hand with the ENB polymer the modulus is independent of the extension ratio and a function of reduced time only. This means that the gel contained in this polymer is microgel.

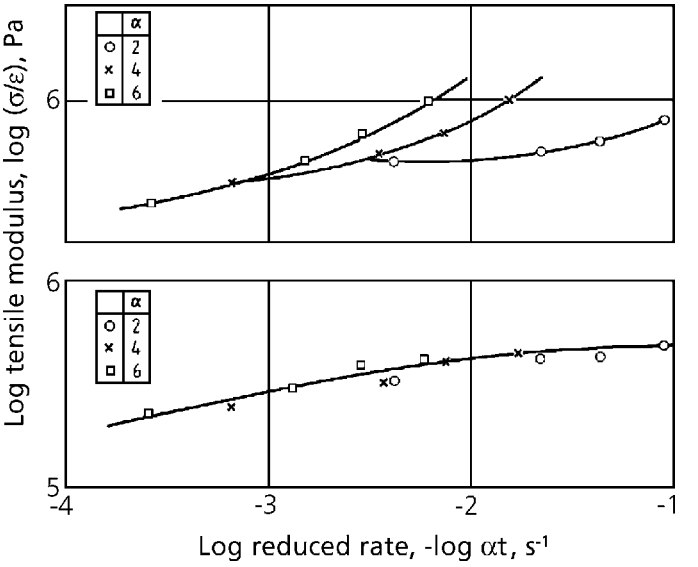

Figure 6.65 Modulus at equal strain observed at different deformation rates plotted as function of reduced time; strain hardening for EP sample (above) and no strain hardening for ENB sample (below).

- *Discussion*
- *Mill processability and viscoelastic properties*

Figure 6.66 (left and right) are photographs, illustrating the major differences in processability.

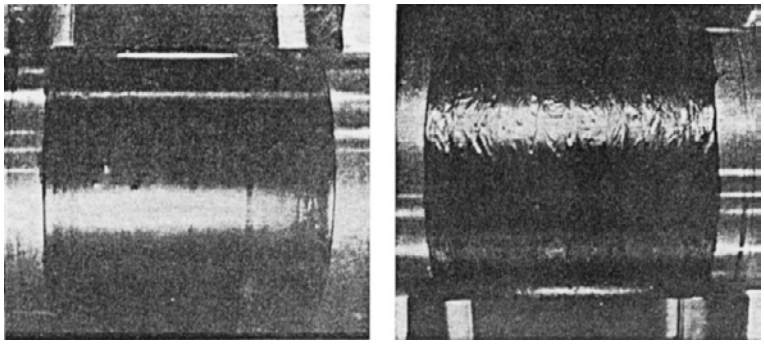

Figure 6.66 Banding characteristics of EP (right) and EMB (left) polyethacrylate at 150 °C.

Reprinted with permission from N. Nakajima, R. A. Miller and E. R. Harrell, International Polymer Processing, 1987, 2, 2, 87. Copyright 1987, Hanser Publishers.

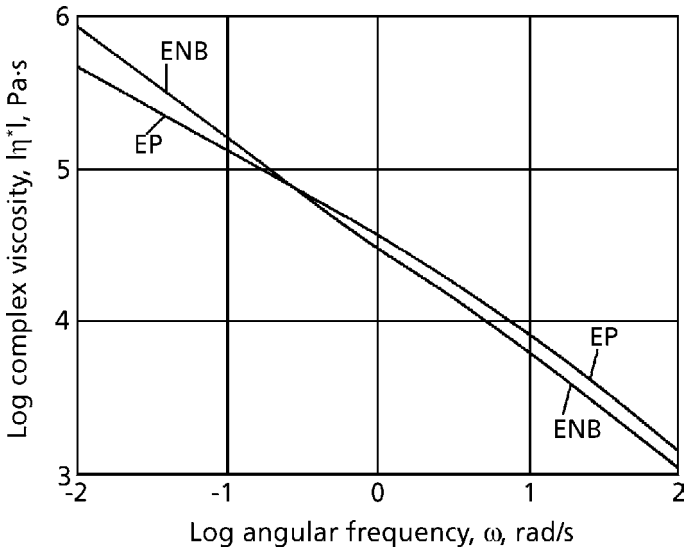

Figure 6.67 Complex viscosity-angular frequency curves of EP and ENB at 150 °C.

Reprinted with permission from N. Nakajima, R. A. Miller and E. R. Harrell, International Polymer Processing, 1987, 2, 2, 87. Copyright 1987, Hanser Publishers.

Whereas, the ENB polymer formed a smooth band around the roll and presented no problem in incorporating carbon black, the EP polymer became sticky and partially transferred into the backroll. There is a clear difference in the mill processability [28]. The ENB polymer exhibited Region II behaviour, which was a highly extensible, elastic state and best suited for mill processing. On the other hand the EP polymer was in Region IV, which was a flow state like a plastic melt. The relative difference in the behaviour may be understood by comparing the data of Figures 6.60 and 6.61 at the lower end of the frequency. Also, the same data at 150 °C are reproduced as the complex viscosity, $|\eta^*|$ as a function of ω, see Figure 6.67. At the lower frequency the viscosity of the EP polymer is lower than that of the ENB polymer. It should be remembered that polyethylacrylate polymer has 73% of its MW in the pendent, ester group [36]. Therefore, it is a relatively short chain for a given MW, with a larger cross-section compared to diene-rubbers, for example. This makes the polymer readily go to the molten state, when the temperature increases. The presence of microgel is known to introduce long relaxation times [38] such that the above undesirable tendency may be overcome. These results of the mill processability depend upon the temperature and the deformation rate; a higher rate corresponds to a lower temperature. Since our mill does not have a precise temperature control, the first batch starts at a lower temperature. The mill-mixing was conducted on different days; one day ENB was milled first and then EP. On another day it was in the reverse order. Although the EP polymer became sticky in both cases, it was less sticky when started with a colder mill.

- *Mechanisms of gel formation*

An inherent tendency for the polyethylacrylate to form long branching and gel has already been discussed in Section 1.1.6. In addition, the data of Table 6.7 show that the EP polymer crosslinked during pressing at 160 °C for 20 minutes. The gel content increased from 9.4 to 15.9%. This must have contributed to the strain-hardening tendency shown in Figure 6.65.

In the polymerisation of the ENB polymer, ENB is copolymerised to give a crosslinkable site. Since ENB is a difunctional monomer, it is hoped that only one functional group is incorporated into polymer chain. However, there must be a finite probability that the second functional group also becomes incorporated in the chain. This reaction leads to the microgel formation.

- *Temperature dependence of viscoelastic property*

The temperature shift factors found in shifting the observed curves of G´ and G´´ are given in Table 6.8. For the accuracy of superposition, the curves of G´ and G´´ are shifted together. The time shift factor, a_T and modulus shift factor, β_T are both based on 25 °C, T_0 = 298 K. The WLF constants [6], C_1 and C_2 are also given in Table 6.8:

$$-\log a_T = \frac{C_1(T - T_0)}{C_2 + (T - T_0)} \tag{6.40}$$

As far as the time-shift factor, a_T, is concerned, the EP polymer has a higher temperature-dependence, compared to the ENB polymer. This difference is apparent in the C_2 values, C_1 values being approximately equal. This result is similar to the temperature dependence of branched EPDM and linear EPM elastomers [39], where the branched elastomer had a higher temperature-dependence.

Table 6.8 Temperature Dependence of Viscoelastic Properties

Sample	Temperature °C	a_T	β_T	C_1	C_2
EP	25	1.0	1.0	10.0	160
	60	1.7×10^{-2}	0.86		
	100	6.2×10^{-4}	0.82		
	150	6.3×10^{-5}	0.82		
ENB	25	1.0	1.0	11.4	227
	60	3.2×10^{-2}	0.92		
	100	1.2×10^{-3}	0.85		
	150	1.4×10^{-4}	0.83		

However, the present case is more complicated because the EP sample contains macrogel and the ENB sample contains microgel. Therefore, we cannot readily draw an analogy to the result of the previous study.

The modulus shift, β_T, is relatively small and subject to a proportionally large error. However, the shift is required for the superposition. This is in contrast to previous work with EPM and EPDM elastomers where such a shift was not required. The value of β_T decreases with increasing temperature; the extent of decrease is similar to what is expected from the theory, $\rho_0 T_0/\rho T$. However, this subject is not pursued any further, since it is somewhat outside the scope of the present study.

6.8 Linear viscoelasticity

The linear viscoelasticity is a well established science and textbooks are available for understanding theories and practices. Therefore, no review of the subject will be made here. However, it is appropriate to make comments on the importance of linear

viscoelasticity where (i) it has direct revelance to mixing of rubber and (ii) it provides background for understanding rubber behaviour during mixing.

6.8.1 Linear viscoelasticity and mixing of rubber

As has been explained, mixing of rubber involves large deformation and fracture. In the former, non-linear viscoelasticity plays the key role. However, in limited cases linear viscoelastic behaviour also plays a key role. For example, the magnitude of shear storage modulus G′ at the lower frequencies is related to the mill-processability in determining the initial reaction of rubber when it touches the mill-roll. That is, the flow state, rubbery state or rubber-glass transition defined by linear viscoelastic measurements at small deformation provides the practical information. After touching the mill-roll whether or not the rubber stretches and makes a tight band depends upon the non-linear viscoelastic property and fracture characteristics. An exception to this is that some rubber exhibits linear viscoelastic behaviour at a large deformation. Such rubber apparently retains the same internal structure (the arrangement of chains) even after stretching. Otherwise, modulus would change with strain, i.e., nonlinear behaviour.

The exact mechanism of how the linear behaviour is maintained in the large deformation is not known and is the subject of future research.

Another importance of linear viscoelasticity is that it provides a reference for non-linear behaviour; that is, the latter is expressed as a deviation from the former with use of appropriate parameters. First is the universal parameter, the elongation ratio, α, which reduces the time-scale of nonlinear behaviour to that of linear behaviour. Next is the modulus shift factor, $\Gamma(\alpha)$, which indicates the degree of strain-hardening or strain-softening. Finally, comparison of linearised elongation data with that of shear data indicates, if they disagree, the presence of strain-induced crystallisation or strain-induced association. All these deviations from linearity are related to the structure of rubber.

Thus far, a considerable variety of gum rubbers have been investigated and the characterisation scheme defined in this book is satisfactory. However, the applicability of the scheme is limited to the behaviour where strain-dependence and time-dependence are separable.

6.8.2 Relaxation time and its distribution

In order to relate viscoelasticity to processability, it helps to understand the concept of relaxation time. The definition of relaxation time customarily uses a spring and dashpot

for illustration. However, a definition is given here without using the spring and dashpot model.

Starting with a situation, where a stimulus is given to a system to excite it, the extent of the excitation is expressed by C^*. If the system is allowed to return to the ground state spontaneously, the rate $-dC^*/dt$ is proportional to the extent of excitation, C^*.

$$-dC^*dt = kC^* \tag{6.41}$$

The integration of this equation gives a well-known equation,

$$C^* = C_0^* e^{-kt} \tag{6.42}$$

where C_0^* is the value of C^* at $t = 0$.

This equation is for the first order reaction in chemical kinetics.

It is also the equation for the decay of radioisotopes in physics.

In viscoelasticity

$$k = 1/\lambda \tag{6.43}$$

where λ is the relaxation time.

In the field of viscoelasticity there is 'retardation time' and relaxation time. Qualitatively these terms may be understood by analogy to human behaviour.

Suppose the reader has played tennis with his friend at lunch break and just returned to his work. After changing his clothes, he immediately resumes his work. His friend keeps talking about tennis and cannot go back to work. Which one of them has a longer relaxation time is obvious.

On a fine day at the weekend a reader invites his friend for a hike. He is ready to go but his friend is taking a long time in preparing for the hike. Which one of them has the longer retardation time is obvious.

In science, relaxation time and retardation time are quantitatively defined. In the viscoelasticity of polymers, the relaxation time is in general not a constant but it has a broad distribution. The retardation time also has a broad distribution. In linear viscoelasticity the distribution of relaxation time is shown in a stress relaxation experiment. The distribution of retardation time is shown by a creep experiment.

The distribution of relaxation time and that of retardation time are quantitatively related. Also, the result from any linear viscoelastic experiment is quantitatively related to distribution of relaxation or retardation time. Therefore, from the result of one type of linear viscoelastic measurement, the data of any other type of measurement can be calculated, provided the data are available for a wide range of time scales. For example, dynamic shear storage modulus, $G'(\omega)$ and dynamic shear loss modulus, $G''(\omega)$, may be calculated from relaxation modulus, $G(t)$. The method of calculation is described in textbooks [6] and outside of scope of this book. The importance here is to recognise that the distribution of the relaxation time is related to every data of linear viscoelasticity.

Accordingly, 'response time' or 'material time' is used to include both relaxation time and retardation time. Also, relaxation time is used somewhat loosely to represent both relaxation and retardation time for explaining observed phenomena. For discussing processability, it includes nonlinear viscoelasticity and the use of relaxation time tends not to be rigorous in the quantitative sense.

In the foregoing discussion the relaxation time is used in a relative sense invoking only long or short relaxation times.

In equation (6.41) for the chemical reaction, C^* is the concentration of the reactant. In radioisotope chemistry, the identity of the isotope is known. On the other hand in viscoelasticity, a material exhibiting certain relaxation time is often not clearly identified. Considering of the distribution of relaxation time, what is the counterpart of the distribution in material? Although much of this relationship is the subject of current and future studies, a general statement may be made as follows: for linear polymer chains, the size of the molecule and the relaxation time are directly related. However, the relaxation time of a given polymer chain is not only dependent on its size but also on its environment. For monodispersed polymers, when the MW is smaller than the entanglement coupling distance, *Me*, and when it is larger than *Me*, the environmental effect is completely different. For the latter case the environmental effect is called entanglement. For a molecule larger than *Me*, a local motion of a chain segment, which is smaller than *Me*, is also present.

For a given polymer molecule, its motion may be divided into relatively fast motions of the segments which are smaller than *Me* and relatively slower motions of the whole chain, which is larger than *Me*. This interpretation may be expanded to include polymers having MW distribution. Considering the whole polymer there must be a relationship between the longest relaxation time (terminal relaxation time) and its MW. An example is the relationship between low shear Newtonian viscosity, η_0, and MW. With commercial gum rubbers, η_0 is observed only with low MW polymer or a polymer whose MW distribution lacks the high MW tail. Nevertheless, η_0 will be considered for a moment.

The presence of long branches is very common in gum rubbers and the branch pattern varies widely. For simplicity, a 'star-branched' polymer will be taken as an example. The reader should be aware that this type of model polymer does not represent all other types of branched polymers. Nevertheless, some common features of the branched polymers may be extracted by examining these model polymers.

Figure 6.68 presents plots of η_0 against weight average MW, $\overline{M}_w$ for linear, 3 arm-star and 4 arm-star polymers [40].

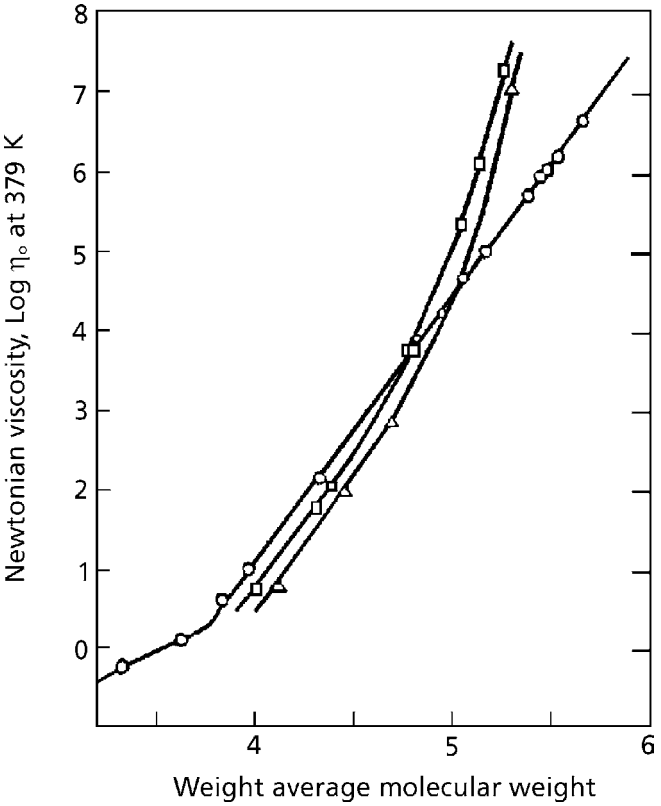

Figure 6.68 Relationship between Newtonian viscosity and MW.
○: Linear molecule
□: Tribranched molecule
△: Tetrabranched molecule

They are BRs prepared through anionic polymerisation. Compared at a fixed MW, the branched polymer has a lower η_0 below certain MW and a higher η_0 above certain MW.

The relaxation time apparently depends upon not only the size of molecule but also its shape, which is branching in this case. Compared at the same size, the branching makes relaxation time shorter below certain branch length and longer above this branch length. The critical branch length is 3 to 4 times of *Me* [41, 42, 43, 44]. Above this crossover MW, the long branch enhanced viscosity.

With a branched polymer exhibiting viscosity enhancement, the extent of the enhancement decreases with increasing shear rate, eventually crossing over the viscosity curve of the linear polymer. That is, at the high shear rate the viscosity is reduced by the presence of long branches. The commercial gum rubbers have branch patterns quite different from the model star polymers. However, often branching is present in the high MW fraction so that the viscosity enhancement at the low shear rates and viscosity reduction at the high shear rates are common observations. This crossover behaviour is also observable in the frequency dependence of the dynamic viscosity, see Figure 6.13 [32].

The long relaxation times introduced by the long branches of commercial gum rubbers have significant influence, even though the amount of the branched fraction may be very small. In the characterisation using dilute solution methods sometimes the branched fraction is filtered off. Then, the interpretation of the processability becomes very difficult.

The presence of gel molecules may be interpreted as a part of the size distribution. The effect of gel is to introduce a very long relaxation time. It exhibits viscosity enhancement at the low shear rate and viscosity reduction at the high shear rate. This occurs with both macrogel and microgel. The details of this mechanism are subjects for future study.

When a polymer blend has island-and-sea morphology, the deformation of the island has a very long relaxation time. The viscosity enhancement was observed at the low shear rate [45].

6.8.3 Linear viscoelasticity as a conceptual background for the mixing of rubber

Different deformational measurements are used to obtain linear viscoelastic data. It may be in simple shear or in elongation. However, the behaviour of rubber during

mixing is neither simple shear nor elongation. Also, in the laboratory measurements, conditions are imposed to be a constant temperature, a constant rate of deformation, a constant frequency, a constant strain or a constant stress over a period of time. Neither one of these conditions are met by the behaviour of rubber during mixing. Then, what is the use of these idealised measurements?

There are two important answers to satisfy the question: one is that the information obtained for a given gum rubber with the above measurements are all related and that from the result of one type of measurement, the result of any other type of measurement, can be calculated. The implication is that if one type of measurement is made then everything about a given gum rubber is known with respect to its linear viscoelastic behaviour. The information is, of course, limited to the range of time scale and the range of temperature of observation.

The other importance is the additivity of the memory. That is, using shear stress relaxation as an example, the cumulative memory of stresses imposed at different times may be calculated with a theory of Boltzmann's superposition principle.

The implication of these two statements is profound. When the separability of time and strain holds for a given gum rubber, subsequent linearisation of the data enables one to describe the behaviour of a gum rubber under any situation, at least in principle. This means that with the understanding of linear viscoelasticity plus the parameters for linearisation, there is adequate information for diagnosing processing problems.

6.8.4 Viscoelasticity and memory

The concept of memory is well accepted today. Memory tapes, memory discs and other memory storage devices are an integral part of our society. However, they are usually either electromagnetic or optical devices. Actually material possesses the ability to retain memories of various kinds; it is also capable of losing memory. In the field of viscoelasticity, the memory appears as a change of shape. If a body is elastic but non-viscous, the memory is retained while a stress is imposed; upon removal of the stress, the memory recovers by 100% and the shape returns to the original. Then, the memory of the deformation is completely gone. With a viscoelastic body, it is not as simple. When a constant stress is imposed, the deformation is not instant but increases with time; this phenomenon is called creep. When the stress is removed, the memory does not recover instantly. It does not necessarily return to the original shape.

When a constant strain is imposed, the stress decreases with time. This is called stress relaxation. The manner of the relaxing stress is a manifestation of the memory loss.

Creep and stress relaxation are model experiments. The stress-strain relations in polymer processing are much more complex. However, the memory phenomena are observed frequently. A typical example is the extrudate swell [46]. In the mixing of rubber it appears as the mill-shrinkage. When the rubber is sheeted out of the mill roll, the thickness increases, and the width and the length decrease. The extent of the change depends upon the material and therefore, the mill-shrinkage has been used as a measure of the material characteristics. When the manner of the memory-loss in the stress-relaxation is considered, there are memories lost in a short time and those retained for a long time. The former memory arises from short relaxation times and the latter from the long relaxation times. The polymer has a distribution of relaxation times and the memory phenomenon is their manifestation.

The relaxation time, λ, is expressed as the ratio of viscosity, η, and elastic (shear) modulus, G,

$$\lambda = \eta/G \tag{6.44}$$

When a system has a single relaxation time, this relationship is easy to understand. When there is a distribution of relaxation times, the meaning of η and G, is not very simple. Therefore, instead of separating the relaxation time into η and G, the relaxation time itself will be used to describe material behaviour.

In the rubber processing neither stress nor strain remains constant over time. Therefore, creep or stress relaxation is not an appropriate model. On the other hand a very complicated stress-strain history is difficult to interpret. A simpler model which offers some insight into processability may be found in transient behaviour. One example is a stress-growth under a constant rate of deformation and observation of stress relaxation. To be realistic, the strain must be large and the behaviour must be in nonlinear viscoelasticity. The experiments may be carried out with a rotational rheometer but they are restricted to low rates of deformation, because otherwise rubber slips at the rheometer interface [47, 48].

Figure 6.69 shows examples of stress history.

Curve 3 is the stress relaxation from the 'instantaneous' deformation, which retains 100% memory at $t = 0$ and exhibits the memory-loss thereafter.

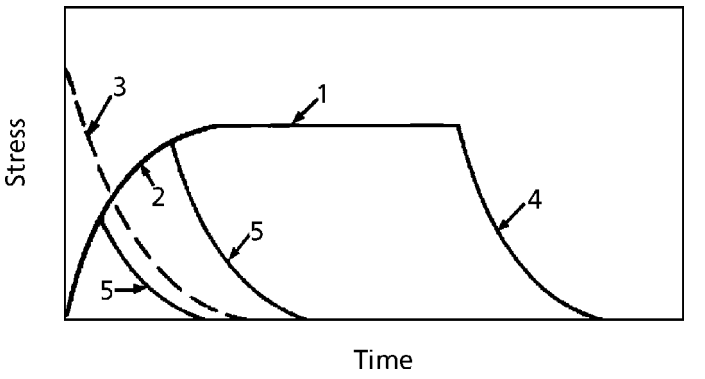

Figure 6.69 Schematic illustration of types of experiments:

1) steady state
2) stress-rise
3) stress relaxation after instantaneous deformation
4) stress relaxation after the cessation of flow
5) stress relaxation after constant rate of deformation

Curve 2 shows stress-growth with low rates of deformation, during which a part of memory is lost. If the deformation is stopped and the strain is held constant, the relaxation shown by curve 5 is observed. When the deformation is carried to the steady state condition, the stress becomes constant, Curve 1. It means that stress is proportional to strain rate and no longer increases with deformation. Curve 4 is the relaxation from the steady state. It is a manifestation of the steady state memory and its dissipation with time. When the relaxation curves, 3, 4 and 5, are expressed as relaxation modulus-time curves, see Figure 6.70, larger differences are observed in the shorter times, but for the longer times the curves merge.

This means that the memory associated with short relaxation times is lost during the imposition of deformation but the memory associated with long relaxation times is retained. Understanding the meaning of the experiment helps interpretation of memory phenomena in processing.

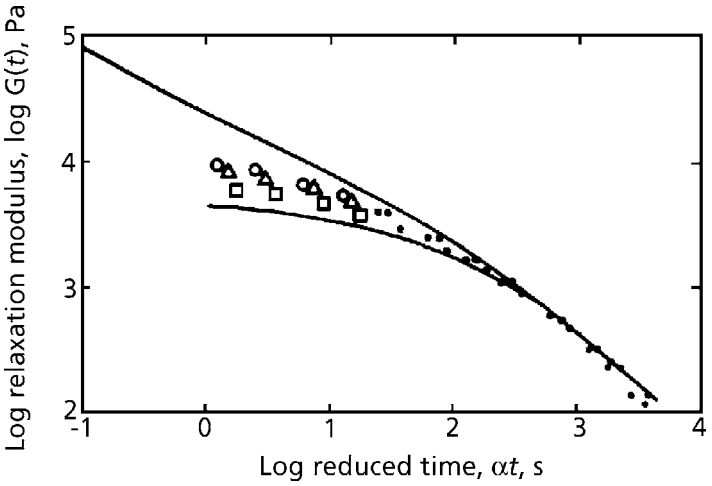

Figure 6.70 Relaxation modulus after constant rate of deformation (•) compared with that after instantaneous deformation (upper curve) and that after cessation of flow (lower curve) for BN-1 sample. Rate of deformation = 0.049-0.050 s^{-1} and strain = 0.405 (O), 0.785 (△) and 1.205 (□).

One drawback of the previous experiment is the slow rate of deformation. In order to match the deformation rate to that in processing, a capillary rheometer may be used. A memory introduced in the deformation at the capillary entrance corresponds to curve 2. Once a material is in the capillary the behaviour is like curve 1, except that some relaxation takes place during the flow through capillary. The recovery of memory appears as the extrudate swell, which is not stress relaxation but like a creep recovery. Because some relaxation takes place during the flow, the recovery depends upon the residence time in capillary which is proportioned to the L/D of the capillary. The higher shear rate results in a shorter residence time in capillary. Therefore less memory is lost and the extrudate swell is higher.

Experiments described in this section concern transient behaviour. Although they are model experiments, they are a closer simulation to the deformational behaviour of gum rubber during mixing than the use of steady state viscosity. The analyses of the transient behaviour with uses of relaxation times, and the interpretation of the memory are a useful way for diagnosing mixing behaviour.

References

1. I. M. Ward, *Mechanical Properties of Solid Polymers*, 2nd Edition, Wiley-Interscience, New York, 1983.

2. R. S. Rivlin, in *Rheology*, Vol. 1, Ed., F. R. Eirich, Academic Press, New York, 1956, Chapter 10.

3. M. Mooney, *Journal of Applied Physics*, 1940, **11**, 582.

4. K. C. Valanis and R. F. Landel, *Journal of Applied Physics*, 1967, **38**, 2997.

5. R. W. Ogden, P. Chadwick and E. W. Hadden, *Quarterly Journal of Mechanics and Applied Mathematics*, 1973, **26**, 23.

6. J. D. Ferry, *Viscoelastic Properties of Polymers*, 3rd Edition, Wiley, New York, 1980.

7. T. L. Smith, *Transactions of the Society of Rheology*, 1962, **6**, 61.

8. R. A. Schapery, *Polymer Engineering Science*, 1969, **9**, 4, 295.

9. B. Bernstein and A. Shokooh, *Journal of Rheology*, 1980, **24**, 189.

10. N. Nakajima and E. R. Harrell, *Rubber Chemistry and Technology*, 1980, **53**, 1, 14.

11. N. Nakajima, J. J. Scobbo, Jr., and E. R. Harrell, *Rubber Chemistry and Technology*, 1987, **60**, 742.

12. N. Nakajima, *Journal of Non-Newtonian Fluid Mechanics*, 1983, **12**, 349.

13. P. A. Small, *Advances in Polymer Science*, 1975, **18**, 1.

14. ASTM D 1646-96a
Standard Test Methods for Rubber - Viscosity, Stress Relaxation, and Pre-Vulcanisation Characteristics (Mooney Viscometer).

15. N. Nakajima and E. A. Collins, *Rubber Chemistry and Technology*, 1974, **47**, 2, 333.

16. M. Mooney and W. E. Wolstenholme, *Journal of Applied Physics*, 1954, **25**, 1098.

17. N. Nakajima and E. R. Harrell, *Rubber Chemistry and Technology*, 1979, **52**, 1, 9.

18. K. Ninomiya, S. Kusamizu, E. Maekawa and G. Yasuda, *Progress in Polymer Science in Japan*, Vol. 1, Eds., M. Imoto and S. Onogi, Kodansha, Tokyo, 1971, p.377.

19. N. Nakajima and E. R. Harrell, in *Current Topics in Polymer Science*, Vol. II, Eds., R. M. Ottenbrite, L. A. Utracki and S. Inoue, Hanser Publications, New York, 1987, p.150.

20. ASTM D 3616-95.
Standard Test Method for Rubber, Raw - Determination of Gel, Swelling Index, and Dilute Solution Viscosity.

21. N. Nakajima, E. R. Harrell, P. R. Kumler, D. A. Seil and A. H. Jorgensen, *Advances in Polymer Technology*, 1984, **4**, 3/4, 267.

22. N. Nakajima, C. D. Huang, J. J. Scobbo, Jr., and W. J. Shieh, *Rubber Chemistry and Technology*, 1989, **62**, 2, 343.

23. N. Nakajima, D. Erbe, A. Maeda and H. Yamazaki, *Rubber World*, 1991, **205**, 2, 33.

24. N. Nakajima and E. R. Harrell, *Rubber Chemistry and Technology*, 1983, **56**, 5, 1019.

25. E. R. Harrell and N. Nakajima, *Journal of Applied Polymer Science*, 1984, **29**, 3, 995.

26. N. Nakajima, M. H. Chu and R. Babrowicz, *Rubber Chemistry and Technology*, 1990, **63**, 4, 624.

27. N. Nakajima, W. J. Shieh and Z. G. Wang, *International Polymer Processing*, 1991, **6**, 4, 290.

28. N. Tokita and J. L. White, *Journal of Applied Polymer Science*, 1966, **10**, 7, 1011.

29. W. H. Whittington and M. E. Woods, Presented at the 100th Meeting of the ACS Rubber Division, Cleveland, OH, Fall 1971, Paper No.38.

30. N. Nakajima and Y. Yamaguchi, *Journal of Applied Polymer Science*, 1996, **61**, 9, 1525.

31. ASTM D412-98a
Standard Test Methods for Vulcanised Rubber and Thermoplastic Rubbers and Thermoplastic Elastomers - Tension

32. N. Nakajima and E. R. Harrell, *Rubber Chemistry and Technology*, 1980, **53**, 1, 14.

33. N. Nakajima and Y. Yamaguchi, *Journal of Applied Polymer Science,* 1996, **62**, 13, 2329.

34. M. Takayanagi, Presented at the 19th Annual Meeting of the International Institute of Synthetic Rubber Producers, Inc., Hong Kong, 1978, Paper No.21

35. N. Nakajima and Y. Yamaguchi, *Journal of Applied Polymer Science*, 1997, **65**, 10, 1995.

36. R. D. DeMarco, *Rubber Chemistry and Technology*, 1979, **52**, 1, 173.

37. *Encyclopedia of Composite Materials and Compounds*, Ed., M. Grayson, Wiley, New York, 1983.

38. N. Nakajima and E. A. Collins, *Journal of Rheology,* 1978, **22**, 5, 547.

39. N. Nakajima and E. R. Harrell, *Journal of Rheology*, 1982, **26**, 5, 427.

40. G. Kraus and J. T. Gruver, *Journal of Polymer Science*, 1965, **A3**, 105.

41. V. R. Raju, G. G. Smith, G. Marin, J. R. Knox and W. W. Graessley, *Journal of Polymer Science: Polymer Physics*, 1979, **17**, 7, 1183.

42. W. E. Rochefort, G. G. Smith, H. Rachapudy, V. R. Raju and W. W. Graessley, *Journal of Polymer Science: Polymer Physics*, 1979, **17**, 7, 1197.

43. H. Rachapudy, G. G. Smith, V. R. Raju and W. W. Graessley, *Journal of Polymer Science: Polymer Physics*, 1979, **17**, 7, 1211.

44. V. R. Raju, H. Rachapudy and W. W. Graessley, *Journal of Polymer Science: Polymer Physics*, 1979, **17**, 7, 1223.

45. N. Nakajima and P. S. L. Wong, *Journal of Applied Polymer Science*, 1965, **9**, 9, 3141.

46. N. Nakajima, *Journal of the Rheology Society*, Japan, 1990, **18**, 5.

47. N. Nakajima and E. R. Harrell, *Journal of Rheology*, 1983, **27**, 3, 241.

48. N. Nakajima and E. R. Harrell, *Journal of Rheology*, 1986, **30**, 2, 383.

7 Viscoelastic Characterisation of Rubber Compounds

7.1 Introduction

The viscoelasticity of a compound is intimately related to its processability in the post-mixing operation such as extrusion and injection moulding. In this chapter, however, viscoelasticity is used to characterise the end-product of mixing. One area of importance is to relate the viscoelastic properties to the composition of the compounds. Because the rubber formulation usually contains many additives, only the additives which have a significant influence on mixing and on viscoelastic properties of the compound are discussed. This narrows down the material variables to rubber grades and fillers. The low MW additives such as extending oils, plasticisers and tackifiers are important but are not included here except for an example of the oil-extended rubber. All the compounds were mixed to give a satisfactory degree of homogeneity, judged to be acceptable on the basis of commercial standards.

7.2 Viscoelastic properties of compounds

The mechanical properties pertinent to the mixing of rubber include viscoelastic properties at small as well as large deformation and failure behaviour. An overriding question is how the viscoelastic properties of gum rubber contribute to these properties of the compounds. This question is answered by choosing several grades of gum rubbers which have the same chemical composition but are different in molecular architecture and therefore, have different viscoelastic properties. Selecting a standard formulation which gives satisfactory mixing, the viscoelastic properties of gum rubbers and compounds may be compared. Samples for this experiment were NBRs with 33% acrylonitrile content [1] (see Table 7.1).

The characterisation of gum rubber is discussed extensively in Chapter 6 and reference [2]. Samples A and B are gel-free if analysed using ASTM D3616-95 [3]. The main difference is in the Mooney index [4]. Samples B, C, and D have similar Mooney values but their viscoelastic properties are very different from each other. Sample C contains 50% microgel, crosslinked particles, whereas Sample D has 75% macrogel, a molecule having many long branches. The compounds contain 40 phr N550 carbon black.

Table 7.1 Butadiene-acrylonitrile Copolymer Samples				
Sample code for filled elastomer	**Sample code for raw elastomer**	**Raw elastomer Hycar[a]**	**T_g (°C)**	**Mooney (ML-4) at 100 °C**
1	A	1052-30	-37, -24	35
2	B	1042	-36, -24	78
3	C	1042X82	-34, -24	81
4	D	1002	-28	85

Stress relaxation, capillary extrusion, dynamic and tensile stress-strain were measured [1]. The results of stress relaxation are presented in Figure 7.1a for the gum rubbers and Figure 7.1b for the compounds.

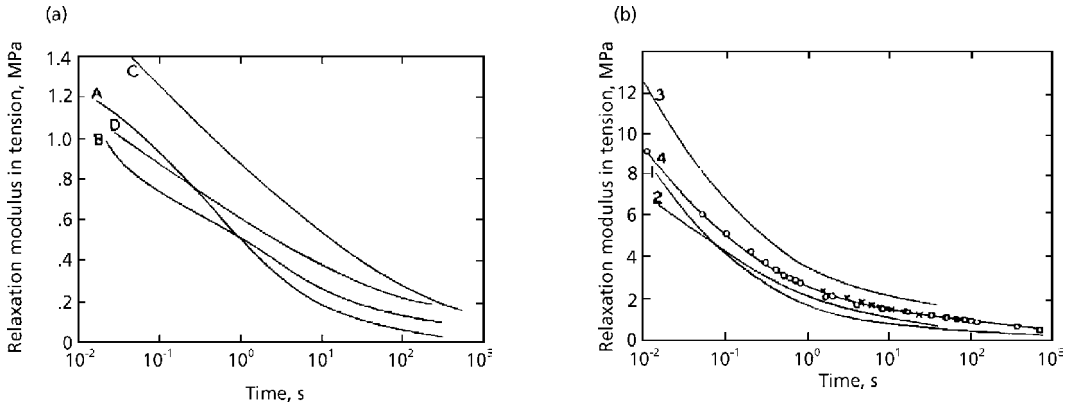

Figure 7.1 (a) Stress relaxation curves, reduced to 25 °C, of unfilled elastomers. (b) Stress relaxation curves, reduced to 25 °C, of four carbon black filled elastomers. 25 °C (O) ; 54→25 °C (x); 98.5→25 °C (□).

Reprinted from N. Nakajima, Polymer International, 1996, 40, 2, 141. Copyright 1996, SCI. Reproduced with permission.

The capillary extrusion data [5] are shown in Figures 7.2a and 7.2b. As seen in these figures, the relative differences between the gum rubbers remain in the filled compounds. Moreover, the magnitudes of the differences are not diminished in the presence of carbon black.

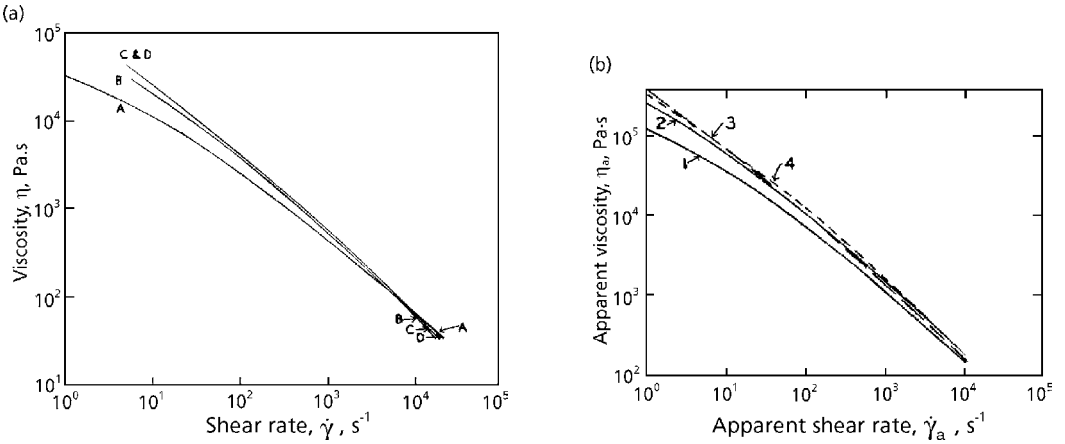

Figure 7.2 (a) Steady shear flow curves, reduced to 100 °C, of unfilled elastomers. (b) Steady shear flow curves, reduced to 100 °C, of carbon black filled elastomers.

In Figure 7.3 the tensile strength and the strain at break for the gum rubbers are shown as functions of strain rate. Each gum rubber has its own unique behaviour. The locus of tensile strength and strain at break is known as the failure envelope, which is a characteristic for a given rubber [6]. The failure envelope is in turn related to the mill processability of the gum rubber, as explained in Chapter 2 and [7].

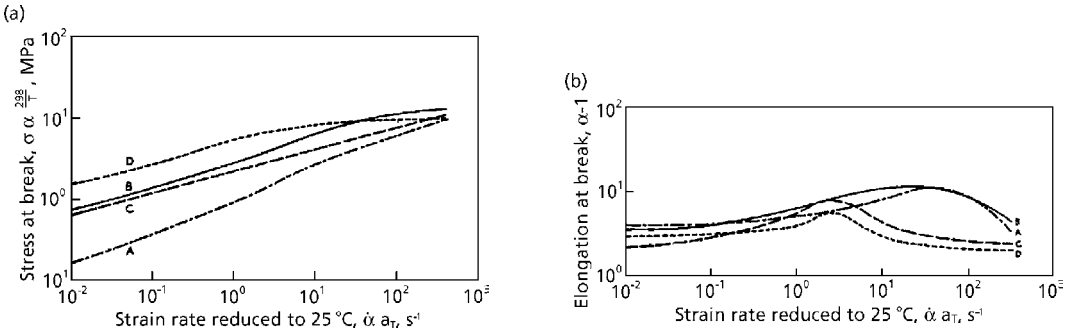

Figure 7.3 (a) Stress at break as a function of strain rate, reduced to 25 °C, of unfilled elastomers.
(b) Elongation at break as a function of strain rate, reduced to 25 °C, of unfilled elastomers.

Reprinted from N. Nakajima, Polymer International, 1996, 40, 2, 141. Copyright 1996, SCI. Reproduced with permission.

The tensile strengths of the compounds are shown in Figure 7.4a, where the relative differences among the gum rubbers are more or less retained. However, some parts of the curves are not exactly in the same order as those of the gum rubbers. Also, at higher strain rates the differences between the samples becomes very small.

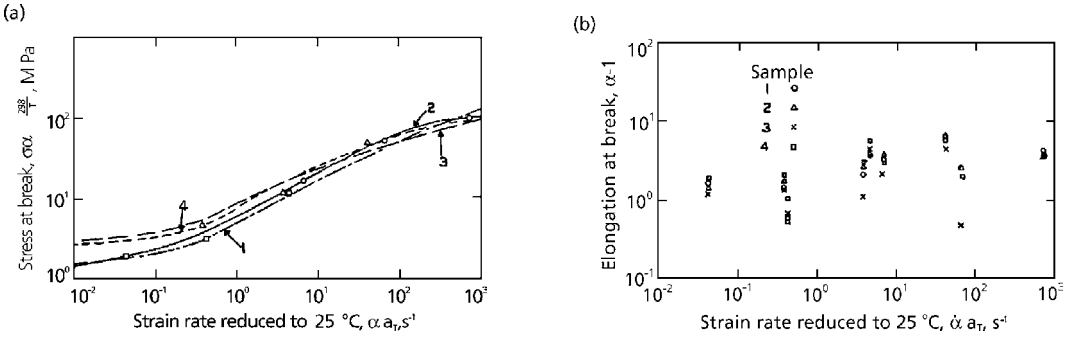

Figure 7.4 (a) Stress at break as a function of strain rate, reduced to 25 °C, of carbon black filled elastomers. 25 °C (O), 56→25 °C (△), 98.5→25 °C (□).
(b) Elongation at break as a function of strain rate, reduced to 25 °C, of carbon black filled elastomers.

Reprinted from N. Nakajima, Polymer International, 1996, 40, 2, 141. Copyright 1996, SCI. Reproduced with permission.

The strain at break (Figure 7.4b) shows no difference among samples, nor any specific pattern. Fracture of gum rubber during mixing has been discussed in Chapter 4. The compounds consist of mixtures of carbon black and comminuted rubber particles. The tensile strength and tensile strain at break depend largely on the strength of cohesion between the rubber particles and the extent of recovery of entanglement in the interparticle boundary. They must also depend upon the growth of the bound rubber. These mechanisms may exert an overriding influence on the tensile strength and the differences among the gum rubbers become secondary. Considering that fracture is initiated from flaws in the material, there must be a wide distribution of flaws in the compounds so that the strain at break data are scattered at random. Why the stress at break data are not scattered is an unanswered question.

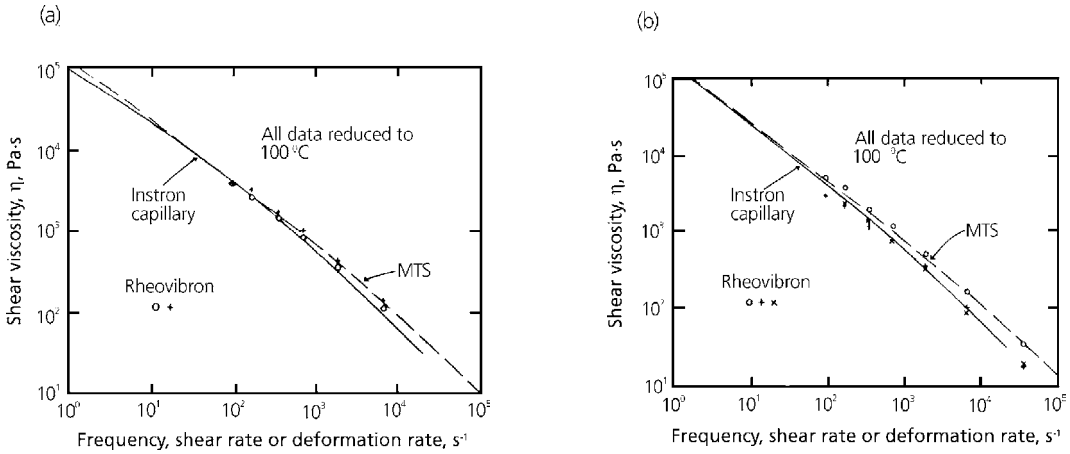

Figure 7.5 (a) Viscosities of gum rubber B obtained by capillary extrusion, dynamic oscillatory and tensile stress-strain measurements.
(b) Viscosities of gum rubber C obtained by capillary extrusion, dynamic oscillatory and tensile stress-strain measurements.

In Figures 7.5a and 7.5b the tensile stress-strain, dynamic and capillary extrusion data are compared for samples B and C, respectively. The tensile data obtained using a High Speed Tension Tester (MTS Systems), are linearised according to the method described in Chapter 6 and [2, 7], i.e., strain-time correspondence. The results are presented as the equivalent of shear viscosity. The results obtained show good agreement with the dynamic data (Rheovibron) within the reproducibility of the experiments. The steady state viscosities from capillary extrusion are also in approximate agreement, and the Cox-Merz empirical rule is applicable in these cases [8].

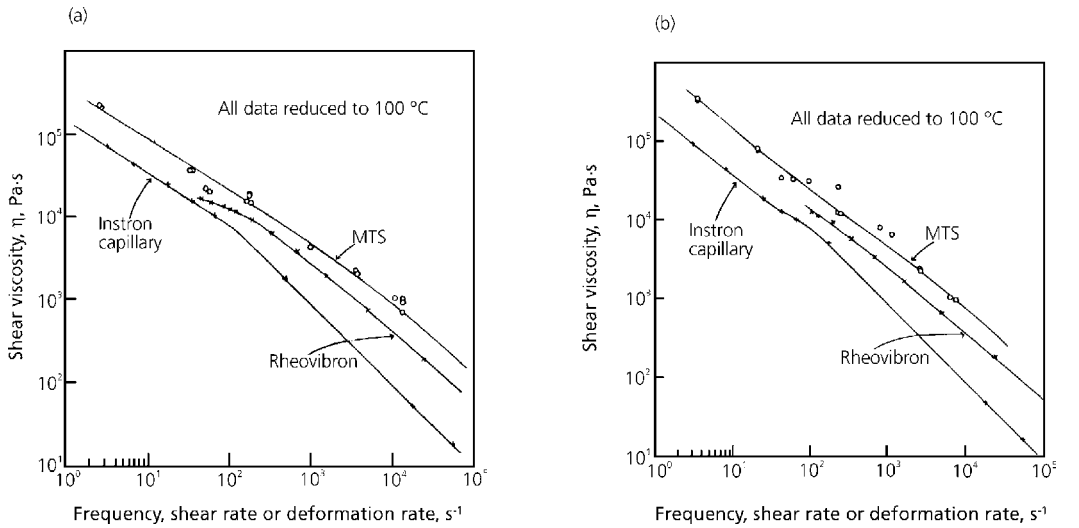

Figure 7.6 a) Viscosities of compound 2 obtained by capillary extrusion, dynamic oscillatory and tensile stress-strain measurements.
b) Viscosities of compound 3 obtained by capillary extrusion, dynamic oscillatory and tensile stress-strain measurements.

Reprinted from N. Nakajima, Polymer International, 1996, 40, 2, 141. Copyright 1996, SCI. Reproduced with permission.

The result for the compounds from the same sets of the experiments are shown in Figures 7.6a and 7.6b. The viscosities evaluated through the three different experiments differ significantly.

The reason for this lies in the fact that it is a dispersed system. The dispersed carbon black is a complex-shaped fine particle, which is hard and not deformable. The matrix rubber is soft and easily gives a large deformation. Also, the dispersed carbon black usually forms a network consisting of strings of particles. The network crumbles easily upon deformation, resulting in a decrease of modulus [9]. Moreover, a part of the rubber is adsorbed on the surface of the carbon black, forming bound rubber, which does not dissolve in solvent. The amount of bound rubber may be as much as 25%. When the temperature is raised, more rubber is extracted and at certain elevated temperatures all the rubber dissolves [10, 11]. In summary the compound consists of carbon black, bound rubber and unbound rubber; each component responds differently at small deformations (Rheovibron) and large deformations (MTS), and with shear (capillary) and elongation (Rheovibron and MTS).

Even though the viscoelastic behaviour is complex, characterisation methods may be developed for relatively easy interpretation. One is the dynamic shear measurement, which provides storage modulus and loss modulus as functions of angular frequency. Because the behaviour of compounds is strain-dependent, the strain amplitude must be kept at a constant value for all samples.

The tensile stress-strain measurements are conducted at different strain rates [12]. These characterisation methods are the same as those for gum rubbers [2]. The tensile data for five different strain rates are shown to form a master curve upon application of the strain-time correspondence, which requires modification of the observed time by multiplying by the extension ratio, α (see Figure 7.7). This conclusion is the same as the case for gum rubbers [2, 7]. However, an important difference of the compound behaviour is the yielding which does not occur in gum rubbers. Therefore, the data up to the yield point are used for the master curve. The data after yielding are inaccurate because deformation often becomes non-uniform.

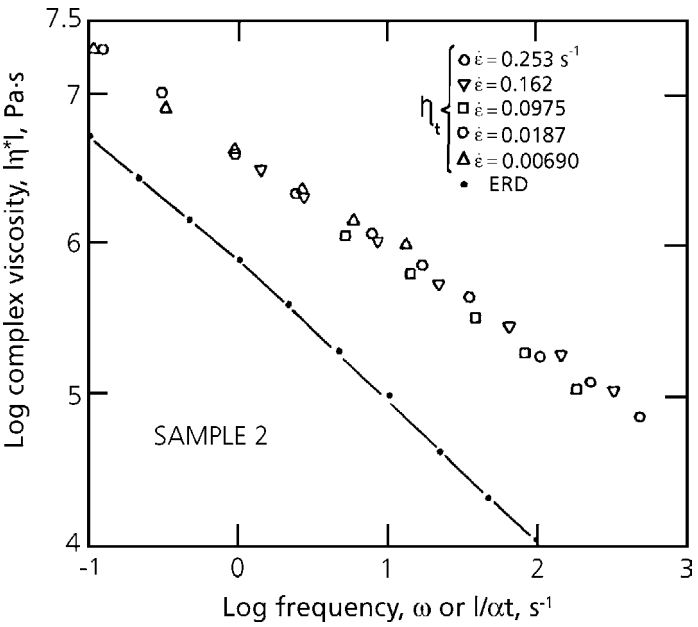

Figure 7.7 Tensile stress-strain data reduced to a master curve compared with dynamic shear data for Sample 2.

The master curve obtained from the tensile data is compared with the curve obtained from dynamic shear measurements in Figure 7.7.

Unlike the gum rubbers, these two curves are in disagreement. Because Poisson's ratio of the compound is not 0.5, the disagreement is expected. However, the shear viscosity calculated from tensile data with the use of the factor 3 is about one order of magnitude higher than that of the dynamic shear data; hence Poisson's ratio alone does not provide the explanation for the disagreement, see Figure 7.7. The following is the explanation for the difference in the internal mechanism of deformation in tension and shear. When a test piece is elongated to twice its original length, it contracts by $\sqrt{2}$ in the crosswise direction, if the volume change is negligible. If the affine deformation (the same deformation at both macroscopic and molecular scale) is assumed, this change of the dimensions must be valid even at the molecular level. However, the affine assumption brings the following contradiction [12, 13]. Figure 7.8 illustrates the elongation in a two-dimensional model, where the short lines may be assumed to be the molecules.

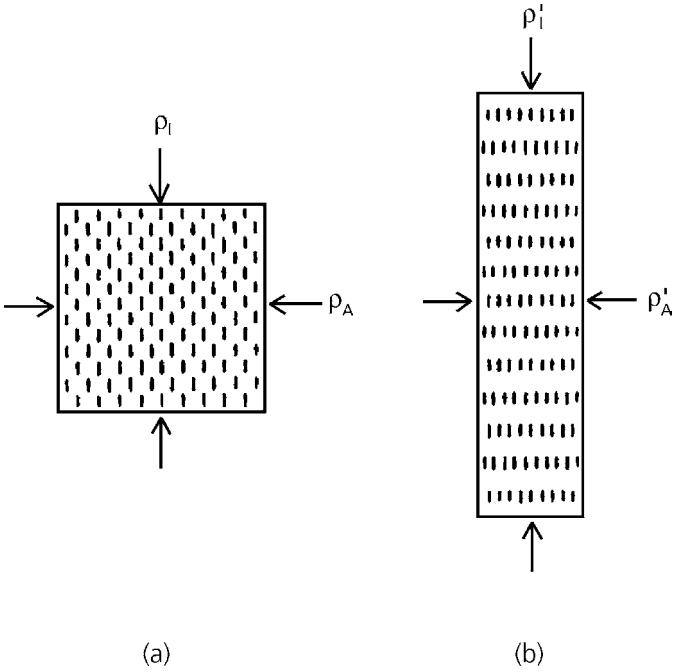

Figure 7.8 Hypothetical model of filled rubber: a) before elongation; b) during elongation.

For an extension ratio of 2 (Figure 7.8b), the density of molecules in the stretch direction, ρ_1' and that before stretching, ρ_1 are related as

$$\rho_1' = \rho_1/2 \tag{7.1}$$

and the density in the cross-direction is given by

$$\rho_A' = 2\rho_A \tag{7.2}$$

In reality the compression in the cross-direction to a half width is impossible. This contradiction does not occur with gum rubbers, because of the liquid-like motion of the chain segments shorter than *Me*; and consequently density rearrangement maintains isotropic density:

$$\rho_1 = \rho_A = \rho_1' = \rho_A' \tag{7.3}$$

The density rearrangement requires additional energy over the thermal motion but it is negligibly small.

With regard to the behaviour of compounds, the short lines in Figure 7.8 represent carbon black with adhered rubber. The size of these particles is about 100 nm, and they are not in a liquid-like motion. Therefore, the density rearrangement must occur through the considerable internal movement which is much larger than the macroscopically imposed deformation.

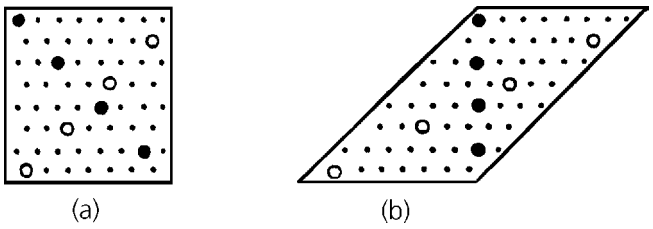

Figure 7.9 Hypothetical model of filled rubber: a) before shear; b) during shear.

On the other hand, in shear deformation (Figure 7.9), the internal deformation requires little density rearrangement, because it is like the sliding of a deck of cards. The density

rearrangement in the direction of the black dots (contraction) and that in the direction of the white dots (expansion) may be insignificant. This explains the disagreement in Figure 7.7 between the complex viscosity calculated from tensile data and the shear viscosity.

7.3 Strain- and strain-rate amplification

The nonlinear viscoelasticity modulus $E(t, \varepsilon)$ is a function of time, t and strain, ε. The compound behaviour is nonlinear even at very small deformation [9]. As described in Chapter 6, the presentation of modulus data requires t and ε axes. The plot is a curved surface. When we consider the property changes resulting from physical ageing and from various deformational history [14], the separability of time and strain does not hold and linearisation of nonlinear data will not work.

The complicated nature of the viscoelastic properties of compounds arises from three contributions. The first is the matrix rubber; the second is the carbon black, with its structure, spatial arrangement and self-interaction, and the third is the interaction between the rubber and the carbon black, including the bound rubber [15]. These three contributions each have a different temperature dependence and a different response to deformation.

In order to simplify the characterisation of the compounds a pragmatic approach is adopted. The following questions represent some of the objectives of this approach:

(i) How is the nonlinear viscoelasticity of the compound affected by changing the rubber grade?

(ii) How is it affected by changing the carbon black grade?

(iii) How can we characterise the physical ageing of the compound?

There must be many practical questions of this nature. The proposed approach is the use of strain amplification.

The concept of strain amplification has been around for many years. When a compound is deformed, the matrix must bear a strain larger than that imposed by the macroscopic deformation, because carbon black does not deform. However, establishing a rigorous theory of strain amplification is almost impossible [16] because the microscopic deformation is very different from the macroscopic one. For example, when the macroscopic deformation is elongation, the microscopic deformation includes shear as well as rotation and the spatial rearrangement of fillers. Use of the elongation-equivalent

of strain amplification is proposed here, which includes all the non-elongational contributions described above. Therefore, it is an 'apparent strain amplification'.

Mullins and Tobin used a simple equation for strain amplification [17], where the apparent amplification is assumed without explicitly stating so. The amplification factor χ is

$$\chi = \varepsilon_0/\varepsilon \tag{7.4}$$

where ε_0 is the matrix strain expressed as the elongation equivalence and ε is the observed strain of the compound specimen. If the stress, σ, is uniform throughout, then

$$\chi = E/E_0 \tag{7.5}$$

where E is the modulus of the compound and E_0 is that of the rubber. In order to evaluate χ, the value of E_0 must be known. Mullins and Tobin prepared filled and unfilled vulcanisates with the same crosslinking recipe, through which E_0 was estimated. In order for this method to be valid, the degree of crosslinking for the filled and unfilled rubber must be the same. In general, the presence of carbon black influences the degree of crosslinking [18]. In Equation (7.5), E and E_0 are equilibrium moduli, so they are functions of strain only. Mullins and Tobin evaluated E and E_0 from the linear portion at small strains in tensile stress-strain curves. No treatment was given for the strain-dependence of χ.

The strain amplification proposed here is very different from that given by Mullins and Tobin. Uncrosslinked rubbers are used and therefore they are not in equilibrium deformation. The material behaviour is time dependent, i.e., viscoelastic. Therefore, the modulus $E(\varepsilon, \dot{\varepsilon})$ is a function of strain and strain rate, $\dot{\varepsilon}$. If the stress is uniform throughout the specimen, Equation (7.5) may be adopted for the dynamic situation. If the matrix is a glass, a stress concentration may occur in the vicinity of fillers. When the matrix is a rubber, the stress concentration dissipates quickly. If the rate of dissipation is much faster than the deformation rate, the stress may be regarded as uniform, and this is the approximation used. At large deformations close to failure, stress concentration may occur and the approximation may not be valid. In such a case the amplification defined by Equation (7.5) includes the effect of the non-uniform stress. The equation is rewritten for the dynamic behaviour as

$$\chi = E_{cp}/E_g \tag{7.6}$$

where E_{cp} is the compound modulus calculated from the stress (σ_{cp})-strain (ε_{cp}) measurement, and E_g is the matrix modulus:

$$E_{cp}(\varepsilon, \dot{\varepsilon}) = \sigma_{cp}/\varepsilon_{cp} \tag{7.7}$$

Likewise the matrix modulus is

$$E_g(\varepsilon, \dot{\varepsilon}) = \sigma_g/\varepsilon_g \tag{7.8}$$

The uniform stress distribution means

$$\sigma_{cp} = \sigma_g \tag{7.9}$$

In Equations (7.7), (7.8) and (7.9) the unknown is ε_g and therefore E_g is also unknown. As it is, Equation (7.6) cannot be solved.

The following method is suggested for the solution. First, a master curve for gum rubber is prepared from the tensile data obtained with several rates of elongation. When the strain-time correspondence is applicable, the master curve gives the relationship [19, 20] :

$$\sigma(\varepsilon, \dot{\varepsilon}) / \varepsilon = E(\alpha t) \tag{7.10}$$

where α is the extension ratio. When strain-hardening occurs

$$\sigma(\varepsilon, \dot{\varepsilon})/\varepsilon/\Gamma(\alpha) = E(\alpha t) \tag{7.11}$$

where $\Gamma(\alpha)$ represents the degree of strain-hardening.

The calculation involves iterative steps; first an arbitrary value is taken for χ, e.g., $\chi = 3$. Inserting this value into Equation (7.12):

$$\chi = \varepsilon_g / \varepsilon_{cp} \tag{7.12}$$

ε_g is obtained as a first approximation ε_{g1} for the given value of ε_{cp}.

Because

$$\alpha_{g1} = \varepsilon_{g1} + 1 \tag{7.13}$$

and

$$t = \varepsilon_{cp} / \dot{\varepsilon}_{cp} \tag{7.14}$$

E_{g1} can be estimated from the master curve, either Equation (7.10) or (7.11), whichever the case may be. From Equations (7.8) and (7.9):

$$\varepsilon_g = E_g / \sigma_{cp} \tag{7.15}$$

Using E_{g1} and Equation (7.15), the second approximation ε_{g2} is obtained. This completes the first cycle of calculation. The next cycle gives ε_{g3}. After repeating the cycle a few times, ε_{gi} no longer changes. Then χ is calculated from Equation (7.12).

Examples of strain amplification for different gum rubbers with the same formulation (see Table 7.2) are shown in Figures 7.10a and 7.10b [19].

Table 7.2 Diene Rubber Samples

Type	Trade Mark[a]	Code for gum	Code for compound	Mooney index of gum[b]	% gel of gum	Carbon black, N550 (phr)
NBR	Hycar 1052	A	1	35	0[c]	40
NBR	Hycar 1042x82	C	3	81	48.6	40
NBR	Hycar 1002	D	4	85	74.3	40
SBR	Ameripol 1502	H	5	52	1.8[d]	40
SBR	Ameripol 1712	I	7	55	4.4	40[d]

a : Registered trademark of the BFGoodrich Company
b : Reference 4
c : Reference 3
d : A method similar to that of Reference 3 but toluene was used instead of MEK
e : Parts per hundred of gum rubber plus extending oil

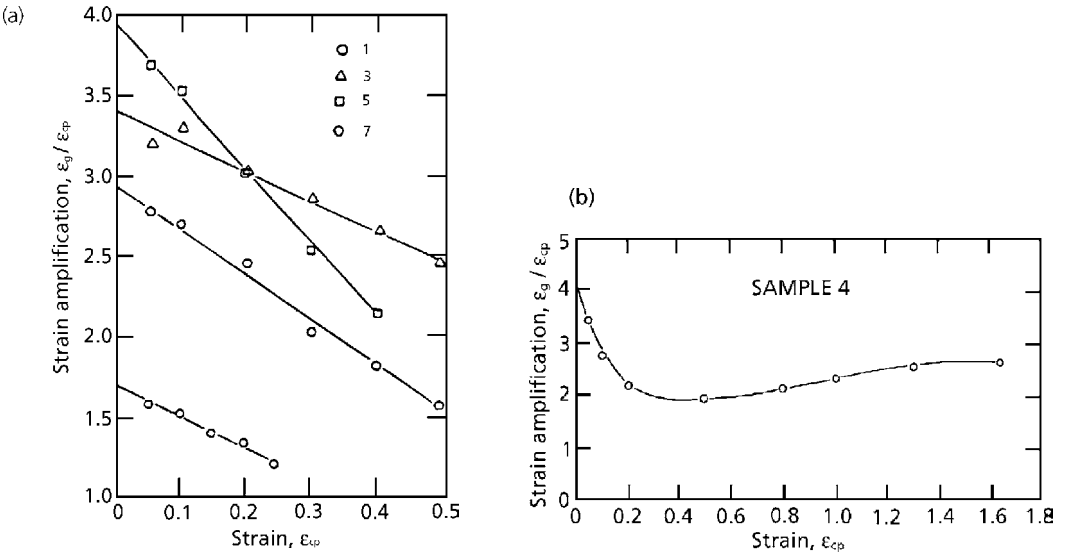

Figure 7.10 a) Strain amplification factor as a function of strain for Samples 1, 3, 5 and 7. b) Strain amplification factor as a function of strain for Sample 4.

As shown in Figure 7.10 the extent of strain amplification varies significantly among the different rubbers. The common trend is a decrease of the amplification with increasing strain. In general, compounds do not elongate much before the yield point is reached; in most cases, less than 50% elongation. Compound 3 contains about 50% microgel [2]. Compound 4 containing 75% macrogel [1] is the only sample giving a large elongation 160%, before yielding. The amplification for Compound 4 decreases up to 20% elongation but thereafter stays about constant. As explained before, the strain amplification arises from multiple sources but may be regarded as the all-inclusive manifestation of rubber-carbon black interaction. For further details the results must be compared with the bound-rubber content, the amount of adsorbed rubber on the carbon black, which may be estimated by nuclear magnetic resonance (NMR) [21, 22, 23], and the extent of development of the secondary network of carbon black (the Payne effect) [10].

Figure 7.11 shows the effect of carbon black grade on the strain amplification [24]. The rubber is ACM having ethylidene norbornene as the cure-site. ACMs in general give a large extension and in this case 500% even as a compound.

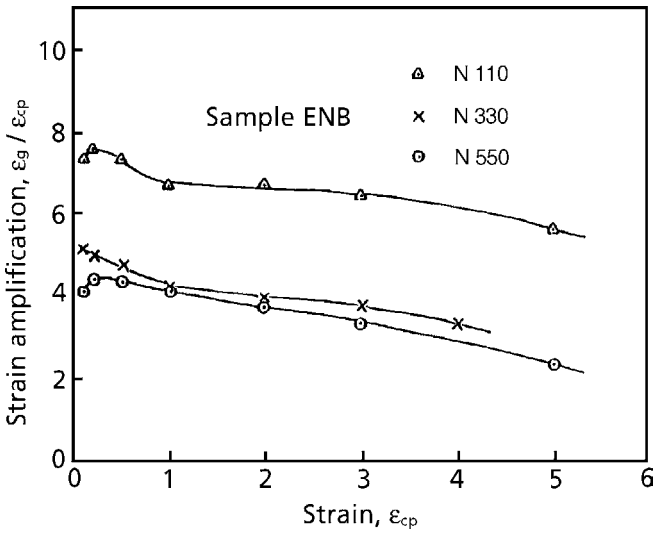

Figure 7.11 Strain amplification of ACM compound ENB, containing 50 phr of carbon black – N110, N330 and N550.

Carbon black N110, which has the smallest particle size of the three, gives the largest strain amplification. Carbon black N330, which has an intermediate particle size, gives a somewhat larger amplification than carbon black N550, having the largest particle size.

When ε_g is found by this procedure, it may be presented as a function of time (Equation 7.14). From this relationship, the strain rate of the matrix rubber, $\dot{\varepsilon}_g$, may be estimated. It follows that the strain-rate amplification, $\dot{\chi}$, is

$$\dot{\chi} = \dot{\varepsilon}_g / \dot{\varepsilon}_{cp} \tag{7.16}$$

Figure 7.12 shows the strain-rate amplification calculated from the data of Figure 7.11 [20].

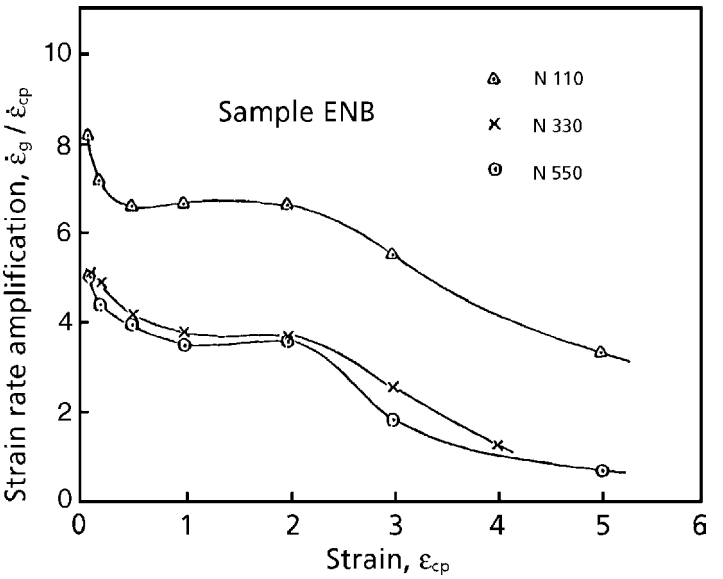

Figure 7.12 Strain-rate amplification of ACM compound ENB, containing 50 phr of carbon black – N110, N330 and N550.

The strain-rate amplification decreases with increasing elongation in two stages. After the initial decrease, the amplification remains constant or increases slightly and then decreases again. At the last point, which is near the yield point, the amplification becomes 1 or even less than 1 with N330 and N550. The strain rate of the matrix is either the

same as, or less than, that of the compound as a whole, suggesting the separation of rubber from the surface of the carbon black.

Figures 7.13 and 7.14 are the strain-amplification and the strain-rate amplification, respectively, of the compounds made with sample EP of ACM. The effect of the particle size of carbon black is the same as that with sample ENB, but the magnitude and the patterns of the amplifications are different between the two gum rubbers.

Figures 7.15 and 7.16 show the effect of the structure of carbon black on the strain amplification. The highest structure, N358, gave the highest amplification but the order is reversed between N330 and N326. This was shown with both samples ENB and EP. The reason for the reversal is not known at this time. Overall, sample ENB gave more pronounced amplification than EP did. This may come from the differences in gel-type and gel-content; ENB containing 70% microgel and EP only 10% macrogel.

Figure 7.17 shows the effect of ageing on the strain amplification [24]. The previous data on the strain amplification (Figure 7.11) were determined within a week after compounding. The aged sample was stored for 2 months. The strain amplification increased almost 50% in 2 months. However, after a slight remilling the original value of the amplification is recovered.

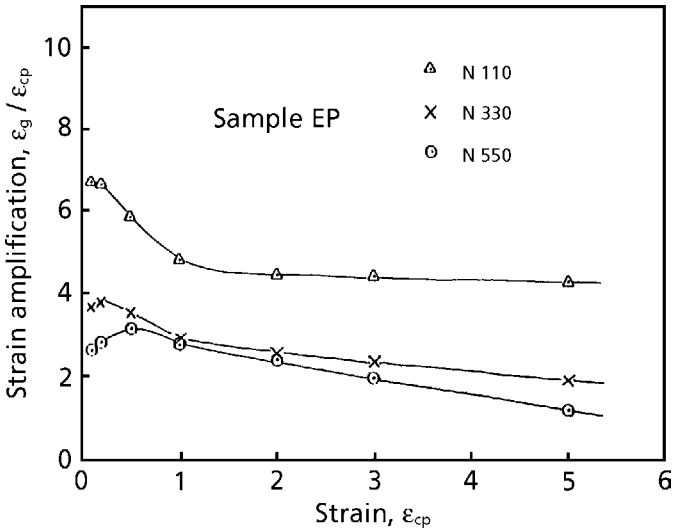

Figure 7.13 Strain amplification of ACM compound EP, containing 50 phr of carbon black – N110, N330 and N550.

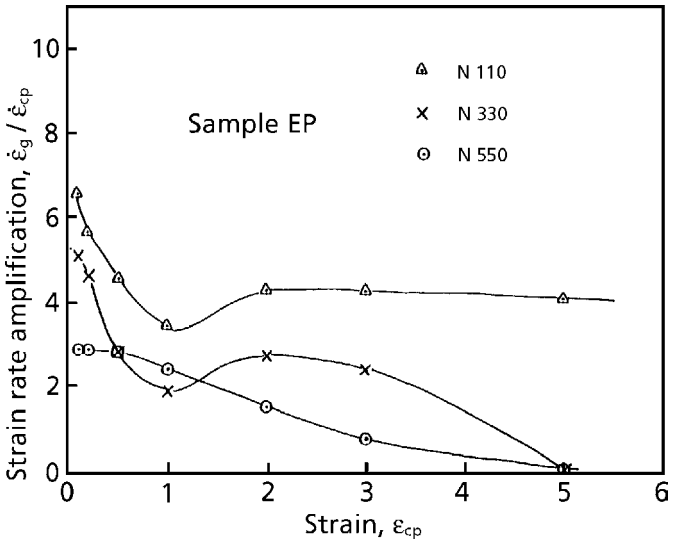

Figure 7.14 Strain-rate amplification of ACM compound EP, containing 50 phr of carbon black – N110, N330 and N550.

Reprinted with permission from N. Nakajima, Rubber Chemistry and Technology, 1988, 61, 5, 938. Copyright 1988, Rubber Division of the ACS.

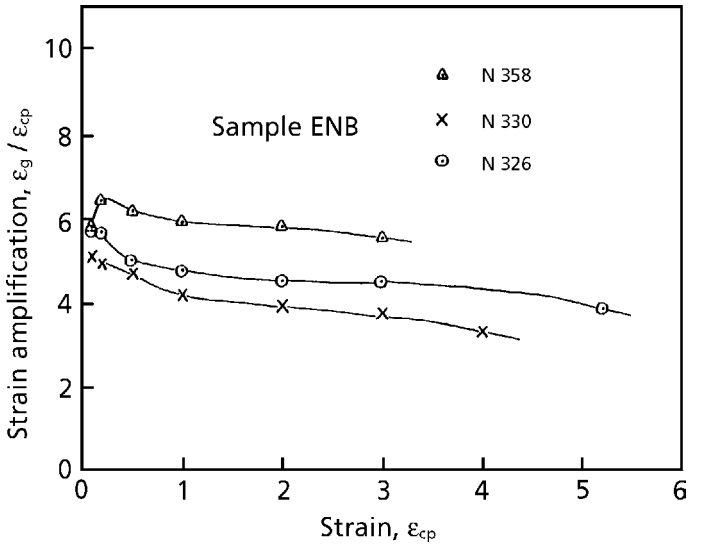

Figure 7.15 Strain amplification of ACM compound ENB, containing 50 phr of carbon black – N358, N330 and N326.

Reprinted with permission from N. Nakajima, Rubber Chemistry and Technology, 1988, 61, 5, 938. Copyright 1988, Rubber Division of the ACS.

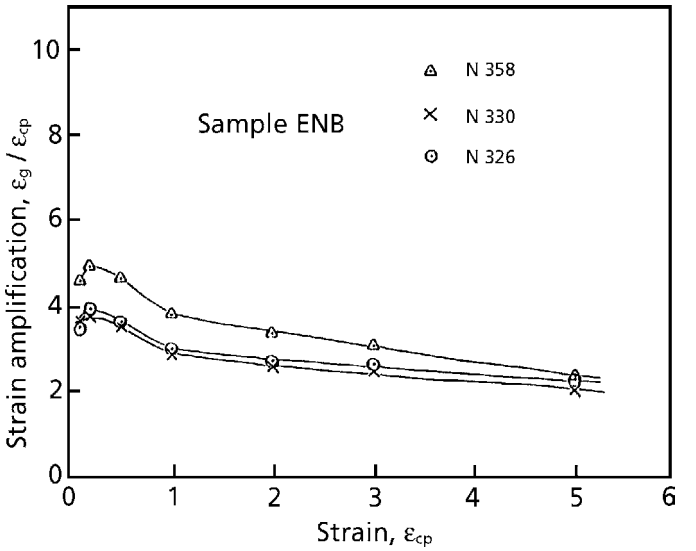

Figure 7.16 Strain amplification of ACM compound EP, containing 50 phr of carbon black – N358, N330 and N326.

Reprinted with permission from N. Nakajima, Rubber Chemistry and Technology, 1988, 61, 5, 938. Copyright 1988, Rubber Division of the ACS.

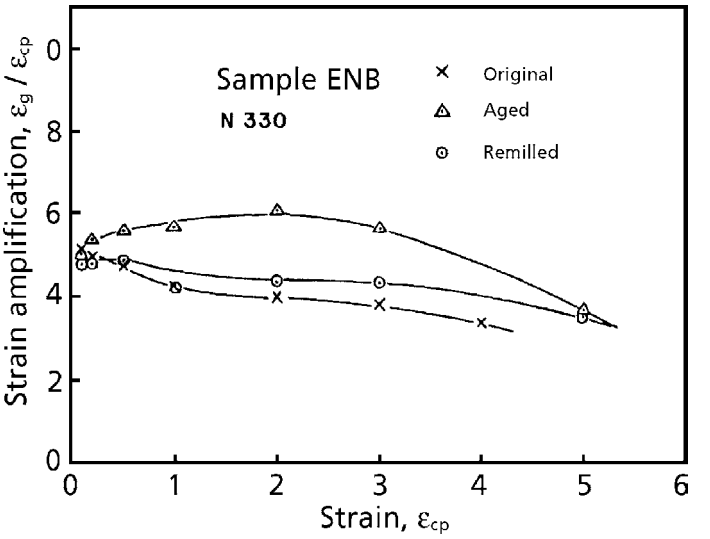

Figure 7.17 Effects of ageing and remilling on strain amplification of ENB compound.

Reprinted from N. Nakajima, Polymer International, 1996, 40, 2, 141. Copyright 1996, SCI. Reproduced with permission.

The increase of the compound modulus on ageing may result from an increase of bound rubber and regeneration of entanglement at the interface of the comminuted rubber particles, as discussed in section 4.4 and [24]. Also, a spatial rearrangement of carbon black caused by the memory of the matrix rubber may occur. As the memory recovers very slowly, the compound tends to go back to the previous state, where the dispersion was poorer and the modulus was higher. These three effects may be erased by remilling.

The evaluation of ageing with a Mooney rheometer is not accurate because charging of the specimen erases a part of the ageing. In the strain amplification, a tensile specimen may be stored for ageing and then subjected to the test without loss of the ageing effect.

7.4 Unique characteristics of compounds

The first part of this chapter concerned the viscoelastic properties of gum rubber and how they affect those of the compound. The second part discussed the use of strain amplification as a quantitative measure of the compound characteristics, where the effect of the formulation, i.e., rubber and carbon black variation, were investigated.

There are other qualitative aspects which are unique to rubber compounds and different from gum rubber behaviour. The increase of modulus as a result of physical ageing has already been discussed in section 7.3.

Rubber compounds tend to give a smooth extrudate without melt fracture. Also, the magnitude of the extrudate swell is smaller than that of the gum rubber [5]. Compounds consist of supermolecular flow units, which form during compounding. No fracture occurs at the entrance of the capillary because it is a fluid material. Consequently, the memory of deformation at the entrance is smaller than that of gum rubber, which is an elastic material. This explains the low extrudate swell. The supermolecular flow units are carbon black with adsorbed rubber and comminuted particles of the matrix rubber. There is some resemblance between the rheology of rubber compounds and that of PVC; both are in a particulate state during flow [5].

Compounds tend to slip more easily at the metal-rubber interface compared with gum rubbers. This is observable in extrusion with use of a colour-marker on the specimen [25].

Yielding is observed in elongation of compounds. This occurs at large deformations. The decrease of modulus with increase of the strain amplitude occurs at very small deformations (Payne effect) [9]. This may also be regarded as a yielding of the carbon black network. When the steady state flow measurement is carried to very low shear

rates, the viscosity increases toward infinity [26]. This is interpreted as the manifestation of yield stress. All these yieldings are not the same kind; nevertheless they are unique to compounds and do not occur with gum rubbers. These aspects will be discussed in Chapter 8.

7.5 Application of characterisation methods for a specific problem

In section 7.2 it was shown that the differences in the viscoelastic behaviour among gum rubbers are carried into the differences among corresponding rubber compounds. The observation is semi-quantitative but it is important to demonstrate the trend.

In section 7.3 a quantitative relationship between a gum rubber and its compound in the elongational behaviour is described in terms of strain- and strain-rate amplification. The variables are

(a) differences among the matrix rubbers with the same filler

(b) differences among fillers in the same matrix rubber

(c) differences in aged and unaged compound.

In this section even more detailed questions are asked about the specific effect of branching and that of crystalline particle fillers in gum rubbers on the elongational behaviour of compounds. The filler type is also a variable. A quantitative comparison is intended in this section [27].

7.5.1 Effect of fillers and rubber structures on tensile behaviour of filled, unvulcanised compounds of cis-1,4-polybutadiene

- *Experiment*
- *Sample*

Samples of gum rubbers and fillers used for the compounds are listed in Table 7.3. These gum rubbers were chosen from eight previously studied samples, which represented three different groups. These groups were titanium-, neodymium-, and cobalt-polymerised polymers. The titanium-polymerised CB11 had a higher degree of branching but the branches were relatively short, causing strain softening. Neodymium-polymerised CB22 had a lower degree of branching than CB11, but the branches were relatively long and exhibited strain hardening. The cobalt-polymerised VCR 412 contained 12% crystalline

particles made from a block copolymer of *cis*-1,4- and 1,2-polybutadiene [28]. The particles produced strain softening. The *cis*-1,4-branches attached to the surface of the particles were relatively short and facilitated the elongation.

Table 7.3 Samples

Sample Designation	Catalyst Type	*cis* Content	Mooney Index of gum	Filler Loading (phr)
BUNA[a] CB11	Ti	*cis*-BR, 93%	47	N110[b] 50 N330[b] 50
BUNA[a] CB22	Nd	*cis*-BR, 98%	63	N110[b] 50 N330[b] 50 VN3[c] 56 VN3[c] 56 Si 69[d] 5.6
VCR[e] 412	Co	*cis*-BR, 91% and SPB[f]	45	N110[b] 50 N330[b] 50

a: Registered trademark of Bayer AG
b: Produced by Cabot
c: Silica produced by Degussa
d: Bis(3-[triethoxisilyl]propyl)tetrasulphane-coupling agent produced by Degussa
e: Registered trademark of UBE Industry
f: Crystalline particles made of block copolymer of *cis*-1,4- and syn-1,2-polybutadiene

The amount of silica was adjusted to make its volume equal to the volume of 50 phr carbon black by taking account of the density difference.

- *Mixing*

A Banbury-type internal mixer with a 250 ml capacity was used. The fill factor was 0.7 and the rotor speed was 100 rpm. First the mixer was cleaned with gum rubber.

Then, fresh rubber was charged and masticated for 1 minute. At this time half of the carbon black was added over a period of 1 minute. After an additional 30 seconds of mixing the rest of the carbon black was added. After mixing for another 2 minutes, the compound was dumped. For mixing silica, one-third was added every minute. After an additional 4 minutes of mixing the compound was dumped. The coupling agent was added with the second addition of silica. All dumped compounds were crumbly and a small amount of the free filler remained.

The dumped compounds were milled and sheeted with a 6-inch two roll mill to develop further mixing and to observe mill behaviour of the compounds. All compounds were pressed at 140 °C for 10 minutes for preparation of tensile specimens.

- *Tensile measurement*

Tensile measurements were performed with a Monsanto Tensometer 500. The strip chart recorder recorded force against time. The force was measured with a 45 kg load cell. The extent of deformation was measured by recording with a video camera. The measurements were performed at room temperature with deformation rates of 0.035, 0.082, and 0.176 s^{-1}.

- *Results and discussion*

Examples of stress-strain curves at various deformation rates are shown in Figures 7.18-7.21 where the stress is the true stress, assuming incompressibility of the compounds.

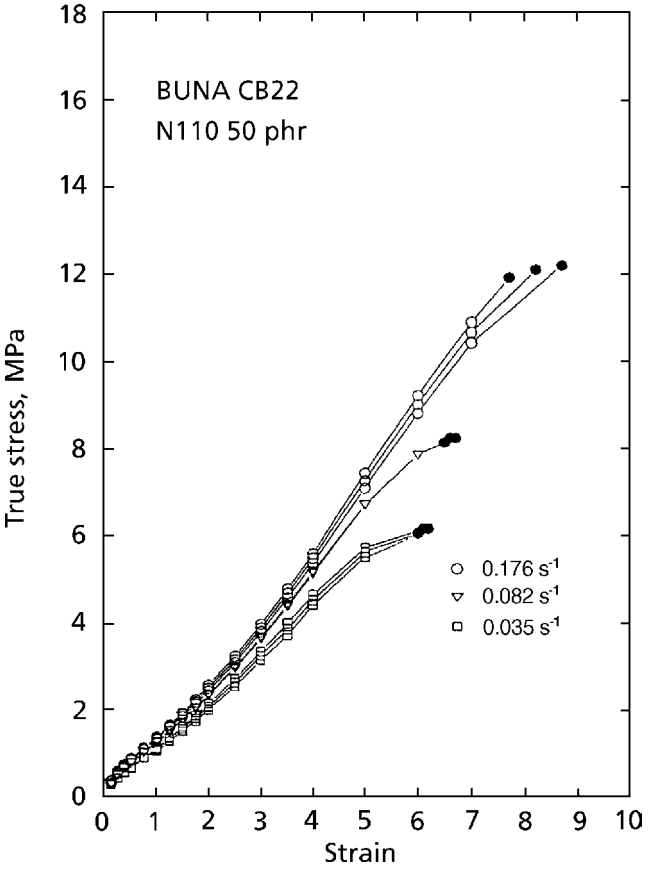

Figure 7.18 Tensile stress-strain curves of CB22 compound with carbon black N110.

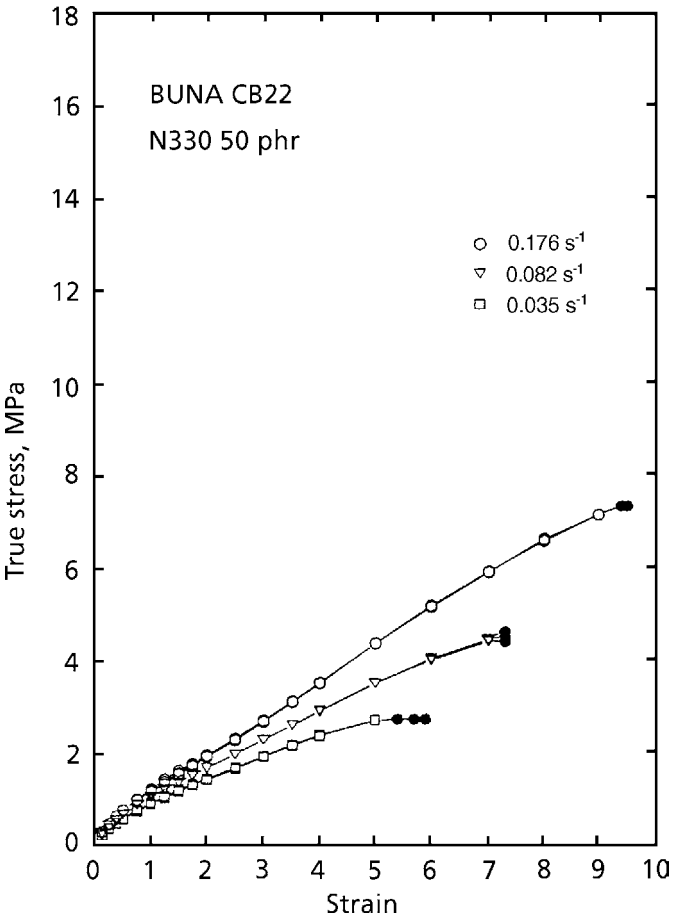

Figure 7.19 Tensile stress-strain curves of CB22 compound with carbon black N330.

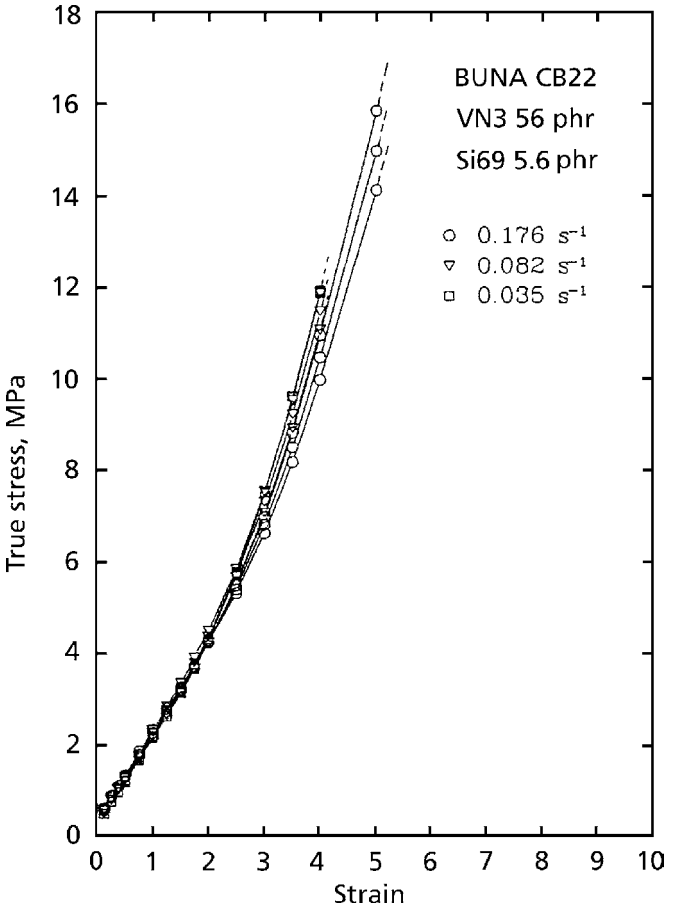

Figure 7.20 Tensile stress-strain curves of CB22 compound with silica and coupling agent.

Reprinted from N. Nakajima and Y. Yamaguchi, Journal of Applied Polymer Science, 1997, 66, 8, 1445. Copyright 1997, reprinted by permission of John Wiley & Sons, Inc.

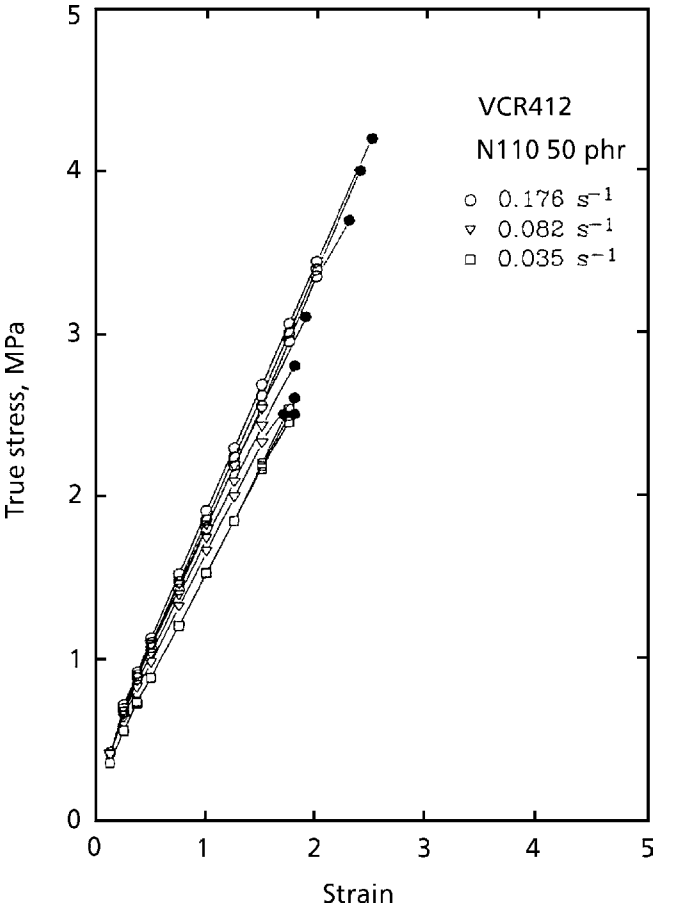

Figure 7.21 Tensile stress-strain curves of VCR412 compound with carbon black N110.

Reprinted from N. Nakajima and Y. Yamaguchi, Journal of Applied Polymer Science, 1997, 66, 8, 1445. Copyright 1997, reprinted by permission of John Wiley & Sons, Inc.

The data with the same symbol shows reproducibility of the measurement, which was within ±3%. It was smaller compared to that of the gum rubbers, ±15%. The stress-strain curves of the carbon black compounds include failure data shown by filled circles. The silica-filled compound of CB22 with coupling agent was very stiff and the specimen slipped out of the grips at the high elongation. With this compound the stress decreased slightly with the increasing deformation rate at the large deformation. This may be the error resulting from slipping. However, the silica-filled compound without the coupling agent and the carbon black filled compounds showed the increase of stress with increasing deformation rate.

In Figures 7.22-7.24, stress-strain curves of gum rubbers and their filled compounds are compared.

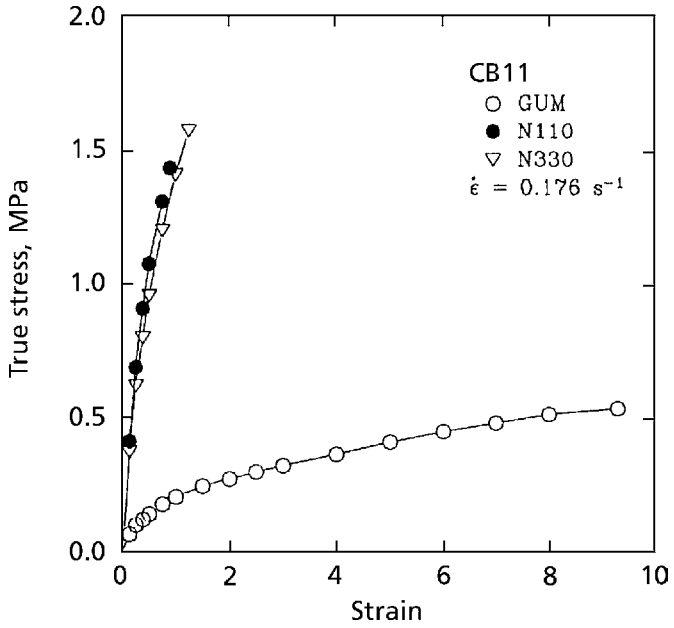

Figure 7.22 Comparison of tensile stress-strain curves of gum rubber and compounds of CB11.

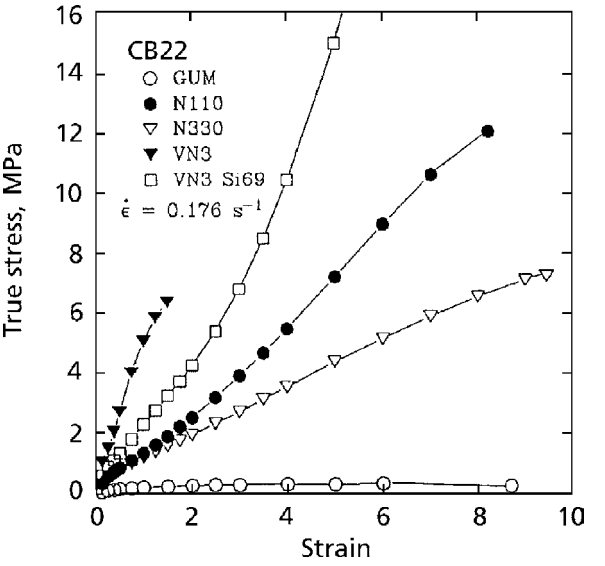

Figure 7.23 Comparison of tensile stress-strain curves of gum rubber and compounds of CB22.

Reprinted from N. Nakajima and Y. Yamaguchi, Journal of Applied Polymer Science, 1997, 66, 8, 1445. Copyright 1997, reprinted by permission of John Wiley & Sons, Inc.

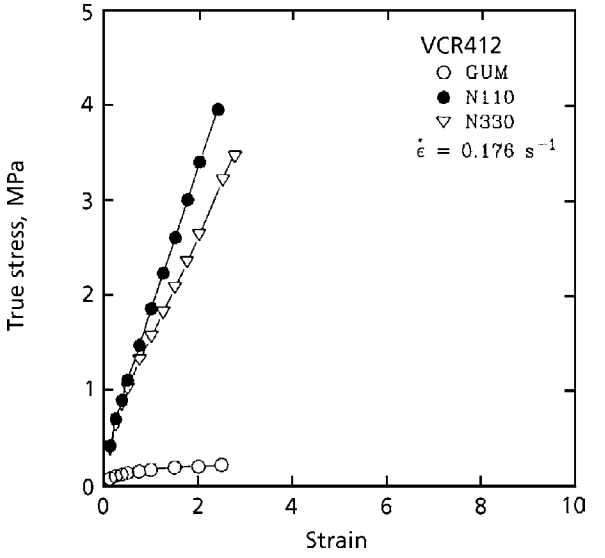

Figure 7.24 Comparison of tensile stress-strain curves of gum rubber and compounds of VCR412.

Reprinted from N. Nakajima and Y. Yamaguchi, Journal of Applied Polymer Science, 1997, 66, 8, 1445. Copyright 1997, reprinted by permission of John Wiley & Sons, Inc.

The stresses for all the compounds are greatly increased by the filler. The gum rubbers of CB11 and CB22 showed a similar elongation at break. However, the elongation at break of the CB11 compound was considerably reduced in the presence of carbon black whereas that of the CB22 compound was unaltered. From previous work [29], CB11 was known to have a higher degree of branching than CB22, but the branches of the former were found to be relatively short whereas those of the latter were long. The more branched rubber is generally known to have a higher affinity to carbon black. This together with the shortness of the branches may be the cause of the reduced elongation at break of the CB11 compound.

On the other hand, long branches are known to aid the retention of elongation at break upon loading with carbon black [19]. This fact accounts for the behaviour of the CB22 compound.

Gum VCR 412 has a much lower strain at break compared to CB11 and CB22. The matrix rubber of VCR 412 is not significantly different from that of CB22, except that it contains crystalline particles. Therefore, the crystalline particles must be affecting the decrease of strain at break. The addition of carbon black does not decrease the strain at break. In this respect it is similar to the CB22.

Referring to Figure 7.23, the silica-filled compound without the coupling agent shows the highest modulus. This is because of the poor dispersion of the filler [30]. The compound with silica and the coupling agent show lower modulus because of a better dispersion. This compound behaves like a crosslinked network; the stress rise indicates limited extensibility. The coupling agent is known to give premature crosslinking during compounding [31]. The carbon black filled compounds show lower modulus than those of silica-filled compounds because of the better dispersion. The compounds with smaller particles of carbon black (N110) show higher modulus than that with larger particles (N330); the better reinforcement from smaller particles is well recognised.

Figures 7.25 and 7.26 show modulus as a function of reduced time (Equation 6.27).

The lines connect the data at the same strain and parallel lines at different strains were obtained. Master curves after application of the modulus shift, Equation. 6.29, are shown in Figures 7.27 and 7.28.

With all compounds the master curves were obtained after the time and the modulus shift. As shown in Figures 7.29-7.31, the direction of the modulus shift was that of strain softening for all compounds.

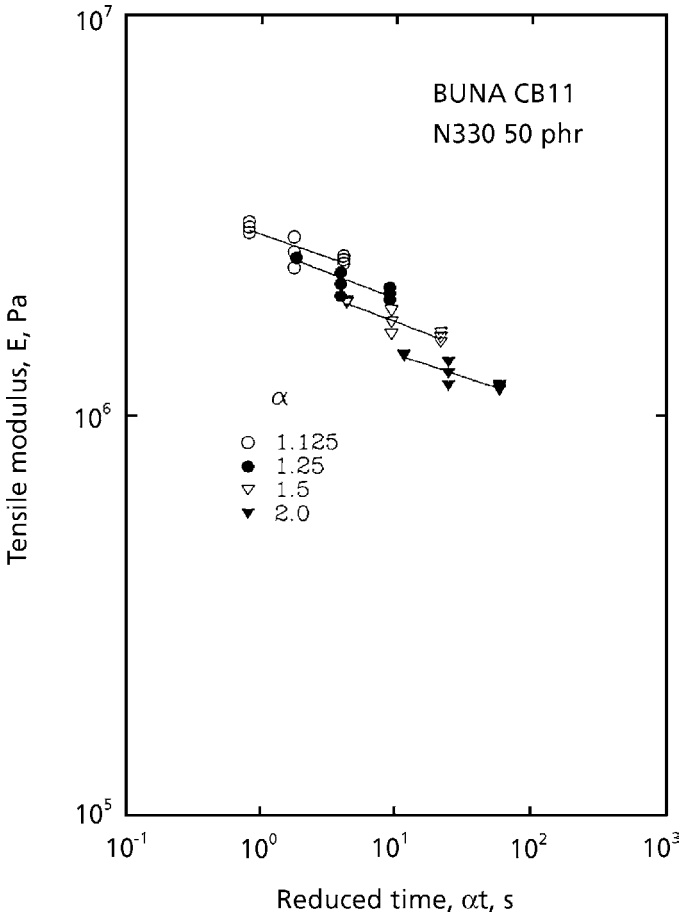

Figure 7.25 Tensile modulus as a function of reduced time at fixed extension ratios for CB11.

The different behaviour of gum rubbers CB11 and CB22 (i.e., strain softening versus strain hardening [29]) is apparently carried over to the difference in the behaviour of the corresponding compounds; that is, the initial strain softening of the CB11 compounds is much higher than that of the CB22 compounds. Also, the softening trends were reversed at the higher elongation in the CB22 compounds (Figure 7.30), indicating the strain hardening of the matrix rubber.

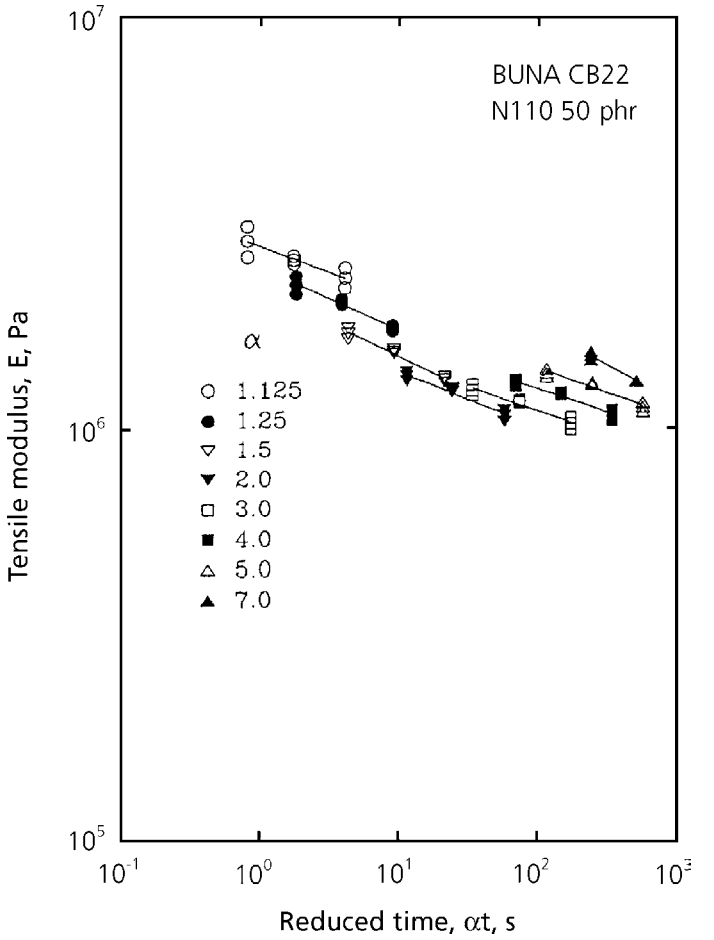

Figure 7.26 Tensile modulus as a function of reduced time at fixed extension ratios for CB22.

Reprinted from N. Nakajima and Y. Yamaguchi, Journal of Applied Polymer Science, 1997, 66, 8, 1445. Copyright 1997, reprinted by permission of John Wiley & Sons, Inc.

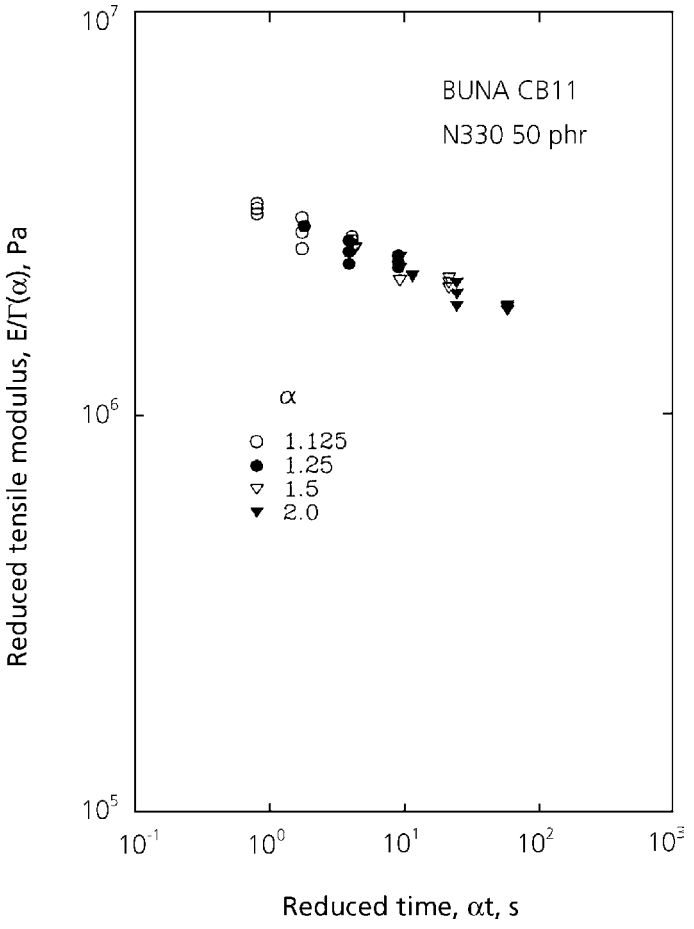

Figure 7.27 Reduced tensile modulus as a function of reduced time at fixed extension ratios for CB11.

Reprinted from N. Nakajima and Y. Yamaguchi, Journal of Applied Polymer Science, 1997, 66, 8, 1445. Copyright 1997, reprinted by permission of John Wiley & Sons, Inc.

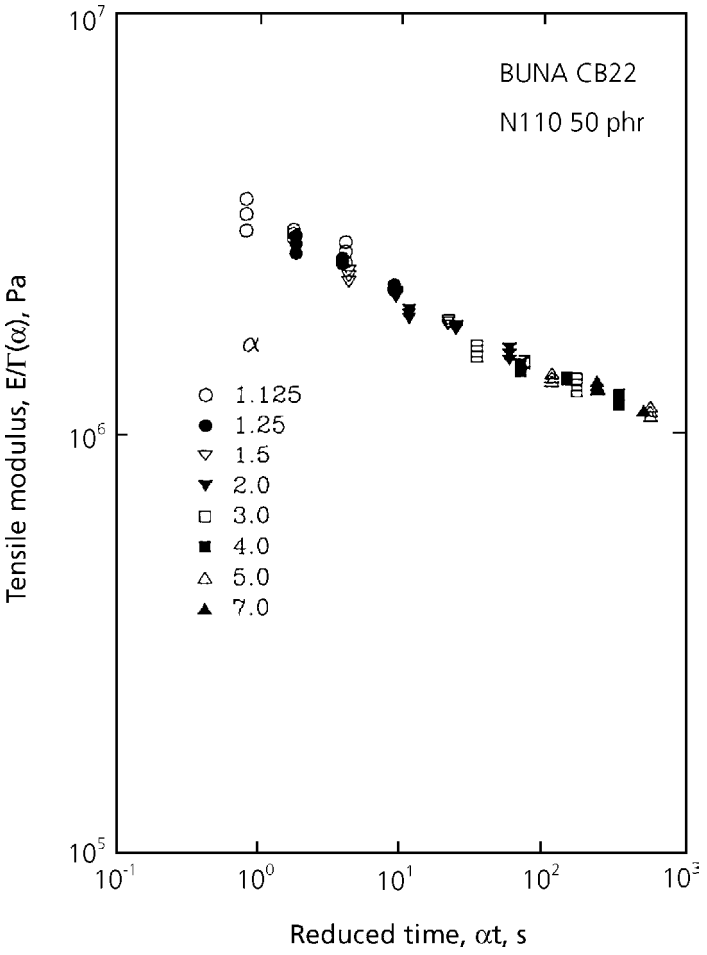

Figure 7.28 Reduced tensile modulus as a function of reduced time at fixed extension ratios for CB22.

Reprinted from N. Nakajima and Y. Yamaguchi, Journal of Applied Polymer Science, 1997, 66, 8, 1445. Copyright 1997, reprinted by permission of John Wiley & Sons, Inc.

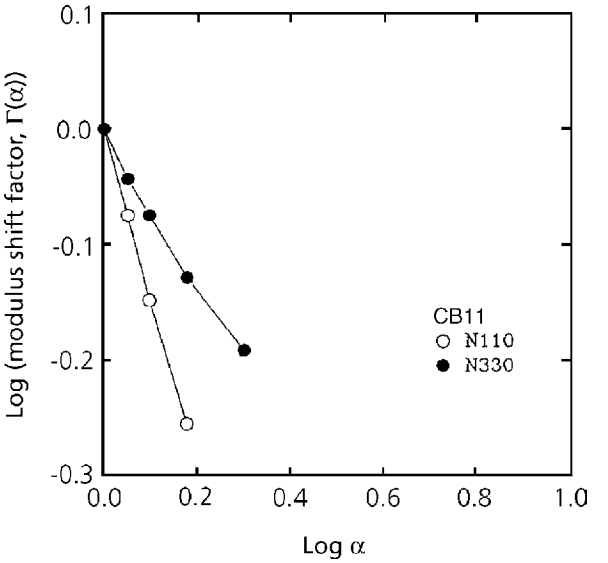

Figure 7.29 Modulus shift factors as a function of extension ratio for CB11 compounds indicating degree of strain softening.

Reprinted from N. Nakajima and Y. Yamaguchi, Journal of Applied Polymer Science, 1997, 66, 8, 1445. Copyright 1997, reprinted by permission of John Wiley & Sons, Inc.

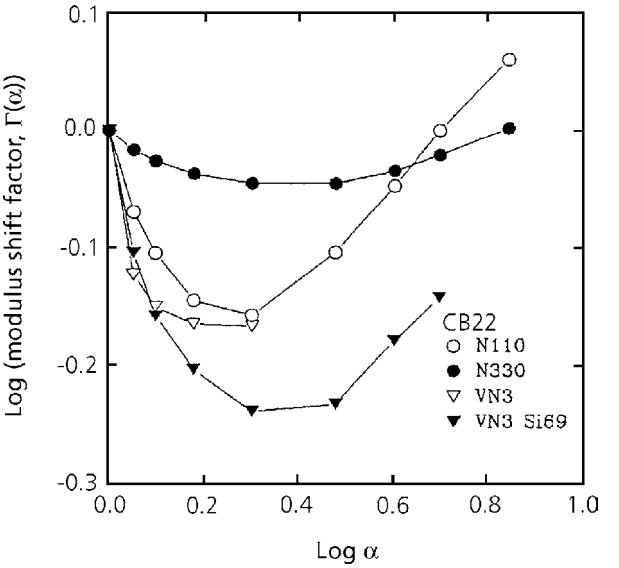

Figure 7.30 Modulus shift factors as a function of extension ratio for CB22 compounds indicating degree of strain softening.

Reprinted from N. Nakajima and Y. Yamaguchi, Journal of Applied Polymer Science, 1997, 66, 8, 1445. Copyright 1997, reprinted by permission of John Wiley & Sons, Inc.

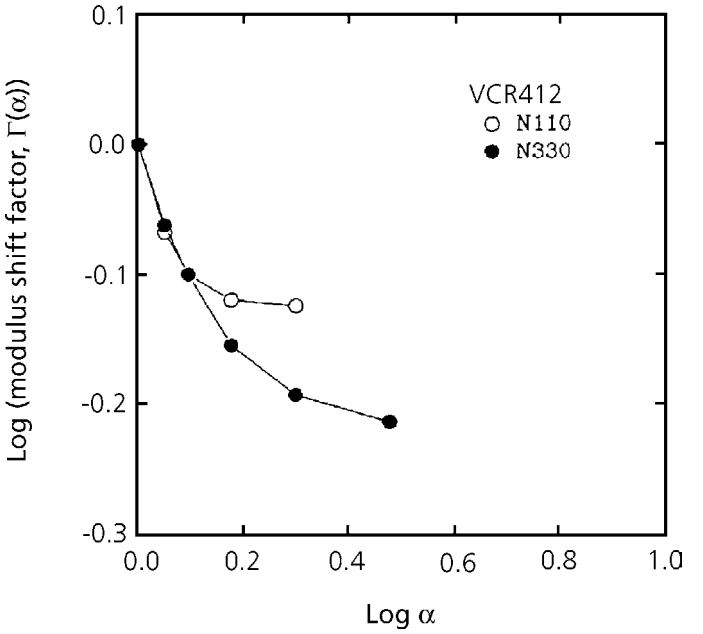

Figure 7.31 Modulus shift factors as a function of extension ratio for VCR412 compounds indicating a degree of strain softening.

Reprinted from N. Nakajima and Y. Yamaguchi, Journal of Applied Polymer Science, 1997, 66, 8, 1445. Copyright 1997, reprinted by permission of John Wiley & Sons, Inc.

The N110 filled compounds of CB11 and CB22 show large degrees of strain-softening compared to those filled with N330 compounds. On the other hand VCR412 compounds with N110 and N330 behave similarly. The carbon black N110 is more difficult to disperse than the N330. The compounds exhibiting a greater degree of strain softening, when other variables are unchanged, have relatively poor dispersion of the filler. VCR412 was the easiest to handle on the mill when either of the carbon blacks was incorporated. This accounts for the same degree of strain softening for N110 and N330. On the other hand, if we compare CB22 and VCR412 compounds with carbon black N330 (see Figures 7.30, and 7.31), the CB22 compound shows much less strain softening than the VCR412 compound does. The difference must come from the difference of the behaviours of the matrix rubbers: CB22 produces strain hardening and VCR412 strain softening. These rubbers with N110 show the same degree of strain softening. As mentioned, the explanation is a poor dispersion of N110 in CB22, a fact that resulted in substantial strain softening.

The effect of silica on strain softening is larger than that of carbon black. This is because of the poorer dispersion of silica compared to that of carbon black. Because of the poor dispersion of the silica and anomalous crosslinking due to the coupling agent, no further comment can be made for the silica-filled compounds.

Whereas the extent and the manner of the strain softening provides useful information on the effects of fillers and that of the structure of matrix rubbers, the data are taken relative to the moduli at the infinitesimal strain. Therefore, the absolute magnitude of moduli must also be examined. The data in Table 7.4 indicate clearly that the moduli of CB22 compounds are significantly lower than those of CB11 and VCR412 at all strain rates. In the previous observations [29, 32] with gum rubbers, CB22 did not give a noticeable strain-induced crystallisation while CB11 and VCR412 clearly indicated crystallisation. Therefore, the above differences in the compound moduli are attributable to the difference in the ease of strain-induced crystallisation of the matrix rubbers.

Table 7.4 Tensile Modulus of Compound

	CB11			CB22			VCR412		
	M50	**M100**	**M200**	**M50**	**M100**	**M200**	**M50**	**M100**	**M200**
$\dot{\varepsilon}$=0.176 s^{-1}									
N110	1.08	–	–	0.85	1.34	2.48	1.10	1.86	3.40
N330	0.96	1.41	–	0.76	1.19	1.93	1.01	1.57	2.64
$\dot{\varepsilon}$=0.082 s^{-1}									
N110	1.03	–	–	0.77	1.24	2.33	1.03	1.74	–
N330	0.85	1.27	–	0.66	1.05	1.67	0.87	1.36	2.36
$\dot{\varepsilon}$=0.035 s^{-1}									
N110	0.92	–	–	0.66	1.08	2.06	0.89	1.53	–
N330	0.88	1.18	–	0.57	0.91	1.43	0.82	1.33	2.27
M50, M100 and M200 are the modulus at 50, 100 and 200% strain, respectively									

References

1. N. Nakajima, H. H. Bowerman and E. A. Collins, *Journal of Applied Polymer Science,* 1977, **21**, 11, 3063.

2. N. Nakajima, *Polymer International,* 1995, **36**, 2, 105.

3. ASTM D3616-95
Standard Test Method for Rubber, Raw - Determination of Gel, Swelling Index and Dilute Solution Viscosity.

4. ASTM D1646-96a
Standard Test Methods for Rubber - Viscosity, Stress Relaxation and Pre-Vulcanization Characteristics (Mooney Viscometer).

5. N. Nakajima and E. A. Collins, *Rubber Chemistry and Technology,* 1975, **48**, 4, 615.

6. T. L. Smith in *Rheology: Theory and Applications*, Volume 5, Ed., F. R. Eirich, Academic Press, New York, 1969, Chapter 4

7. N. Nakajima, *Polymer Engineering and Science,* 1979, **19**, 3, 215.

8. W. P. Cox and E. H. Merz, *Journal of Polymer Science*, 1958, **28**, 118, 619.

9. A. R. Payne and R. E. Whittaker, *Rubber Chemistry and Technology,* 1971, **44**, 2, 440.

10. *Reinforcement of Elastomers*, Ed., G. Kraus, Wiley, New York, 1965, Chapter 3.

11. A. K. Sircar and A. Voet, *Rubber Chemistry and Technology,* 1970, **43**, 5, 973.

12. N. Nakajima, J. J. Scobbo, Jr., and E. R. Harrell, *Rubber Chemistry and Technology,* 1987, **60**, 5, 761.

13. N. Nakajima, *Journal of Non-Newtonian Fluid Mechanics*, 1983, 12, 349.

14. S. Montes, J. L. White and N. Nakajima, *Journal of Non-Newtonian Fluid Mechanics*, 1988, 28, 183.

15. N. Nakajima and E. R. Harrell, in *Encyclopedia of Fluid Mechanics,* Volume 9, Ed., N. P. Cheremisinoff, Gulf Publishing Co., Houston Texas, 1990, p.277-314.

16. F. Bueche in *Reinforcement of Elastomers*, Ed., G. Kraus. Wiley, New York, 1965, p.6.

17. L. Mullins and N. R. Tobin, *Rubber Chemistry and Technology*, 1967, **39**, 4, 799.

18. G. Kraus in *Science and Technology of Rubber*, Ed., F. R. Eirich, Academic Press, New York, 1978, p.339.

19. N. Nakajima and J. J. Scobbo, Jr., *Rubber Chemistry and Technology*, 1988, **61**, 1, 137.

20. N. Nakajima, *Rubber Chemistry and Technology*, 1988, **61**, 5, 938.

21. H. Serizawa, M. Ito, T. Kanamoto, K. Tanaka and A. Nomura, *Polymer Journal, (Japan)*,1982, **14**, 2, 149.

22. H. Serizawa, T. Nakamura, M. Ito, K. Tanaka and A. Nomura, *Polymer Journal (Japan)*, 1983, **15**, 3, 201.

23. H. Serizawa, T. Nakamura, M. Ito, K. Tanaka and A. Nomura, *Polymer Journal (Japan)*, 1983, **15**, 3, 543.

24. N. Nakajima and R. A. Miller, *Rubber Chemistry and Technology,* 1988, **61**, 2, 362.

25. C. Y. Ma, J. L. White, F. C. Weissert, A. I. Isayev, N. Nakajima and K. Min, *Rubber Chemistry and Technology,* 1985, **58**, 4, 815.

26. H. J. Song, J. L. White, K. Min, N. Nakajima and F. C. Weissert, *Advances in Polymer Technology*, 1988, **8**, 4, 431.

27. N. Nakajima and Y. Yamaguchi, *Journal of Applied Polymer Science*, 1997, **66**, 8, 1445.

28. M. Takayanagi, Presented at the 19th Annual Meeting of the International Institute of Synthetic Rubber Producers, Hong Kong, 1978, Paper No.21.

29. N. Nakajima and Y. Yamaguchi, *Journal of Applied Polymer Science,* 1996, **61**, 9, 1525.

30. M. P. Wagner, *Rubber Chemistry and Technology*, 1976, **49**, 3, 703.

31. N. Nakajima, W. J. Shieh and Z. G. Wang, *International Polymer Processing*, 1991, **6**, 4, 290.

32. N. Nakajima and Y. Yamaguchi, *Journal of Applied Polymer Science*, 1996, **62**, 13, 2329.

8 Rheology of Gum Rubber and Compound

8.1 Rheometry

Rheology is a study of deformation and flow. In a simplistic way the deformation may be associated with elasticity and the flow with viscosity. Then, rheology is synonymous to viscoelasticity. Indeed, sometimes these terms are used interchangeably. An extensive treatment has already been given for the viscoelastic behaviour of gum rubbers and compounds in Chapter 6 and 7.

The reasons why rheology is selected as a separate chapter is as follows: the capillary rheometer and the rotational rheometer, which had originally been designed for the rheological measurements of liquids have been used for the observation of gum rubber and compound behaviour. The question is what these measurements really mean, because gum rubbers as well as compounds are not liquids but they are in the rubbery state. However, in this chapter, the conventional practice of treating the material as if it were liquid is followed. Not only is the viscosity-shear rate relationship discussed but also the melt fracture, extrudate swell and slip. Shown in Figure 8.1 are 'flow curves' of NBR samples, A, B, C, and D at 100 °C [1].

These curves are very much like the ones obtained with thermoplastic melts, exhibiting a non-Newtonian behaviour. The only difference is that with the plastic melt the curves become flatter, decreasing the negative slope with the decreasing shear rate. This suggests that if the lower shear-rate-data were obtained, the extension of the curves of Figure 8.1 would become like those of the thermoplastics.

From this discussion the question arises, of whether or not the flow mechanism is the same for plastic melt and rubber throughout the shear-rate range of non-Newtonian flow. As pointed out with the curve A, the melt fracture occurs at a shear rate higher than that indicated by the arrow. With the other three samples the melt fracture occurred over the entire range of the shear rate. The appearance of the extrudates is depicted in Figure 8.2. Onset of the melt fracture suggests some sort of a discontinuity.

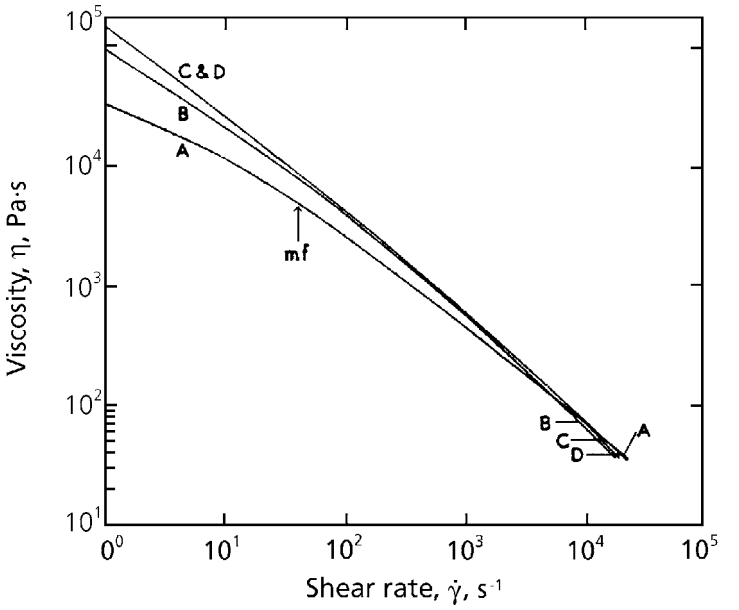

Figure 8.1 Flow curves of Samples A, B, C and D at 100 °C; mf is the onset of melt fracture.

Reprinted from N. Nakajima and E. A. Collins, Polymer Engineering and Science, 1974, 14, 2, 137. Copyright 1974, Society of Plastics Engineering.

This is consistent with the previously described viscoelastic behaviour of gum rubber where there is a transition from the rubbery state to the flow state over a longer time scale. The longer time scale corresponds to the lower shear rate where the material is in the flow state.

With the higher MW rubber the flow-rubber transition occurs at the lower shear rate so that the transition does not appear in Figure 8.1 for samples B, C, and D. When the gum rubbers in the rubbery state are pushed from the barrel of the rheometer into the capillary they break because the large deformation from the barrel to capillary exceeds the breaking strain.

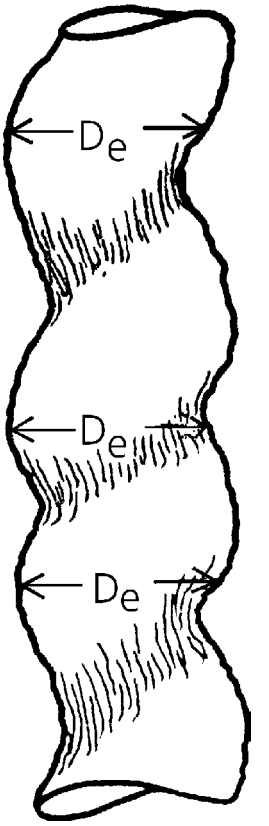

Figure 8.2 Shape of distorted extrudate. De is the extrudate diameter.

Reprinted from N. Nakajima and E. A. Collins, Polymer Engineering and Science, 1974, 14, 2, 137. Copyright 1974, Society of Plastics Engineering.

Next the behaviour of the 'flow', which is in reality a combination of the fracture and a bulk transport through capillary will be examined.

Figure 8.3 is a plot of pressure (expressed as a force on the piston) against the L/D of the capillary at fixed shear rates.

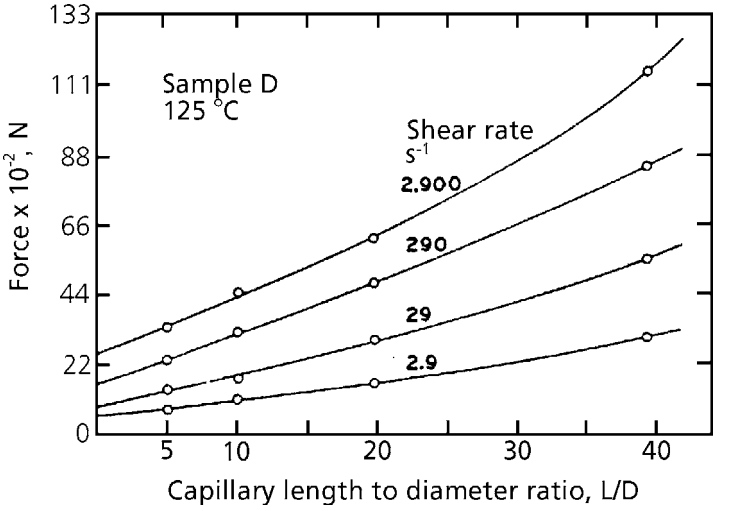

Figure 8.3 Pressure versus capillary L/D at constant shear rate for Sample D at 125 °C.

Reprinted from N. Nakajima and E. A. Collins, Polymer Engineering and Science, 1974, 14, 2, 137. Copyright 1974, Society of Plastics Engineering.

These curves look very much like the ones obtained with thermoplastic melts, except that the entrance pressure loss (the force at L/D = 0 in the figure), is much larger. With thermoplastic melt, this loss consists of the viscous resistance of flow in the barrel and the elastic energy associated with deformation at the constriction leading into the capillary. With rubbers the energy of break must have a significant contribution.

The behaviour of rubber at the capillary entrance is similar to that in the transient region observed by the rotational rheometer, see Figure 4.6 [2]. The peak of the torque-rise curve is interpreted to be breaking strain and compared to that observed with the tensile stress-strain measurement, see Figure 8.4 [3].

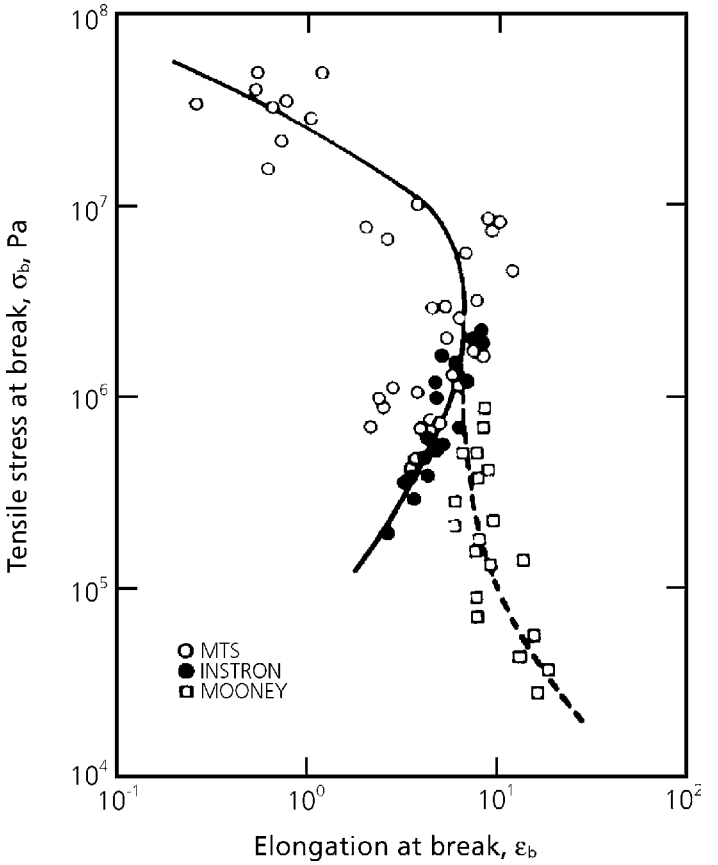

Figure 8.4 Ultimate properties.

Reprinted from N. Nakajima and E. A. Collins, Rubber Chemistry and Technology, 1977, 50, 4, 791. Copyright 1977, Rubber Division of the ACS.

The solid curve represents locus of the stress and strain at break, observed with elongation and the broken curve with shear after converting the shear strain to the elongational equivalent. A reasonable agreement between the elongation data and shear data shows that rubber breaks prior to exhibiting a flow-like behaviour. Because the rotational rheometer used has a wide distribution of the strain, the highest strain was used in the above calculation.

A gradual decrease of the torque curve passing the peak in Figure 4.6 indicates that the break is progressing in the rubber contained in the rheometer cavity.

In Figure 8.3, the curves are concave-upward in shape and the trend becomes more prominent at the higher shear rate. In this plot the slope of the curve is the shear stress, τ.

For a constant shear rate, $\dot{\gamma}$, the stress must be constant and independent of L/D. The increasing slope implies that the viscosity increases with L/D.

$$\tau = \eta \dot{\gamma} \tag{8.1}$$

This was previously interpreted as a pressure effect because with the larger L/D, a higher pressure is required to extrude the rubber. However, this interpretation may be incorrect, because gum rubber is practically incompressible and therefore, viscosity is not expected to depend upon pressure. This is demonstrated in the following experiments.

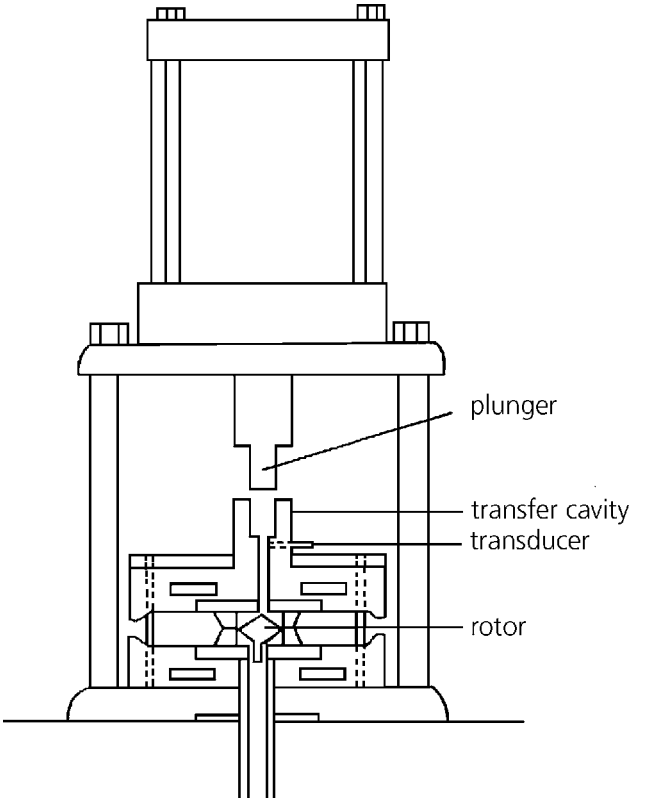

Figure 8.5 Schematic of rebuilt pressurised multispeed viscometer.

Figure 8.5 shows a rotational rheometer, which is modified to apply static pressure on the sample in the rheometer cavity [4]. This is done by charging an excess sample from the top and pressing it with a plunger. This device enables the maintenance of a constant pressure during the measurement of viscosity. On the other hand with a capillary rheometer the static pressure on the sample is variable, decreasing from the barrel pressure to near ambient pressure at the exit. With this rotational rheometer a number of measurements were made with NR, *cis*-1,4-BR, S-SBR, NBR, EPDM and FPM fluoroelastomer at 44, 60, 80 and 100 °C over the shear rate range of 3 x 30^{-2} and 2.5 s^{-1}. No perceptible pressure effect was found at the applied pressure of 1.1 and 6.4 MPa. Examples of the pressure effects are shown in Figures 8.6 and 8.7.

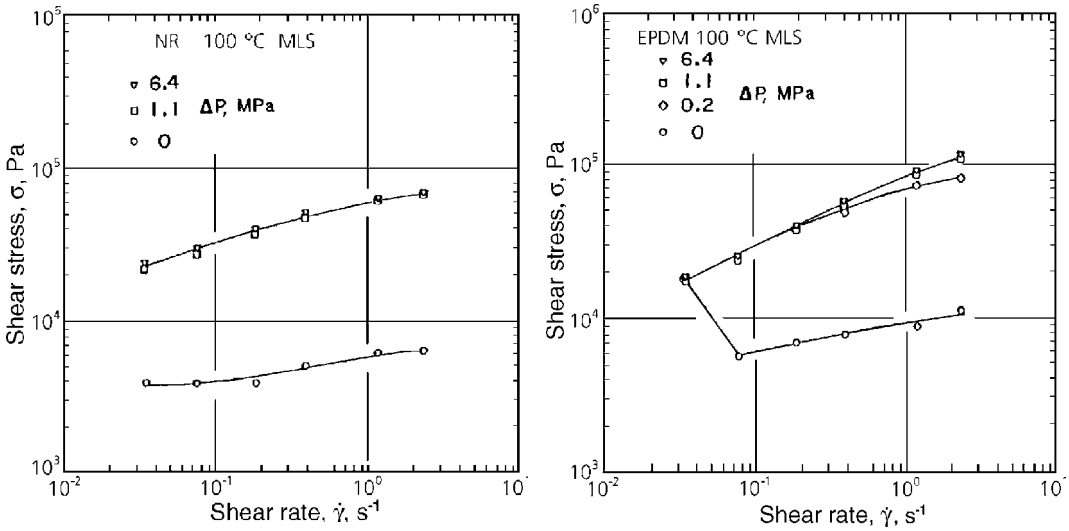

a) b)

Figure 8.6a Shear stress σ_{12} as a function of shear rate $\dot{\gamma}$ for gum NR (SMR-5) from a Mooney disk rheometer with a smooth rotor. The influence of pressure is shown. T= 100 °C.
Figure 8.6b Shear stress σ_{12} as a function of shear rate $\dot{\gamma}$ for gum EPDM from a Mooney disk rheometer with a smooth rotor. The influence of pressure is shown. T= 100 °C.

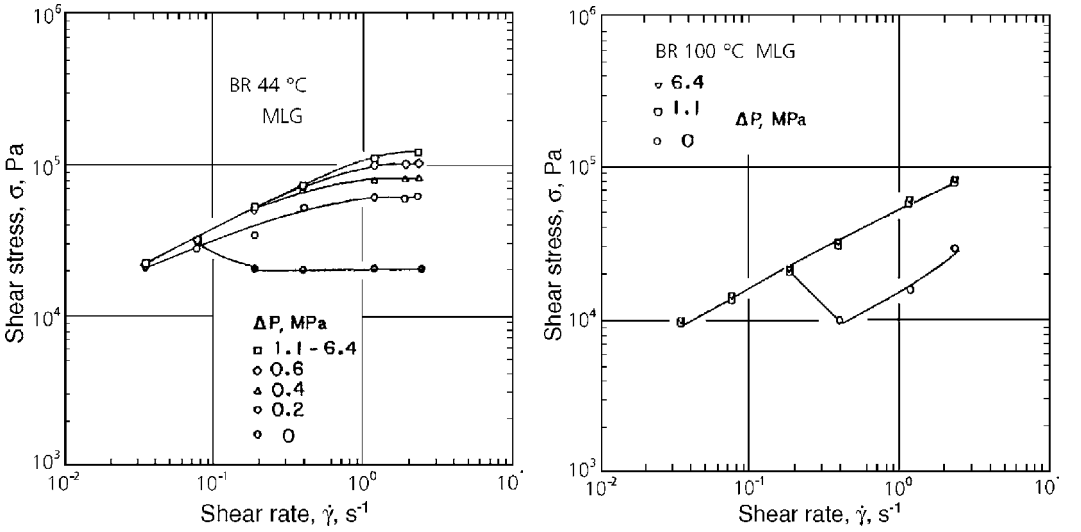

a) b)

Figure 8.7a Shear stress σ_{12} as a function of shear rate $\dot{\gamma}$ for gum BR from a Mooney disk rheometer with a grounded rotor. The influence of superposed pressure is shown at 44 °C.

Figure 8.7b Shear stress σ_{12} as a function of shear rate $\dot{\gamma}$ for BR from a Mooney disk rheometer with a grounded rotor. The influence of superposed pressure is shown at 100 °C.

These results show that the upwardly concave curves of Figure 8.3 are not due to the pressure-effect on viscosity. For some reason a higher pressure is required to extrude gum rubber for a longer L/D. A possible explanation is that the behaviour of gum rubber is not really a flow, a fact which is obvious in the fractured extrudate. The fracture is initiated by a vacuole formation as explained in Chapter 4. The higher pressure suppresses the vacuole formation; therefore, a higher force is necessary for the fracture to occur.

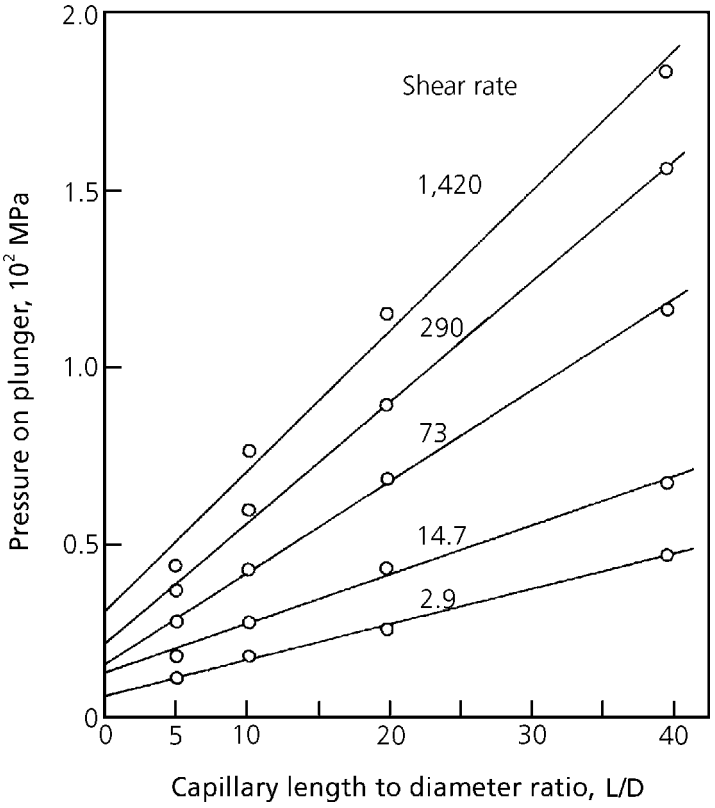

Figure 8.8 Pressure as a function of capillary L/D. Sample 2; shear rates in s^{-1} as indicated; 125 °C.

Reprinted from N. Nakajima and E. A. Collins, Rubber Chemistry and Technology, 1975, 48, 4, 615. Copyright 1975, Rubber Division of the ACS.

Figure 8.8 is a plot similar to Figure 8.3 except that the sample is an NBR compound containing 40 phr of carbon black N550 [5]. The plots are not concave upward. The compound consists of supermolecular flow units, created during mixing. Therefore, it is a flowable material and no fracture is required. In a closer examination these curves may be concave downward. If this trend is real, there are possible explanations; one is a possible inward migration of the filler particles away from the capillary wall. The other is a slip at the capillary wall. Both phenomena may become prominent at the higher shear rate and with the larger L/D.

8.2 Slip

It is obvious that in rubber processing there will be slip, because the surface of processing equipment in contact with gum rubbers and compounds is usually shiny. This is in contrast to plastic processing equipment, in which the surfaces become coated with a thin layer of the degraded material. With plastics this fact indicates the velocity of the melt at the metal interface is zero, i.e., laminar shear flow. A study of slip is multi-faceted, because there are many types of slip, a steady slip, slip with a lubricated layer, slip-stick, slip involving a fracture at the interface or rubbing like a dynamic friction measurement.

In this section slip is treated as if it were one type of behaviour. In Figures 8.6 and 8.7 at the static pressure of 0.6 MPa or lower the shear stresses are considerably lower than the values at 1.1-6.4 MPa. The deviation is larger at the lower pressure and also at the higher shear rate. This indicates the presence of slip. At atmospheric pressure, there is a large reduction of the resistance (expressed as shear stress). However, at very low shear rates, there is no reduction of the resistance, indicating that the sample contact with the rotor is good.

A similar observation is made with carbon-black compounds. Examination of the sheared samples indicated a failure of adhesion of material to the rotor, starting from the location of the highest deformation, i.e., the periphery of the rotor, and progressing inward.

The movement of material in the barrel of a capillary rheometer was used to observe the wall slip [6]. SBR 1500 (E-SBR) and its compounds are used with a flow marker as illustrated in Figure 8.9.

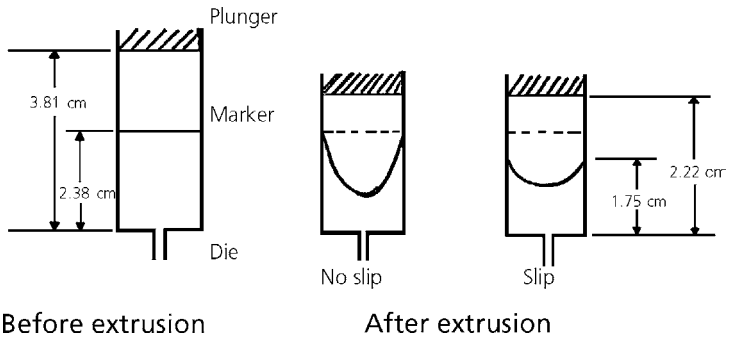

Figure 8.9 Marker technique used for observing wall slippage of elastomer compounds.

Reprinted from C-Y. Ma, J. L. White, F. C. Weissert, A. I. Isayev, N. Nakajima and K. Min, Rubber Chemistry and Technology, 1985, 58, 4, 815. Copyright 1985, Rubber Division of the ACS.

In this experiment the gum rubber did not show a slip but the compounds slipped at a higher loading of the filler (20% volume) see Figure 8.10.

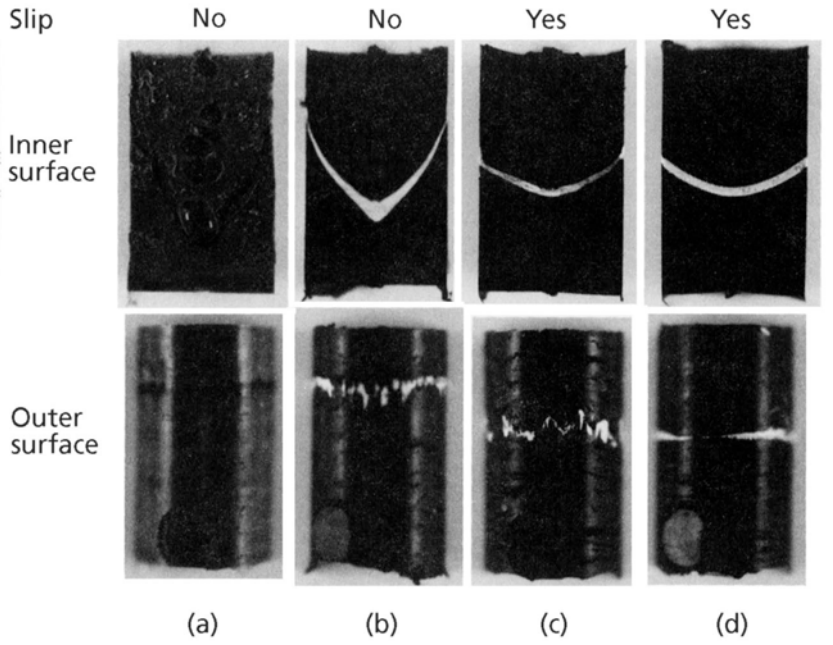

Figure 8.10 Detailed observation of wall slippage for E-SBR and its compounds at 100 °C, $\dot{\gamma}_a = 1.78 \times 10^{-2}\ s^{-1}$.
a) gum E-SBR
b) E-SBR + 10 vol% carbon black
c) E-SBR + 20 vol% carbon black
d) E-SBR + 30 vol% carbon black

It showed a slip only at the higher extrusion rate, Figure 8.11.

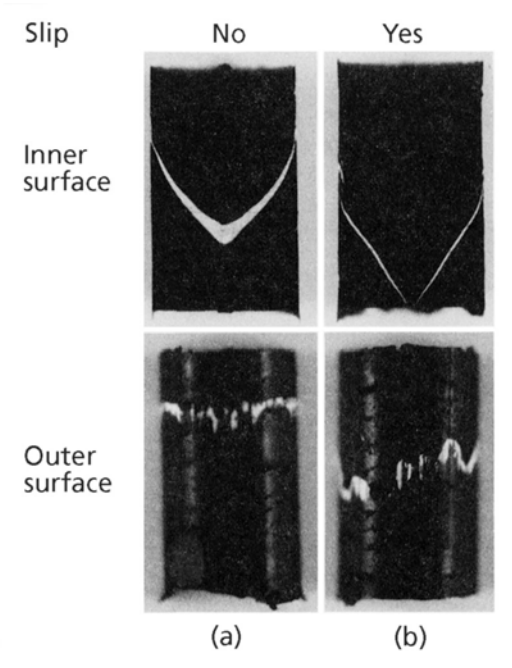

Figure 8.11 Influence of extrusion rate on wall slippage for E-SBR + 10 vol% carbon black at 100 °C.
a) $\dot{\gamma}_a = 1.78 \times 10^{-2}\ s^{-1}$.
b) $\dot{\gamma}_a = 1.78 \times 10^{-1}\ s^{-1}$

Reprinted from C-Y. Ma, J. L. White, F. C. Weissert, A. I. Isayev, N. Nakajima and K. Min, Rubber Chemistry and Technology, 1985, 58, 4, 815. Copyright 1985, Rubber Division of the ACS.

8.3 Extrudate shrinkage

Extrudate shrinkage is another way of expressing so-called 'die swell'. In the rubber industry, shrinkage is one of the serious concerns, because the extrudate is cut at a certain length. When there is non-uniform shrinkage, the length of the cut pieces becomes non-reproducible. This causes various problems of material handling. A well-known example is in tyre-building, where the ends of the piece wound around a drum fail to meet.

In this section the phenomenon is described as extrudate swell. Although the practical problem is usually with compounds, the swell of both gum rubbers and compounds will be discussed.

Between gum rubber and compound there are number of differences in the 'extrusion mechanisms'. The gum rubber usually fractures in extrusion but with compounds there is no melt fracture or very slight, when it occurs. The extrudate swell of gum rubber is very large but it is considerably reduced in the presence of filler.

With the plastic melt it was shown that the extrudate swell is a recovery of memory, which was introduced by the deformation of the melt at the entrance to the capillary rheometer. As the melt flows through a capillary, the memory fades by relaxation. Therefore, the shorter the residence time in the capillary, the less memory is lost. This results in the higher swell at the higher shear rate, where the residence time is shorter. Also, the swell decreases with a longer capillary, because the residence time is longer.

Apparently the above interpretation is not applicable to the extrudate swell of gum rubbers. Shown in Figure 8.12 are the shear-rate dependence of swell data of four NBR [1].

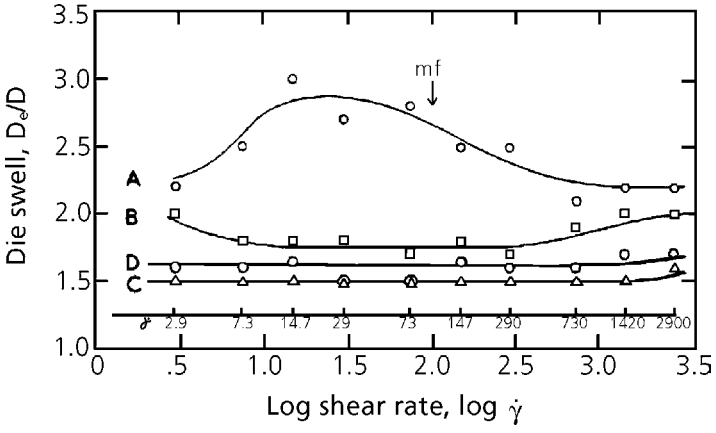

Figure 8.12 Shear rate dependence of die swell at 125 °C, L/D = 5 for samples A, B, C and D. See Table 7.2 for description of samples; mf is the onset of melt fracture.

Reprinted from N. Nakajima and E. A. Collins, Polymer Engineering and Science, 1974, 14, 2, 137. Copyright 1974, Society of Plastics Engineering.

Only for the lower MW rubber, A, at low shear rate, did the swell increase with increasing shear rate. This shear-rate region of sample A is in the flow state and therefore, the behaviour is similar to that of plastics melt. However, at the higher shear rate, and particularly after the melt fracture the swell decreased significantly. The extrudate going over maximum swell is not generally recognised.

A possible explanation for the decreasing swell with the increasing shear rate is as follows: with the plastic melt and the flow state of rubber, the memory loss results from the relaxation mechanism. In the rubbery state the fracture of the material is involved. The fracture brings about memory-loss also. When the relaxation mechanism contributes less and less and the fracture becomes more dominant, the swell decreases, eventually reaching a constant value.

The decrease of the swell of sample B at the lower shear rate may also be similarly explained. The samples C and D containing a large amount of gel reflect the fracture and consequence of the loss of memory. There is a tendency to increase the swell slightly at the very high shear rate, see Figure 8.12. This behaviour may be attributable to the more elastic nature of the material at the higher shear rate.

The L/D dependence of the swell is shown in Figure 8.13 [1]. The decrease of the swell with the increase of L/D indicates that the relaxation mechanism is also operating with samples A and B. A mechanism of the memory loss with the samples C and D is through fracture.

Figure 8.14 shows the shear rate dependence and L/D dependence of extrudate swell of compound [2]. Both dependencies are there even though they are rather small compared to those of gum rubbers. The trend is to imply a relaxation mechanism, the higher swell at the higher shear rates and the lower swell with the larger L/D. The deformation of the supermolecular flow units and their relaxation may be the explanation.

There is a longstanding question as to whether long branching increases extrudate swell or not. One argument is that it does increase swell. This opinion is based on the observations on melt processing of plastics, for example, film-drawing. When the drawing-speed is increased, the film eventually becomes stiff and difficult to draw. Sometimes, the film vibrates and tears. When long branches are present in the polymer the above behaviour is accentuated. In general, behaviour like this observed in plastic processing is loosely termed ‘elastic’. When the behaviour becomes more elastic because of the presence of long branches, elastic memory increases. Therefore, the extrudate swell, being recovery of memory, increases.

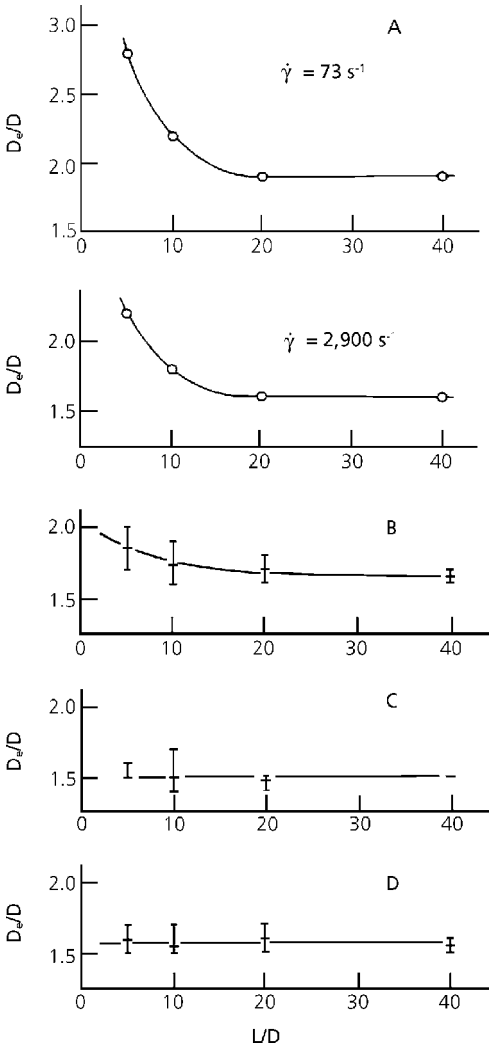

Figure 8.13 Dependence of die swell on capillary L/D at 125 °C for Samples A, B, C, and D. See Table 7.1 for description of samples.

Reprinted from N. Nakajima and E. A. Collins, Polymer Engineering and Science, 1974, 14, 2, 137. Copyright 1974, Society of Plastics Engineering.

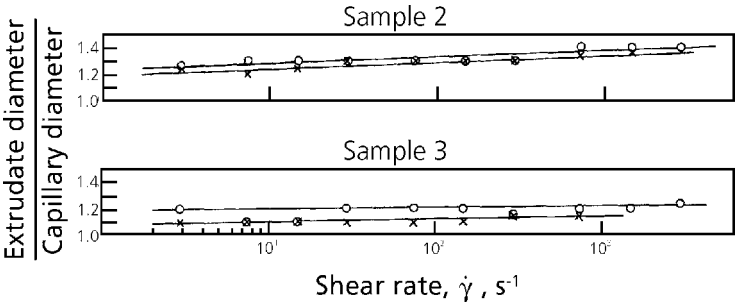

Figure 8.14 Extrudate diameter as a function of shear rate, Samples 2 and 3 of Table 7.1.
L/D = 5 (o); L/D = 40 (x).

Reprinted from N. Nakajima and E. A. Collins, Rubber Chemistry and Technology, 1975, 48, 4, 615. Copyright 1975, Rubber Division of the ACS.

The other argument which opposes to the previous argument is based on fundamental viscoelastic studies with 'monodispersed' polymers, where the only variable is the long branch, linear versus equal-arm star branch molecule. The steady state compliance of the branched polymer is lower than that of the linear polymer; therefore, the steady state memory in the former is less than that in the latter. This means the extrudate swell of the branched polymer is less than that of the linear polymer.

The error in both arguments is that the variety of branch pattern is not recognised. The error in drawing the conclusion from the fundamental study is that it does not recognise the distinction between linear and nonlinear viscoelastic behaviour. Whereas the fundamental studies are conducted under small deformations where the material behaviour is linear, the extrudate swell concerns nonlinear, large deformation. There is a possibility that the relative degree of swelling between two samples at the small deformation may be reversed at the large deformation. This is one of the 'crossover' phenomena.

The crossover may occur also with shear rate such that the relative degree of swell at the lower shear rate may be reversed at the higher shear rate. At the lower shear rate the relaxation of memory is operating but at the higher shear rate the memory loss resulting from fracture may dominate. If the branching introduces long relaxation times, it enhances the swell at the lower shear rate. If the branching results in fracture, the swell is decreased at the higher shear rate. Therefore, whether long branches increase the swell or not depends upon the branch pattern and the extrusion conditions.

This discussion concerns the fully recovered extrudate. In reality the recovery of memory is time-dependent. Cotten conducted a detailed study of the time-dependence with a use of laser beam [7, 8]. SBR 1500 containing 50 phr of carbon black of representative commercial grades was used. A major discovery was the presence of two mechanisms; one was a very fast recovery at less than 0.1 seconds. The other was a much slower recovery towards an equilibrium. The latter is what may be expected from the viscoelastic nature of the material and similar to that observed with plastic melts [9]. The fast recovery had never been observed before, although the die swell of plastic melts had sometimes been arbitrarily classified into a fast and a slow part. The magnitudes of the fast and slow swell were about the same at 25 – 37% at 350 s^{-1} shear rate.

In detail, the fast recovery is clearly related to the surface area and the structure of carbon black, the larger the surface areas by nitrogen absorption (see Chapter 9) and the lower the structure by dibutyl phthalate (DBP) absorption (see Chapter 9) the larger is the swell. The slow recovery was not clearly related to the carbon black properties. What causes the fast and slow recovery is the subject of future study. The fast recovery may primarily be related to the deformation of carbon black network and the slow recovery to the deformation of the rubber matrix.

8.4 Yielding

The yielding of compounds have been observed in elongational as well as in flow measurements. An example of the latter is shown in Figure 8.15 [10].

An extensive examination was conducted on the yielding phenomena associated with various rheological measurements with an NR and S-SBR. Carbon blacks were N110, N326 and N990 at 0, 10, 20 and 30% by volume. Experiments carried out were (i) stress relaxation, (ii) transient and steady state shear flow, (iii) stress relaxation after steady flow, (iv) sequential shear flow history and (v) storage effect.

The yielding was observed in all these measurements with N110 and N326 at the volume concentration of 20% and higher. This implies the presence of structure built by carbon black. The yield value was significantly dependent on the previous shear history; the milder the shear treatment the larger was the yield value, as shown in Figure 8.16, of the relaxation curves and in Figure 8.17 of relaxation after cessation of flow. Destruction of the structure occurs to a different degree depending upon the severity of the shear history.

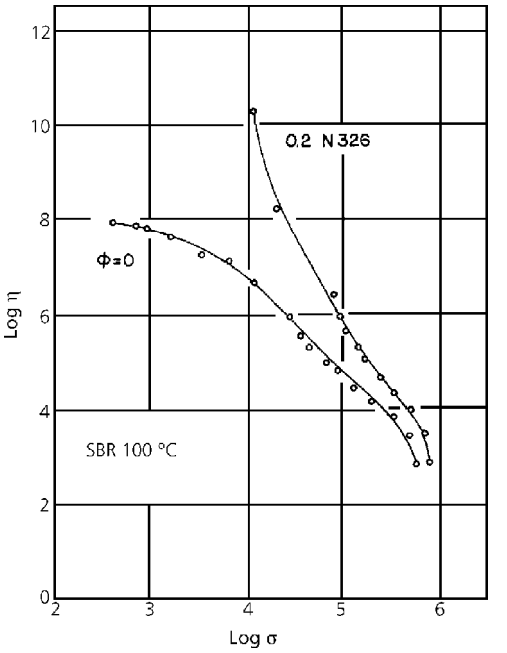

Figure 8.15 Steady state shear viscosity η as a function of shear stress for SBR and its 0.2 phr N326 carbon black compounds, T = 100 °C.

Reprinted from S. Montes, J. L. White and N. Nakajima, Journal of Non-Newtonian Fluid Mechanics, 1988, 28, 183. Copyright 1988, with permission from Elsevier Science.

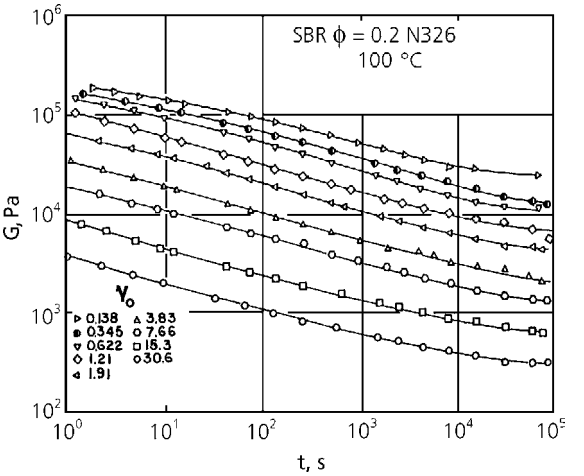

Figure 8.16 Relaxation modulus G (t) from small instantaneous strains. SBR + 0.2 phr volume fraction black, T = 100 °C.

Reprinted from S. Montes, J. L. White and N. Nakajima, Journal of Non-Newtonian Fluid Mechanics, 1988, 28, 183, Copyright 1988, with permission from Elsevier Science.

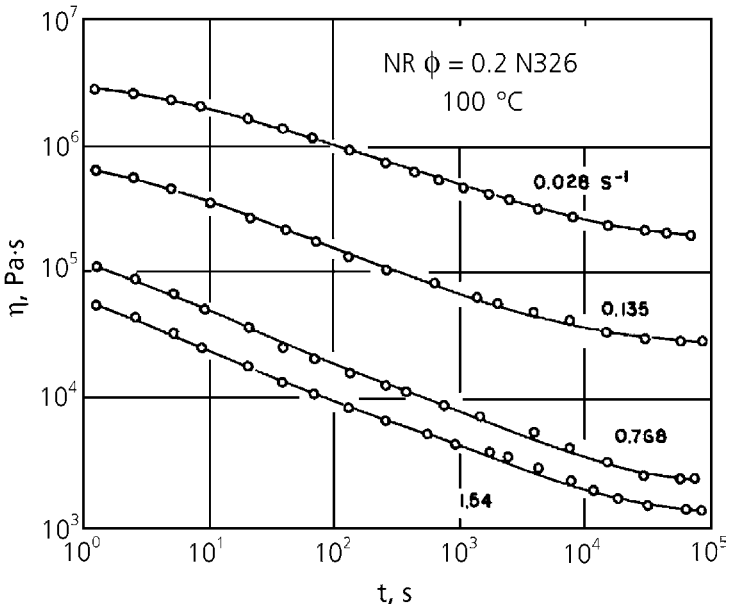

Figure 8.17 Shear viscosity relaxation following flow for NR + 0.2 phr N236 black, T = 100 °C.

Reprinted from S. Montes, J. L. White and N. Nakajima, Journal of Non-Newtonian Fluid Mechanics, 1988, 28, 183, Copyright 1988, with permission from Elsevier Science.

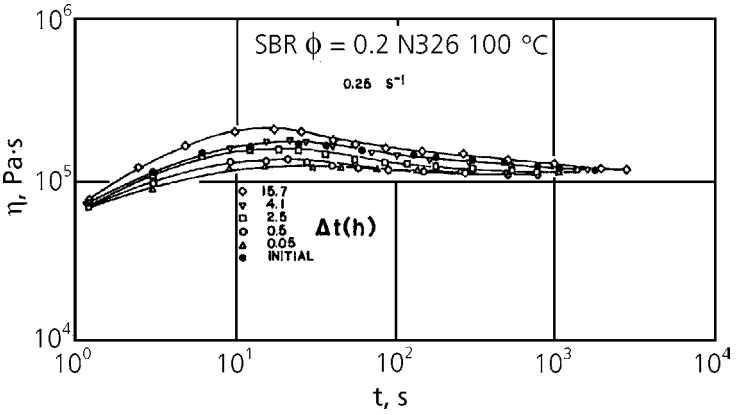

Figure 8.18 Sequential transient shear viscosity after various periods of rest for SBR. SBR + 0.2 phr N236 black, T = 100 °C.

Reprinted from S. Montes, J. L. White and N. Nakajima, Journal of Non-Newtonian Fluid Mechanics, 1988, 28, 183, Copyright 1988, with permission from Elsevier Science.

With storage, the modulus and yield value recover to the original values and eventually even surpass them.

Recognising that the original sample had some prior shear treatment, such as charging into the rheometer or even history of mixing, the recovery surpassing the original value is not surprising.

What we learn from the yielding study is that the mutual arrangement of carbon black aggregates, sometimes called 'carbon black network', takes a variety of forms, which are quasi-stable. It changes slowly with time towards a more stable form. Because diffusion of carbon black particles is negligible, the driving force of the aggregate-structure change must come from viscoelastic memory of the compound. The detail of this mechanism will be the subject of future study.

8.5 Effect of concentration and structure of carbon black

8.5.1 Hydrodynamic theories

The starting point for discussion is an idea that the modulus, E of the filled rubber is related to the modulus, E_0, of the unfilled counterpart:

$$E = f(v)\, E_0 \tag{8.2}$$

Where $f(v)$ is a function relating these two moduli which is dependent on the volume fraction, v, of the filler. This relationship is sometimes given in the following form,

$$E = E_0(1 + c_1 v + c_2 v^2) \tag{8.3}$$

where

$$f(v) = 1 + c_1 v + c_2 v^2 \tag{8.4}$$

Physical explanation of this expression is usually given in steps. Smallwood [11] derived a theoretical expression for modulus increase by the presence of an isolated, rigid sphere. Complete adhesion of the rubber matrix on the surface of the sphere is assumed. For a small deformation, i.e., extrapolated to zero elongation, it gives an expression:

$$E = E_0\,(1 + 2.5v) \tag{8.5}$$

Smallwood noted the similarity of this equation to Einstein's viscosity equation [12]

$$\eta = \eta_0\,(1 + 2.5v) \tag{8.6}$$

where η and η_0 are the viscosity of suspension and that of the medium, respectively.

Subsequently, Guth and Gold [13], considering the interaction of a pair of spheres embedded in a moving fluid, added the higher term in the concentration dependence as,

$$\eta = \eta_0 (1 + 2.5v + 14.1 v^2) \tag{8.7}$$

In recognising a similarity between Equations 8.5 and 8.6, Guth [14] adopted Equation 8.7 for the modulus of rubber containing a pair of interaction spheres.

$$E = E_0 (1 + 2.5v + 14.1 v^2) \tag{8.8}$$

This equation is still for a low concentration of the filler, where only binary interaction is considered. The Equations 8.5 and 8.8 are sometimes called hydrodynamic theories [15]. For a yet higher concentration Guth produced a model that showed that the filler particles line up in a straight line forming a rod-like chain. For this rod a shape factor, f, is assigned, representing the length to breadth ratio. With this rod-model, Guth [14] considered inter-rod binary interaction and derived the following expression,

$$E = E_0 (1 + 0.67 fv + 1.62 f^2 v^2) \tag{8.9}$$

where f>>1. The shape-factor was interpreted later to represent the anisotropic shape of the single filler particle as rod-like [15].

Considering a highly irregular shape and a presence of 'occluded rubber' in cavities of the carbon black aggregates, Medalia [16] introduced 'effective volume' to represent filler concentration. His effective volume fraction, V, replaces the real volume fraction, v, in Equation 8.8. The effective volume fraction, V, is not an adjustable parameter, but calculated from the DBP absorption [17] (see also Chapter 9). The shear storage modulus, G', was measured at 25 °C and 0.25 Hz, with 20 phr of carbon black loading where G' was practically independent of the strain amplitude. With 12 carbon blacks of varying particle size and structure, the calculated, G', from the equation,

$$G' = G'_0 (1 + 2.5V + 14.1 V^2) \tag{8.10}$$

were in agreement with observed values to within 5%.

Recalling the assumptions involved in deriving Equation (8.8), it may be concluded that when the occluded volume correction is made as suggested by Medalia [16], the sphere model for an isolated filler particle is a good approximation; this conclusion is valid only at a low loading, where the modulus is practically independent of strain amplitude, and only binary interaction between particles needs to be considered.

For a higher loading where the modulus decreases [18] with the increasing strain amplitude, Medalia [16] took the G' values at 10% strain amplitude. At this point the modulus has decreased significantly, presumably as a result of breaking the carbon black network. The calculated G' were in good agreement with the observed ones within 10% for the same 12 carbon blacks.

Medalia [16] demonstrated a further usefulness of this approach by using graphitised carbon blacks, which are known to have a weaker surface-affinity towards rubber. Thus, the method provides a means of examining the filler-rubber interaction. However, by the conditions set for deriving Equation 8.10, its applicability is limited to a small deformation. Also, only bi-particle interactions are considered in the equation and multi-particle interactions are assumed to be negligible. For the filled-rubber with the normal loading of 40-50 phr, the carbon black particles are crowded and the multi-particle interaction is important.

Because of the assumption involved in deriving Equations 8.7 and 8.8, the above correlations should be regarded as an empirical nature. With this and with consideration of the dependence of the viscoelastic properties on the time scale, the quantitative relationship of the viscoelastic properties to the concentration and properties of the carbon black must be examined case-by-case.

8.5.2 Concentration dependence

In general the concentration dependence of viscosity of dispersed spheres may be described with a form of equation given by Eilers [19].

$$\eta_r = \left[1 + \frac{2.5v}{2\left(1 - \frac{v}{b}\right)} \right]^2 \tag{8.11}$$

when η_r is the ratio of the viscosity of the dispersion to that of the medium and b is a constant determined by the mode of packing of spheres. For infinite dilution, Equation 8.11 is reduced to Einstein's equation, Equation 8.6. As the concentration is increased, the viscosity increases rapidly towards infinity when v approaches b. At $v = b$, the tight packing of spheres presumably prevents flow. A more general form of Eiler's equation is given by Maron and Belner [20] as

$$\eta_r = \left[1 + \frac{\alpha v}{1 - \beta v}\right]^2 \tag{8.12}$$

where α and β are constants determined by the nature of the dispersion.

Many equations similar to Eilers' equation have been proposed; for example, Maron's [21] equation is,

$$\eta_r = \frac{(\varepsilon v)^m}{(1 - \varepsilon v)^n} \tag{8.13}$$

where ε, m, and n are material constants; the exponent, m, may be zero or positive and n is a positive non-zero number. There are many variations of these equations, which reduce to the identical forms at the infinite dilution and at the highest allowable concentration at the tight packing. Therefore, the variation of the forms concerns the concentration dependence between the two limits.

In applying these equations other important considerations, namely the non-Newtonian nature of the flow also needs to be considered. A similar form of equation may be used to represent the modulus of the dispersed systems. However, for the modulus both strain- and strain-rate dependence must be considered.

References

1. N. Nakajima and E. A. Collins, *Polymer Engineering and Science,* 1974, **14**, 2, 137.

2. N. Nakajima and E. A. Collins, *Rubber Chemistry and Technology*, 1974, **47**, 2, 333.

3. N. Nakajima and E. A. Collins, *Rubber Chemistry and Technology,* 1977, **50**, 4, 791.

4. S. Montes, J. L. White, N. Nakajima, F. C. Weissert and K. Min, *Rubber Chemistry and Technology*, 1988, **61**, 4, 698.

5. N. Nakajima and E.A. Collins, *Rubber Chemistry and Technology*, 1975, **48**, 615.

6. C-Y. Ma, J. L. White, F. C. Weissert, A. I. Isayev, N. Nakajima and K. Min, *Rubber Chemistry and Technology,* 1985, **58**, 4, 815.

7. G. R. Cotten, *Rubber Chemistry and Technology,* 1979, **52**, 1, 187.

8. G. R. Cotten, *Rubber Chemistry and Technology*, 1979, **52**, 1, 199.

9. N. Nakajima and M. Shida, *Transactions of the Society of Rheology*, 1966, **10**, 299.

10. S. Montes, J. L. White and N. Nakajima, *Journal of Non-Newtonian Fluid Mechanics*, 1988, **28**, 183.

11. H. M. Smallwood, *Journal of Applied Physics*, 1944, **15**, 11, 758.

12. A. Einstein, *Annals of Physik*, 1906, **19**, 289.

13. E. Guth and O. Gold, *Physics Review*, 1938, **53**, 322.

14. E. Guth, *Journal of Applied Physics*, 1945, **16**, 1, 20.

15. E. M. Dannenberg, *Rubber Chemistry and Technology,* 1975, **48**, 3, 410.

16. A. I. Medalia, *Rubber Chemistry and Technology,* 1973, **46**, 4, 877.

17. ASTM D 2414-99
S*tandard Test Method for Carbon Black-n-Dibutyl Phthalate Absorption Number.*

18. A. R. Payne, *Journal of Applied Polymer Science*, 1962, **6**, 19, 57.

19. H. Eilers, *Kolloidnyi Zhurnal,* 1941, **97**, 313.

20. S. H. Maron and R. J. Belner, *Journal of Colloid Science,* 1955, **10**, 6, 523.

21. S. H. Maron and P. E. Pierce, *Journal of Colloid Science*, 1956, **11**, 1, 80.

9 Reinforcing Fillers and Liquid Additives

9.1 Reinforcing fillers

9.1.1 Introduction

In this chapter, reinforcing fillers, carbon black and precipitated silica, will be discussed. Because a reference book on carbon black [1] and a review article on silica [2] are available, the discussion will be limited to the aspects that are pertinent to mixing.

Major properties characterising these fillers are surface area (particle size) and structure (bulkiness). The commercial grades of carbon black and their characteristics are given in Table 9.1 [3]. When discussing mixing one more property must be considered, the mixing ease, which will be part of the discussion that follows.

9.1.2 Mixing ease of fillers

The ease of mixing has two aspects, one is ease of incorporation and the other is dispersion. How can the ease of mixing be quantified and how can it be related to the appropriate properties of a filler? These questions concern characterisation of fillers and may be called the property-processability relationship. Whereas the effect of fillers on the performance of vulcanisates has been quite extensively researched and the reinforcing mechanisms have been examined, the ease of mixing has not been investigated as much. This chapter is also limited to primarily qualitative discussions. Scientific investigation is very much in order.

Consider first the phenomenon, which is called rejection of a filler by rubber. When a silica filler is charged onto premasticated natural rubber, fine particles of the filler are blown out from the charge hole of the internal mixer like smoke. It is interpreted as a repulsion by the electric charge built in the rubber during mastication. When silica is premixed with carbon black or fine powdered metal carbonates, the repulsion is significantly reduced [9].

The second aspect is the affinity between filler and rubber which, affects incorporation. The stronger this affinity the easier that incorporation appears. Concerning the filler-

Table 9.1 Properties of Rubber-Grade Carbon Blacks								
ASTM[a] designation	Former industry designation	I_2 absorption number (D1510) [4], g/kg	DBPA[b,] (D2414) [5], $cm^3/100$ g	DBPA[b,d] (compressed sample) (D3493), $cm^3/100$ g	CTAB[c,e] surface area (D3765), m^2/g	Nitrogen surface area[f] (D3037), m^2/g	Tinting strength (D3265) [7],	Pour density (D1613) [6], kg/m^3
N110	SAF	145	112	98	126	143	124	335
N121	SAF-HS	121	132	112	121	132	121	320
N220	ISAF	121	114	100	111	119	115	345
N231	ISAF-LM	121	92	86	108	117	117	390
N234	ISAF-HS	120	125	100	119	126	124	320
N299	ISAF-HS	108	124	105	104	108	113	335
N326	HAF-LS	82	72	69	83	84	112	465
N330	HAF	82	102	88	83	83	103	375
N339	HAF-HS	90	120	101	95	96	110	345
N347	HAF-HS	90	124	100	88	90	103	335
N351	HAF-HS	68	120	97	74	73	100	345
N358	HAF-HS	84	150	112	88	87	99	290
N375	HAF-HS	90	114	97	98	100	115	345
N539	FEF	43	111	84	41	41	0	385

Table 9.1 Properties of Rubber-Grade Carbon Blacks (continued)								
ASTM[a] designation	Former industry designation	I_2 absorption number (D1510) [4], g/kg	DBPA[b,] (D2414) [5], $cm^3/100$ g	DBPA[b,d] (compressed sample) (D3493), $cm^3/100$ g	CTAB[c,e] surface area (D3765), m^2/g	Nitrogen surface area[f] (D3037), m^2/g	Tinting strength (D3265) [7],	Pour density (D1613) [6], kg/m^3
N550	FEF	43	121	88	42	42	0	360
N650	GPF-HS	36	122	87	38	38	0	370
N660	GPF	36	90	75	35	35	0	425
N683	GPF-HS	35	133	0	39	37	0	335
N762	SRF	27	65	57	29	28	0	505
N765	SRF-HS	31	115	86	33	31	0	375
N774	SRF	29	72	62	29	29	0	495
N990	MT	0	43	40	9	9	0	0

a: ASTM D1765-99a [8]
b: Dibutyl Phthalate (*84-74-2*) absorption
c: Cetyl trimethylammonium bromide (*57-09-0*)
d: ASTM D3493-99
Standard Test Method for Carbon Black-n-Dibutyl Phthalate Absorption Number of Compressed Sample
e: ASTM D3765-99
Standard Test Method for Carbon-Black-CTAB (Cetyltrimethylammonium Bromide) Surface Area
f: ASTM D3037
Test Methods for Carbon-Black-Surface Area by Nitrogen Adsorption (Discontinued 1999)

rubber affinity, for quantifying the filler-rubber interaction, the conventional method has been to measure the bound-rubber content [10]. More recently, NMR has been used for characterising the interaction [11]. Because the present interest is in the processing behaviour of the material, mechanical methods are also needed. In Chapter 7, a method of evaluating the strain-amplification was developed [12]. The method was designed to treat dynamic conditions rather than quasi-equilibrium conditions of Mullins and Tobin [13]. Using dynamic conditions, the new method yields the strain amplification as a function of strain and strain rate. Subsequently, the strain-rate amplification had also been evaluated [14]. In this work, three NBRs, two SBRs and two ACMs were examined together with several grades of carbon black having different particle size and different structure.

However, the method requires elongational measurements of gum rubber and its unvulcanised compound. The experiments as well as the calculation are somewhat involved. If only a relative measure of the filler-rubber interaction is needed, dynamic mechanical measurements and subsequent comparison of modulus of the compound against that of the gum rubber are much simpler. Such comparisons with N550 carbon black were made with the samples listed in Table 9.2 and the moduli data of Figures 9.1 and 9.2 [12]. The modulus ratio is found to be independent of the frequency of the dynamic measurements but varies considerably among different gum rubbers.

Table 9.2 Samples

Type	Trade Mark	Code for gum[g]	Code for compound[g]	Mooney index of gum[b]	% gel of gum	Carbon black phr	Modulus ratio[f]
NBR	Hycar[a] 1052	A	1	35	0 [c]	40	1.94
NBR	Hycar[a] 1042x82	C	3	81	48.6	40	1.21
NBR	Hycar[a] 1002	D	4	85	74.3	40	3.30
SBR	Ameripol[a] 1502	H	5	52	1.8 [d]	40	1.49
SBR	Ameripol[a] 1712	I	7	55	4.4	40 [e]	1.21

a: Registered trademark of the BFGoodrich Company
b: ASTM D1646 [15]
c: ASTM D3616 [16]
d: A method similar to that of *c*, but toluene was used instead of MEK
e: Parts per hundred of gum rubber plus extending oil
f: Modulus ratio is the absolute value of shear complex modulus of compound, $|G^*|_{cp}$, over that of gum rubber, $|G^*|_g$
g: Sample codes for the experiment

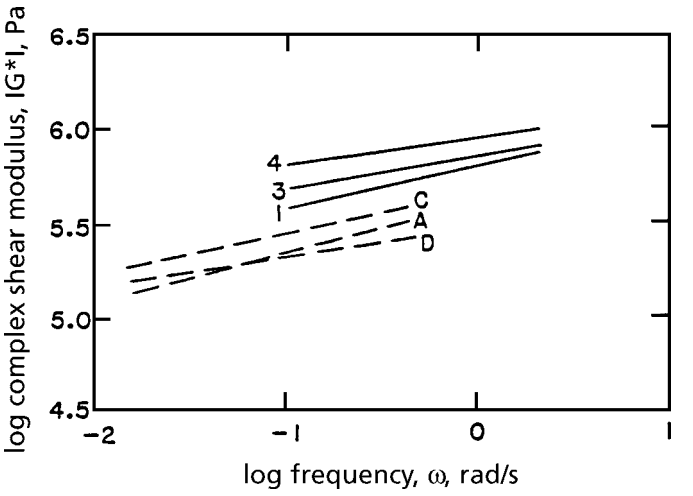

Figure 9.1 Complex shear modulus as a function of frequency for filled and unfilled NBRs.

Reprinted with permission from N. Nakajima and J. J. Scobbo, Jr., Rubber Chemistry and Technology, 1988, 61, 1, 137. Copyright 1988, Rubber Division of the ACS.

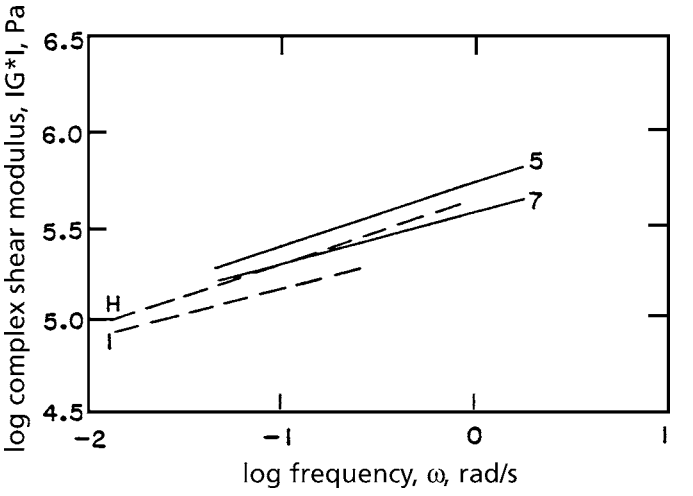

Figure 9.2 Complex shear modulus as a function of frequency for filled and unfilled SBRs.

Reprinted with permission from N. Nakajima and J. J. Scobbo, Jr., Rubber Chemistry and Technology, 1988, 61, 1, 137. Copyright 1988, Rubber Division of the ACS.

The strain amplification, is expressed as a ratio of the absolute value of the complex shear modulus $|G^*|_{cp}/|G^*|_g$. The value of compound 4 is very high compared to the others. The gum rubber D has long branches and a large amount (75%) of macrogel (see also sections 4.1 and 6.5). The long branches are known to have a higher affinity to carbon black but the reason why is not clear. However, if the branches of one gel-molecule tie up a number of carbon black particles, the modulus may become higher than those containing unbranched rubber. The gel in the compound 3 is a microgel. Since the microgel is a particle of crosslinked network, it may be ineffective in tying up the carbon black particles; and therefore the amplification is rather low.

In comparing compounds 5 and 7, the oil-extended rubber, SBR 1712, shows a lower amplification. A smaller amount of rubber against the amount of carbon black may be the reason.

Whether or not there is a difference between NBR-A and SBR-H in the affinity towards carbon black is not certain with this data alone, because the Mooney indices are different. If the difference is significant, NBR has somewhat higher affinity than SBR toward carbon black.

Rather unexpectedly a build-up of bound-rubber of the polyisoprene was observed on the surface of silica in the absence of the coupling agent. Polyisoprene is usually considered to be unreactive with silica. The compound was kept at 120 °C for up to 18 hours and the development of the bound rubber was examined with NMR [17].

Nakajima preheated silica in an oven set at 200 °C to remove water. When the hot silica was added directly from the oven to the premasticated NR, it dispersed without use of a coupling agent. When the silica was removed from the oven and cooled to room temperature, mixing the heated silica was just as difficult as mixing silica without heat-treatment. Evidently the hot silica helped mixing. Examples in literature about interaction with silica are mostly with polar rubbers [2]. The above examples illustrate that even nonpolar rubber like NR interacts with silica [18].

Neither silica nor carbon black fillers are pure material. Their surfaces have chemically reactive groups. Their physical-chemical interaction and chemical reaction with rubber have been extensively investigated as a part of the reinforcing mechanisms [19]. How these chemical groups contribute to the mixing mechanism is an obvious interest. Wang, Wolff and Donnet investigated the surface energies of fillers and their interaction with model compounds using an inverse gas chromatography. The model compounds were selected to simulate various rubbers including polar rubbers. Both carbon black and silica were studied [20, 21, 22, 23], to characterise the rubber-filled interaction.

The next subject is the ease of dispersion. Generally, when the incorporation of rubber is difficult the problem is carried over into the dispersion of the rubber. The filler-rubber interaction also plays an important role here. In addition, there are cases where the ease of dispersion is significantly different among the same grade of silica for a reason that is not exactly clear [24].

The sample used was Hycar 4051EP (ACM), a product of the BFGoodrich Company. The Hycar homoploymer, has a glass-transition temperature of –14 °C and a Mooney index (ML-(1 + 4) at 100 °C), in the range of 35-50.

The silica fillers used are given in Table 9.3. All the compounds contained 50 phr of a filler by weight. The compounds were prepared with a Haake Buchler Rheocord 750 laboratory mixer at 50 rpm and a machine temperature of 100 °C. The fresh rubber was charged and masticated for one minute. After that silica was added over a period of about 2.5 minutes. An additional 6.5 minutes was required to complete the mixing. No coupling agent was required.

Table 9.3 Silica Fillers used with Hycar 4051EP

Compound Code	Filler	Identification Surface Area, m^2/g	Manufacturer
1	Precipitated silica	170	Manufacturer A, spray-dried commercial product
2	Precipitated silica	200	Manufacturer B, rotary-dried commercial product
3	Precipitated silica	150	Manufacturer B, rotary-dried commercial product
4	Precipitated silica	200	Manufacturer B, spray-dried experimental product

All compounds were compression moulded at 100 °C for 30 minutes. The spray-dried silicas were found to be much easier to disperse than the rotary-dried ones. This was readily seen in the mixed compounds, for which a good dispersion resulted in a transparent material, whereas the poor dispersion gave an opaque white material, Figure 9.3.

When the opaque compounds were remilled many times through a roll-mill with a tight gap (no clearance), they became transparent. This fact is a further confirmation that the opaqueness comes from poor dispersion.

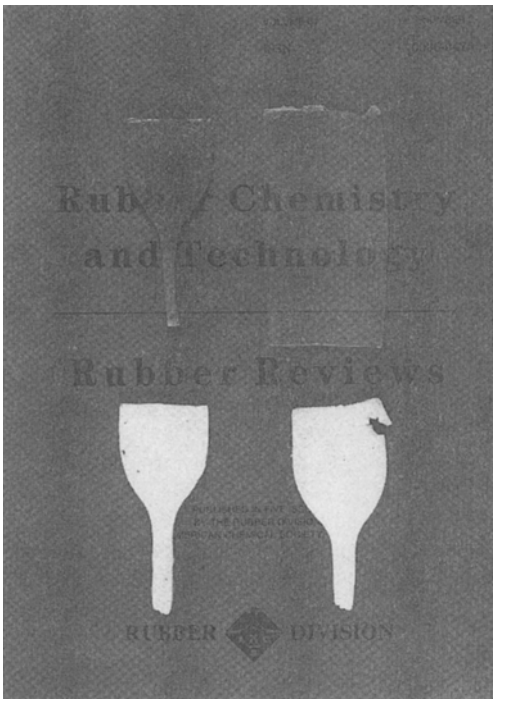

Figure 9.3 Silica compound specimens: transparent specimens with spray-dried silica and white specimens with rotary-dried silica.

The rotary-dried silica presumably contained more water. This is thought to be the reason why the silica agglomerates are not easily broken down to the aggregates. In addition, the spray-drying might have given a more uniform and milder heat history, so that the agglomerates are more friable. The difference in friability of the agglomerates causes the difference in the dispersibility.

However, the above interpretation must be confirmed. The presence of some additive is also suspected.

Just how friable the filler agglomerates should be, is an important question. For the ease of dispersion, a more friable filler is desirable. But, this brings a material-handling difficulty at any time before the filler is added to a rubber [25]. Incorporation is facilitated if the agglomerates retain their integrity. This means that a delicate control of the cohesive strength among aggregates is necessary for providing sufficient resistance to break before

incorporation is completed. Then, they must break up easily as soon as dispersion starts. Such a contradicting requirement is common in industrial practice and this is one of the best examples.

9.1.3 Structure of aggregate and agglomerate

A question of the friability of agglomerates leads to an inquiry into structure of both agglomerate and aggregate. The structure of aggregate has been a subject of intensive study. A review of this subject is given by Medalia [26], who produced the electron microscope images in Figure 9.4.

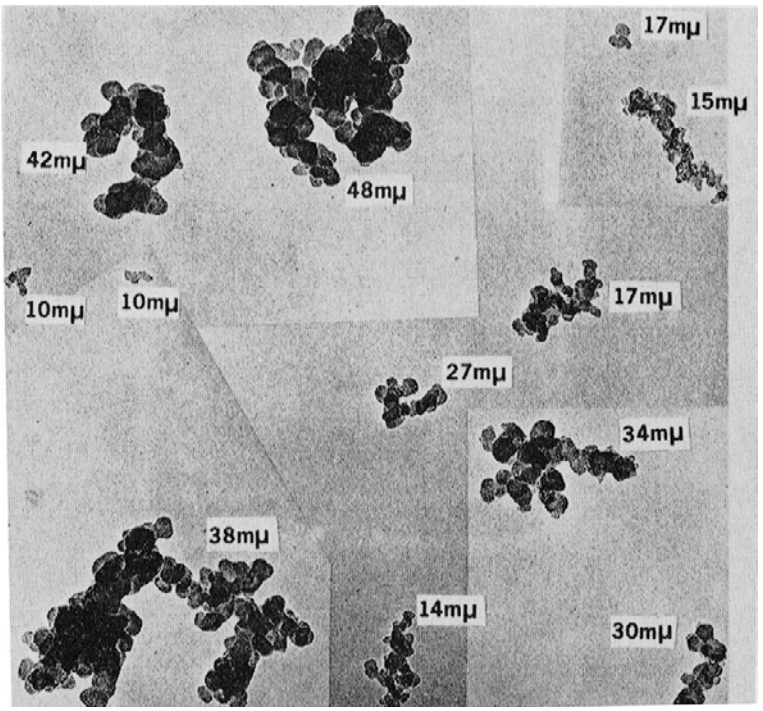

Figure 9.4 Montage of aggregates in a single field of N220 carbon black. Numbers beside each aggregate indicate average particle size.

The aggregates are in the size range of approximately 10 to 100 nm in diameter. They consist of strings of smaller spheres fused together. The size of the sphere determines the total surface area, and the manner by which the spheres are strung together determines structure. More recent studies are directed toward converting the electron microscopic images to three-dimensional morphology [27].

The application of fractal analysis enabled the characterisation of the aggregates, which by nature consisted of wide varieties of size and shape.

One method is called the perimeter-area (*P-A*) relationship, $P - A^{D_p/2}$, where the perimeter fractal, D_p, relates to the degree of irregularity or ruggedness of the perimeter of the two-dimensional profile. Gerspacher and O'Farrell [28] applied the method to 15 commercial grades of carbon black. The values of D_p were from 1.14 to 1.34 and tended to be higher for more reinforcing, smaller particle size grades.

Herd, McDonald and Hess [29] applied both the perimeter-area relationship and the mass-size (*M-R*) relationship, $M - R^{D_m}$ to 19 grades of commercial carbon blacks. On-line transmission-electron-microscopy/automated-image-analysis was used for rapid sampling of 1,000 aggregates per grade. Values of D_p and D_m were 1.05 – 1.23 and 2.47 – 2.85, respectively, and they were related to the structure and size characteristics observed with the conventional methods. Further, they classified a variety of shapes into four categories, spheroidal, ellipsoidal, linear and branched. For each category fractal analysis was applied to determine D_p and D_m. From the mass fraction of each category and their D_p and D_m values, the composite fractal indices, D_p* and D_m*, were calculated for each grade. The composite fractal indices are more sensitive than D_p and D_m for distinguishing between different grades of carbon black.

For very practical reasons simple tests are needed to determine the surface area and structure of fillers. However, defining the test condition is not without problems. The surface area based on a monolayer adsorption of a small molecule depends upon the size of the adsorbent molecule, because the filler surface is made up of irregular topology.

A practical definition of surface area must be related to the adsorption of rubber molecules. Upon consideration the current choice of adsorbent is cetyltrimethylammonium bromide (CTAB). However, nitrogen adsorption (BET) is also in common use.

The structure determination utilises absorption of liquid into pores of agglomerate. Therefore, it depends not only upon the structure of the aggregate but also how tightly aggregates are packed in an agglomerate. The usual procedure is to compress the sample under a very high pressure prior to the absorption of DBP [30]. More detailed discussion on the surface area and structure are given by Donnet and Voet [1]. In addition to the

surface area and structure, another parameter called 'occluded volume' is frequently used [26]. This parameter has multi-meanings or multi-purposes, which require some clarification. The first meaning is the assigning of a volume of an equivalent sphere for the complexed shape of the aggregates. The second is a volume of an aggregate plus the volume of the immobilised rubber trapped by the aggregate. The third is an assumed existence of the rubber, which has penetrated and filled voids of the agglomerate. In practice all three definitions are interpreted to give the same quantity. The concept has been used to explain the mixing mechanisms and rheology. These are discussed later in this chapter.

The structure of the agglomerates has escaped the attention of researchers. Figure 9.5 is an imaginary structure of agglomerate, showing a small section, 100 x 100 nm, out of the overall diameter of 10-100 μm [31]. It is based on the crushed DBP value of 95 cm^3/100 g for N339 carbon black, the data reported by Cotten [32]. Using the density of 1.86g/cm^3 for the carbon [33], the volume fraction occupied by carbon in the agglomerate is calculated to be 0.36. The area it corresponds to is about 50% occupied and 50% void. In the lower left corner the 20 nm square shows 50% of the area occupied by carbon. In the rest of the area, a model of stacking of aggregates is illustrated; one in the lower left is drawn to fit in the 20 nm square; others are made to fit either a 40 nm square or 20 x 40 nm area. The shapes of the aggregates are made to resemble to those in Figure 9.4, except that the particles are represented with squares instead of circles. This is to make the estimate easier for 50% area occupancy. Also, it is drawn to make the aggregates touch their neighbour at some point. This model assumes that the void is more or less uniformly distributed within the agglomerate.

A similar structure was observed by Misono for N330 carbon black. Much denser packing is shown for the low structure, N880, Figure 9.6 [30].

A variation in the strength of the pellet has been recognised and a test method is defined in ASTM D1937-62T [35]. The fact indicates that the packing of the aggregates is variable.

Then, the packing within an agglomerate may be non-uniform.

According to Donnet and Voet [36] in Carbon Black: Physics, Chemistry and Elastomer Reinforcement (Reproduced by permission of Marcel Dekker, Inc.): 'the pelletisation is not merely a physical densification, since many properties of the black appear to undergo irreversible changes, incompatible with a mechanical or physical view of pelletisation. The change in free radical content upon pelletisation supports the argument that chemical bonding is involved'.

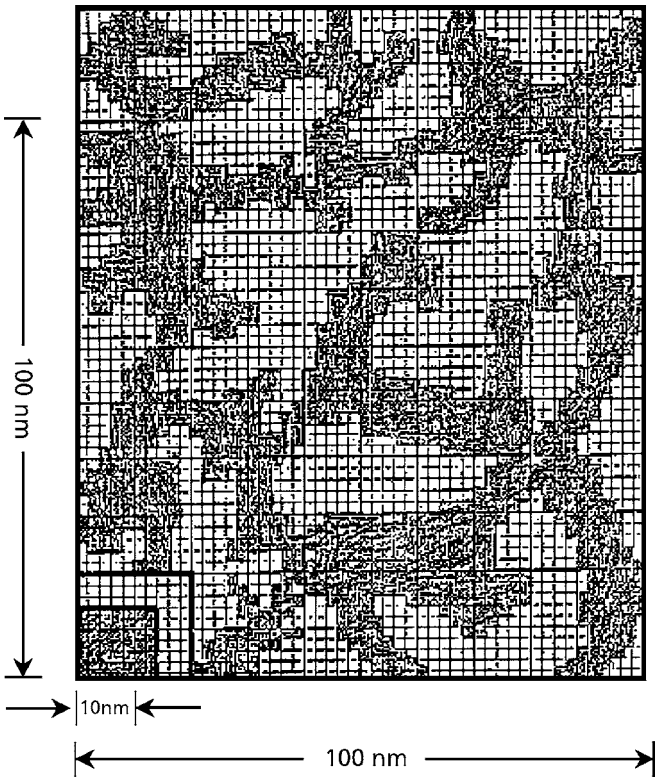

Figure 9.5 Imaginary structure of carbon black agglomerate.

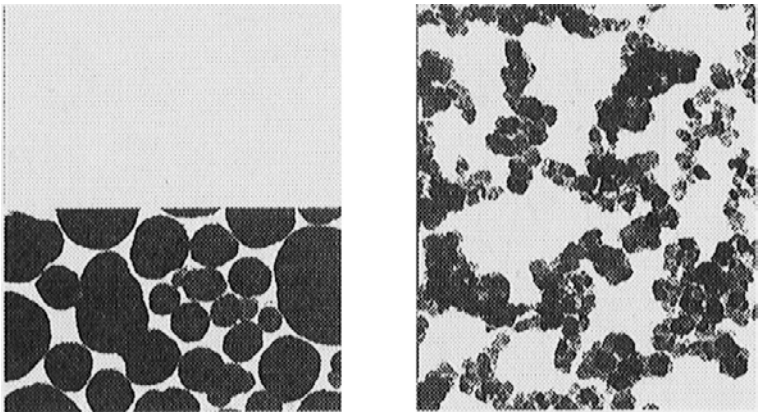

Figure 9.6 Carbon blacks having different agglomerate structure.

They state further that 'generally, to promote the formation of firm, yet easily dispersible pellets and to minimise the presence of undesirable fines, additives are used in the water of pelletisation for rubber grade of blacks' [37]. Molasses and lignosulphonic acids are mentioned as examples of additives. 'These additives function as binders only upon carbonisation in the dryer. It seems likely that the free radicals formed during carbonisation tend to create carbon-to-carbon bonds, thereby promoting the formation of firmer pellets, which are still dispersible in elastomers'.

Previous examples of silicas show that there is a difference of friability, i.e., dispersibility among the same grade of fillers. As discussed before, a control of the friability plays an important role in dispersing fillers. Cotten [32] examined the dispersion rate in mixing of oil-extended *cis*-1,4-BR with thirteen grades of carbon black varying the surface area and structure. The decreasing torque after the second peak in mixing with a miniature mixer was used as the indication of the dispersion rate. The curve was fitted to an empirical equation of a form:

$$\ln[(P_t - P_\infty)/(P_0 - P_\infty] = -kt \tag{9.1}$$

where P_0 and P_∞ are limiting torques at the assumed initial and final condition and P_t is the torque at time, t. Therefore, k is the rate constant of the progress of dispersion. The value of k was related to the surface area (CTAB) and structure (DBPA) with a correlation coefficient of 0.98. Because the surface area and the structure are assigned as the properties of the aggregate, this result indicates that the friability of the agglomerate is controlled solely by the properties of the aggregate. Because the previous discussion points towards variation in the friability of agglomerate for the same aggregate properties, the samples chosen by Cotten may have been manufactured to give the same degree of friability. Another possibility is that because DBPA was measured with the agglomerates, it might have represented a variation in the agglomerate structure as well as the aggregate structure.

Donnet and Voet [38] state that the DBP number is somewhat dependent upon the mechanical treatment of the carbon black during pelletisation. An increase in work done leads to an increase in pellet density and a reduction in DBP number. The variation in DBP number is partially related to a variation in the agglomerate morphology.

Jansen and Kraus [25] evaluated the dispersibility of two commercial N220 carbon blacks. The rubber used was SBR and the amount of oil was varied at 0, 15, 30, 45 or 60 phr. The mixing was done with a miniature mixer. The same mixing condition was used for two carbon blacks. The dispersion rating with a photomicrographic technique gave an identical rating within experimental error if no oil was present. However, at all concentrations of added oil, there were differences of the rating between two carbon blacks.

Jansen and Kraus state that two oil levels (30 and 60 phr) are adequate to define relative dispersibility of carbon blacks. Evidently, there is a subtle difference in the friability of the

agglomerate even if the aggregate properties are the same. The reason why the difference is magnified in the presence of oil is that the oil makes dispersion more difficult. In the same article Jansen and Kraus present two more examples of the differences in dispersibility within a given grade. One example was with N339 carbon black. A significant difference in dispersibility was observed in mixing with S-SBR and SBR as well as in dispersion in chloroform by ultrasonic device.

An even more dramatic example was obtained with N326, a low structure carbon black, known to be difficult to disperse. The results are reproduced in Figure 9.7. More discussion on the subject of friability in relation to mixing mechanisms is given in Chapter 11.

Shiga and Furuta [39] investigated the breakdown mechanisms of agglomerates of N330 and N550 carbon black in mixing with six grades of EPDM. An optical-micrograph was used with samples taken during both the incorporation and dispersion stage. The breakdown was found to proceed in two steps: first is the breakdown of large agglomerates into smaller agglomerates (see Figure 9.8), and second is the disintegration of the surface layer of the agglomerate in a way which has been compared to the way an onion peels, see Figures 9.9 and 9.10. The explanation given is from the point of view of the mechanical action of rubber onto the agglomerate.

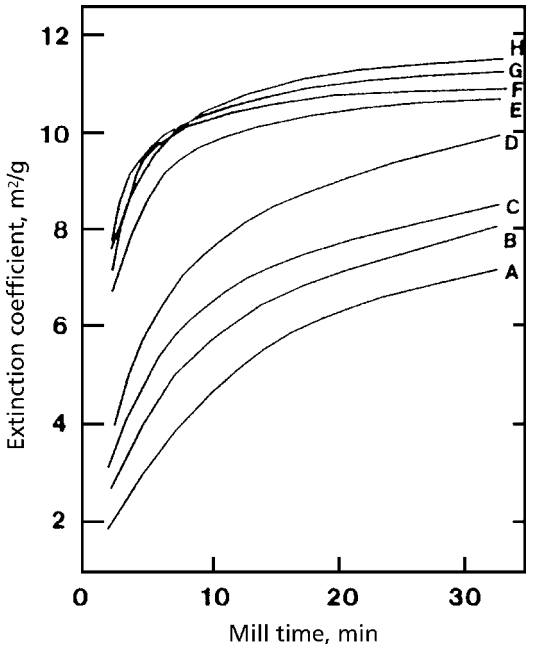

Figure 9.7 Dispersion of N326 blacks in polybutadiene.

Reprinted with permission from J. Jansen and G. Kraus, Rubber Chemistry and Technology, 1990, 63, 1, 110. Copyright 1990, Rubber Division of the ACS.

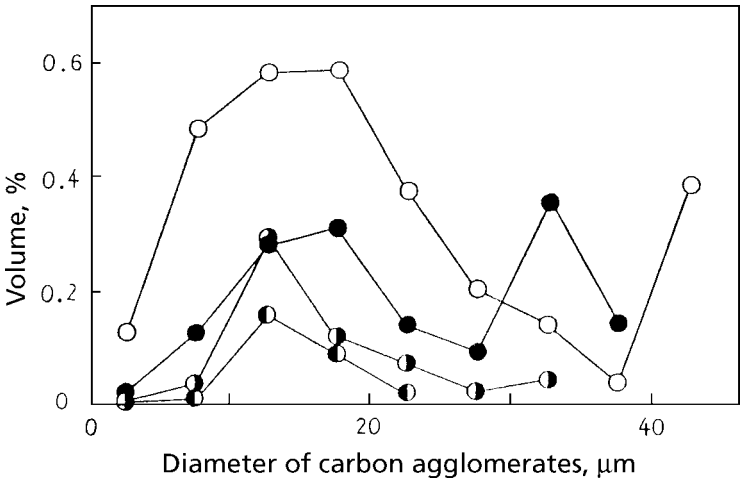

Figure 9.8 Distribution of diameter of carbon agglomerates at each mixing time. Recipe: EPDM, 100; N330, 10; oil, 10; zinc oxide, 5; stearic acid, 1. ○, 30 seconds mixing; ●, 2 minutes mixing; ◑, 4 minutes mixing; ◐, 6 minutes mixing.

Reprinted with permission from S. Shiga and M. Furuta, Rubber Chemistry and Technology, 1985, 58, 1, 1. Copyright 1985, Rubber Division of the ACS.

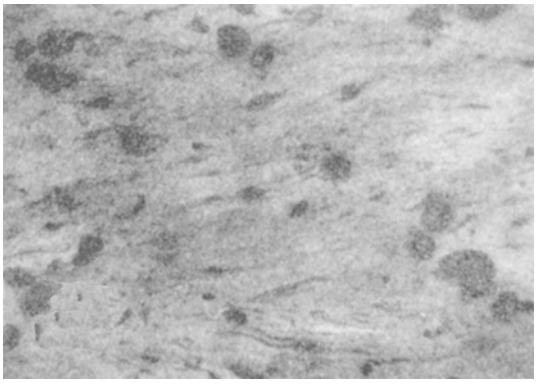

Figure 9.9 Photomicrograph of EPDM compound after 2 minutes mixing. EPDM, 100; N330, 10; oil, 10; zinc oxide, 5; stearic acid, 1.

Reprinted with permission from N. Nakajima and E. R. Harrell, Rubber Chemistry and Technology, 1984, 57, 1, 153. Copyright 1984, Rubber Division of the ACS.

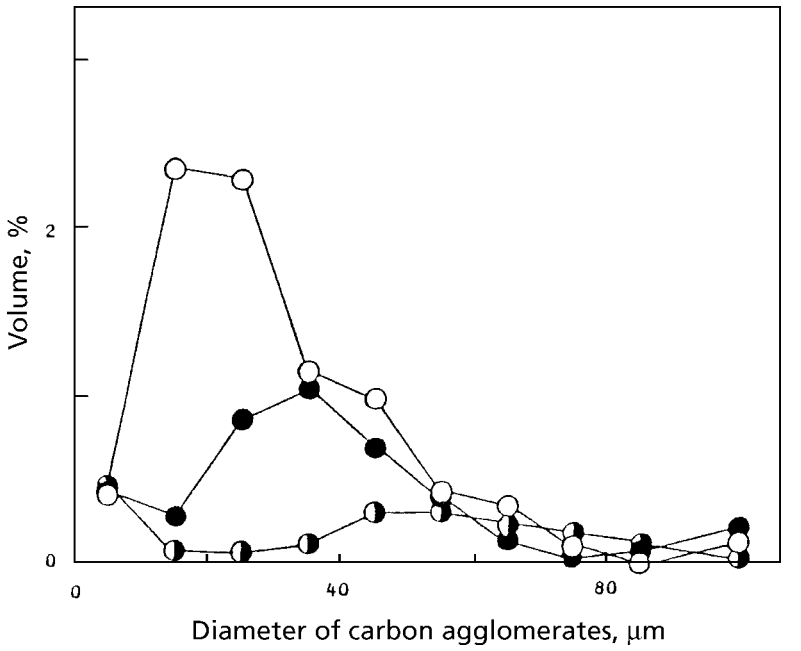

Figure 9.10 Distribution of diameter of carbon agglomerates for Sample E at each mixing time (PI recipe). ○, 2 minutes mixing; ●, 5 minutes mixing; ◑, 10 minutes mixing.

Reprinted with permission from S. Shiga and M. Furuta, Rubber Chemistry and Technology, 1985, 58, 1, 1. Copyright 1985, Rubber Division of the ACS.

These two steps of the breakdown may also be related to the morphology of the agglomerate. The first step appears to be the generation of a large number of smaller agglomerates, the size of which is centred around 25 μm diameter. This suggests that the larger agglomerates and pellets are made up of units of smaller agglomerates. The scanning electron micrographs, Figures 9.11 and 9.12 are suggestive of this point of view.

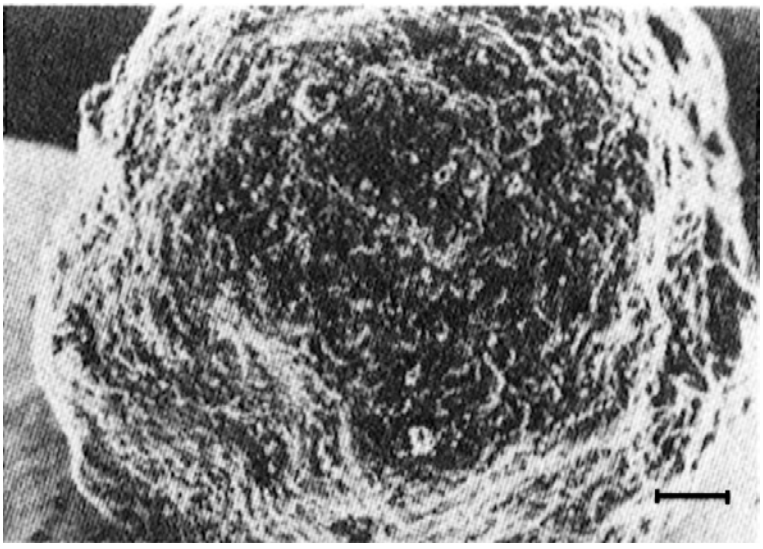

Figure 9.11 Scanning electron micrograph of N330 pellet. Scale bar 100 μm.

Reprinted with permission from S. Shiga and M. Furuta, Rubber Chemistry and Technology, 1985, 58, 1, 1. Copyright 1985, Rubber Division of the ACS.

Figure 9.12 Scanning electron micrograph of N330 carbon black after mixing or crushing for one minute. Scale bar 100 μm.

Reprinted with permission from S. Shiga and M. Furuta, Rubber Chemistry and Technology, 1985, 58, 1, 1. Copyright 1985, Rubber Division of the ACS.

The second stage (peeling of an onion), may be related to the presence of a shell-over-shell structure with a fault between the shells. Such a structure is conceivable from rolling actions involved in the process of pelletisation.

Even identical molecules in the process of crystallisation generate defects and dislocations. The aggregates having a wide variation in size and shape are not likely to pack uniformly like the one depicted in Figure 9.5. Recognising that even equal sized spheres may pack into varying degree of tightness, it is conceivable that both larger and smaller agglomerates consist of non-uniformly packed aggregates. The loosely packed location may be the inter-particle boundary between the smaller agglomerates and inter-shell faults in the smaller agglomerates.

The morphological causes of the agglomerate break down may be examined by proper sampling during carbon black manufacture. The nascent carbon particles, i.e., aggregates, go through several steps before ending up as a pellet. The carbon particles coming out of the furnace are cooled with water and carried through an electrostatic precipitator of the Cottrel type at 60,000 V DC [40]. What do the precipitated carbons look like? After precipitation they are collected in a number of cyclones and bag filters. Then, they are pulverised in a micropulveriser. They are described as 'the fluffy black'. What does it look like? According to Donnet and Voet [36] in Carbon Black: Physics, Chemistry and Elastomer Reinforcement (Reproduced by permission of Marcel Dekker, Inc.): 'The 'fluffy black' is charged into a pin type mixer and agitated with an approximately equal quantity of water. Firm, spherical pellets are formed within minutes and the quantity of water used is critical. Fully automatic proportioning systems are used to control water addition simultaneously with the charging of the carbon black into the pelletiser with an accuracy of at least ± 0.5%' [41]. Evidently, water plays a critical role in the manner of packing of particles.

Recent advances in the characterisation of carbon blacks have been reviewed by Gerspacher *et al* [42]. Among the new methods scanning tunnelling microscopy and atomic force microscopy have revealed fine details of the surface topology.

The question is whether or not the surface topology may be modified to our benefit. A recent development by Cabot [43] on doping carbon black with silica achieved this objective. The carbon-silica dual phase fillers (CSDP) consist of two phases, a carbon phase and finely divided silica phase dispersed in it. A higher filler-rubber interaction is demonstrated by the higher amount of bound rubber at less than 10% silica and mostly at the few percent level. The scanning tunnelling microscopy revealed the surface topology, where the area of well-organised structure (quasi-graphitic) is smaller and more surface defects are present.

The ease of mixing of CSDP was demonstrated by a lower mixing torque and a shorter incorporation time, compared to the counterpart grade of carbon black or silica-coupling agent. The resulting CSDP compound showed better dispersion.

9.2 Liquid additives

Liquid additives such as extending oil often play a unique and decisive role in mixing of rubber. Hess *et al* [44] conducted an extensive mixing study involving a variety of rubbers, carbon blacks and oils. The rubbers were SBR1712, SBR1500 and EPDM1070. Seven grades of carbon black were selected to statistically represent particle size and structure of commercially available carbon blacks. Variable amounts of aromatic and paraffinic oil were used. The degree of dispersion was evaluated after mixing under controlled conditions. Capillary rheometry was used to characterise viscosity and die-swell of the compounds. Properties of the vulcanisate were also measured, to establish the relationship amongst the variables.

There are three kinds of liquid additives: plasticiser, extending oil and tackifier. Plasticisers usually have a T_g lower than those of gum rubbers, extending oils have similar T_g tackifiers have higher T_g, although exceptions are found in the literature [45]. Most tackifiers are solid at room temperature and require heating during mixing. Once mixed a tackifier remains as a liquid and forms a rubber solution. Therefore, it is classified here as one of the liquid additives. Some tackifiers are only partially soluble so that a broadening of the glass transition peak is observed in the dynamic mechanical studies [46]. Plasticisers and extending oils are absorbed quickly and almost instantaneously by gum rubbers. They are completely soluble with gum rubbers, unless the solubility is mismatched. The purpose of using a plasticiser is to lower the T_g of the composition, and it also facilitates the mixing of rubber with fillers. Plasticisers are polar liquids and are usually used with polar rubbers such as NBR and ACM, which have relatively high T_g.

The reasons for using an extending oil are not necessarily economic. Extending oil facilitates the mixing of difficult-mixing rubbers which provides the desired properties in the finished products. In this book the plasticiser and extending oil will be discussed primarily. The order of addition is very important; if the liquid is added first to the rubber followed by the other additives, it is similar to using an oil-masterbatch, because the oil mixes quickly with rubber. If the liquid and filler are added together to the rubber, it becomes mixing of rubber with an oil-filler mixture. In the former case the viscoelastic characterisation method is applicable to the mixture of the liquid-rubber composition in just the same way as the oil-extended gum rubbers. From the characterisation results processability may be assessed as explained in Chapter 6.

The latter case is more complicated. A part of the liquid is absorbed in the filler. Eventually the liquid migrates into rubber and at the same time the rubber becomes adsorbed onto the filler. More discussion is given on this subject in Chapter 11.

The interaction between a liquid additive and a rubber is an obvious interest not only from the solubility point of view but also from the resulting mechanical properties. Scientific studies of this subject belong to current and future activities [47, 48, 49].

References

1. J-B. Donnet and A. Voet, *Carbon Black, Physics, Chemistry and Elastomer Reinforcement*, Marcel Dekker, Inc., New York, 1976.

2. M. P. Wagner, *Rubber Chemistry and Technology*, 1976, **49**, 3, 703.

3. E. M. Dannenberg, *Carbon Black, Encyclopaedia of Composite Materials and Components*, Wiley, New York, 1983, p.230.

4. ASTM D1510-98
Standard test method for carbon black-iodine adsorption number.

5. ASTM D2414-99
Standard test method for carbon black-n-dibutyl phthalate absorption number.

6. ASTM D1513-99a
Standard test method for carbon black, pelleted-pour density.

7. ASTM D3265-99
Standard test method for carbon black-tint strength.

8. ASTM D1765-99a
Standard Classification System for Carbon Blacks used in Rubber Products.

9. N. Nakajima, W. J. Shieh and Z. G. Wang, *Polymer Engineering Science*, 1992, **32**, 15, 981.

10. E. M. Dannenberg, *Rubber Chemistry and Technology*, 1975, **48**, 3, 410.

11. J. O'Brien, E. Cashell, G. E. Wardell and V. J. McBrierty, *Rubber Chemistry and Technology*, 1977, **50**, 4, 747.

12. N. Nakajima and J. J. Scobbo, Jr., *Rubber Chemistry and Technology*, 1988, **61**, 1, 137.

13. L. Mullins and N. R. Tobin, *Rubber Chemistry and Technology*, 1967, **39**, 4, 799.

14. N. Nakajima, *Rubber Chemistry and Technology*, 1988, **61**, 5, 938.

15. ASTM D 1646 – 98a
Standard Test Methods for Rubber – Viscosity, Stress Relaxation, and Pre-Vulcanisation Characteristics (Mooney Viscometer).

16. ASTM D 3616 – 95
Standard Test Methods for Rubber, Raw – Determination of Gel, Swelling Index, and Dilute Solution Viscosity.

17. M. Ito, T. Nakamura and K. Tanaka, *Journal of the Society of the Rubber Industry, Japan*, 1985, **58**, 7, 468.

18. Y. Hirata, *Journal of the Society of the Rubber Industry, Japan*, 1986, **59**, 450.

19. J-B. Donnet and A. Voet, *Carbon Black, Physics, Chemistry and Elastomer Reinforcement*, Marcel Dekker, Inc., New York 1976. Chapter 4 and Chapter 8.

20. M-J. Wang, S. Wolff and J-B. Donnet, *Rubber Chemistry and Technology*, 1991, **64**, 4, 559.

21. M-J. Wang, S. Wolff and J-B. Donnet, *Rubber Chemistry and Technology*, 1991, **64**, 5, 714.

22. M-J. Wang and S. Wolff, *Rubber Chemistry and Technology,* 1992, **65**, 5, 890.

23. E-H. Tan, S. Wolff, M. Haddeman, H. P. Grewatta and M-J. Wang, *Rubber Chemistry and Technology*, 1993, **66**, 4, 594.

24. N. Nakajima and M. H. Chu, *Rubber Chemistry and Technology*, 1990, **63**, 1, 110.

25. J. Jansen and G. Kraus, *Rubber Chemistry and Technology*, 1980, **53**, 1, 48.

26. A. I. Medalia, *Rubber Chemistry and Technology*, 1974, **47**, 2, 411.

27. T. C. Gruber, T. W. Zerda and M. Gerspacher, *Rubber Chemistry and Technology*, 1994, **67**, 2, 280.

28. M. Gerspacher and C. P. O'Farrell, *Elastomerics*, 1991, **123**, 4, 35.

29. C. R. Herd, G. C. McDonald and W. M. Hess, *Rubber Chemistry and Technology*, 1992, **65**, 1, 107.

30. S. Misono, *Journal of the Society of the Rubber Industry, Japan*, 1997, **70**, 10, 564.

31. N. Nakajima, Presented at the *International Seminar on Elastomers*, 1985, Itoh, Shizuoka, Japan, p.182.

32. G. R. Cotten, *Rubber Chemistry and Technology*, 1984, **57**, 1, 118.

33. B. B. Boonstra and A. I. Medalia, *Rubber Chemistry and Technology*, 1963, **36**, 1, 115.

34. ASTM D1937-98
Standard test method for carbon black, pelleted-mass strength.

35. J-B. Donnet and A. Voet, *Carbon Black, Physics, Chemistry and Elastomer Reinforcement*, Marcel Dekker, Inc., New York, 1976, p.12.

36. J-B. Donnet and A. Voet, *Carbon Black, Physics, Chemistry and Elastomer Reinforcement*, Marcel Dekker, Inc., New York 1976, p.9 and p.11.

37. J. V. Day, inventor; Godfrey L Cabot, Inc., assignee, US Patent 2,850,403, 1958.

38. J-B. Donnet and A. Voet, *Carbon Black, Physics, Chemistry and Elastomer Reinforcement*, Marcel Dekker, Inc., New York, 1976, p.201.

39. S. Shiga and M. Furuta, *Rubber Chemistry and Technology*, 1985, **58**, 1, 1.

40. J-B. Donnet and A. Voet, *Carbon Black, Physics, Chemistry and Elastomer Reinforcement*, Marcel Dekker, Inc., New York, 1976, p.3.

41. J-B. Donnet and A. Voet, *Carbon Black, Physics, Chemistry and Elastomer Reinforcement*, Marcel Dekker, Inc., New York, 1976, p.9 and p.11.

42. M. Gerspacher, C. P. O'Farrell, L. Nikiel and H. H. Yang, *Rubber Chemistry and Technology*, 1996, **69**, 3, 569.

43. N. Tokita, M. J. Wang, B. Chung and K. Mahmud, *Journal of the Society of the Rubber Industry, Japan*, 1998, **71**, 9, 522.

44. W. M. Hess, R. A. Swor and E. J. Micek, *Rubber Chemistry and Technology*, 1984, **57**, 5, 959.

45. N. Nakajima, *Rubber World*, 1996, **215**, 3, 33.

46. J. B. Class and S. G. Chu, *Journal of Applied Polymer Science*, 1985, **30**, 2, 825.

47. N. Nakajima and S. Okuno, *Journal of Rheology*, 1994, **38**, 3, 541.

48. N. Nakajima and J. P. Varkey, *Polymer International*, 1998, **46**, 4, 298.

49. N. Nakajima, *Journal of Applied Polymer Science*, 1994, **53**, 39.

50. ASTM D 3493-99
Standard Test Method for Carbon Black-n-Dibutyl Phthalate Absorption Number of Compressed Sample.

51. ASTM D3765-99
Standard Test Method for Carbon-Black-CTAB (Cetyltrimethylammonium Bromide) Surface Area.

52. ASTM D3037
Test Methods for Carbon-Black-Surface Area by Nitrogen Adsorption. (Discontinued 1999).

10 The Energy Aspects of Mixing Rubber

10.1 Introduction

The energy aspects of rubber mixing have been a focal point of some research activity. Particular attention has been given to the process involving internal mixers. A state-of-art review was published on this subject [1]. A method was proposed for control and scale-up which was based on the energy input for mixing [2]. Those properties affected by the degree of mixing were evaluated as functions of mixing energy [2, 3, 4]. This method was used for evaluating the performance of different types of elastomers and carbon blacks in internal mixers [5, 6]. Although the method treats the internal mixers essentially as a 'black box', it represents significant progress in understanding the mixing process. It permits comparison of the efficiency of different types of equipment and the evaluation of the ease of mixing of a given formulation.

The energy aspect is not only of technological importance but also an economic concern. It leads to two questions: how the input energy is spent and how much is actually necessary. The answer to the first question is to take an energy balance, which is a method of 'book keeping' on the income and expenditure in terms of energy. The second question requires elucidation of mixing mechanisms and calculation of theoretical energy requirements. The mill-mixing involves human participation. Therefore, the energy spent in the machine operation is only a part of the overall energy aspect. It is not easy to quantify the energy balance. On the other hand mixing with an internal mixer is amenable to taking energy balance. The foregoing discussion is about the operation of internal mixer only and an example is a Banbury type mixer.

The examination of mixing mechanisms will also deal primarily with the internal mixer, because the energy requirements must be determined quantitatively. A discussion of this subject will be given in Chapter 11.

10.2 Energy balance

Because mixing involves viscous heat generation and simultaneous cooling, heat transfer measurement is a necessary part of calculating the energy balance.

Precise data gathering requires extensive instrumentation, which becomes prohibitively expensive. However, with reasonable assumptions and approximations, an overall energy balance of the mixing operation may be obtained using relatively simple instrumentation. This work is an example of such a study of the operation of a laboratory Banbury mixer with a powdered rubber compound.

10.2.1 Experiment

The aim of the experimental work is:

(1) to define the operating conditions of the machine as closely as possible,
(2) to establish a reproducible operation,
(3) to collect as much data as possible within a rather short time operation, i.e., about 1.5 minutes.

The characterisation of the mixing results is outside the scope of this work. The emphasis is on the analysis and not on the optimisation of the process.

- *Sample*

A preblended powdered rubber compound was charged into the mixer, instead of separately charging a slab of rubber and carbon black. This was done to minimise the variability in the charging procedure and to avoid gross inhomogeneity at the beginning of the mixing.

The formulation is given in Table 10.1. The raw elastomer was an NBR copolymer powdered rubber with a Mooney index of 80 (ASTM D1646 [7]). The powder was preblended with a high-intensity Henschel mixer.

Table 10.1 Compound Formulation

Material	Quantity phr
Rubber	100.0
ZnO	5.0
Stearic acid	1.0
N550 carbon black	65.0
DOP	15.0
TMTD	1.5
4,4′-Dithiodimorpholine	1.5

DOP: dioctyl phthalate
TMTD: tetramethyl thiuram disulphide

- *Equipment and operating conditions*

The internal mixer and measuring instruments were as follows:

(1) A Banbury mixer (size BR) with the narrowest gap between the blade and the wall of 2.39 mm and a sectional chamber diameter of 101.6 mm.

(2) A built–in thermocouple for stock temperature measurement which was in a thermocouple well located above the rotors in the middle of the chamber and extending about 25 mm in a 45 degree downward direction from the right–hand wall.

(3) A recording watt–meter and a power integrator.

(4) A portable pyrometer for direct measurement of the stock temperature and temperatures of various parts of the machine.

(5) Thermometers for the measurement of the cooling-water temperature.

(6) A flow meter for the cooling water.

All thermometers had been precalibrated. The operating conditions of the mixer are given in Table 10.2.

Table 10.2 Operating Conditions

Sample charge	1,400 g
Revolution rate	77 rpm
Ram pressure	0.24 MPa
Cooling water flow rate (Full cooling)	~440 cm^3/s

10.2.2 Experimental programme

The programme consisted of three sets of experiments. The first set, Experiment I, was performed in 1972; the second, Experiment II and the third, Experiment III, were performed in 1981. A different operator performed the mixing for each set of experiments.

In Experiment I, the machine had been prewarmed by circulating cooling water which had been adjusted to 35-40 °C. The circulation of water had been started well ahead of

the mixing runs so that the machine, a metal block of large mass, was preheated to an approximate equilibrium temperature. Five runs were made to assure energy data reproducibility. The sixth run was terminated at an intermediate stage of mixing for the direct measurement of the stock temperature at this stage.

The thermometer for the outlet water did not register a significant temperature rise. The subsequent calculation of the heat transfer indicated that the expected temperature rise was so small that a more precise thermometer was required.

In Experiment II, the cooling water was at room temperature in the beginning. The machine was prewarmed by the first three mixing runs; the energy data of these runs were not used for the present calculation. Subsequently, another three runs were made for obtaining the energy balance. In order to measure the total heat removed by the cooling water, a given amount of water in a reservoir of 84 litres was recirculated and the temperature difference between the beginning and the end of the mixing was measured with a thermometer accurate to 0.05 °C.

Experiment III was essentially the same as Experiment II, except that the curatives were omitted from the formulation. This was done to ensure that a premature cure, which might contribute to errors in the energy balance, did not take place. The first two somewhat longer runs were used for prewarming the machine. The subsequent four runs were made for obtaining the energy balance. Each run was terminated at a different stage of mixing in order to measure the stock temperature directly.

The mixing performance, as observed by the power input and the stock temperature, was quite reproducible for all mixing runs in the three sets of the experiment. This confirmed that a premature cure reaction did not take place.

- *Measurement of machine temperature*

The machine temperature was measured immediately before and after the runs with a portable pyrometer. The measurements were always made at the same place on the machine. The outside wall had a square bulge, which was a convenient spot to use. It was approximately 50 mm from the right-hand wall of the chamber. The rotor temperature was measured in the centre of the broad side of the blade at the largest gap from the wall. This part is thought to represent the average temperature. At the edge of the blade, the temperature may be higher because of the high shear rate at the narrowest gap. The chamber-wall temperature was measured near the top of the door. The order of temperature measurements was first the rotor, followed by the chamber-wall, and then the outside wall. After each run, the stock temperature was taken first, and then the machine temperatures were measured. The measurements were made rapidly, and the highest temperature was measured first in order to minimise the error due to cooling.

- *Measurement of stock temperature*

The final stock temperature was measured immediately after the door was opened at the corresponding spot where the rotor temperature was measured. However, because the stock was still banded on the rotor, it was not possible to see whether or nor the spot was exactly at the centre of the broad side of the blade.

10.2.3 Results

- *Temperature measurements*

The temperature data of some of the mixing runs are given in Table 10.3; the data of the runs not shown here were very similar to the ones in the table. Within a given set of experiments, the cooling-water temperature gradually increased a few degrees. However, during each mixing run, the cooling-water temperature remained approximately constant.

Table 10.3 Temperature Measurements

Experiment No.	**I**		**II**		**III**	
Run No.	2	4	4	6	3	6
Run time, *s*	78	84	105	100	100	75
Cooling water, °C						
Inlet (start/finish)	35/35	38/38	–	–	–	–
Reservoir (start/finish)	–	–	28.7/29.4	30.0/30.7	26.2/26.9	28.1/28.5
Machine temperature, °C						
Rotor (start/finish)	32/48	40/49	32/41	31/40	37/43	29/36
Chamber wall (start/finish)	35/45	41/49	29/37	30/36	30/40	28/36
Outside wall (start/finish)	32/33	35/36	27/29	29/30	27/30	28/30
Stock temperature at finish, °C						
Direct measurement, t_1	127	143	156	156	133	119
Thermocouple, t_2	110	112	117	120	115	107
t_1-t_2	17	32	39	36	18	12

The temperatures of the rotor and chamber-wall were not exactly reproducible, partly because of the non-uniform temperature within the compound. Moreover, the measurement of the steel surface with a temperature probe involves a somewhat larger

error. However, the average temperature rise of these parts can easily be estimated. The temperature of the outside wall of the machine increased by 1-3 °C during a run. This must have resulted from the temperature rise of the compound rather than from the cooling water, which was in many cases warmer than the outside wall.

Direct measurements of the stock temperature indicated that there was a large run-to-run variation. This was interpreted to represent temperature non-uniformity within one batch, which was as much as ± 13.5 °C. Also, the direct measurements indicated a 12-39 °C higher temperature than that indicated by the built–in thermocouple. The latter, being placed in a rather large well, might have been cooled by the large heat sink of the machine body.

Examples of the continuous recording of the stock temperature are shown in Figure 10.1. The recorded starting temperature is that of the machine rather than the stock temperature, which was 24 °C. In all three sets of experiments, the temperature readings increased as the mixing runs were repeated. However, there is a reproducible pattern in all the temperature recordings, namely, the initial rapid increase tapers off at about 25-30 seconds and then, another rapid increase occurs until 40-50 seconds. Thereafter, the temperature increase is much more gradual.

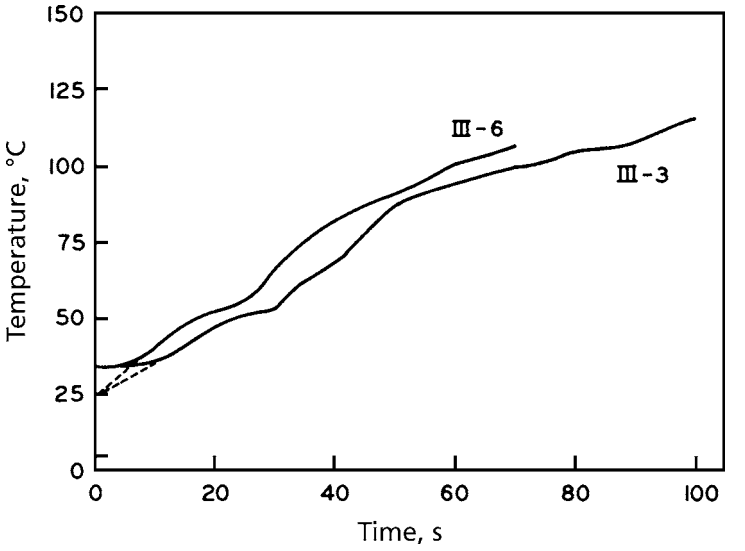

Figure 10.1 Temperature curves recorded by the thermocouple for Experiment III, Runs 3 and 6 (see Table 10.3 for experimental details).

A method for estimating the true compound temperature is illustrated in Figure 10.2, which shows the temperature recorded by thermocouple, t_2, the stock temperature, t_1, measured directly by a probe and the stock temperatures estimated from the temperature difference, $t_1 - t_2$, of other runs. These $t_1 - t_2$ values were added to the t_2-curve of this run to obtain the t_1-curve. It was assumed that the temperature difference between the t_1-curve and the t_2-curve increased smoothly with the rise of the stock temperature. This is based on the previously stated interpretation that the temperature difference, $t_1 - t_2$, is caused by the heat-sink effect on the thermocouple. Such an effect is expected to increase with rising stock temperature. The fact that the pattern of t_2-curves is very reproducible means that the temperature non-uniformity within the compound is not registered by the thermocouple. This is probably due to the time lag of the thermocouple, which averages out the temperature non-uniformity of the very rapidly sweeping compound.

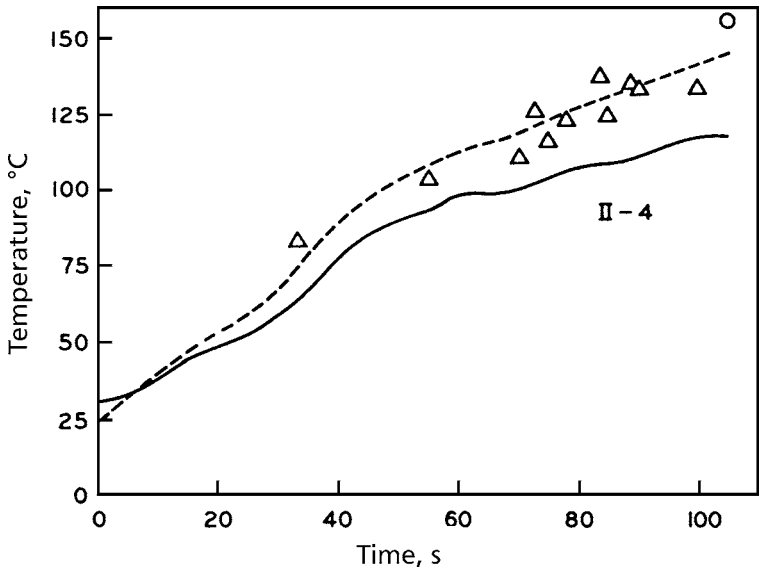

Figure 10.2 Method of estimating correct temperature of the compound for Experiment II, Run 4 (see Table 10.3 for experimental details). Solid curve, temperature recorded by thermocouple, t_2; broken curve, estimated stock temperature, t_1; ○ stock temperature measured by probe, t_1; △ stock temperature estimated from the temperature difference, $t_1 - t_2$, of other runs.

- *Mechanical energy input*

Figure 10.3 shows a recorder trace of the power input; the input of mechanical energy is the area under the curve. Also, shown is the stock temperature, estimated according to the method described previously. Initially, the power level is high and approximately constant. This part corresponds to the rapid increase of the stock temperature. The carbon black incorporation is almost completed before the dusting period. The dusting period occurs when the ram is lifted up and the material remaining in the charge hole is swept down into the chamber. That is why the power input during the dusting period is lower. After the ram is down, the power goes up again but then gradually decreases. This part corresponds to the more gradual increase of the stock temperature.

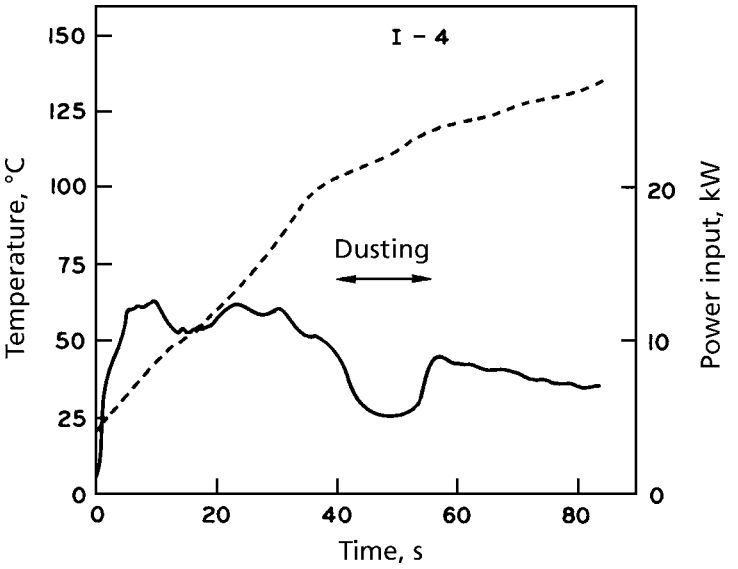

Figure 10.3 Power input (____) and temperature curves (------) for Experiment I, Run 4 (see Table 10.3 for experimental details).

- *Method for evaluating energies*

Mechanical energy input. The mechanical energy input was calculated in the following sequence. First, the area under the kW-time recorder trace was integrated. This gives the energy input as a function of time. The total energy input was checked against the reading of the power integrator. This energy, however, does not represent the real work done on

the material because one part of the energy represents the electrical loss in the motor and another the mechanical loss in the machine.

The efficiency cannot be obtained from the differences of the energy inputs between loaded and unloaded operations, because the losses depend upon the load. In the present operations, the energy required to run the unloaded machine for the corresponding period of time was only 6-6.5% of the total energy input for mixing. However, for a large mixing machine, the real loss is usually 10-15% [1]. On the other hand, an example involving the extrusion of thermoplastic materials gave an efficiency of 75%. Since a small mixer was used in this experiment, the efficiency may be somewhat lower than that of the large mixers. From the energy calculation at the end of the mixing cycle, the efficiency was estimated to be 79%, as will be shown later. Then the 79% efficiency was assumed to be independent of the progress of mixing. This approximation is justified, because the power input does not change enough to affect the efficiency.

- *Enthalpy increase of the compound*

As the mixing progresses, the temperature of the stock rises. The accompanying increase of enthalpy, ΔH, was calculated according to

$$\Delta H = \sum_i m_i C_{pi} \left(t - t_0 \right) \tag{10.1}$$

where m_i is the mass,

C_{pi} is the specific heat of the components,

t is the stock temperature;

t_0 is the room temperature, 20 °C for Experiment I and 24 °C for Experiments II and III.

The mass–average value of C_p of the compound, 1.5 J/g-K, was used for the actual calculation. This value was estimated, assuming that the C_p of SBR rubber, 1.9 J/g-K [8], represented the C_p of rubber and ingredients other than carbon black, while C_p of carbon was taken to be 0.76 J/g-K [9].

- *Heat loss from the machine surface to the room.*

The following formulae [10] were used to estimate the heat loss from the machine surface.

For convection,

$$q_c = hA\Delta t_s \tag{10.2}$$

where q_c is the rate of heat loss to the room by convection in watts,

h is a convection coefficient in $W/(m^2 \cdot K)$,

A is an effective surface area of the machine in m^2,

Δt_s is the temperature difference between the machine surface and the room in K.

The convection coefficient for heat loss from surfaces by convection to air at atmospheric pressure and ordinary temperatures is given by the equation for vertical plates as

$$h = 0.28(\Delta t_s / L)^{1/4} \tag{10.3}$$

where L is the characteristic dimension of machine in metres.

For radiation,

$$q_R = A\varepsilon\sigma(T^4 - T_0^4) \tag{10.4}$$

where q_R is the rate of heat loss by radiation in watts,

σ is the Stefan–Boltzman constant for a black body in $W/(m^2 \cdot K^4)$,

ε is emissivity, a coefficient for a particular surface,

T is the absolute temperature of the surface in K,

and T_0 is the room temperature in K. The numerical values of the constants are given in Table 10.4.

Table 10.4 Quantities for Heat Transfer Calculation

Convection	Radiation
A=0.24 m^2 *a* L=0.25 m *b*	σ =5.67 x 10^{-8} $W/(m^2 K^4)$ *c* ε=0.8 *d*

a : Approximate surface area of the mixing chamber
b : Approximate dimension of the vertical surface
c : [11]
d : Painted surface or oxidised steel surface [12]

The overall rate of heat loss from the machine surface is

$$q_L = q_c + q_R \tag{10.5}$$

Because the temperature difference between the room and the machine surface remains approximately constant throughout the run, the total heat loss is

$$Q_L = q_L \theta \tag{10.6}$$

where θ is the time in seconds.

- *Machine body as a heat sink*

If the machine is cold at the start of the mixing operation, a large amount of heat is used to raise the machine temperature, which eventually reaches approximately a steady state after several mixing cycles. In the present case, the machine body was pre-equilibrated either by circulating warm water or by performing a few mixing runs. In this way, the bulk of the heat sink effect was eliminated. The observations in Table 10.3 show that the outside-wall temperature of the machine remained approximately constant during a mixing cycle. However, the temperature of the outside wall went up 1-3 °C during the mixing cycle. This means that the heat-sink effect still existed. It is difficult to calculate the heat loss from this temperature-rise, because the exact portions of the machine which are involved cannot be estimated. Instead, the heat flow from the compound to the environment was evaluated in the following manner. One part of the heat flow was to the metal block between the mixing chamber and the cooling water. This part of the heat flow, Q_m, raised the temperature of the metal block and also was partially removed by the cooling water, Q_w. Another part of the heat flow, Q'_m occurred through non–jacketed regions of the machine, e.g., the charge hole, the ram, and the rotor shafts. The sum of $Q_m + Q'_m = Q_M$ constitutes the total magnitude of the heat-sink effect.

The magnitude of Q_m was calculated from

$$Q_m = C_p m \Delta t_{av} \tag{10.7}$$

where $C_p = 0.46\ J/g \cdot K$ for steel, and the mass of the block and the rotor, m, is estimated to be 21 kg, where jacketed. The average increase of the temperature was calculated from:

$$\Delta t_{av} = (\Delta t_m + \Delta t'_m) / 2 \tag{10.8}$$

where Δt_m is the observed temperature rise at the chamber wall (and the rotor surface) and $\Delta t'_m$ is the temperature rise at the jacket surface. The latter was estimated from the known value of the heat transfer coefficient between steel surface and cooling water, U_w, and from the rate of heat transfer to the cooling water, $dQ_w / d\theta$. The averaging in equation (10.8) assumes a constant temperature gradient across the chamber wall, i.e., a steady state. This somewhat overestimates the actual heat loss because the heat flow is

not at a steady state [1]. Moreover, linear increases of Δt and $\Delta t'$ with time were assumed, and this also somewhat overestimates the heat loss. However, these approximations do not seriously affect the present calculation.

For the calculation of heat flow through the unjacketed part of the machine, a semi-infinite solid wall with a uniform, unidirectional temperature gradient was assumed. On the assumption of a temperature rising linearly with time at the chamber wall and at the rotor surface, $\Delta t_{x0} = C\theta$, the equation for the heat flow becomes [13]:

$$\Delta t_x = C\theta[\{1+(x^2/2\alpha\theta)\}erfc\{x/2(\alpha\theta)^{1/2}\}-\{x/(\pi\alpha\theta)^{1/2}\}\exp(-x^2/4\alpha\theta)] \qquad (10.9)$$

where Δt_x is the temperature difference between the location x and infinite distance at a fixed time θ. The other parameters are C, the coefficient of the linear temperature rise and α, the thermal diffusivity of steel, given by

$$\alpha = k/(\rho C_p) \qquad (10.10)$$

where the thermal conductivity, k, of steel is 45 $W/m \cdot K$,

the density, ρ, is 7.8 x 10^6 g/m^3,

and the specific heat, C_p is 0.46J /($g \cdot K$). These values give a thermal diffusivity of

$$\alpha = 12.5 \text{ x } 10^{-6} \text{ m}^2/\text{s}$$

The values of Δt were calculated as functions of x at fixed values of θ. This permitted evaluation of the temperature gradient, $(\partial t / \partial x)_{\theta,x}$ at $x = 0$. The corresponding heat flux is,

$$f = -k(\partial t / \partial x) \qquad (10.11)$$

The total heat flow by conduction is,

$$Q'_m = A\int_0^\theta f d\theta = -kA\int_0^\theta (\partial t / \partial x) d\theta \qquad (10.12)$$

where the estimated surface area, A, is 0.04 m^2.

- *Heat removed by cooling water*

The heat removed by cooling water was calculated in two ways. The first used the observed temperature rise, Δt_R, of the cooling water in the reservoir:

$$Q_w = mC_p\Delta t_R \qquad (10.13)$$

The second method evaluated Q_w from the difference according to

$$Q_w = Q_t - (\Delta H + Q_M + Q_L) \tag{10.14}$$

The first method was used only with the data at the end of the run. As stated before, the energy balance at this stage gave an average 79% efficiency for the machine. The second method was used to evaluate Q_w as mixing progressed. The total energy input, Q_t was calculated as previously explained, using 79% efficiency.

Table 10.5 Energy Balance at End of Mixing Cycle

Experiment No.	**II**			**III**			
Run No.	**4**	**5**	**6**	**3**	**4**	**5**	**6**
Input, *k*J (Power Integrator)	738	702	724	695	648	396	540
ΔH, *k*J	254	246	256	244	231	176	210
Q_L, *k*J	1	1	1	1	1	1	1
Q_M, *k*J	75	75	75	75	67	41	52
Q_w, *k*J	246	211	246	246	246	105	140
Total Output, *k*J	576	533	578	566	545	323	403
Efficiency, %	78	76	80	81	84	82	75

- *Energy Balance*

The energy balance data at the end of the mixing runs for Experiments II and III are summarised in Table 10.5. This calculation was not performed for Experiment I because direct measurements of Q_w were not available. From these seven runs, the average efficiency of the machine was found to be 79%.

An example of the energy balance during the mixing is shown in Figure 10.4. For this example, the following values prevailed at the end of the mixing cycle:

$\Delta H/Q_T = 41.3\text{-}46\%$

$Q_L/Q_T = 0.2\text{-}0.6\%$

$Q_M/Q_T = 12.3\text{-}14.6\%$

Q_W/Q_T = 39.6-45.1%

For the runs terminated after 30-55 seconds, the values were:

$\Delta H/Q_T$ = 54.5-55.4%

Q_L/Q_T = 0.3-0.4%

Q_M/Q_T = 10.0-12.7%

Q_W/Q_T = 32.5-34.5%

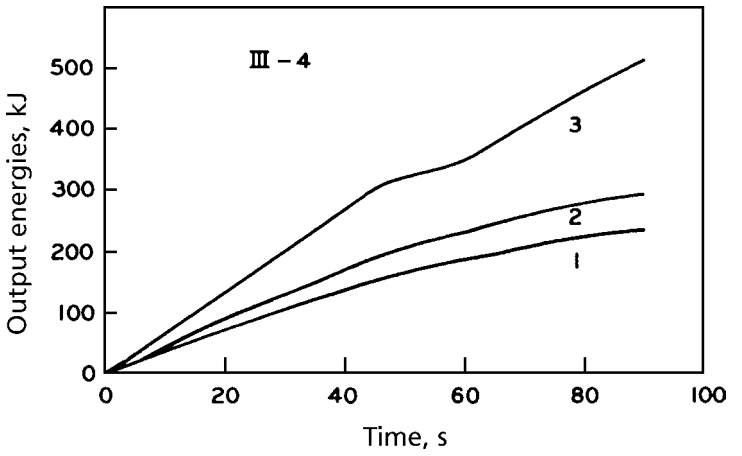

Figure 10.4 Energy balance of internal mixer during mixing of powdered rubber compound. Curves: 1, ΔH; 2, $Q_M + Q_L$; 3 Q_W. Results obtained from Experiment III, Run 4 (see Table 10.3 for experimental details).

- *Heat Transfer*

Calculation of heat transfer coefficient. The heat removed by the cooling water, Q_w is plotted with time, θ in Figure 10.5, for Experiment III, Run 4. The slope of this curve is the rate of heat transfer from the compound to water, $dQ_w / d\theta$.

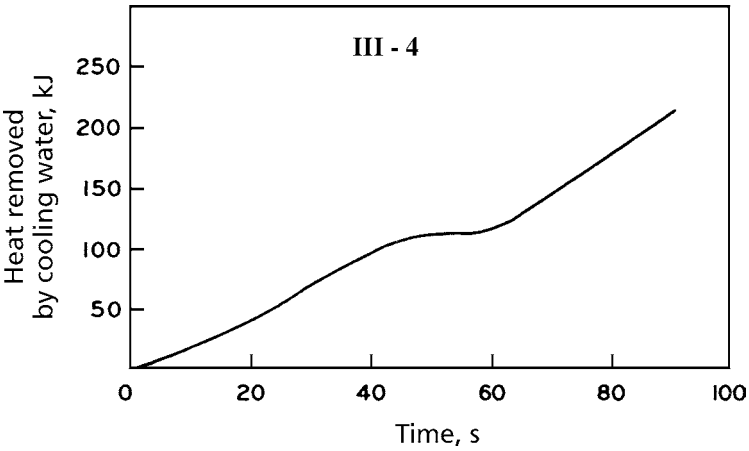

Figure 10.5 Heat removed by cooling water. Results obtained from Experiment III, Run 4 (see Table 10.3 for experimental details).

The overall heat transfer coefficient for heat transfer from the stock to cooling water is calculated from

$$UA = dQ_w / d\theta(t - t_w)^{-1} \tag{10.15}$$

where U is the overall heat transfer coefficient, W/(m^2·K),

A is the area of heat transfer, m^2,

t is the average stock temperature,

and t_w is the cooling water temperature, °C.

The values of U are plotted in Figure 10.6 for the period when the ram was down. The points indicated by the circles are the averages obtained from all the runs. Each data point fell within the range indicated by the error bars. In spite of the considerable scattering of the data, there are two observable trends: the heat transfer coefficient decreases as the mixing progresses and tends to level off; the scatter of the data diminishes as mixing advances. The scatter of the data may be related to inhomogeneity of the material and non–uniform temperature, both of which must decrease with the progress of mixing.

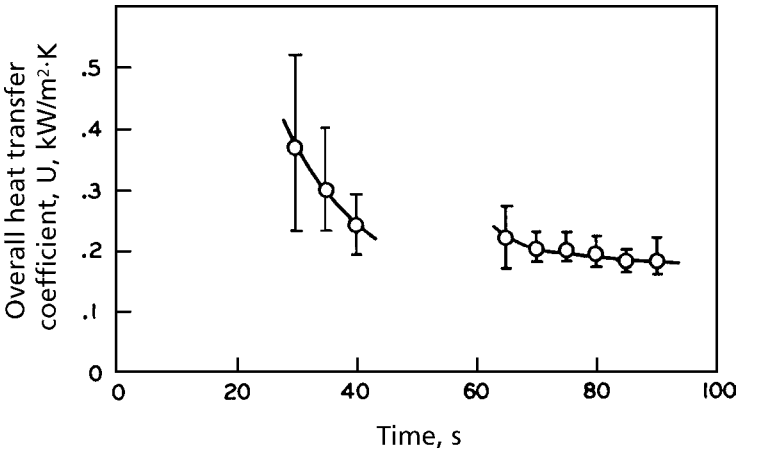

Figure 10.6 Overall heat transfer coefficient in heat transfer from compound to cooling water.

Reprinted with permission from N. Nakajima, E. R. Harrell and D. A. Seil, Rubber Chemistry and Technology, 1982, 55, 2, 456. Copyright 1982, Rubber Division of the ACS.

The data for the early stage for the mixing and the dusting period are not shown because they were not reproducible.

The high value of the heat transfer coefficient early in the process may be related to the carbon black that is exposed to the chamber wall. As the carbon black becomes completely incorporated, the heat transfer is between the rubber and the chamber wall. This explains the constant values eventually reached. From the heat transfer data, the incorporation of carbon black is seen to be almost complete after 40-45 seconds of mixing. This is the beginning of the dusting, which, experience had taught us, coincides with the completion of incorporation of carbon black.

10.2.4 Summary

An energy balance was obtained for the mixing of an elastomer compound in the internal mixer. The mixing operation was done reproducibly, and pertinent data were collected with relatively simple instrumentation. Out of the total mechanical energy input into the compound, 41-46% went to raise the temperature of the compound, and 40-45% was removed by the cooling water. The heat loss from the mixer wall to the room was very

small and negligible. This energy balance is based on the average temperature profile, which assumes uniform temperature of the stock.

The actual temperature measurement of the stocks gave temperature differences of as much as ±13.5 °C, indicating temperature non-uniformity within the stock. This is very plausible because rubber is a poor conductor, the shear field within the mixing chamber is exceedingly non-uniform, and thus, the viscous heating of the material is very non–uniform.

Heat transfer coefficients were evaluated for the overall heat transfer from the stock to the cooling water and for the heat transfer from the stock to the chamber wall. The data indicate that the compound was not uniform at the beginning of the mixing, in spite of the fact that a premixed powdered rubber was used. The non-uniformity must be in the degree of incorporation of carbon black rather than in the composition. There is also non-uniformity in the temperature. The heat transfer coefficient has a high value when the carbon black is on the surface of rubber but decreases to a constant value with the incorporation of carbon black into the rubber.

Although it is not the objective of this chapter to evaluate the effectiveness of mixing, the compound after curing gave mechanical properties which indicated thorough mixing.

References

1. H. Palmgren, *Rubber Chemistry and Technology*, 1975, **48**, 3, 462.

2. P. R. Van Buskirk, S. B. Turetzky and P. F. Gunberg, *Rubber Chemistry and Technology*, 1975, **48**, 4, 577.

3. F. S. Myers and S. W. Newell, *Rubber Chemistry and Technology*, 1978, **51**, 2, 180.

4. G. E. O'Connor and J. B. Putman, *Rubber Chemistry and Technology*, 1978, **51**, 4, 799.

5. S. B. Turetzky, P. R. Van Buskirk and P. F. Gunberg, *Rubber Chemistry and Technology*, 1976, **49**, 1, 1.

6. E. S. Dizon, *Rubber Chemistry and Technology*, 1976, **49**, 1, 12.

7. ASTM D1646-99
Standard Test Methods for Rubber-Viscosity, Stress Relaxation and Pre-Vulcanised Characteristics (Mooney Viscometer).

8. *Polymer Handbook*, 4th Edition, Eds., J. Brandrup, E. H. Immergut and E. A. Grulke, Wiley–Interscience, New York, 1999.

9. *Handbook of Chemistry and Physics*, 32nd Edition, Chemical Rubber Publishing Co., Cleveland, Ohio, 1950-51, p.1871.

10. R. H. Perry, C. H. Chilton, and S. D. Kirkpatrick, *Chemical Engineer's Handbook*, 4th Edition, McGraw-Hill Book Company, New York, 1963.

11. R. B. Bird, W. E. Stewart, and E. N. Lightfoot, *Transfer Phenomena*, John Wiley and Sons, Inc., New York, 1960, p.433.

12. D. Q. Kern, *Process Heat Transfer*, McGraw-Hill Book Company, New York, 1950.

13. H. S. Carslaw and J. C. Jaeger, *Conduction of Heat in Solids*, 2nd Edition, Oxford Press, 1959, p.63.

11 Mixing Mechanisms

11.1 Introduction

Rubber is an elastic material and it is often called an 'elastomer'. It also possesses a viscous nature, which is manifested in temperature-rises during mixing, i.e., viscous energy dissipation. Although its viscoelastic nature has been recognised for some time, the discussion on mixing of rubber often ignores viscoelasticity. One reason for this may lie in the fact that many people are unfamiliar with viscoelasticity. Another reason may be that methods for applying viscoelasticity to practical situations are not adequately developed. The latter concerns the handling of non-linear viscoelasticity in particular. It also includes fracture behaviour of rubber.

This chapter will discuss the mechanisms of mixing fillers with gum rubbers. It is primarily concerned with the use of internal mixers.

11.2 Problems associated with internal mixers

In discussing problems associated with internal mixers, we begin with the differences in operation between the mill and the internal mixer. In the mill operation, it is possible to observe what is happening, whereas with internal mixers, direct observation is not possible. In mill mixing, the operator participates in the production process by adjusting mill gap, cutting and rolling rubber sheet, and recharging. The repeated take-off and recharging are to give a uniform treatment of the compound. With internal mixers, the gap between the rotor wing and the chamber wall corresponds to the mill gap. However, the contents of the mixer do not necessarily pass the gap uniformly; some parts may go through more times than other parts. Some parts may even remain stagnant. In general, the history of deformation and fracture of rubber during mixing is non-uniform. The degree of non-uniformity depends on the rotor configuration and on whether the rotors are intermeshing or non-intermeshing. In addition, the viscoelasticity of a given gum rubber has a decisive influence on the uniformity. The uniformity in this discussion primarily concerns the macroscopic differences but it is indirectly related to microscopic inhomogeneity also.

The fill factor most suitable for the mixing of rubber is about 70-75%, which was determined through experience. In order for the mixer's contents to move uniformly, a

vacant space is necessary. With 100% fill factor, the contents are prevented from moving easily; only a small part is sheared and a large part is stagnant. With an insufficient amount of charge, the contents are not carried through the gap efficiently. The above material behaviour is associated with the solid-like nature of rubber. Sometimes, a gum rubber is considered to be a fluid having a very high viscosity, but an inelastic fluid would behave differently.

The meaning of a solid-like behaviour has been explained in Chapter 1 [1]. It is the dominance of elasticity over viscous contribution. In other words, when a polymer is in the rubbery state, the entanglement of the rubber chains (see section 1.2) cannot be disentangled within a given time-temperature window. If the deformation exceeds the fracture limit (see section 4.4), rubber breaks primarily through the slipping of the entanglement near the chain ends. If either temperature or time exceeds the limits set by the time-temperature window, the rubber enters into the flow region. Its behaviour is no longer rubbery. Because the content of the internal mixer is non-uniform, the dumped compound is homogenised in the mill. The milling must be done immediately, otherwise the compound tends to become too stiff to be millable. Once milled and sheeted, the aged and stiffened compound may be remilled easily.

In addition to the non-uniformity within a batch, there is a batch-to-batch reproducibility problem. In general the extent of non-reproducibility depends upon the configuration of the mixer, the size of the machine, operating conditions such as the temperature of the machine, and the viscoelastic nature of the rubber. Therefore, the two most important problems of the mixing operation are the process control and scale-up.

In earlier days, process control was based on the mixing time. The rationale was that when the same operating conditions were maintained, mixing for the same period of time yielded the same product. In reality this was not true. Because there was a larger batch-to-batch difference in a short time, excessive time was spent in ensuring that all batches became acceptable. This resulted not only in a waste of energy but also reduced production capacity. In some cases, even an extended mixing time does not improve batch-to-batch reproducibility. The compound temperature monitored with a built-in thermocouple indicates batch-to-batch variation although the general pattern of the temperature-rise may be very similar. For a batch, where the temperature rises quickly, the rubber may enter into the flow region and the dispersion of filler may become difficult. If the compound contains curatives, it may become scorched.

As a solution to the reproducibility problem, energy rather than time-based control was proposed [2-6]. For examining the reproducibility, the dynamic stress relaxometer was used [4]. This idea is called the unit work concept or energy-based control. A power integrator is used for the control. The energy-based control is also reported to be useful

for scale-up [2]. However, in this case, the temperature profile as well as the total mixing energy must be the same. In general, the cooling of the mixer contents depends upon the surface-to-volume ratio in that duplicating the same temperature profile for different sized mixers is not always possible.

An extensive review article on the internal mixer was published by Palmgren [7, 8, 9]. This review made two significant contributions to the progress of mixing technology. One was to summarise the state-of-the-art at the time of its publication and another was to help define needs for further investigation. Therefore, it is convenient to use this review for contrasting the knowledge then and now. For example, the article makes no mention of viscoelasticity, which is the theme of this chapter. The knowledge at that time was to treat rubber as a high viscosity fluid and steady-state viscosity was used.

Up until the mid 1970s, investigation on the operation of internal mixers relied on instruments for monitoring temperature, torque and energy input. Samples were removed at certain intervals to examine the state of mixing [10, 11]. With these methods, the movement of the contents of the mixer was not observed.

Direct observation of mixing, so-called 'flow visualisation' was reported by Freakley and Wan Idris [12]; he adopted a transparent plastic chamber for a miniature mixer, the Brabender Plastograph, and observed the dynamics of mixing in detail using silicone rubber. Realising that silicone rubber is soft and has a rather unique viscoelasticity, he also examined an oil-extended natural rubber (NR) and an oil-extended, carbon black-filled styrene-butadiene rubber (SBR). However, these were mixed in a metal chamber and by monitoring pressure at one location; therefore, they were not visualised.

Visualisation with common commercial rubbers, SBR, BR and NR, was handled by Min and White [13]. A miniature mixer with a glass window was used. There are no examples of visualisation with commercial sized mixers. Toki *et al* [14] installed several pressure sensors at key locations of a 3.6 litre Banbury mixer and observed the movement of the contents. A very similar experiment was conducted by Freakley and Patel [15] with a 1.57 litre Banbury mixer. There are a number of significant discoveries from the visualisation. The most important one is the material behaviour, which relates to previously known behaviour of the mill processability [16]. The movement of the rubber is not flow, although it is wrongly called flow visualisation. It is deformation, failure and changes of location. The visualisation contributed to further progress in understanding of the mixing.

11.3 Approach to simulation

Process simulation is a popular subject nowadays. Simulation is used to design machinery, optimise a process, scale-up and even interpreting a process for problem solving.

However, simulation of mixing of rubber is still in the early stages of development. There are two approaches: one is based on a conceptual model, sometimes called the theoretical approach. The other is based on a model which, derives from systematised knowledge of accumulated experience, the empirical approach. The theoretical model must be modified by correcting concepts which contradict reality. The empirical model needs to rely on the scientific concepts in the course of systematising the experience. In the end, both approaches must produce the same result.

This book emphasises the empirical approach and it is not intended to include a review on the theoretical approach here. The theoretical approach at this stage contains many crude assumptions; for example, gum rubber is considered to be an inelastic, viscous fluid and consequently the steady-state viscosity is used. The fill factor is ignored; the presence and importance of the vacant space in the chamber is not recognised. Generally, slip at the rubber-metal interface is not considered. Non-affine deformation at the microscopic level for the filled system is not treated.

11.4 Proposed model of a mixing mechanism

In constructing a model, it is better to describe the outline first and fill in the details later. Such an outline should be left flexible enough to accommodate various details. If the initial model is too detailed, it tends to be too rigid to modify later. Then, the modification of the outline requires a fresh start each time it occurs.

The outline of the model proposed here consists of (i) changes in the material during mixing, (ii) mechanical actions and (iii) material-machine interaction.

11.4.1 Changes in material during mixing

The first question in describing the changes in material is how to treat an extremely non-uniform system. Figure 11.1 is a simplified model illustrating a proposal. The model treats the contents of mixing as a multi-phase system. The number of phases may be increased later, when the model becomes ready to accept more details. In rubber mixing, diffusion of polymer molecules and of the filler does not occur. Therefore, it is not a randomisation process. Consequently, the phase boundaries are relatively clear. The phases in Figure 11.1(b) during incorporation correspond to those observed by Shiga and Furuta [17], Figures 11.2(a) and (b). The phases in Figure 11.1(c) before dusting correspond to Figure 11.2(c) and (d).

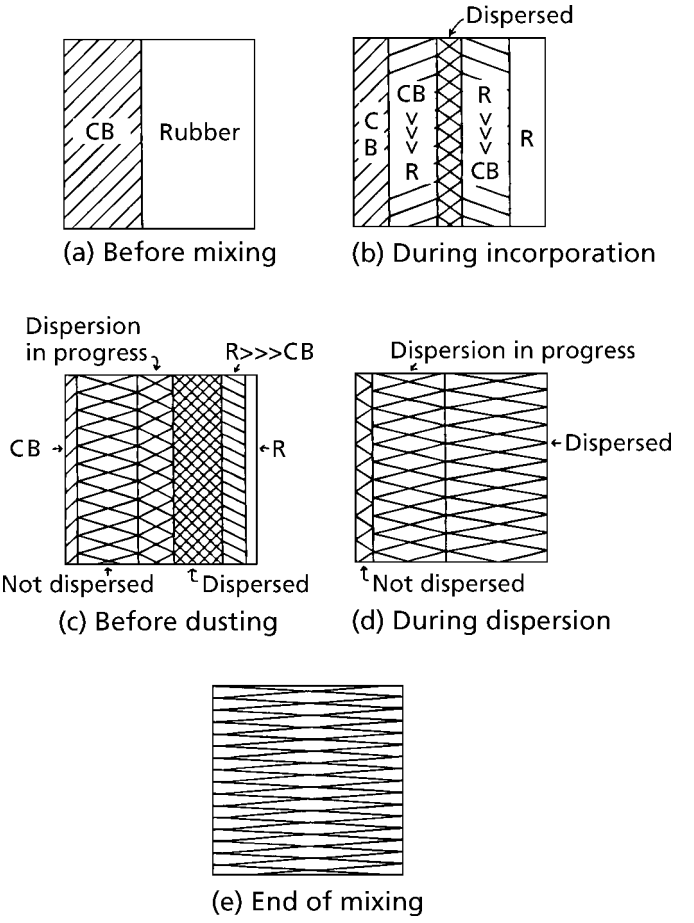

Figure 11.1 Multiphase model for rubber mixing. CB: carbon black; R: rubber.

Even at the end of mixing, the system is not uniform and consists of parts having different viscoelastic history. The model described here represents only macroscopic changes. Microscopic change such as growth of bound rubber must be accommodated later. This type of phase-modelling is in progress in the field of polymer blends and a similar approach may be adopted here.

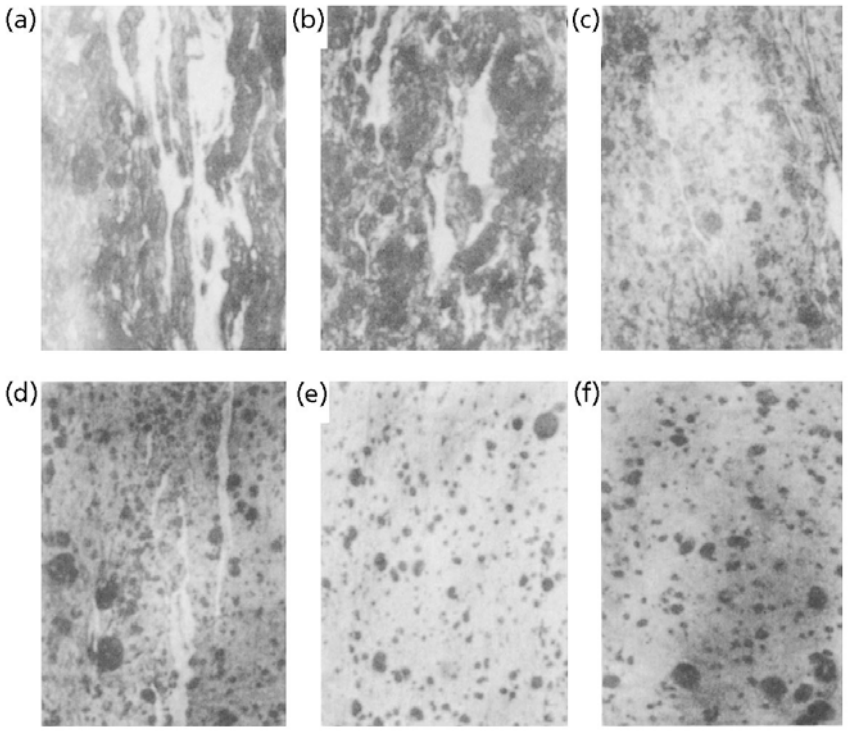

Figure 11.2 Photomicrographs of EPDM compound, with mixing time of a) 30 s, b) 45 s, c) 60 s, d) 75 s, e) 90 s and f) 105 s.

11.4.2 Mechanical actions

For illustrating the mechanical action, Figure 11.3 is used in Farrel's technical brochure [18].

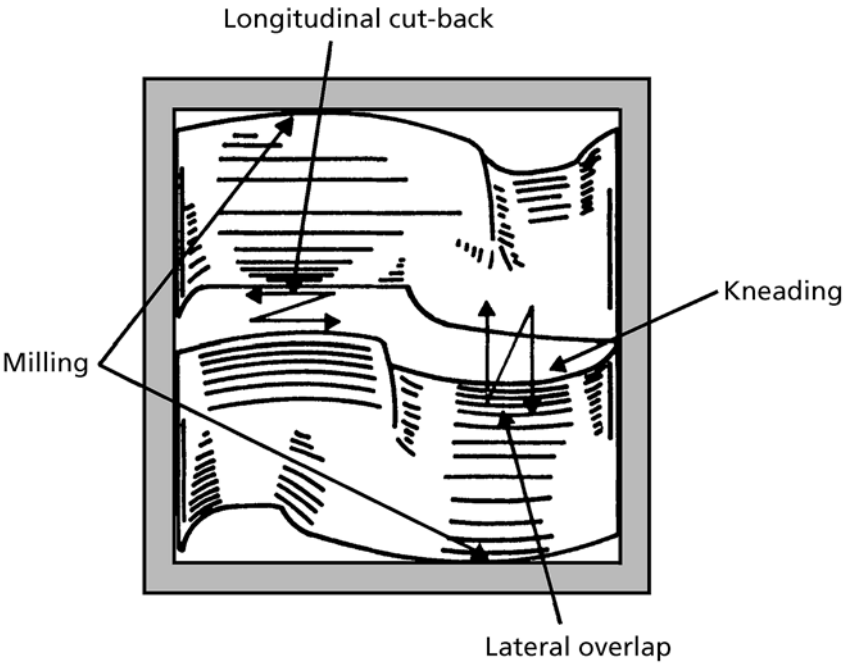

Figure 11.3 Behaviour of compound in the internal mixer.

Reprinted with permission from Understanding the Banbury Mixer, Farrel Company, Division of USM Corporation. Copyright Farrel Company.

The mechanical actions are classified into four kinds. As a starting point, they may be simplified to only two kinds, which are (a) milling and (b) the other three kinds. At the milling zone, much shear and elongational deformation occurs. It helps incorporation and dispersion. The longitudinal cut-back, kneading and lateral overlap are dependent upon the properties of rubber, the formulation and how they are charged. It was observed in visualisation with a miniature mixer that part of the rubber passes through the milling zone and another part moves through the wide gap. The latter movement involves the axial direction and the transfer from one rotor to another. This is illustrated in Figure 11.4 [9].

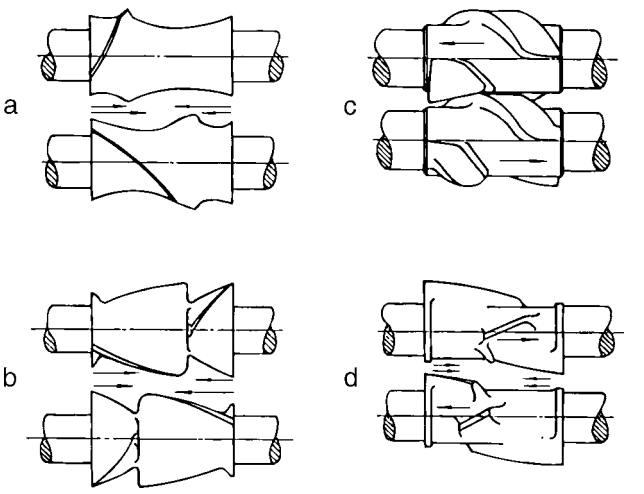

Figure 11.4 Examples of rotor designs (arrows indicate pumping action of wings).
a) Banbury two-wing, wings pumping form ends to centre section;
b) Banbury four-wing, wings pumping form ends to centre section;
c) Shaw Intermix three-wing, the large wings on each rotor pump to opposite ends, while the smaller ones do not contribute very much to axial flow;
d) Werner & Pfleiderer four-wing, the two large wings on each rotor pumping from ends to centre section, while the two small ones operate to give a reversing action.

The movement of the contents depends significantly upon the rotor configuration. It also varies depending upon the viscoelasticity of the material. This suggests that for each material there is an optimal configuration of the rotor.

One common feature for all the rotors is the presence of the milling zone. This corresponds to the gap in the roll mill. In mill mixing an operator performs cut-back with the use of a knife. He takes up the sheet and rolls it up to make the overlap. When the rolled sheet is recharged into the mill, kneading occurs. Therefore, in roll milling, the operator plays a role, which corresponds to those at the wide space in the internal mixer. There is one critical difference in the operation of the mill and that of the internal mixer. In the former, the entire compound is passed through the mill-gap repeatedly. In the internal mixer, only a part goes through the gap and the other moves slowly in the wide space. Some parts may go through the gap many more times than other parts. An extreme case of this

is stagnation. The manner of the non-uniform treatment depends upon the viscoelastic properties and also upon the mixer design.

11.4.3 Material-machine interaction

The previous sub-sections have involved material-machine interaction. In this section, the discussion will be expanded. The mill processability discussed in Chapter 2 [16] is the material-machine interaction, which was related to the behaviour of gum rubber. It is also directly related to the ease of mixing with carbon black. This conclusion is the same with internal mixers. It is most important to recognise the fact that the mixing result is determined by the ease of mixing in the beginning. In other words, the viscoelasticity of gum rubber has a decisive influence on the mixing result, which is a cumulative history of the viscoelastic events.

The progress of mixing modelled in Figure 11.1 is strongly influenced by the viscoelasticity of gum rubber. It also depends upon the carbon black type and the extending oils used. These are details to be considered in the future.

With the progress of incorporation, viscoelasticity of carbon black-filled compounds must be considered. The well-dispersed compounds have been discussed in Chapter 7 and in [19]. Viscoelasticity of compounds during mixing must also be investigated.

In order to relate the machine operation and the material behaviour, the deformational behaviour must be described. In Palmgren's review [8], this is represented by shear rate, $\dot{\gamma}$, which is defined by the linear rotational velocity, v of the rotor tip and the narrowest gap h:

$$\dot{\gamma} = v / h \tag{11.1}$$

This description assumes the steady-state flow of inelastic fluid, which is not the behaviour of rubber as pointed out in Chapter 4 and [20].

The behaviour of rubber at the milling zone is primarily a large extension with some contribution of shear. How should we describe the large deformation, which is changing every instant, i.e., non-steady state? In order to solve this problem, we need to consider the presence of empty space in the mixer. In other words, we need to know which part of the mixing chamber is occupied with rubber and which part is empty. At present, we have no way of predicting it. With a miniature mixer this may be observed through the transparent windows. With larger mixers, pressure taps at different locations may be helpful [14, 15]. The finite element approach is not feasible at present for the following reasons:

(1) as stated, the exact location of the empty space cannot be defined

(2) the geometry of the empty space is not very reproducible

(3) the extent of slip at the material machine-interface is unknown.

In order to circumvent this difficulty, an energy-based approach is suggested instead of the momentum-based approach [1], which usually assumes steady-state flow.

Next is a mechanism for rejoining the part of the compound, which has just passed the milling zone, to another part of the compound in the wide space. It was treated before as if it were stirring [21]. However, the stirring implied randomisation, which certainly does not happen with rubber compounds. The returning part lays over onto the existing material like a jelly roll. This is similar to the action of the mill operator rolling up the sheet. Freakley observed the layering action in visualisation with a miniature mixer [12]. The layering is also seen in Shiga and Furuta's observation [17] (Figure 11.5).

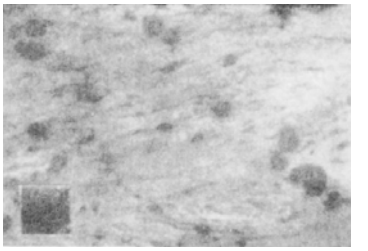

Figure 11.5 Photomicrographs of EPDM compound; EPDM 100, N330 10, oil 10, ZnO 5, stearic acid 1, after 2 minutes.

11.4.4 Macroscopic versus microscopic deformation

The above outlines of the model deal with the macroscopic changes. The details remain to be refined. The remaining problem lies in the differences between macroscopic and microscopic deformation. With the progress of incorporation, this problem becomes critical. In pursuing the progress of dispersion, in what way is the onion model related to matrix deformation? As modelled in Figure 11.6(a) and (b) [22], the agglomerate particle

lies between two layers of matrix, which were formed in the process of incorporation [23]. Regardless of whether the two layers are sheared or stretched, the force acting on the surface of the agglomerate is microscopic shear, which acts to peel the skin of the agglomerate [17]. This is the reverse of making a 'snowball', the mechanism by which agglomerates were made from aggregates in the manufacture of carbon black.

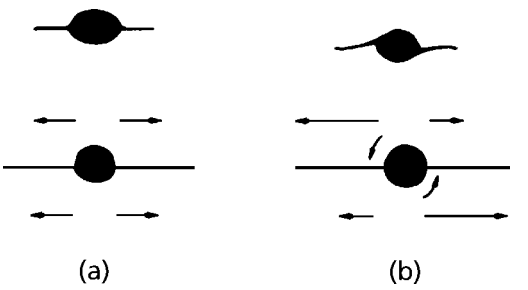

Figure 11.6 Modelling of elastomer behaviour contributing to the peeling of an 'onion' during dispersion of carbon black.

11.5 Modelling of the fracture of rubber particles

11.5.1 Material

In the present work, the mixing of only elastomer and carbon black is considered; mixing of other additives and the effect of other additives on the mixing of elastomer and carbon black are assumed to be insignificant. Of course, this is not true, and the contribution of the additives to the mixing mechanism may be considered in the future as a modification of the present model.

Further, mixing of powdered rubber is considered here because of the simplicity of the treatment, Figure 11.7. The model will be modified in the future to include slabs of rubber.

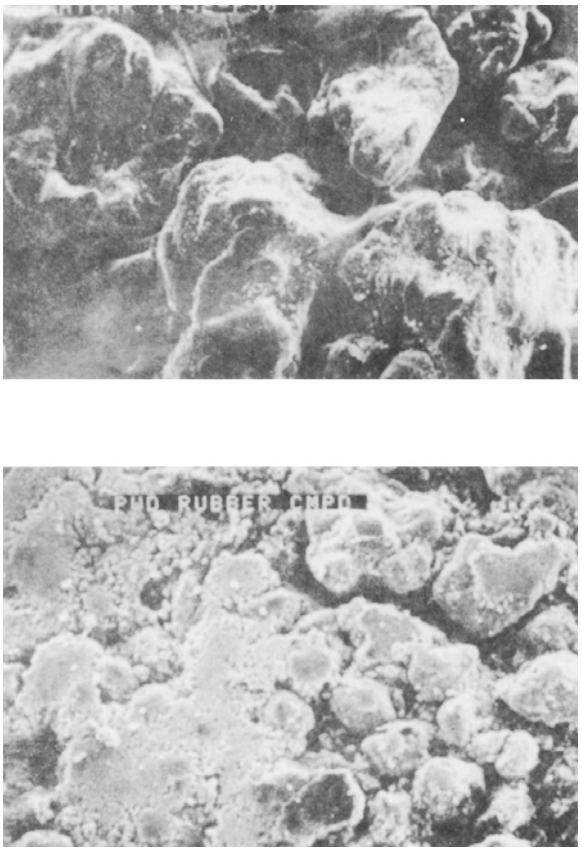

Figure 11.7 Scanning electron micrographs of a) the powdered rubber (x 30) and b) the powdered rubber compound (x 13).

Reprinted with permission from N. Nakajima and E. R. Harrell, Rubber Chemistry and Technology, 1984, 57, 1, 153. Copyright 1984, Rubber Division of the ACS.

11.5.2 Dynamic state of the elastomer

The state of elastomer in the processing behaviour is assumed to be Region II of Tokita and White [24], that is, the polymer is in the elastic state. The behaviour involves a large deformation, breaking of material, and recovery of the deformation [25, 26]. This will be discussed next.

11.5.3 Basic mixing model

The basic model is very simple: particles of elastomer break down to smaller and smaller size of particles with the progress of the mechanical treatment. As the particle size becomes smaller, the homogenisation with carbon black is improved, and at the same time the desired degree of dispersion of the carbon black is achieved.

An example of the calculation may be given for powdered rubber mixing. The powder has an average particle diameter, ϕ_0, of approximately 250 μm. After satisfactory mixing is achieved, the size is decreased to an average diameter, ϕ_f, of approximately 0.1 μm [27]. The break-down of the particles takes place during 1.5 minutes at 77 rpm [28]. This corresponds to a volumetric size reduction, $(\phi_0 / \phi_f)^3$, of 1.56×10^{10} during the course of 115.5 revolutions. If we assume uniform breakage of rubber particles, an average size reduction per revolution, f_0, may be calculated according to

$$f_0^n = \left(\phi_f/\phi_0\right)^3 \tag{11.2}$$

where n is the total number of revolutions. In the present example $f_0 = 0.816$ for $n = 115.5$.

The present model treats the average particle size; it does not consider the particle size distribution, nor changes in the distribution during the breaking of particles. This aspect is a refinement to be made in the future, when experimental data on the particle size distribution become available.

For simplicity, it is assumed that each particle breaks exactly in half each time it breaks and that only average particle size needs to be considered. These assumptions allow us to calculate the volume fraction of particles, ν_b, which break during one revolution of the rotor and the volume fraction, ν_u, which does not break. Both ν_b and ν_u are assumed to be constants independent of the cycle.

First, the average size reduction per cycle, f_0, is related to the increase in the number of particles per cycle as

$$N_{i+1} / N_i = 1 / f_0 \tag{11.3}$$

where N_i is the total number of particles before the i -th cycle is started and N_{i+1} is that after the cycle is completed. Therefore,

$$N_i = N_b + N_u \tag{11.4}$$

$$N_{i+1} = 2N_b + N_u \tag{11.5}$$

where N_b is the number of particles to be broken in half during the cycle and N_u is that remaining unbroken.

Combining equations (11.3), (11.4), and (11.5), we obtain,

$$1 / f_0 = (2N_b + N_u) / (N_b + N_u) \tag{11.6}$$

The volume of rubber breaking during the cycle, V_b, and that remaining unbroken, V_u, are related to the corresponding number of particles and their sizes as follows: before starting the i-th cycle,

$$V_b = N_b \phi_i^3 \tag{11.7}$$

$$V_u = N_u \phi_i^3 \tag{11.8}$$

where ϕ_i is the particle diameter before the break.

Substitution of Equations (11.7) and (11.8) into Equation (11.6) gives

$$1 / f_0 = (2V_b + V_u) / (V_b + V_u) \tag{11.9}$$

Division of the numerator and the denominator of the right side of the equation by the total volume gives f_0 in terms of volume fractions,

$$1 / f_0 = 2v_b + v_u = v_b + 1 \tag{11.10}$$

for $f_0 = 0.816$, $v_b = 0.225$, and $v_u = 0.775$.

11.5.4 Model of unit processes

The present model considers three unit process, (i) incorporation of carbon black, (ii) dispersion of carbon black, (iii) macroscopic homogenisation of the compound. The incorporation process is predominant in the beginning, rapidly tapering off and ending, for example, after 0.9 minutes of mixing [28]. The progress of this process may be semi-quantitatively characterised by direct observation of the unmixed carbon black. A quantitative measure may be obtained from the change in the heat transfer coefficient [28]. The dispersion and homogenisation processes are assumed to start from the beginning and progress steadily with time.

The dispersion process takes place primarily between the rotor edge and the chamber wall, where the deformational stress is the highest, i.e., the milling zone in Figure 11.3 [18]. The volume of material swept through this gap per revolution is given by

$$V_s = 2\pi DSL(1 - F) \tag{11.11}$$

where D is the diameter of the chamber,

S is the gap,

L is the length of the chamber, and

F is the fraction of the circumference of the two chambers which is open between them.

For example [28], D = 10.16 cm, S = 0.239 cm, L = 15.24 cm, F = 0.25 and V_s = 174 cm^3.

In the same example, the total amount of the compound was 1.4 kg. On the assumption that the average density of elastomers and other additives is 0.98 g/cm^3 and that of carbon black is 1.88 g/cm^3 [29], the density of the compound is calculated to be 1.17 g/cm^3. The total volume (V_T) was then 1,200 cm^3. Even under 0.24 MPa of ram pressure, the actual volume of the compound changes with the progress of mixing. However, the 'compacted' volume may be taken as a reference equal to 1,200 cm^3. The powdered rubber compound is macroscopically uniform in composition. Therefore, the composition of the material in V_s and the rest of the volume are the same. Because the material in V_s is compacted, it may be compared to the total compacted volume of the compound, i.e., $V_s = 0.146V_T$. If all the rubber particles going through the gap break once and break in half, then 14.6% of the rubber particles break in half in one revolution of the rotor blades. In this example, the rotors are the two-wing type [30], and therefore, the material goes through the gap only once in each revolution.

The fraction of the rubber particles breaking in half per revolution was previously estimated to be $\nu_b = 0.225$. Therefore, $\nu_b - \nu_s = 0.079$ of rubber particles must be breaking in the space other than the milling zone which is defined by Equation 11.11. However, the breaking must be taking place in the vicinity of the milling zone. This is in agreement with the previously described compaction study in Chapter 3 that the break up of the rubber particle takes place only at and near the narrow gap. This finding is different from the view that the effective mixing takes place in one-quarter of the chamber space, which is in front of the rotor blades [9].

During the dispersion process, not only the rubber particles but also the carbon black agglomerates break. Therefore, the mechanism of breaking of carbon black must be included in the dynamic model of mixing. However, this aspect is relegated to the future refinement of the model.

11.6 Model of material behaviour in the internal mixer

11.6.1 Material properties

The behaviour of material in the internal mixer is assumed to be in the elastic state, Region II, which may be contrasted to the melt-flow state, Region IV [24]. In the latter state, the material undergoes a large deformation resulting in molecular flow. On the other hand, in the elastic state, even when the bulk material appears to be flowing, the flow units are supermolecular in size [31]. Such supermolecular units were created as a result of breaking of material under a large deformation which exceeds the ultimate strain [32].

In the elastic state, even though the bulk behaviour involves flow (that is, a significant part of the bulk deformation is permanent), the behaviour of the flow unit itself is elastic. Under the imposed large deformation, the elastic flow unit deforms to its ultimate strain, breaks up, and recovers its strain [26]. This process is schematically depicted in Figure 11.8.

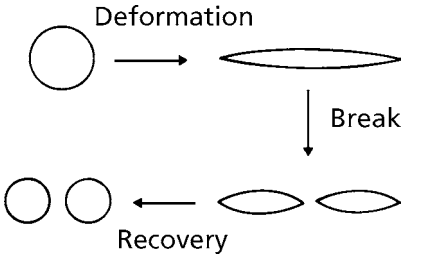

Figure 11.8 A model of the breaking process of rubber particles.

Initially, the flow units in the present model are the particles of the powdered rubber. They become smaller and smaller as the process of breaking is repeated. For simplicity and a first approximation, the particles are assumed to be spherical in their relaxed state, although this condition is not necessary for the modelling of the material behaviour.

The present approach is to treat the behaviour of the particle as solely responsible for the mixing behaviour. Also, the behaviour of the particle is assumed to be characterised by testing the bulk rubber [16].

This is a reasonable assumption, which is based on the Author's observation of large deformation and fracture under shear, [32, 33].

11.6.2 Pressure profile in the internal mixer

The net volume of the mixing chamber is 1,690 cm^3, and the compacted volume of the compound is 1,200 cm^3. This gives a fill factor of 71%. The material just in front of the rotor is under pressure. At 70% fill factor, a sharp pressure peak of approximately 0.85 MPa at the rotor front has been reported [12]. The ram pressure in the present example is 0.24 MPa. In general, the material in the chamber is under a large and constantly varying pressure gradient. The pressure profile is expected to vary not only in the direction of rotation, but also in the radial and axial directions of the rotors.

Because in this mixer, the two rotors take different positions with respect to each other for each turn [18] and come back to repeat the same relative position only every eleventh turn, the pressure profile is different for each turn. The pressure profile also depends upon the material properties and is, therefore, expected to change with the progress of mixing.

Quantitative information on the pressure profile is necessary for the detailed definition of the flow and deformation in the internal mixer. However, it requires extensive instrumentation, which has not been available as yet. For the purpose of the present paper, only a semi-quantitative discussion is given.

11.6.3 Deformation of material between rotor edge and chamber wall

The material in front of the rotor is pushed in directions dictated by the geometry of the rotor blades and the chamber wall. The material movement is in both axial and lateral directions, resulting in kneading and cutback. However, the material sufficiently close to the front of the rotor edge may be modelled independently from the other part of the chamber. This approximation is reasonable on the basis of visualisation and a sharp rise of the pressure, which appears to be essentially independent of the pressure generated from other parts of the rotor [12].

The material behaviour is depicted in Figure 11.9 where (a) shows the relative directions of the material movement [18] and (b) the deformation and the postulated breaking of the material. The major importance of the model is that at this location the deformation far exceeds the ultimate strain, which is about 200-300% [25] for the powdered rubber at the rate of deformation estimated to be 200 s^{-1} [20] in the temperature range 25-97 °C.

Whether the particles of rubber break only once or more than once, whether every particle breaks or only a fraction of particles break, and whether one particle breaks in approximately half or not are the questions to be answered in the future. For this purpose, the use of powdered rubber, especially when a portion of it is dyed, may be very useful.

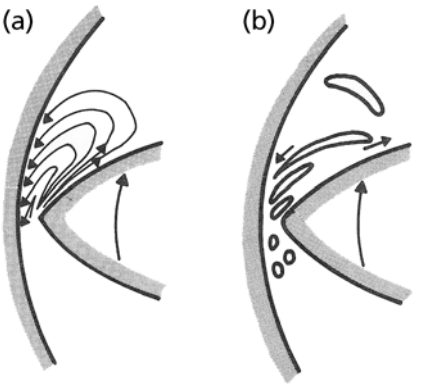

Figure 11.9 a) Flow lines in the milling zone and b) deformation and rupture of rubber particles.

a) Reprinted with permission from Understanding the Banbury Mixer, Farrel Company, 1968.
b) Reprinted with permission from N. Nakajima, Rubber Chemistry and Technology, 1981, 54, 2, 266. Copyright 1981, Rubber Division of the ACS.

11.6.4 Probability and distribution in mixing

As mentioned already, the powdered rubber initially has a certain particle size distribution. This distribution changes as the particles break. The probability of the breaking of a particle is influenced by the transport and exchange of material to and from the kneading zone, the cut-back zone, and the milling zone.

Without considering the probability and distribution, the details of the mixing model cannot be constructed. However, in the absence of experimental data, such a statistical treatment is meaningless at this time. Therefore, this is a subject for future study.

11.6.5 Calculation of mixing energy

Because a number of approximations have been made to simplify the model, the purpose of calculating the mixing energy is to compare only its order of magnitude with the

observed value. In the volume of the milling zone per revolution, V_s = 174 cm^3, the actual amount of rubber in the compound is 63.3% of V_s that is V_s' = 110 cm^3. The rupture energy for this rubber in the range of temperature and at the deformation rates is approximately w_b =10 MJ/m^3 [25]. Therefore, the energy of break in the milling zone is:

$$W_s = w_b V_s' n \tag{11.12}$$

where n is the total number of revolutions. For n = 11.5, W_s = 127 kJ.

If we consider the total volume of rubber particles which are breaking per revolution:

V_b' = 0.633,

= (0.633 x 0.225) V_T

=171 cm^3.

V_T is the total volume of the compound in the mixer, which in this case is 1,200 cm^3 (see also section 11.5.4). Therefore, the total energy expended in breaking the rubber particles for the entire period of the mixing cycle is:

$$W_M = w_b V_b' n = 189 \text{ kJ} \tag{11.13}$$

This energy compares well with the observed data, W_0 = 552 kJ in magnitude. The difference, W_L, is,

$$W_L = W_0 - W_M = 354 \text{ kJ} \tag{11.14}$$

This energy consists of the energy required to break carbon black, H_C, the frictional loss among carbon black particles, W_F, and the energy expended to deform rubber particles without resulting in the rupture of the particles, W_D

$$W_L = H_C + W_F + W_D \tag{11.15}$$

Here, H_C is the cohesive energy and, for the time being, it is assumed to be much smaller than the mechanical energies. The magnitude of W_F is small and occurs only when free carbon black is present. Therefore, W_L can be approximately identified with W_D.

According to the present model of mixing, W_D appears to be a wasted energy, because it is not contributing to the breaking of the rubber particles. However, W_D is a significant part of the observed energy input to the material.

$$W_D / W_0 \approx W_L / W_0 = 66\%$$

If we consider the material behaviour in the kneading and cut-back zones, we realise that a significant volume fraction, v_c = 85.4%, of the total charge is present and that the material is repeatedly deformed and relaxed. The deformational energy per volume, w_d,

is expended here and may be estimated as follows. Because the volume fraction of rubber, which is breaking is

$$v_b = 0.225$$

the volume fraction of rubber deforming without break is 77.5% or $V_d' = 589$ cm^3. Assuming that the deformation-relaxation process takes place only once per revolution with all the rubber particles which are not breaking,

$$w_d = W_L / V_d' n = 5.4 \text{ MJ/m}^3 \tag{11.16}$$

The deformational energy, w_d, is about 54% of the rupture energy. This translates to a strain, which is about 55-65% of the ultimate value. The magnitude of the ultimate strain is anywhere between 100 and 700%, depending upon the temperature and the deformation rate [25].

Up to this point, we have assumed that the mixing mechanism is essentially the same for every revolution of the rotor. This is true only approximately. The effective energy of mixing, W_M, may be converted to the average wattage input:

$$E_M = W_M / t_M \tag{11.17}$$

where t_M is the total time of mixing. For $t_M = 90$ s, $E_M = 2.2$ kW, Figure 11.10 is an example of a recording of the power input, the magnitude of which was reduced to 75% of the observed value [26]. The 75% is an estimated efficiency of the power input, when the machine is loaded. The area under the broken line is the energy required for breaking rubber particles.

If a slab of rubber is charged instead of powdered rubber, additional energy is required to grind the rubber down to the size of the powdered rubber. If rubber is polymerised in the presence of carbon black [34, 35], and if the latex size is about 0.1 μm in diameter, the mixing energy is for dispersion and homogenisation, assuming that the carbon black is in the agglomerate form. Such an experiment is expected to yield the data needed to refine the present mixing model.

11.7 Discussion

The mechanical energy input to the material in the mixer is converted to heat, a part of which is removed by cooling and the reminder raises the temperature [28]. Traditionally, the behaviour of the material is interpreted as viscous heat generation. This view has several shortcomings. First, it ignores the elastic nature of the material; second, it has no

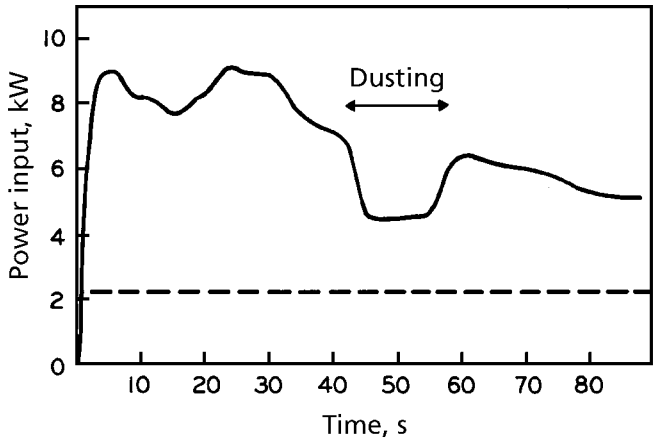

Figure 11.10 Power input curve and power required for breaking rubber particles. Ordinate values have been reduced to 75% of the observed values (75% in the estimated efficiency).

specific relation to the mixing mechanism; third, it assumes the viscosity to be that of the steady-state and laminar flow. None of these is valid [20].

On the other hand, the present model is based on the large viscoelastic deformation and breaking of material. This behaviour is realistic and may be demonstrated with laboratory instruments under conditions corresponding to those in the internal mixer.

Further, the breaking of the rubber particles to a smaller size can be quantitatively related to the mixing results. The mixing energy estimated from this mechanism is about 36% of the observed value.

The following discussion is an attempt to analyse the data more in detail. The numerical analyses are approximate and presented for the purpose of illustrating the approach. Referring to the power-input curve of Figure 11.10 the input is low during dusting. In this period no ram pressure is acting on the material and the material hardly passes through the milling zone. Therefore, no progress is made in mixing. The contents of the mixer are moving around the wide space and undergoing deformation and relaxation process. As a first approximation, it is assumed that the same material behaviour occurs at the wide space even when ram is down. The average energy under the solid line in Figure 11.11 corresponds to this behaviour.

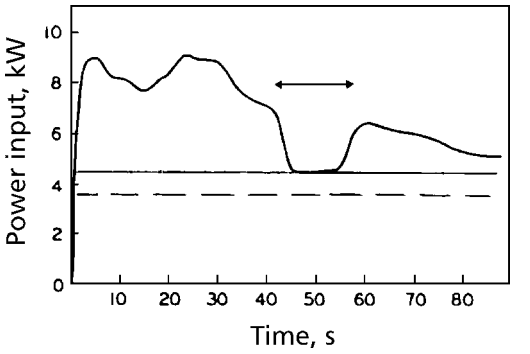

Figure 11.11 Power input curve.

Reprinted with permission from N. Nakajima, Polymer International, 1996, 41, 1, 23. Copyright 1996, SCI.

The amount of energy above the solid line is about 185 kJ, which is very similar to the theoretical comminution energy, $W_M = 198$ kJ.

Thus far, the energy calculation considered the comminution mechanism only [23]. At the incorporation stage there are lamination and comminution mechanisms. The former does not involve fracture. Therefore, in reality the mixing energy is larger than that considering fracture only.

In the dispersion stage also, the required energy is not limited to that required to fracture the rubber. It must include the energy required to 'peel' the aggregates from the surface of the agglomerates in the 'onion model' [17]. In order to treat this situation, a well-known fact of fracture mechanics may be applied: that is, the energy required for pulverising carbon black is not just the energy required for creating new surfaces, but many more times the energy must be spent. This energy corresponds to the force exerted by the medium, i.e., the viscoelastic energy due to the deformation of rubber.

The amount of rubber participating in this deformational process is difficult to estimate at this time. However, it must be similar to V_b, i.e., 0.225, where the effective comminution is taking place, $V_b' = 171$ cm^3. An equation analogous to equation (11.12) for the energy of deformational process is:

$$W_{CD} = w_{CD} V_b' n \tag{11.18}$$

where $W_{CD} = 445$ MJ/m^3 is the estimated energy of the viscoelastic deformation of rubber, which is necessary for fracturing carbon black agglomerate down to aggregates [36].

This energy is about 45% of that required to fracture rubber itself. The extent of deformation corresponding to W_{CD} is about 200-300% [36]. When the comminution energy W_M = 198 kJ and the deformation energy W_{CD} = 88 kJ are added, the sum is the total energy necessary for mixing. This gives a revised efficiency for mixing of:

$$(198 + 88)/552 = 0.52, \text{ i.e., } 52\%$$

The balance, 48%, is the energy spent by the machine, which corresponds to the work by the mill operator in the roll mill. Attempts are continuing to improve the efficiency of this operation by modifying the rotor configuration.

One remaining question is why the breaking of the rubber domain stops at the 0.1-1.0 μm size. The ultimate size attainable for pulverising or crushing a material depends upon the design and mode of operation of a given machinery and the property of material to be comminuted. This is well-known for crushing ores and ball-milling solid material. Even for a soft solid, there must be a reason why the comminution of rubber ceases at certain size level. For breaking rubber in the rheometer to form supermolecular flow units, Mooney [37] estimated the ultimate size to be in the order of 10 μm. Does the size of the serrations of rotor and cavity determine this size? The ultimate size of the rubber domain in the mixing must be related to the size of carbon black particles, which are acting like sand paper. This subject is open for future investigation.

11.8 Nano and molecular scale of mixing

The previous sections dealt with mixing mechanisms down to the order of 0.1 μm in the rubber domains, which were also interpreted to be the ultimate size of the supermolecular flow units.

However, the growth of bound rubber onto the surface of fillers must also be accounted for, because it is an important part of the dispersion mechanism. The mechanism of growth of the bound rubber concerns molecular interaction between rubber and filler surface; this is a nano-scale phenomenon.

In order to understand the growth of the bound rubber, we need to start from the incorporation of the filler, when the rubber-filler interaction commences. Boonstra and Medalia [11] interpreted the occurrence of the torque maximum (the second peak) as the result of filling the void of the agglomerate with rubber. This view was supported by the density measurements. The dispersion did not start, because no brown tint appeared in the rubber phase. Thus, the increase of the torque was interpreted as the result of the effective increase of the filler concentration, when the increasing amount of rubber becomes

occluded inside of agglomerate. The decrease of the torque after the peak was interpreted as the effective decrease of the filler concentration when a significant fraction of rubber presumably occluded inside of agglomerates was released in the course of dispersion.

However, under the conditions of mixing, rubber is usually a soft solid and it does not diffuse spontaneously into the void of agglomerates. Even if rubber were assumed to be a high-viscosity fluid, it would not flow into and fill the void under the pressure generated by the rotor blade and within the incorporation time of only 1.5 - 5.0 minutes [38]. The density measurements were made with vulcanised specimens. The amount of the penetrated rubber might have increased during vulcanisation. Significant increases of the bound rubber as a result of vulcanisation were detected with the NMR by Wardell and McBrierty [39].

Table 11.1 Properties of Compounds Containing 50 phr N339 Carbon Black (a part of the original table in [40])

Mixing time, min	Comments	Torque, kg m	Density, g/cm^3	Unincorporated carbon black, %	Bound rubber, %
SBR-1712					
1.0	1st Peak	4.20	1.064	16.8	8.7
2.5	–	3.37	1.106	5.6	16.1
4.0	2nd Peak	3.95	1.112	4.0	23.9
6.0	–	3.55	1.124	1.0	27.0
20.0	–	2.40	1.128	0.0	27.2
CB-411(BR)					
1.0	1st Peak	3.50	1.055	13.3	3.7
2.5	–	2.98	1.068	9.6	10.3
5.5	2nd Peak	3.43	1.087	4.5	17.4
8.0	–	2.95	1.097	1.8	19.6
20.0	–	2.02	1.104	0.0	22.0

More recently, Cotten conducted a systematic examination on the subject [40]. Rubber samples were SBR 1712 and *cis*-1,4-BR-441 and with 50 phr of carbon black N339. A miniature mixer was used at a condition yielding a reproducible torque curve. In the incorporation step rubber is assumed to penetrate into the void of agglomerate, wetting the carbon black and building the bound rubber. The results are reproduced in Table 11.1.

The percentage of unincorporated carbon black is defined as unpenetrated agglomerate, U;

$$U = \{[\frac{B}{d'} - \frac{B}{d}]/[CS]\} \times 10^4 \qquad (11.19)$$

where B is the batch weight (phr), d' and d are densities at time t and 20 minutes after the start of mixing, respectively. After 20 minutes carbon black dispersion is rated as B3 or better as determined by ASTM D2663 [41] and the penetration is assumed to be completed. The volume of air, A, in the batch at time t is

$$A = \left[\frac{B}{d'} - \frac{B}{d}\right] \tag{11.20}$$

Therefore

$$U = \left[\frac{A}{CS}\right] \times 10^4 \tag{11.21}$$

where S is the crushed DBPA value (in $cm^3/100$ g) and C is the carbon black loading (in phr). The data in Table 11.1 indicate that at the second peak only 4 - 4.5% of the void of agglomerate is still unfilled. The time of mixing measured from the first power peak is only 4.0 minutes with the SBR and 5.5 minutes with the BR.

It is inconceivable that within such a short time rubber molecules can diffuse into the tortuous passage of approximately 20 nm size (see Figure 9.5), and fill 95% of the void volume. Knowing that both SBR 1712 and BR 411 were oil extended rubbers, the oil could have filled the void. Along with the oil a small amount of rubber molecule could also have been carried into the void.

On the other hand the bound rubber at the second peak was already 90% of the ultimate value. Because the agglomerates were essentially intact at that time, the implication was that the void of agglomerates was almost filled with rubber. Apparently, there is a contradiction.

A possible answer to this puzzle is the growth of the bound rubber during its determination. The bound rubber was measured by extracting rubber with toluene at room temperature. Toluene would rapidly diffuse into the void replacing the oil. Toluene has a lower viscosity than the oil and its good solubility for rubber facilitates diffusion of rubber molecules into void, eventually replacing toluene. The period for extraction was 4 days, and it may be sufficient to replace toluene with rubber molecules, which have a much higher MW and thus are adsorbed preferentially onto the surface of carbon. Whether or not this view is correct, the method of determining bound rubber needs re-examination.

Concerning the growth and the nature of the bound rubber, much insight may be gained from the book by Donnet and Voet [29]. The bound rubber also forms from rubber

solutions. This presents a possibility of the increase of the bound rubber during the extraction. The formation of the bound rubbers is an adsorption process. The unextracted amount decreases linearly with the increasing temperature of extraction, extrapolating to zero at a certain temperature. This indicates that only a small part of bound rubber is chemically bound.

The rate of agitation also has an effect on the unextracted amount of bound rubber [42]. As the agitation rate was increased, the unextracted amount decreased, then reached approximately constant value in the intermediate range of the rate and increased again at the higher rate. This indicated the presence of loosely-bound and tightly-bound fractions. The compounds were NBR-N774, SBR-N330, and *cis*-1,4-BR-N330.

Ito, Nakamura and Tanaka using NMR detected a loosely-held and a tightly-held fraction in polyisoprene bound-rubber on silica fillers [43]. Shiga [44] observed by using NMR that the tightly-bound rubber became denser with progress of mixing.

In some of the literature, two different types of agglomerates are cited without making a clear distinction. One type is a fragment of the carbon black pellet in the size range of approximately 10-100 μm. The other type is a flocculate consisting of once-dispersed aggregates. The former type is called agglomerate throughout this book. Speaking of the latter type and judging from a rapid growth of the bound rubber, the aggregates in a flocculate must be coated with bound rubber. Therefore, the break up of the flocculate involves primarily a rubber-rubber interaction. The break-up of agglomerate involves rubber-filler interaction and the friability of the agglomerate as discussed in Chapter 9.

Just what the bound rubber looks like and how it responds mechanically may be learned from a study by Ban *et al* [45]. They published many photographs taken with a high resolution electron microscope, see Figures 11.12 and 11.13. There is carbon black encapsulated with rubber forming networks, and voids are presumably formed where the soluble fraction had been extracted. A string of rubber forms between the adjacent aggregates.

For 50 phr of carbon black and assuming the amount of bound rubber to be 30% of total rubber, the rubber-coated aggregates occupy almost 50% of the volume. At 50% volume-filling the irregularly-shaped dispersion can occupy 100% of the available space. Figure 11.12 appears to show this situation. The rubber-coated aggregates form a network of the 'carbon gel'. The unbound and extractable rubber appears to be filling the voids of the network rather than providing matrix for the dispersed carbon black.

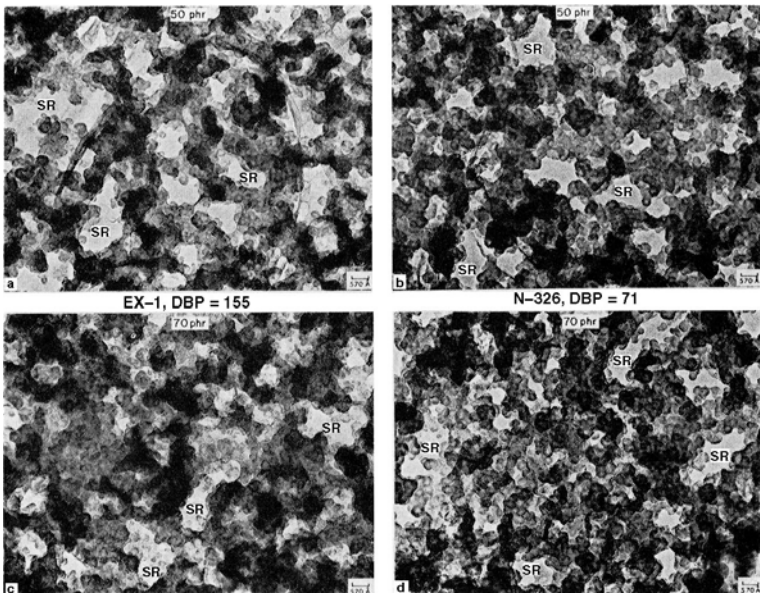

Figure 11.12 Carbon-rubber gel network in SBR-1500: a) EX-1 50 phr; b) N-326 50 phr; c) EX-1 70 phr; d) N-326 70 phr. SR denotes missing soluble rubber.

Reprinted with permission from Rubber Chemistry and Technology, L. L. Bon, W. M. Hess, and L. A. Papazian, 1974, 47, 4, 858. Copyright 1974, Rubber Division of the ACS.

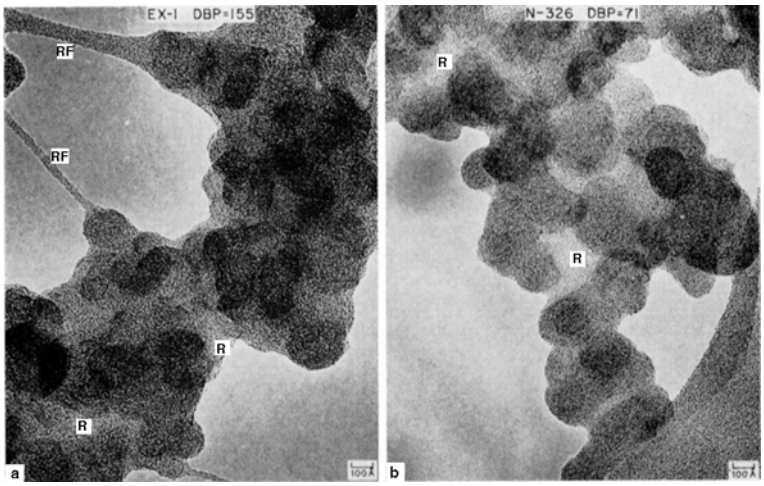

Figure 11.13 High resolution image of SBR-1500 carbon-rubber gel networks at 50 phr. R indicates trapped rubber, RF designates filaments between network segments.

Reprinted with permission from Rubber Chemistry and Technology, L. L. Ban, W. M. Hess and L. A. Papazian, 1974, 47, 4, 858. Copyright 1974, Rubber Division of the ACS.

If the manner of packing is denser in some locations than others, the denser parts may be regarded as the previously mentioned flocculates. The other extreme is the presence of unmixed rubber, which is an oversized rubber domain. Both types of the inhomogeneity are very difficult to break up; they are similar to the formation of lumps in a flour-water mixture. The presence of unmixed rubber is reported to occur sometimes in the mixing of EPDM [46].

Once these inhomogeneities are created, it is very difficult to remedy the situation. Therefore, it is important to avoid creating this problem. How do we avoid it? This question brings us back to the beginning of the book and to the ongoing theme of the gum-rubber processability, i.e., the 4 regions of Tokita-White. For a given gum rubber there is an optimum processing condition in terms of temperature and deformation rate. Major guidance has already been given in Chapters 1 to 6. The details on how to apply to a specific example may still be a case-by-case, leaving room for the future research.

11.9 Chemical reactions during mixing

Chemical reactions often take place during mixing. It may be an intended reaction like that between the silica filler and a coupling agent. It may be used for a grafting reaction and a dynamic vulcanisation. On the other hand there are many unintended reactions such as the polymer chain-break, resulting free-radical formation [47], generation of long branches and gels, and the premature start of a crosslinking reaction. This subject is so varied that it requires another book to cover.

However, not mentioning the subject leaves a gap in a book on the mixing of rubber. Therefore, some of the examples will be presented here with an acknowledgement that a thorough coverage of the subject is not intended.

Ito *et al* [43] examined reactions between silica filler and IR using the pulsed NMR method. Three commercial silicas having different amounts of silanol were selected. First, the bound rubber was generated by mixing the polymer solution in benzene and the silica suspension was also mixed in benzene. Then, the silica-rubber composite was obtained by freeze-drying. After extracting for 24 hours with benzene at room temperature, the sample was vacuum dried at room temperature. The procedure was to prevent chemical reactions during the preparation of the samples. The amount of bound rubber was higher for the silica having a higher amount of the silanol. The composites were heat-treated under vacuum at constant temperatures between 50-150 °C for a period of 1 to 18 hours. The rubber alone was stable during the period of the heat-treatment. The bound rubber of both untreated and heat treated composites consisted of the tightly bound and loosely bound phase. With the highest-silanol silica, the amount of the bound rubber increased

with the heat treatment, a part of the loosely bound fraction changed to the tightly bound fraction and the mobility of both fractions decreased. With the lower silanol-silica the effect of the heat treatment was very small. The nature of the interaction between silanol and polyisoprene was not elucidated, although the researchers postulated a formation of the polymer free-radical by the action of silanol.

Gotoh examined the cause of gel-formation during mixing of a high-structure carbon black and EPDM [48, 49]. Both the rotational rheometer and the internal mixer (1.7 litre volume) were used at 130 °C. Even though there was no crosslinking agent, a significant increase of the torque was observed after certain period of mixing. With the addition of a free-radical catcher the torque-rise disappeared. The mixing time before the start of torque-rise was shorter for the higher amount of dienes, for the higher MW fraction, M_Z and for the higher ethylene content. It was also shorter for the higher structure carbon black. The higher structure presumably enhanced the chain-cission and the free-radical formation. The radical generated in the early stage of mixing reacted later when the temperature of the compound reached a higher temperature. Various methods of preventing the gel formation are discussed.

The previous examples of the reaction involving IR-silica and EPDM-carbon black are caused by the free radical formation. Jamroz *et al* used electron spin resonance (ESR) for investigating the formation of free radicals on compounding rubbers with carbon black [50]. The rubbers were NR and SBR1500. A roll mill with the cooling water was used for the compounding with 10 to 70 phr of carbon black. The increased amount of free radical was formed with the increasing amount of carbon black. The radicals are assumed to react with carbon black, participating in the bound rubber formation.

11.10 Optimisation of operation and improvements of mixers

11.10.1 Introduction

For the purpose of understanding the mixing, the usual practice involves sampling of the contents of the mixer at various stages of mixing. This presents a problem, because the contents are not uniform. When a miniature mixer is used, the entire contents of the mixer may be treated as one sample. However, with a production machine and a laboratory sized mixer like a BR Banbury, one sample is only a small portion and would not be representative. This problem has been recognised for a long time. Therefore, either an average value of many samples is taken or if the entire contents may be dumped, it is lightly mill-mixed, hoping that the contents are sufficiently homogenised.

Improving the uniformity has been high on the list of optimising operation and improving mixers. Other items are improvement of the efficiency from the point of view of both

time and energy, and of course, achieving satisfactory quality of the mix. For this purpose, the rubber-processors have been devising in-house knowledge for a type of mixer available to them. Such knowledge depends upon a given mixer, a particular formulation to be mixed, and economic factors. Examples are upside-down mixing, and multi-steps of charging additives. Sasai [46] reported techniques of mixing EPDM along these lines. Problems unique to mixing of FKM are discussed by Tomoda [51] and those concerning CR and CSM are discussed by Okutsu [52]. As discussed before, incorporation and dispersion are different unit processes, of which the objectives are different. Using the same machine for the different objectives is far from ideal. This has been recognised for a long time. When a large quantity of compound is made, the usual practice has been to use an internal mixer for the incorporation. As soon as the free carbon black disappears and the compound is massed, it is dumped onto a mixing roll and the dispersion is completed with the mill. The mill operation is often assisted by an operator, who cuts a band of the compound, raises it to an overhead roll, and brings it down to the mill roll. In this way, a portion of the compound is re-circulated to the mill. A mechanical device moves the band side-ways to the left and right, to ensure uniform mixing. In addition to assisting the milling, the operator may take a sample and inspect the progress of dispersion. When the dispersion is completed the band is transported toward the down stream operation. Finish mixing with a roll-mill is considered to be necessary for difficult-dispersing fillers.

In spite of the importance of the dispersion process, the description of the mill operation is scarce in literature. In order to automate the operation, a recycling conveyor is used, Figure 11.14 [53]. Air-cooling during recycling is another advantage of this system. In place of the mill, a single screw, e.g., Transfermix or a twin screw mixer is used for the automatic and continuous operation.

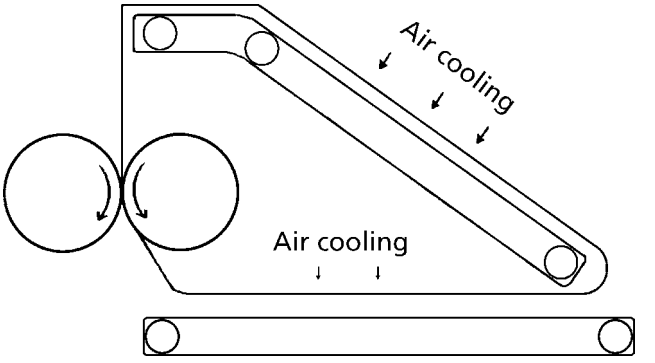

Figure 11.14 Open roll with cycling conveyor.

11.10.2 Optimum state of the elastomer for mixing

The mill processability of raw elastomer was classified into four typical regions, of which Region II provides the optimum processability [24]. In this region, an elastomer will undergo a large deformation without breaking. This provides a large surface suitable for incorporating carbon black through a lamination mechanism [20]. Repeating the large deformation and elastic recovery during mixing facilitates incorporation. The accompanying microscopic mechanism is the bringing of the rubber and carbon black surfaces into intimate contact. Because the carbon black has a large surface area with a complex topology, intimate contact with rubber is difficult to attain if the rubber is too stiff, as in Region I. An inspection of failure envelopes [25] shows that for a high deformation rate, e.g., 20,000%/s, the optimum processing temperature, i.e., Region II, is 50-60 °C, although this depends upon the type of rubber and its MW. At a much slower rate, e.g., 200%/s, room temperature may be the optimal condition. In order to have the most effective mixing, the material behaviour between the blade tip and the chamber wall must be considered. This is where the deformation rate is in the order of 20,000%/s. There may be an advantage in pre-warming the rubber [54], although in practice it creates an additional step in material-handling. Nakagawa [54] states that the optimum temperature for the chamber wall is 50-80 °C.

As described in the section on energy balance (see Section 10.2), essentially all the energy input into the material is converted to heat, which raises the compound temperature. When the temperature becomes too high, mixing becomes less effective because the material behaviour moves toward Region IV. There, the modulus of rubber is too low to sustain the level of stress required for effective dispersion. Too high a temperature also causes premature cure. Therefore, efficient cooling is important especially for fast, intensive mixing, and traditionally, this was achieved with the use of cold water.

However, the previous argument suggests that the use of warm water is preferable if very efficient heat transfer can be achieved. Figure 11.15 is an example of such an experiment [54], where a temperature regulator for the cooling water and a mixer designed for very good heat transfer were used. The figure shows that with the increasing temperature, both the time for seating of the ram and the total energy input are decreased, the optimum condition being reached at 50-60 °C. Figure 11.16 is a comparison of the electrical power inputs at the cooling water temperature of 7 °C and 60 °C. At 60 °C control, the cycle time was shortened by 37%, together with at least 10% savings in the required electrical energy.

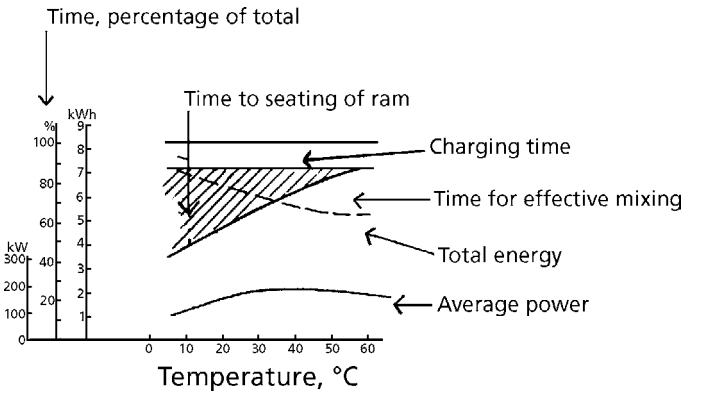

Figure 11.15 Effects of the mixer temperature on mixing performance.

Reprinted with permission from K. Nakagawa and I. Amano, Journal of the Society of the Rubber Industry, Japan, 1980, 53. Copyright 1980.

11.10.3 Improvements in rotor design

Figure 11.3 is a good illustration of an example of rotor design and its mixing actions [18]. According to the previously mentioned model, about 65% of the comminution mechanism takes place within a volume of a shell between the chamber wall and an imaginary wall, swept by the tip of the rotor. Another 35% of comminution must be taking place near the front of the rotor tip. In other words, the comminution mechanism is taking place at and near the milling zone of Figure 11.3. The compaction during incorporation and dispersion processes must be taking place here also.

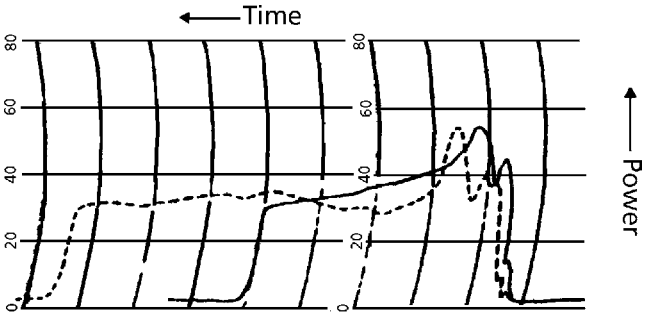

Figure 11.16 Power input curves; ---, 7 °C cooling water; ——, cooling water maintained at 60 °C.

Reprinted with permission from K. Nakagawa and I. Amano, Journal of the Society of the Rubber Industry, Japan, 1980, 53. Copyright 1980.

Then, what is the purpose of the longitudinal cut-back, kneading and lateral overlap? Because these zones have large cross sections, the deformation rates are low. Therefore, the only effective action is the macroscopic transport of the material as indicated by the arrows in Figure 11.3 resulting in macroscopic homogenisation.

In the example of the model-calculation, the comminution mechanism has taken place within 22.5% of the total volume charged. The rest, 77.5% of the volume, is presumably undergoing the macroscopic homogenisation. The question is whether 77.5% of the volume charged is really effectively worked in the mixer or not.

In general, a semi-quantitative interpretation [54] is that effective mixing takes place only in front of the rotor between the rotor tip and the chamber wall. In the backside of the rotor little mixing takes place, but since material occupies this space also, it results in a waste of energy. This means that a larger number of rotor wings would be expected to improve the efficiency of mixing.

The older type Banbury mixer has been of the two-wing rotor type. More recently, however, four-wing rotors have been adopted for reasons of higher productivity; for example, shortening the mixing time by 25% and improving the energy efficiency by 8% [54].

The four-wing type has an added advantage in that it gives a better force-balance on the rotor shaft than the two-wing does. The force in the axial direction is considerably less for the four-wing rotor than the two-wing rotor. This also contributes to a better energy efficiency [54].

An example of the pressure profile is shown in Figure 11.17, where the pressure was recorded in a miniature mixer [12]. Even though the size of the pressure transducer was large compared to the dimension of the rotor tip, a sharp rise in the pressure was registered when the rotor tip swept across the pressure transducer. The actual pressure peak may have been even steeper.

According to the conventional interpretation, the mechanisms of the material transport entail both 'pressure flow' and 'drag flow' [55]. Material transport through the gap between the rotor tip and the chamber wall is affected by the drag flow and a part of the pressure flow, i.e., in the 'through' direction. However, the pressure also pushes the material backwards. The latter does not contribute to effective mixing, except perhaps in macroscopic homogenisation.

The shoulders on the leading edge of the pressure profile of Figure 11.17 are related to the axial flow; however, it might be caused by a pressure wave rather than actual material transport [12]. Whether or not a sharp pressure rise in front of the rotor tip is necessary for effective mixing may be questioned.

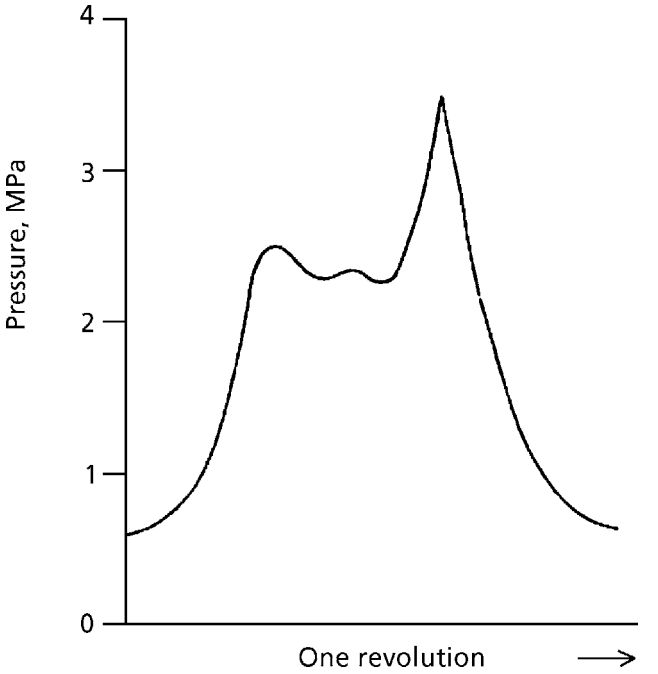

Figure 11.17 Pressure profile observed with a miniature mixer.

Reprinted with permission from P. K. Freakley and W. Y. Wan Idris, Rubber Chemistry and Technology, 1979, 52, 1, 134. Copyright 1979, Rubber Division of the ACS.

In the study of compaction, (see Chapter 2) not a high pressure but a tear was found to be the effective means of mixing.

In the course of developing a new type of four-wing rotor, the design concept was to give more uniform pressure to the material within the chamber. This is based on the interpretation that the action behind the rotor results in wasted energy [54].

The resulting new design of the four-wing rotor has given an energy efficiency 25% better than the conventional two-wing rotor and 16% better than the previous four-wing rotor [54].

The patterns of the material transport are shown in Figure 11.18 for the previous four-wing rotors and the improved four-wing rotors. A major difference between the two designs is that the older type gives impinging streams, whereas the improved design provides smooth transport of one-directional circulation. The latter eliminates the pressure peak in the axial direction.

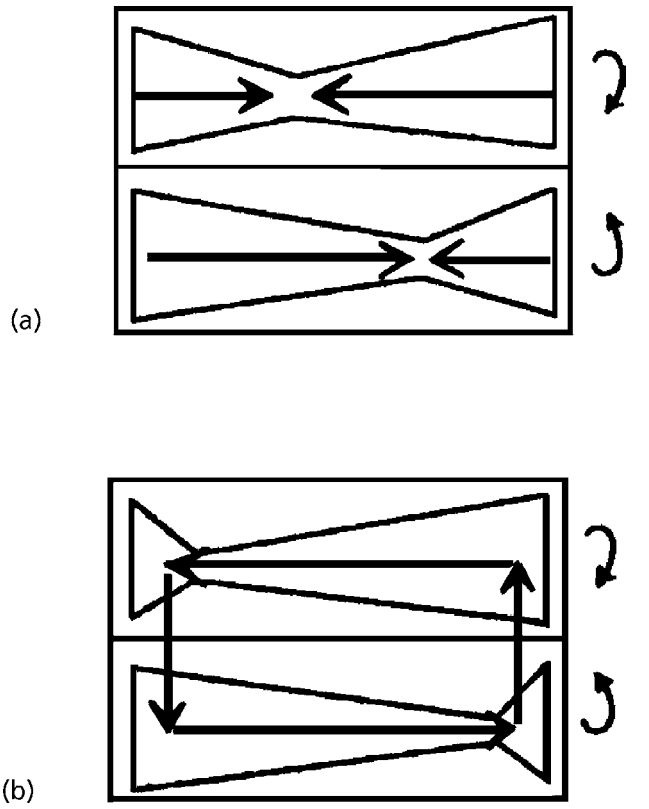

Figure 11.18 Directions of material transport in the mixer with a) an old type four-wing rotor and b) a new type four-wing rotor.

For the reasons explained earlier, impinging streams are effective for mixing low viscosity, inelastic fluids, whereas with elastomers, the opposing transport creates unnecessary resistance, resulting in wasted energy.

Following the previous discussion of the four-wing rotors, the question is whether or not increasing the number of rotor wings further improves the performance of the mixer. Such an investigation was carried out with six-wing rotors [56]. However, an excessive temperature-rise and resulting decrease of the modulus of rubber adversely affected the efficiency of dispersion. For a remedy and a further improvement, the rotor-tip clearance was made variable; that is, along the flight, three sections of different clearances, narrow,

intermediate and wide, were made, Figure 11.19. The narrow section is for the effective dispersion and when plastics instead of rubber are handled, it is for wiping the polymer melt off the chamber wall. Although the intermediate and wide clearance is less effective for dispersion, it improves the circulation of the mixer contents without excessive temperature-rise. A significantly shorter mixing time was achieved, Figure 11.20.

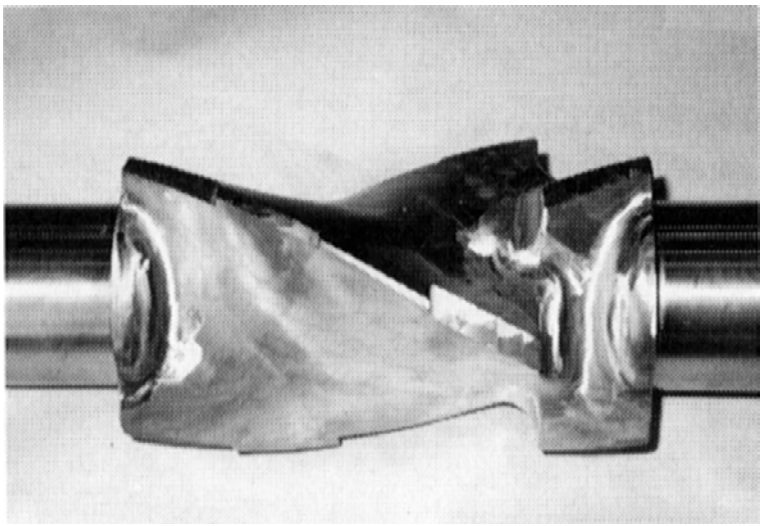

Figure 11.19 Six-wing variable clearance rotor for an internal mixer.

In general, the design of the internal mixer must be flexible enough to accommodate widely varying requirements: they are, for example, providing maximum efficiency for both incorporation and dispersion. At the same time, the temperature-rise must be kept minimum. However, when a rubber is too stiff, a warmer start-up temperature is desired. In the mill operation the usual practice is to make a gap wide. A variable internal clearance (VIC) intermeshing mixer was developed by Pomini [57, 58]. The clearance may be adjusted automatically during the cycle. Making the rotor speed a variable and controlling it, is another option. Both variable clearance and variable speed are made in recognition that each rubber and each formulation have different requirement for the optimum mixing.

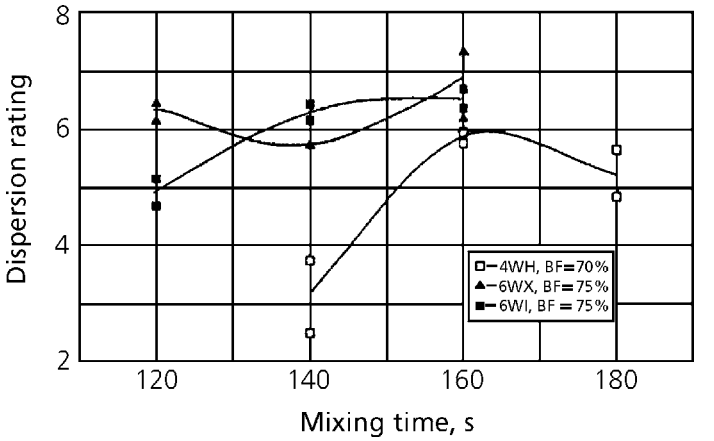

Figure 11.20 Rotor type and dispersion rating. 4 WH - 4-wing rotor with constant clearance; 6WX - 6-wing rotor with constant clearance and 6WI - 6-wing rotor with variable clearance.

References

1. N. Nakajima, *Rubber Chemistry and Technology*, 1981, **54**, 2, 266.

2. P. R. Van Buskirk, S. B. Turetzky and P. F. Gunberg, *Rubber Chemistry and Technology*, 1975, **48**, 4, 577.

3. S. B. Turetzky, P. R. Van Buskirk and P. F. Gunberg, *Rubber Chemistry and Technology*, 1976, **49**, 1, 1.

4. F. S. Myers, and S. W. Newell, *Rubber Chemistry and Technology*, 1978, **51**, 2, 180.

5. G. E. O'Connor and J. B. Putman, *Rubber Chemistry and Technology*, 1978, **51**, 4, 799.

6. E. S. Dizon, *Rubber Chemistry and Technology*, 1976, **49**, 1, 12.

7. H. Palmgren, *European Rubber Journal,* 1974, **156**, 5, 30

8. H. Palmgren, *European Rubber Journal,* 1974, **156**, 6, 70.

9. H. Palmgren, *Rubber Chemistry and Technology*, 1975, **48**, 3, 462.

10. E. S. Dizon and L. A. Papazian, *Rubber Chemistry and Technology*, 1977, **50**, 4, 765.

11. B. B. Boonstra, and A. I. Medalia, *Rubber Chemistry and Technology*, 1963, **36**, 1, 115.

12. P. K. Freakley and W. Y. Wan Idris, *Rubber Chemistry and Technology*, 1979, **52**, 1, 134.

13. K. Min and J. L. White, *Rubber Chemistry and Technology,* 1985, **58**, *5*, 1024.

14. S. Toki, M. Takeshita, Y. Morimoto and M. Okuyama, Presented at the 124th ACS Rubber Division Meeting, Houston, TX, Fall 1983, Paper No.37.

15. P. K. Freakley, and S. R. Patel, *Rubber Chemistry and Technology*, 1985, **58**, 4, 751.

16. N. Nakajima and E. A. Collins, *Transactions of the Society of Rheology*, 1976, **20**, 1, 1.

17. S. Shiga and M. Furuta, *Rubber Chemistry and Technology,* 1985, **58**, 1, 1.

18. *Understanding the Banbury Mixer,* Farrel Company, Division of USM Corporation, Ansonia, CT 06401.

19. N. Nakajima, J. J. Scobbo, Jr., and E. R. Harrell, *Rubber Chemistry and Technology*, 1987, **60**, *5*, 761.

20. N. Nakajima, *Rubber Chemistry and Technology*, 1980, **53**, *5*, 1088.

21. I. Manas-Zloczower and Z. Tadmor, *Rubber Chemistry and Technology*, 1984, **57**, 1, 48.

22. N. Nakajima and E. R. Harrell, *Rubber Chemistry and Technology*, 1984, **57**, 1, 153.

23. N. Nakajima, *Rubber Chemistry and Technology*, 1982, **55**, 3, 931.

24. N. Tokita and J. L. White, *Journal of Applied Polymer Science*, 1966, **10**, 7, 1011.

25. N. Nakajima and E. A. Collins, *Rubber Chemistry and Technology*, 1976, **49**, 1, 52.

26. N. Nakajima, *Polymer Engineering and Science*, 1979, **19**, 3/4, 215.

27. W. M. Hess in *Reinforcement of Elastomers*, Ed., G. Kraus, Interscience Publishers, New York, 1965, p.187.

28. N. Nakajima, E. R. Harrell and D. A. Seil, *Rubber Chemistry and Technology*, 1982, **55**, 2, 456.

29. J-B. Donnet and A. Voet, *Carbon Black, Physics, Chemistry, and Elastomer Reinforcement,* Marcel Dekker, Inc., New York, 1976, p.276.

30. *Banbury Mixers*, Bulletin 215A, Farrel Company, Division of USM Corporation, Anosonia, CT 06401.

31. M. Mooney and W. E. Wolstenholme, *Journal of Applied Physics*, 1954, **25**, 1098.

32. N. Nakajima and E. A. Collins, *Rubber Chemistry and Technology,* 1974, **47**, 2, 333.

33. N. Nakajima and E. A. Collins, *Rubber Chemistry and Technology,* 1977, **50**, 4, 791.

34. S. H. Maron, W. von Fischer, W. M. Ellslager and G. Sarvadi, *Journal of Polymer Science,* 1956, **19**, 29.

35. S. H. Maron, W. von Fischer, W. M. Ellslager and G. Sarvadi, *Journal of Applied Polymer Science,* 1961, **5**, 308.

36. N. Nakajima, *Polymer International*, 1996, **41**, 1, 23.

37. M. Mooney, *Journal of Applied Physics,* 1956, **27**, 7, 691.

38. N. Nakajima, Presented at the *International Seminar on Elastomers*, Itoh, Shizuoka, Japan, 1985, p.182.

39. G. E. Wardell, V. J. McBrierty and V. Marsland, *Rubber Chemistry and Technology*, 1982, **55**, 4, 1095.

40. G. R. Cotten, *Rubber Chemistry and Technology*, 1984, **57**, 1, 118.

41. ASTM D2663 – 95a
Standard Test Methods for Carbon Black – Dispersion in Rubber.

42. K. Kawanishi and K. Agei, *Journal of the Society of the Rubber Industry, Japan*, 1989, **62**, 1, 39.

43. M. Ito, T. Nakamura and K. Tanaka, *Journal of the Society of the Rubber Industry, Japan*, 1985, **58**, 7, 468.

44. S. Shiga, *Journal of the Society of the Rubber Industry*, *Japan*, 1989, **62**, 3, 123.

45. L. L. Ban, W. M. Hess and L. A. Papazian, *Rubber Chemistry and Technology*, 1974, **47**, 4, 858.

46. K. Sasai, *Journal of the Society of the Rubber Industry*, *Japan*, 1992, **65**, 6, 353.

47. J. W. Watson, *Rubber Chemistry and Technology*, 1957, **30**, 3, 987.

48. H. Gotoh, *Journal of the Society of the Rubber Industry, Japan*, 1997, **70**, 11, 641.

49. H. Gotoh, *Journal of the Society of the Rubber Industry, Japan*, 1998, **71**, 6, 340.

50. M. Jamroz, K. Kozlowski, M. Sieniakowski and B. Jachym, *Rubber Chemistry and Technology*, 1978, **51**, 1, 81.

51. M. Tomoda and Y. Ueda, *Journal of the Society of the Rubber Industry, Japan*, 1992, **65**, 6, 336.

52. S. Okutsu, *Journal of the Society of the Rubber Industry, Japan*, 1992, **65**, 6, 346.

53. Y. Yamaguchi, *Journal of the Society of the Rubber Industry, Japan*, 1998, **71**, 9, 578.

54. K. Nakagawa and I. Amano, *Journal of the Society of the Rubber Industry, Japan*, 1980, **53**, 9, 550

55. J. M. McKelvey, *Polymer Processing*, John Wiley and Sons, Inc., New York, 1962, p.229.

56. K. Inoue, *Journal of the Society of the Rubber Industry, Japan*, 1998, **71**, 9, 534.

57. L. Pomini and S. Crespi, *Rubber Chemistry and Technology*, 1992, **65**, 1, 264.

58. J. L. White, *Rubber Chemistry and Technology*, 1992, **65**, 3, 527.

12 Post-Mixing Processes

12.1 Introduction

The results of mixing obviously have a decisive influence on the down-stream processes. Some of the critical points of the influence will be discussed in this chapter. Extrusion and injection moulding are selected as examples, although other processes such as calendering are equally important. Extrusion and injection moulding are automated; as a result they have a strict requirement for the consistency of the compounds. The operation of extrusion will be discussed with respect to feeding problems, the compound uniformity and flow mechanisms. An example of the extrusion problem of silica-filled compounds is also discussed. For the injection moulding a method of dealing with the non-uniformity of the compound is described.

12.2 Extrusion

A brief description of the extrusion of a rubber compound is given with emphasis on the uniformity of the operation. One source of non-uniformity is that originating from the mixing and the other is caused by the extrusion itself. Only the former is related to mixing, but both cases are described here, because they may not be clearly separable in the actual extrusion operation. The purpose of extrusion is to fabricate a continuous object with a precisely defined cross-sectional geometry, i.e., a profile. It follows that the material must be uniform in every part over the cross-section as well as in the machine direction. The material, being viscoelastic, carries deformational memory. Therefore, the uniformity of the memory as well as that of the composition must be concerned with the recovery or else the memory will distort the profile.

12.2.1 Causes of non-uniformity in feeding

The compound fed into extruder may be a ribbon, pellets or premixed powdered rubber. The ribbon is usually cut from sheet taken up from the sheeting mill-roll. The width of the ribbon is uniform but the thickness may be irregular. This is one of the potential

causes of non-uniformity of feeding. However, the non-uniformity of the properties of the compound is the dominant cause of non-uniformity in extrusion. This aspect has already been discussed in previous chapters. If the pellets have been made from an inhomogeneous compound, there is the same problem as with the ribbon. If preblended powder is used, the distribution may be uniform. However, the dispersion of fillers must be achieved during extrusion. Therefore, it becomes a process of the continuous mixing. In addition, the feeding of powder may present a problem of bridging (see section 3.3.5), which is a stoppage of the flow against gravity by friction between the particles. Another problem may be the intermittent non-uniform feeding which is often a characteristic of powder flow. Either of these problems may be overcome by use of mechanical feeding devices.

If a ribbon is too stiff, it slips and becomes difficult to feed. This indicates too high a modulus and hence, a low friction between the compound and the screw surface. The high modulus may be caused by the formulation but also by insufficient dispersion or ageing of compound. Relatively unrecognised is premature crosslinking, which does not appear as scorch [1]. Because the deformation rate is low at feeding, the effect may be significant, but it may not be detectable at the higher rate of deformation used in the Mooney test or with the capillary rheometer.

The feed rate may be controlled by using a forced feeder, but excess material may remain in the gap between the feeder and screw. The behaviour of the material resembles that at the nip of the mill, where some kneading takes place. The material may stagnate here and may not necessarily be fed into the screw continuously. It may be intermittently sucked into the screw. If the amount taken up by the screw is larger than the amount of the feed, there is no excess material stagnating. However, it becomes a starved feed, which presents another control problem. Even, when the amounts of take-up and feed are balanced, non-uniformity can be caused because the screw flight cuts the ribbon in every revolution, introducing intermittent behaviour, (see Figure 12.1) [2].

For a given extruder and die combination the output rate is determined by the screw rpm and the properties of the compounds affecting reverse flow. However, this is only when the channel is full. For the starved operation, the insufficient feeding rate may result in the non-steady operation.

In summary, there are a number of causes for disturbing the steady operation, which may not be completely eliminated. The result is not only the non-steady output rate but also non-uniform shrinkage (die swell), non-uniform surface appearance and other irregularities. Therefore, various homogenising devices are used, some as a modification of screw, others as homogenisers at the screw head or as post-extrusion devices.

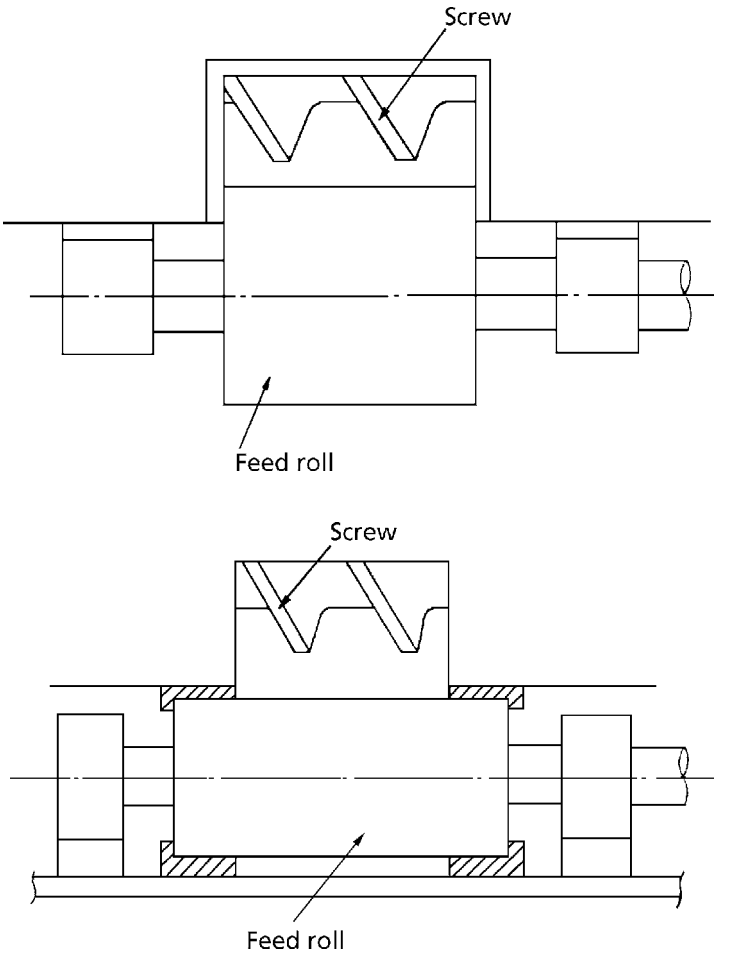

Figure 12.1 Feed port and feed roll.

12.2.2 Material behaviour in the screw

Although the material behaviour at the feed port can be observed, once the compound enters the screw channel, direct observation is not possible. The 'flow visualisation' is accomplished for thermoplastics, by stopping the screw, cooling the machine and pushing out the screw with the material filling the channel. For a rubber compound the rotation

is stopped, and the temperature is raised to vulcanise the material. After that the machine is cooled and the screw is pushed out.

The following is an example of the flow visualisation, where a ribbon consisting of a white and black layer was fed into a screw. The formulations were adjusted to the same rheology for both layers, Figure 12.2 [3]. The sections 1 through 12 are all in the starved condition. Only sections 13-16 are filled; this is where the pressure is increased for extruding through a die.

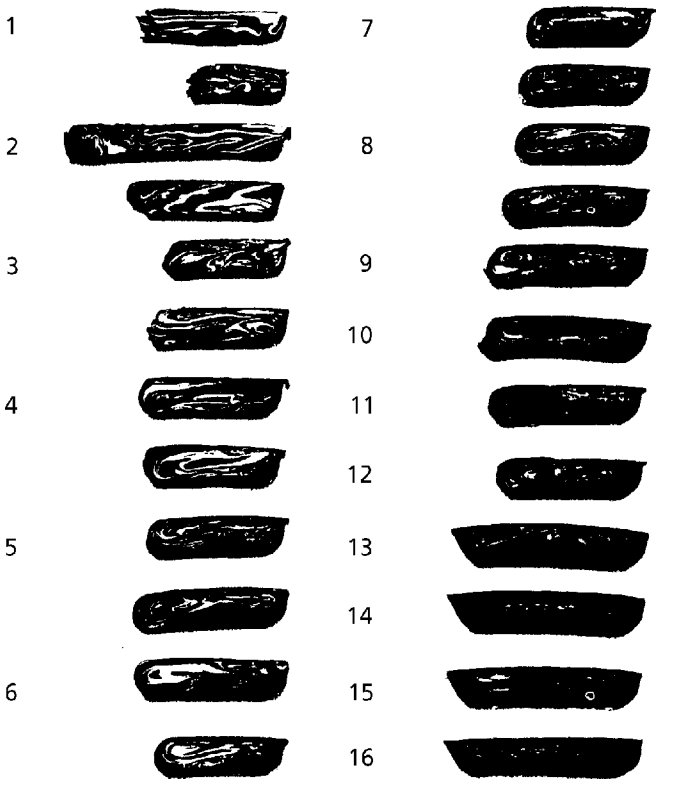

Figure 12.2 NRM Extruder (ITT) (Operating Conditions: $T_b = 65, 55, 55$ °C; $T_s = 65$ °C; N = 20 rpm). T_b is the extruder barrel temperature; T_s is extruder screw temperature and N is the rotational speed of the screw.

The white portion is seen to disappear gradually, indicating the mixing of the compound during flow through the channel. However, the mixing is not very effective. This particular screw has the same channel width in the axial direction. In general, various modifications were made as shown in Figure 12.3 [2] to effect homogenisation.

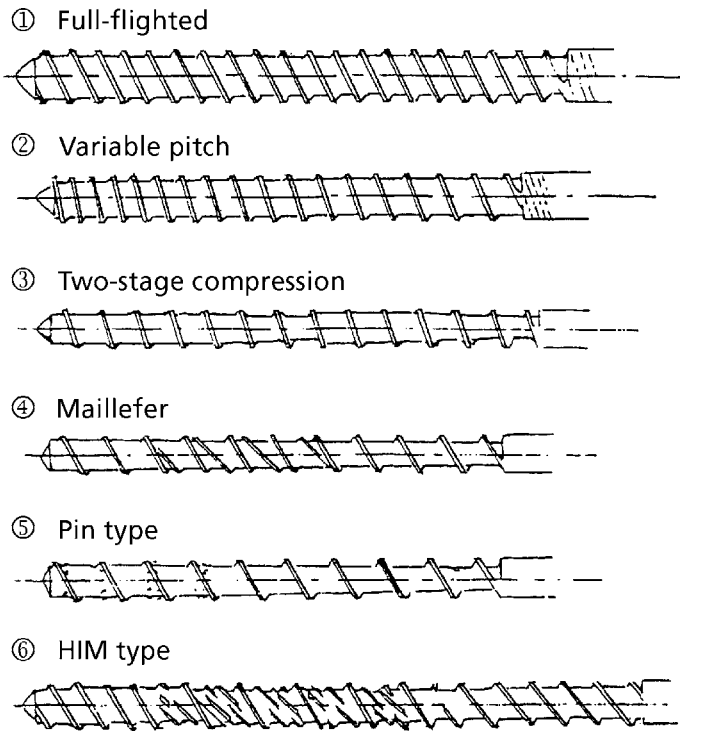

Figure 12.3 Various screws for rubber extrusion.

Among these screws 4, 5 and 6 are intended for the homogenisation. When the screw channel is divided, the resistance increases and the output decreases. It may also result in excess heat generation. The pin-barrel extruder was invented as a homogenisation device with minimum resistance, Figure 12.4 [4].

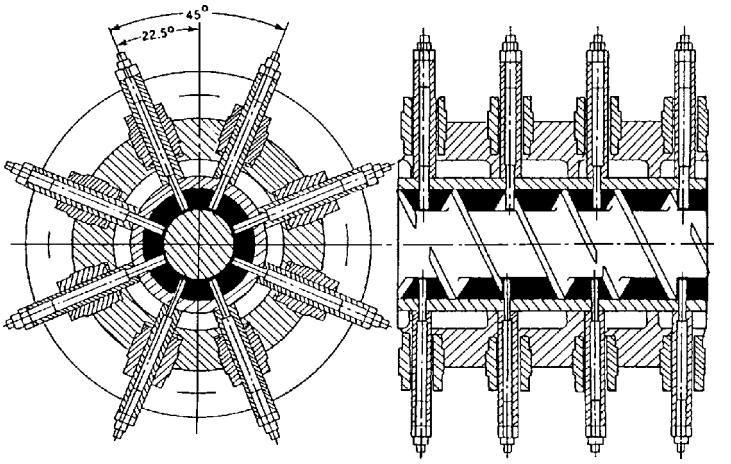

Figure 12.4 QSM pin extruder.

Reprinted with permission from Krupp.
Copyright Krupp.

12.3.3 Flow mechanisms in the extruder

The following equation represents a flow mechanism [5] at the metering section of the extruder

$$Q = Q_D - Q_B \tag{12.1}$$

where the net output rate is the difference between drag flow, Q_D, and pressure flow rate, Q_B. However, this equation does not differentiate two mechanisms:

(A) one extreme is that part of the material in the channel moves forward at the rate, Q_D and the other part moves backwards at rate Q_B.

(B) the other extreme is that the entire material in the channel is moving at a uniform rate, corresponding to the balance of Q_D and Q_B. In the open discharge there is no Q_B. A rod of the compound was pushed out. Also, in the starved feed, sometimes the compound moves forward like the marching of soldiers Figure 12.5 [6]. However, these are cases without back-pressure.

Figure 12.5 Patches of Passenger Tyre Tread (PTT) rubber compound removed from screw.

The reverse flow actually occurs at the gap between the flights which divide the channels and the barrel wall, i.e., leakage flow, see Figure 12.6 [6]. When the flights are cut in the pin barrel extruder to allow the passage of the pin, the leakage flow occurs. For the uniform channel like the one in Figure 12.3, it is not clear how much reverse flow occurs. For the open discharge the following equation may provide a general picture:

$$Q_D = f(V_z wh/2) \tag{12.2}$$

where V_z is the velocity vector in the direction of the channel,

w is the width of the channel,

h is the depth of the channel.

When the channel geometry is not rectangular a geometric factor, f, is applied. When the die is attached and if a part of the material movement is a reverse flow, case A, the actual cross-section of the forward-moving material will be smaller than wh. If the entire material is moving forward, the actual forward velocity V_z' is smaller than V_z.

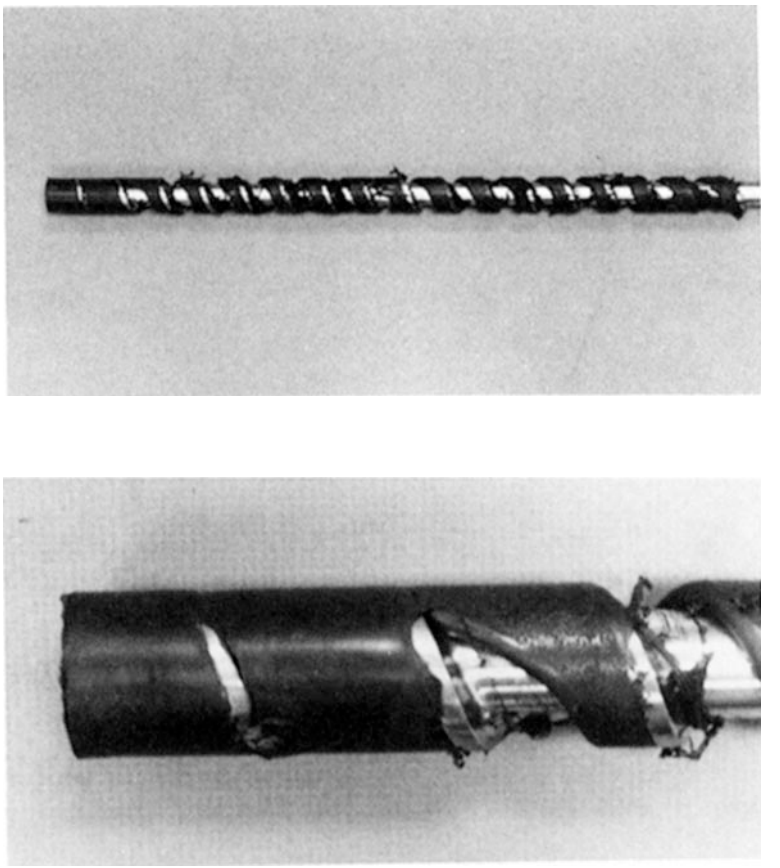

Figure 12.6 Distribution of PTT compound along screw covering of the flights with compound indicates leakage flow.

In this case is a slip or a slip-stick mechanism operating to decrease V_z to V_z'?

Even in the open discharge or in the previously mentioned case of the starved feed, the material is moving as one piece instead of leaving a thin layer behind at the barrel wall. This means that material is slipping at the material-metal interface. Indeed, the screw and barrel wall of the rubber extruder are clean and shiny, implying the slip. However, if it is a steady-slip, the material would not move forward. Therefore, slip-stick must be

the mechanism. Evidently, there is lack of a fully convincing mechanism of material movement in the screw channel.

12.2.4 Homogenisation devices before the die entrance and after the exit

In order to improve the homogeneity of the compound, a device is sometimes attached to the screw head. Among these the Rapra cavity transfer mixer (CTM) is very effective in improving distributive mixing with least resistance to the flow of compound, Figure 12.7 [4]. The improvement of dispersion is not intended.

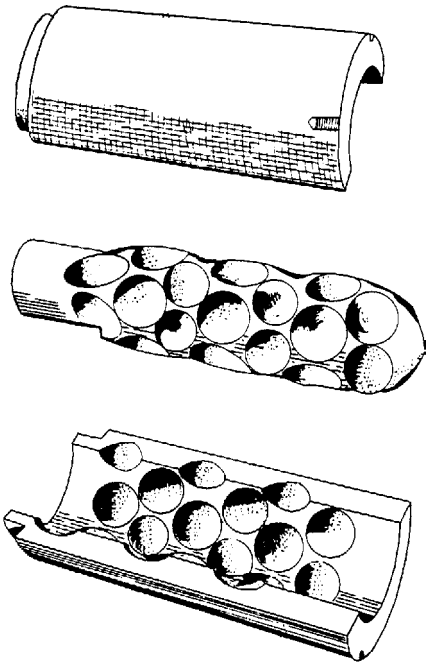

Figure 12.7 Rapra CTM cavity transfer mixer.

Homogenisation in the screws and the screw head is localised. Non-uniformity in the larger scale cannot be treated in this way. To remedy this, a tension device or post-die rollers are used (see Figure 12.8) [4].

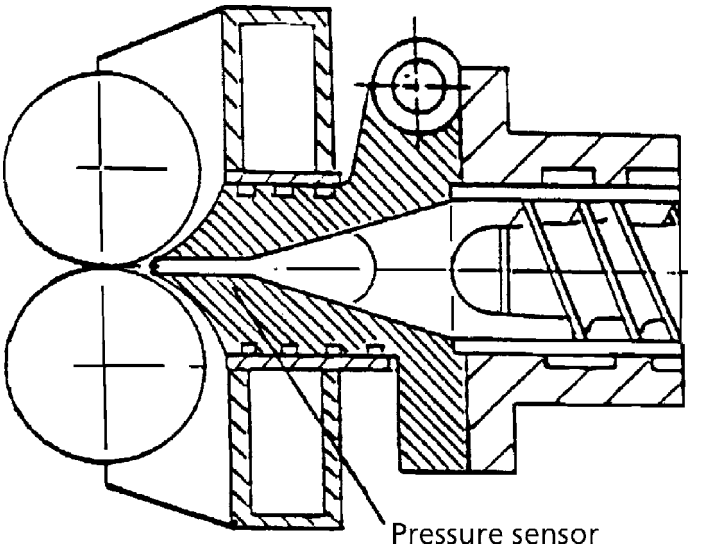

Figure 12.8 Roller head unit.

Reprinted with permission from P. S. Johnson, Rubber Chemistry and Technology, 1983, 56, 3, 575. Copyright 1983, Rubber Division of the ACS.

12.3 Mixing and extrusion of high silica and all silica-natural rubber compounds

12.3.1 Introduction

Silica filler is often used together with carbon black as a reinforcing filler [7]. However, it is usually a minor component of the filler. This section explores the use of silica as a major component (67% or 100%) of the total filler in NR. In order to overcome the mixing difficulty a coupling agent is used. The control compounds contained silica in amounts of 0 or 33% of total filler. A wide ribbon of rubber was extruded from a Monsanto hot-feed extruder and then, the ribbon was fed into an NRM cold feed extruder to test extrudability through a profile die [8].

The control compounds gave extrudates with a smooth surface, but the 67% silica compound extruded with a wavy surface. The 100% silica compound was extruded through the Monsanto extruder but was too stiff to feed into the NRM extruder. Therefore,

the major objective of this study was to find the causes of difficulty in extrusion. A minor objective was to see if the 67% and 100% silica compounds may be made extrudable with smooth surfaces.

12.3.2 Samples

NR was Standard Indonesian Rubber (SIR-10), carbon black was N110 (Cabot) and silica was Ultrasil VN3 Sp (Degussa). The coupling agent was bis-(3[triethoxysilyl]-propyl)-tetrasulphane (TESPT) (Si 69, Degussa) [9]. The compound formulation is given in Table 12.1 and the composition of fillers is given in Table 12.2.

Table 12.1 Compound Formulation

Compound	phr
NR	100
Zinc oxide	4
Stearic acid	3
Carbon black	50 or volume equivalent of the fillers

Table 12.2 Composition of Fillers

Compound number	Fillers		Coupling agent
	Carbon Black phr	Silica phr	phr
1	50	0	0.0
2	34	18	1.8
3	17	37	3.7
4	0	56	5.6
4′	0	56	0.0

The total amount of the filler was adjusted for the difference of densities of carbon black and silica in such a way as to make the total filler volume equal to the volume of 50 phr carbon black. The curatives and retardant are not involved in this study.

12.3.3 Mixer and mixing conditions

The mixer was Moriyama internal mixer, model D3-75, with a 3 litre capacity. The fill factor was 0.7, and the rotor speeds were 72.2 rpm for the front rotor and 52.1 rpm for the back rotor. Also, a laboratory size Banbury mixer was used to assure the similarity of mixing performance.

Table 12.3 Mixing Schedule

		Time (min)
1st Stage	charge NR	0.0
	charge 3/4 filler and additives	0.5
	sweep	2.5
	dump	3.5
2nd Stage	Recharge the above	0.0
	Recharge 1/4 filler	0.5
	Sweep	2.0
	Dump	3.0
3rd Stage	Open mill	4.0

The mixing procedure follows general industrial practice. In this case the three stage mixing given in Table 12.3 was followed.

The order of addition was rubber, carbon black, silica, coupling agent and a mixture of zinc oxide and stearic acid. The filler and other additives were charged very quickly in succession.

The compound temperatures at dump after both first and second stage were specified to be 155 °C. This was to assure the completion of reaction between the silica and the coupling agent [10]. However, the dump temperature, i.e., the highest temperature experienced by the compound, became an important issue and will be discussed later.

Because the Mooney index [11] of SIR-10 was about 100, it was necessary to masticate the compound for several minutes to bring it down to 70 to 75. This may be called the zeroth stage.

The dump temperature was measured by inserting a probe in the compound in several places. Because the dump temperature was an important parameter, it was controlled by the time allowed for the compound to cool to a certain temperature before recharging for the next stage of mixing. The dump temperature control was specified to be a temperature between 140 °C and 160 °C.

12.3.4 Extruder and extrusion test

The mixed compound was sheeted out with a two-roll mill and cut into a strip. This was fed into a Monsanto extruder, 44.8 mm diameter with an L/D ratio of 10.4 mm to obtain a uniform ribbon. Then an NRM extruder of 38.1 mm diameter with an L/D ratio of 20, was used for testing the extrusion performance. The screw geometrics for these extruders are shown in Figure 12.9. The Monsanto extruder is equipped with a power feed whereas the NRM is free-feeding.

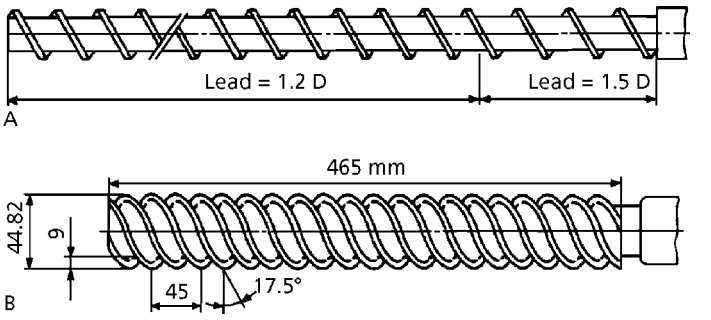

Figure 12.9 Screw geometrics of NRM extruder (A) and Monsanto extruder (B).

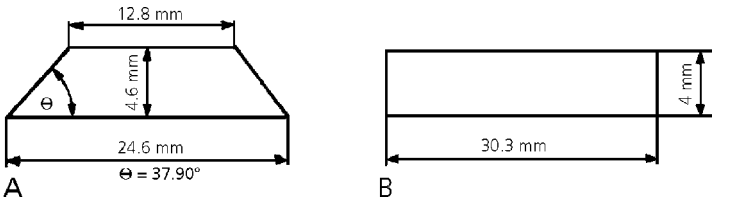

Figure 12.10 Geometry of the profile die of NRM extruder (A) and Monsanto extruder (B).

The die geometries are shown in Figure 12.10. The land-length of the die for the NRM extruder is 28.4 mm with a conical entrance. The extrudate was taken up with a conveyer in order to prevent distortion by sagging. The barrel temperature was set according to those specified in Table 12.4.

Table 12.4 Barrel Temperature Setting for Extruders

Extruder	Zone	Temperature setting °C
Monsanto		100
NRM	1 (feed zone)	77
	2	87
	3	100
	4	100
	5	100

12.3.5 Results and discussion

- *General results of extrusion trials*

The controls, compound 1 and compound 2, gave extrudates with smooth surface. Compound 3 (67% silica), extruded with wavy surface, see Figure 12.11. Compound 4 (100% silica), was extruded through the Monsanto extruder but too stiff to feed into the NRM extruder. The extrudates from the Monsanto extruder also had wavy surfaces, see Figure 12.12.

- *Interpretation of the extrusion problem*

There are at least two separate phenomena which contribute to the extrusion problem of compounds containing a high amount of silica: one is poor dispersion or a poor wettability of silica with NR. The other is a gel or long-chain-branch formation involving the coupling agent.

- *Dispersion problem*

It was found that the silica filler Ultrasil VN3 Sp (spray-dried precipitated silica) even with the coupling agent was more difficult to disperse in NR than the carbon black N110 in NR.

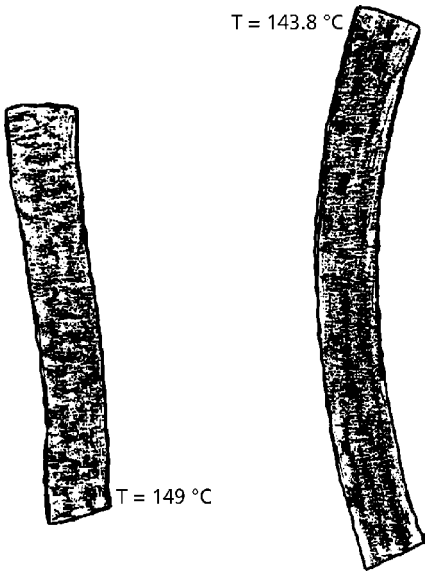

Figure 12.11 Extrudates of compound 3 with wavy surfaces.

Reprinted with permission from N. Nakajima, W. J. Shieh and Z. G. Wang, International Polymer Processing, 1991, 6, 4, 290. Copyright 1991, Hanser Publishers.

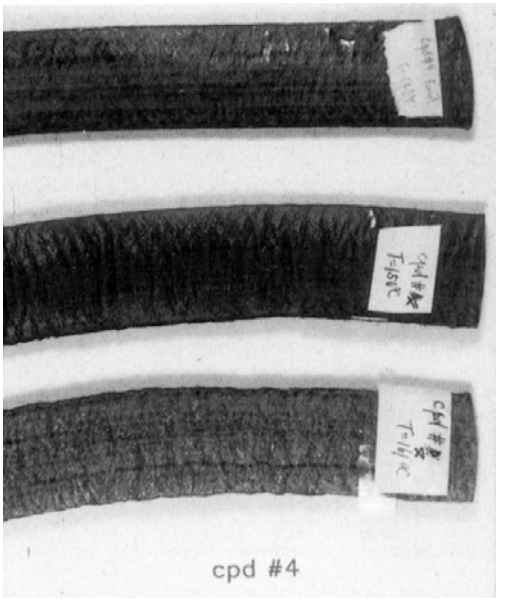

Figure 12.12 Extrudates of compound 4 with wavy surfaces.

Reprinted with permission from N. Nakajima, W. J. Shieh and Z. G. Wang, International Polymer Processing, 1991, 6, 4, 290. Copyright 1991, Hanser Publishers.

Rotary-dried, precipitated silica was found to be even more difficult to disperse [12]. The difficulty was easily observed during mixing in both the open mill and the internal mixer. The silica agglomerates are more difficult to break down to aggregates compared to carbon black agglomerates, because the silica aggregates are held together by hydrogen bonding involving the surface silanols [7].

With either carbon black or silica the poorer dispersion results in a stiffer compound. Medalia [13] explains this phenomenon on the basis of the occluded rubber. He postulates that rubber is trapped inside of cavities of agglomerates, thereby increasing the effective filler-volume. As the agglomerates are broken down to aggregates the trapped rubber is released, and therefore, the effective filler-volume decreases. However, it is doubtful if very highly viscous and elastic rubber could diffuse into the cavities of the agglomerates with a short time-period of mixing [14]. With the silica filler the diffusion of NR into the cavity of the agglomerates is even more unlikely, because of the organophobic nature of the silica surface.

The reinforcing fillers possess a large void-volume. Therefore, the unbroken agglomerates occupy a large effective volume, even though the cavities are not filled with rubber. When the agglomerates break down into aggregates and the surfaces become wet with rubber, the void-volume is significantly decreased.

Together with a large effective volume of the unbroken agglomerates the poorly dispersed filler particles perhaps interfere with each other like a log jam. This is probably why the poorly dispersed compound is stiffer.

- *Reaction between coupling agent and rubber*

Wolff [10] recommends that the compound temperature should reach above 150 °C in order to assure the reaction between silica and TESPT. Unless the compound temperature becomes higher than 160 °C, the reaction between TESPT and NR is not significant. However, since 150 °C is within the temperature range for vulcanisation, the polysulphide linkage would break and react with NR. Datta [15] showed, using gas chromatographic evidence, that the reaction between TESPT and NR occurs even at temperatures as low as 140 °C. This reaction generates gels and long branches. When the amount of silica is small like compound 2, the gels and long branches may be small and their effect on processability may be negligible. However, with the higher amount of silica (and TESPT) this effect is magnified. The generation of gel and long branching needs not be very much in order to cause the extrusion problem of the present investigation [16].

- *Evaluation of degree of dispersion*

Amplitude dependence of storage modulus

Payne [17] observed the dependence of shear storage-modulus (G´), on strain amplitude at a fixed frequency with an SBR-carbon black compound, which is given different degrees of mixing. The G´ value started from a plateau, G_0' at the amplitude close to 0.001 and decreased toward the lower plateau, G_∞', with the amplitude close to 1.0. The values of G_0' and $G_0' - G_\infty'$ decreased with the progress of mixing. This method has been applied for evaluating the degree of dispersion of the present compounds using a dynamic mechanical tester, Mechanical Energy Resolver (MER) [18].

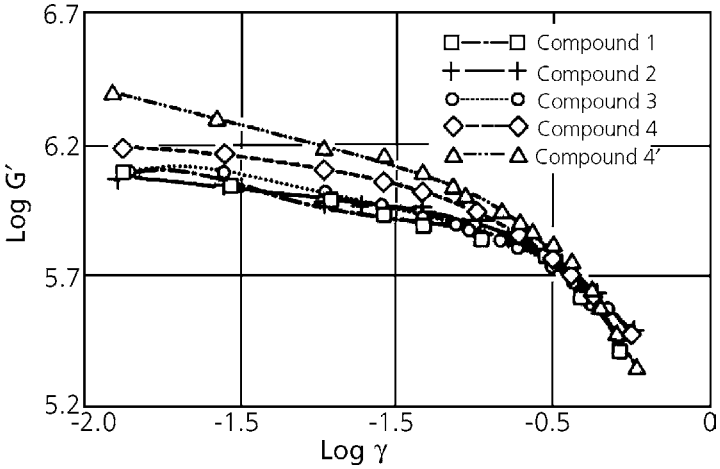

Figure 12.13 Amplitude dependence of shear storage modulus G′, indicating relative degree of dispersion of fillers.

Figure 12.13 shows the results, where approximately plateau values of G´ are observed at the lower strain amplitudes and the G´ decreases at the higher strain amplitude.

The curve of compound 4´, which is known to have a poor dispersion, is the highest as expected; the curves of compounds 1, 2 and 3 are indistinguishable within experimental error, and the degree of dispersion may be considered to be about the same. The curve of compound 4 is somewhat higher than the above three, indicating that compound 4 may have somewhat poorer dispersion.

Even though Figure 12.13 shows a reasonable ranking among the compounds, this method was unsatisfactory for discriminating small differences in the degree of dispersion. The reason is that the G´ value depends on the prior mechanical history in addition to the degree of dispersion. The amplitude dependence of G´ itself implies this. G´ values, particularly those at the lower amplitude depend upon the ageing of compound, loading history of a sample into the tester and any other handling history. The samples used for creating the data of Figure 12.13 were given approximately the same history and therefore, their relative positions of curves are probably correct.

- *Scanning electron microscopy (SEM)*

Figures 12.14A and B show typical cross-sections of compounds 2 and 3 at 1,000x magnification. Particles about 1 μm or smaller can be seen throughout and occasional larger particles of several μm can also be seen.

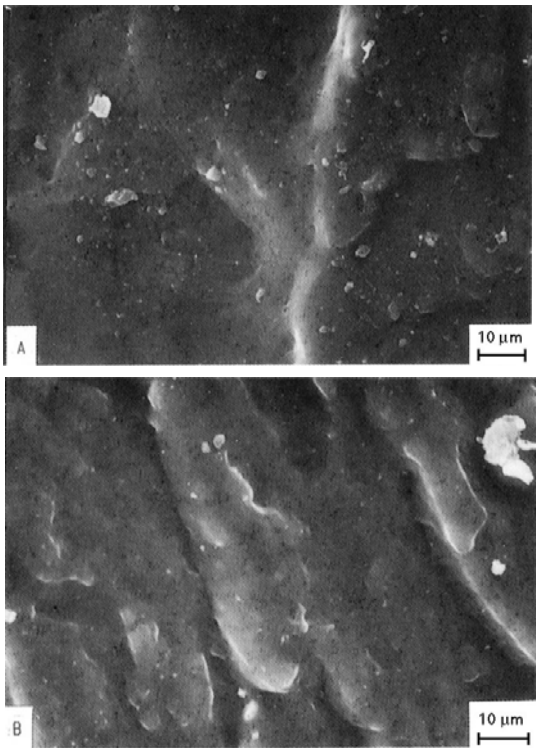

Figure 12.14 Scanning electron micrograph of compounds 2(A) and 3(B), showing some undispersed particles; these compounds have about the same degree of dispersion of fillers.

Figures 12.15A and B show cross-sections of compound 4. Most of the cross-section looks like Figure 12.15A. Many more particles can be seen here than in Figure 12.14A and B. Also, here and there a concentration of undispersed fillers can be seen as in Figure 12.15B. There are no detectable differences at 10,000x magnification.

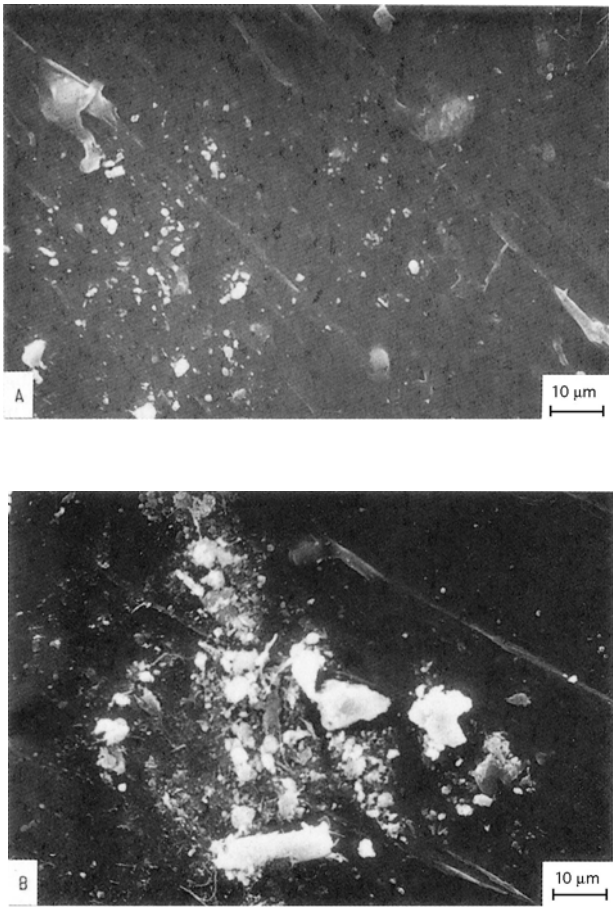

Figure 12.15 Scanning electron micrograph of compounds 4(A), showing many undispersed particles, and (B) undistributed particles.

Reprinted with permission from N. Nakajima, W. J. Shieh and Z. G. Wang, International Polymer Processing, 1991, 6, 4, 290. Copyright 1991, Hanser Publishers.

The SEM results are in agreement with those for the strain-dependence of storage modulus. To the best of our knowledge the degree of dispersion of compounds 1, 2 and 3 are about the same, and the dispersion of compound 4 is poorer.

- *Detection of gel and long branch formation*

Both the storage modulus-strain amplitude measurements and the SEM observation indicated that compound 4 has somewhat poorer dispersion of fillers. However, there was no detectable difference in dispersion of compound 3 compared to the controls, compounds 1 and 2.

The question remains, as to whether or not the gel and long branch formation resulting from the reaction between TESPT and NR may be responsible at least as a part of the extrusion problem. This question may be answered by what is shown in Figures 12.11 and 12.12: that when the dump temperature is higher, the waviness of the extrudate surface is more extensive.

In general, gel formation and long branching introduce very long relaxation times [16]. There is also a strain-hardening tendency [19, 20]. Even when the amount of these structures are very small, e.g., a few percent or less, it is known to cause various processing problems. The present extrusion problem is most probably related to this phenomenon.

The detection of a relatively small increase of the long relaxation time poses a technical problem. A standard technique such as stress relaxation measurement [21] is not suitable, because as the time goes on, the accuracy of the data diminishes. This is because the stress signal becomes weaker and also the baseline may drift. Creep measurement [21] may be more reliable, because it is easier both to maintain the stress constant and to measure displacement accurately. However, it still requires rather an elaborate instrument to measure it. Furthermore, it takes a long time (in the order of hours), to reach a meaningful time region. With gum rubbers, free of fillers, a large deformational measurement, such as tensile stress-strain, may be used effectively to characterise the gel and long branch structure [19, 20]. When the filler is present, the tensile behaviour does not resolve the question unequivocally.

Some time ago another characterisation method was developed utilising a transient shear measurement at a very low deformation rate [22]. In the present study this method is used to discriminate between the samples. Figure 12.16 shows torque-time curves, which were obtained with a rotational rheometer with a biconical rotor [23] at a rotational speed of 0.045 rpm.

Compound 4 at the dump temperature of 150 °C and 160 °C clearly shows that the higher temperature results in the higher torque, i.e., the generation of an increased amount of the long-relaxation-time component. Also, the order in the curves of compounds 1, 2 and 3 indicates that with more TESPT present the torque level became higher. However, the order is reversed between the curves of compounds 3 and 4 (dump temperature 150 °C). Overall these results indicate gel and long branch formation caused by the reaction between NR and TESPT.

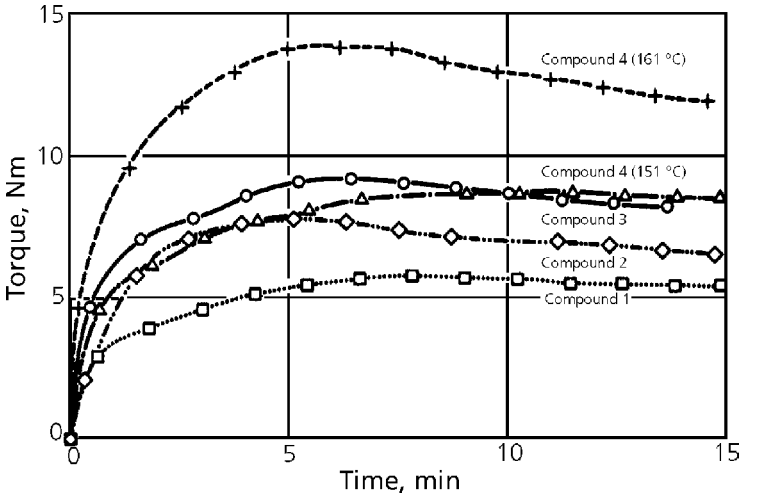

Figure 12.16 Torque-time curves at a very low deformation rate, indicating gel and long branch formation at rotor speed: 0.045 min^{-1}.

Reprinted with permission from N. Nakajima, W. J. Shieh and Z. G. Wang, International Polymer Processing, 1991, 6, 4, 290. Copyright 1991, Hanser Publishers.

- *Reaction between silica and coupling agent*

The studies in the previous section indicate that the higher temperature encountered during mixing generates more gel and long branching, leading to the extrusion problem. A basic problem is whether the dump temperature of 155 °C (or even 150 °C) is necessary or not to complete the reaction between silica and TESPT.

For this purpose a differential scanning calorimeter (DSC) was used to observe the heat of reaction. Figures 12.17a and 12.17b are the temperature scan with silica alone. In the first scan, Figure 12.17a, the calorimeter and its contents was heated to 250 °C; there was some reaction, which might be primarily a removal of water. Evidently it was completed, because it does not appear in the second scan, Figure 12.17b.

Figures 12.18a and 12.8b are the scans obtained for silica and TESPT together in the proportions given by the compound formulation. The reactions were completed when heated up to 250 °C, as there was no reaction seen in the second scan.

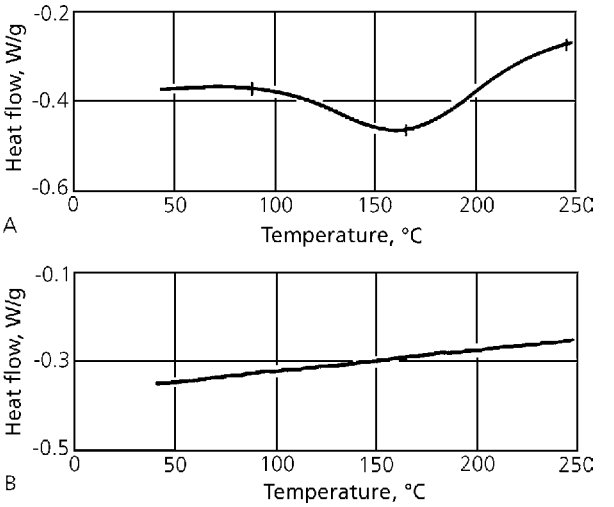

Figure 12.17 First (A) and second scan (B) of differential scanning calorimetry, temperature-sweep, with silica filler.

Reprinted with permission from N. Nakajima, W. J. Shieh and Z. G. Wang, International Polymer Processing, 1991, 6, 4, 290. Copyright 1991, Hanser Publishers.

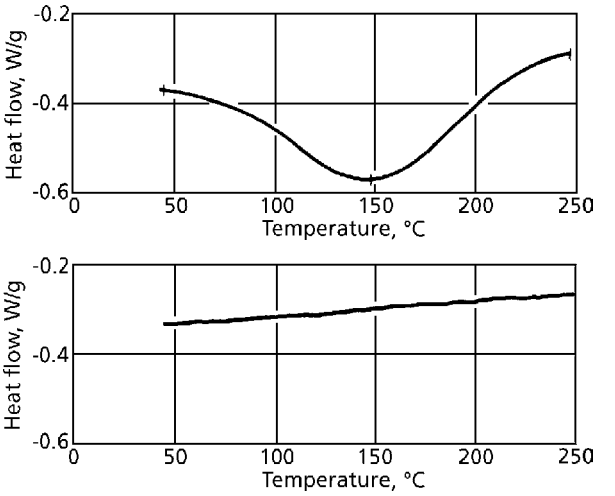

Figure 12.18 First (A) and second scan (B) of differential scanning calorimetry, temperature-sweep, with silica and coupling agent.

Reprinted with permission from N. Nakajima, W. J. Shieh and Z. G. Wang, International Polymer Processing, 1991, 6, 4, 290. Copyright 1991, Hanser Publishers.

In this case the heat balance includes not only the reaction between silica and TESPT but also the evaporation of the reaction product, i.e., ethylalcohol. There may be some side reactions also. What we are looking for is an overall effect of the reaction between silica and TESPT, which is manifest in the heat balance. Figure 12.19 is a composite curve obtained from the difference between Figure 12.17a and 12.18a.

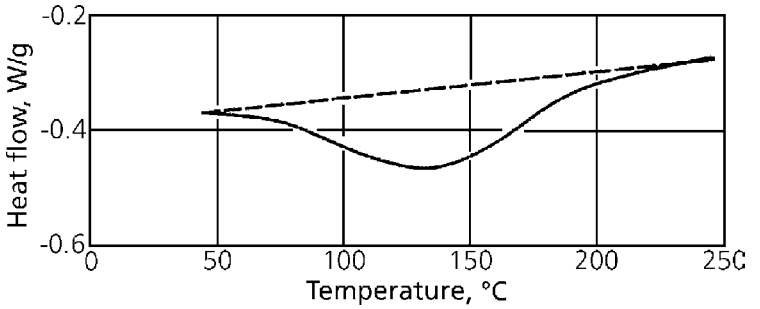

Figure 12.19 Difference of heat of reaction shown in Figures 12.17 and 12.18 indicating the reaction between silica and coupling agent.

Assuming that the reactions of pure silica and the coupling reaction do not interfere with each other, Figure 12.19 represents the reaction between silica and TESPT. Because the measurements include a high temperature range, which is unrealistic with respect to the mixing conditions, quasi-isothermal measurements were made at 140 °C and 155 °C (see Figures 12.20 and 12.21).

There were overshootings of the temperature to 146 °C and 157 °C, respectively, but after about 2 minutes the temperature levelled at 140 °C and 155 °C. There were large endotherms, which correspond to those seen in Figures 12.17 and 12.18. The reaction is completed in about 2 minutes. This suggests that the dump temperature need not be 155 °C but that 140-145 °C may be sufficient to complete the reaction between silica and TESPT.

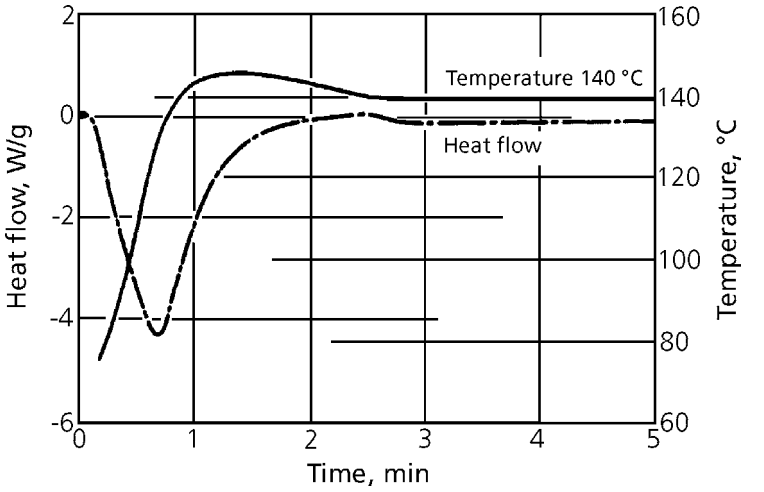

Figure 12.20 Differential scanning calorimetry, isothermal measurement at 157 °C with silica and coupling agent.

Reprinted with permission from N. Nakajima, W. J. Shieh and Z. G. Wang, International Polymer Processing, 1991, 6, 4, 290. Copyright 1991, Hanser Publishers.

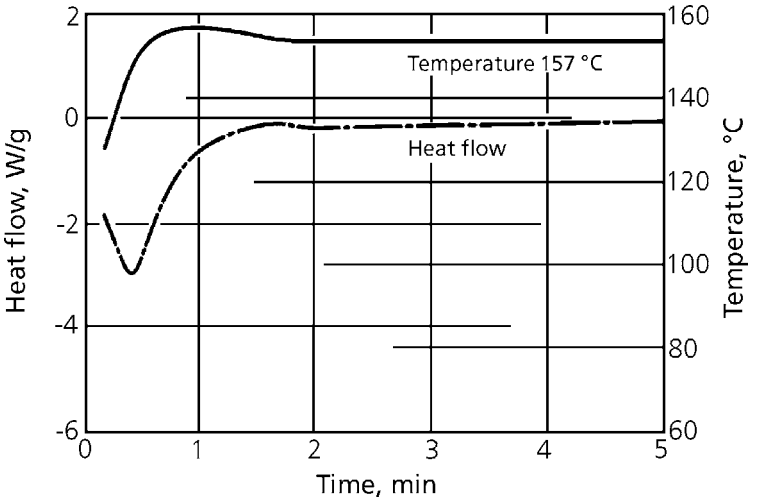

Figure 12.21 Differential scanning calorimetry, isothermal measurement at 140 °C with silica and coupling agent.

Reprinted with permission from N. Nakajima, W. J. Shieh and Z. G. Wang, International Polymer Processing, 1991, 6, 4, 290. Copyright 1991, Hanser Publishers.

- *Mixing and extrusion trial*

Following the findings of the previous section, a new mixing experiment was carried out with compound 3, for which the dump temperature was designed to be as low as 140 °C. The dump temperature after the first stage met the target but that after the second stage somehow overshot to 160 °C. Even then, the extrusion went well and as shown in Figure 12.22, some of the extrudate was smooth (the one at the bottom).

Similar mixing conditions applied to compound 4 did not give a smooth extrudate. It appears that for this compound the degree of dispersion must be improved.

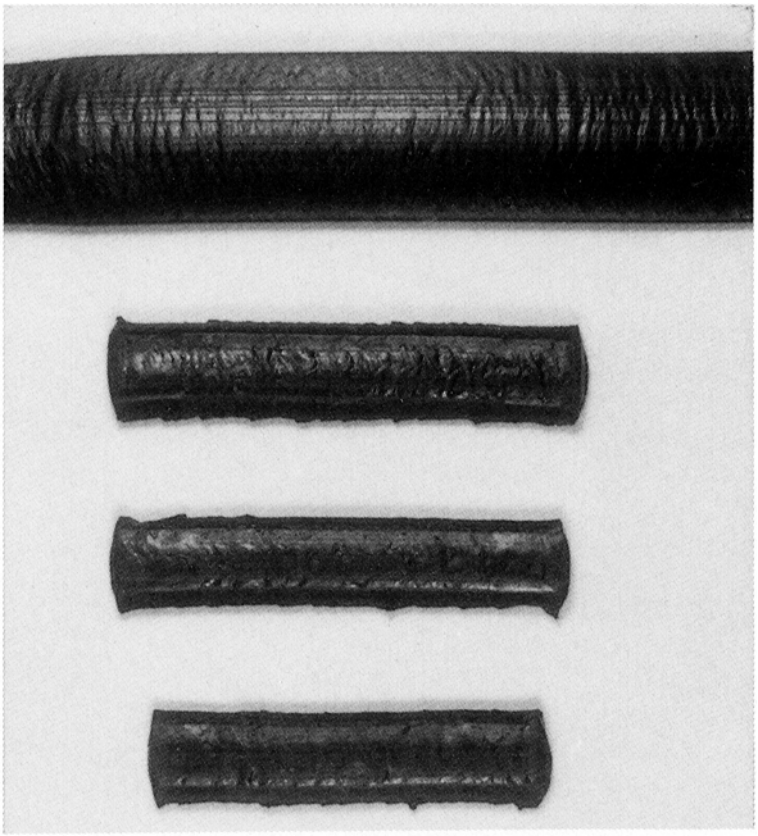

Figure 12.22 Extrudates of compound 3 with smooth surface (bottom).

12.4 Injection moulding

12.4.1 Introduction

Injection moulding is different from extrusion in that it involves a crosslinking reaction. Therefore, the rate and the mechanisms of crosslinking is an integral part of the process. However, in this chapter, chemistry of vulcanisation is not included.

Injection moulding has an advantage over compression moulding and transfer moulding, when a large number of pieces are made because it is rapid and automatic. When a small article is made, every piece must be the same in its shape as well as in its properties. When a thin sheet such as a gasket is made, the properties must be uniform over the whole area. Therefore, the uniformity of the compound is critical. When a multi-cavity mould is used, the material in every cavity must be the same. The automatic operation requires that every shot must have the same rheology. In summary the compound must be uniform in the large scale as well as in the small scale. However, no further comment will be made on the uniformity, because it has been discussed in section 12.2.

12.4.2 Flow mechanisms

The aspect, which requires the most scientific scrutiny is the material flow. The injection is performed at higher shear rates than the extrusion. For this reason, characterisation of a given compound is performed using for example a high-shear capillary rheometer and the high-shear viscosity is used. This approach may satisfy the calculation of flowability; however, a detail of the flow mechanism of the rubber compound at high shear rates is not known. The capillary rheometer was originally designed to measure the steady-state laminar shear viscosity of a homogeneous fluid. Shown in Figures 12.23a and 12.23b are electron micrographs of well-mixed compounds [24].

Apparently, the material is microscopically inhomogeneous; the size of the dispersed carbon black is in the order of 10-100 nm and the size of the rubber domains is approximately 1 μm with irregular topology implying a sub-domain of approximately 0.1 μm. Even though these dimensions are much smaller than the capillary diameter, which is in the order of 1 mm, it may not be appropriate to treat the material as homogeneous.

Does the material look like a flowable liquid? The carbon black forms a ‘network’ structure, which possesses a yield value. Further, the yield value depends upon the previous mechanical history [25].

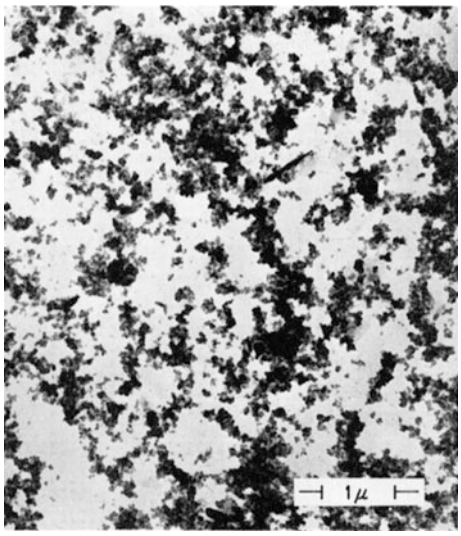

Figure 12.23a Cross-section of ALS-HAF/IIR vulcanisate. Scale bar equals 1.0 μm.

Reprinted with permission from W. M. Hess in Reinforcement of Elastomers, Ed., G. Kraus, 1965, Interscience Publishers, New York. Copyright 1965, John Wiley and Sons.

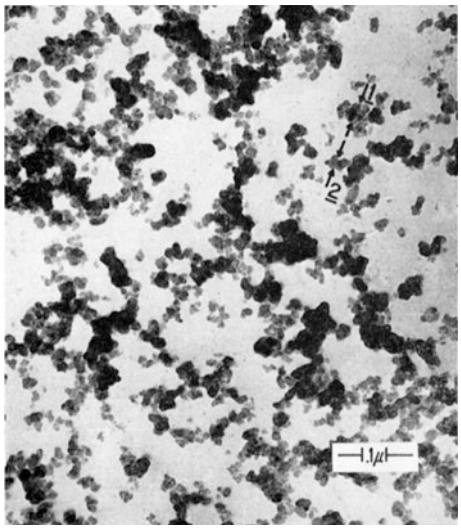

Figure 12.23b Cross-section of ALS-HAF/IIR vulcanisate. Scale bar equals 0.1 μm.

Reprinted with permission from W. M. Hess in Reinforcement of Elastomers, Ed., G. Kraus, 1965, Interscience Publishers, New York. Copyright 1965, John Wiley and Sons.

Is the network destroyed when the strain is increased [26]? Does the bound rubber play any role in flow? Rubber molecules with long branches and gels usually accept a higher loading of carbon black. At the same loading level the mixed compound with branched rubber stretches more than that made with less branched rubber [27]. Evidently, the rubber-carbon black interaction varies with polymer chain structure. A recent development of the chain-end modification also affects this interaction. How do these rubber-carbon black interactions affect the flow mechanism?

Referring to Figure 12.23, the behaviour of the rubber domains are viscoelastic. How does this affect the flow? Does the domain deform during the flow? Does the domain or an assembly of the domains store elastic memories? If the heterogeneous memory is frozen by crosslinking, the moulded article may warp with time, i.e., a memory recovery. How serious is the problem? In the moulded pieces of filled thermoplastics there is often skin-core difference in the concentration of filler. Is this a problem with rubber compound also? In the mould-filling of thermoplastics a jetting or a fountain flow is observed. Does the rubber compound follow these patterns? When a mould has a complex shape, the mould-filling may involve a meeting of two streams. Does the situation create the weld-line problem? What is the mechanism of filling the spider mould?

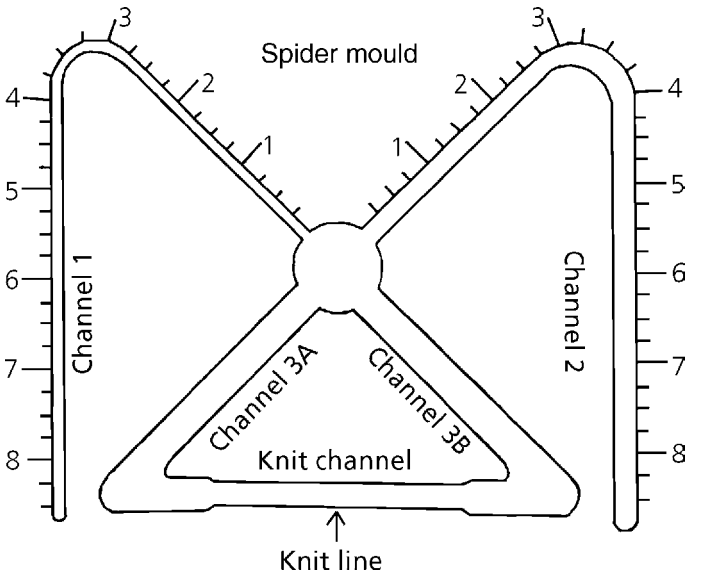

Figure 12.24 Spider mould.

Figure 12.24 shows a spider mould, where a compound is injected vertically in the centre through a gate. The primary purpose of using the spider mould is for evaluating the flowability, i.e., the mould-filling capability. The knit line may also be examined. An example of such an evaluation was made with seven different grades of NBR. The sample characteristics and formulations are given in Tables 12.5, 12.6 and 12.7 [28]. The results are shown in Figure 12.25. The injection condition was selected to give large differences among the compounds made from different grades. The real problem is the difference among the same grade of material. Because the use of the different grades exaggerates the effects of different molecular structure on the flowability, it serves as a background knowledge for diagnosing processing problems.

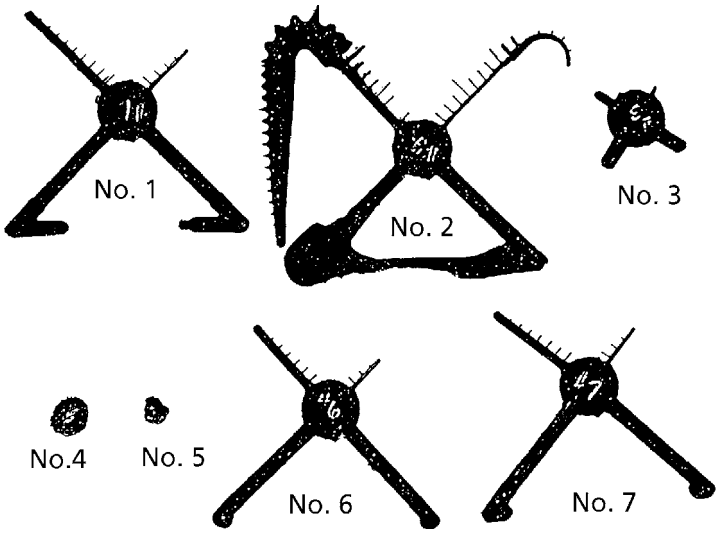

Figure 12.25 Results of filling a spider mould with NBR compounds.

Samples 1, 6 and 7 are commercial products, essentially the same, except for their acrylonitrile content. The mould-filling results are also very similar. Samples 2 and 3 were made in a pilot plant, but using the same polymerisation conditions, as in the commercial plant, except for the amount of MW modifier. For sample 2, more modifier was used giving a lower MW and less long branches. The best flowability out of seven samples was achieved with sample 2. For sample 3, less modifier was used to give a higher MW. A large difference in flowability between 1 and 3 indicates the sensitivity of MW on the flowability. Samples 4 and 5 contained a large amount of gel and they did not even fill the centre of the mould. These results must be interpreted with reference to the rheological data of corresponding compounds without curatives to see if a premature cure during mould-filling had some effect or not.

Table 12.5 Sample Characteristics of NBRs							
Sample No	**1**	**2**	**3**	**4**	**5**	**6**	**7**
MW modifier (relative amount)	1	1.44	0.73	1.44	1.72	0.78	0.75
Conversion, %	75	81	79	92	78	80	80
Mooney Index, ML-4-100[a]	71	22	121	103	88	52	56
Acrylonitrile content of polymer, %	43.7	41.2	39.4	40.3	40.9	33.8	28.4
T_g, °C [b]	–14	–17	–17	–16.5	–17	–33, –22.5	–46, –25
Gel, % [c]	0.9	0.1	0.1	54.7	71.7	0	5.1
a: ASTM D1646-98 [11] *b*: Measured with a DuPont differential thermal analyser with a heating rate of 10 °C *c*: ASTM D3616-95 [29]							

Table 12.6 NBR Compound Formulation	
	phr
Nitrile rubber	100.0
Zinc oxide	5.0
Stearic acid	1.0
N 326 HAF-LS	30.0
N 220 ISAF-HM	20.0
Hi Sil 215	15.0
ARRD (Antioxidant)	3.0
Cumar P25	10.0
DOP	5.0
Spider sulphur	1.75
MBTS	1.75
TETD	0.25
Total	**192.75**
ARRD: Agerite Resin D	

Table 12.7 NBR Solution Properties							
Sample No.	**1**	**2**	**3**	**4**	**5**	**6**	**7**
Gel %	0.9	0.1	0.1	54.7	71.7	0	5.1
Swell Index	29	200	380	32	27	–	40
DSV	1.15	0.66	1.34	0.45	0.39	1.05	1.16

Perhaps the most serious objection to using capillary rheometry to obtain the flowability information is that it assumes a constant temperature. In injection moulding the compound flow is accompanied with the increase of temperature. Scientific treatment of this aspect is rather difficult, for at least two reasons. One is that the increase of temperature affects viscosity, which is a cause for the temperature rise. The other is the non-uniform distribution of the temperature rise, presumably more severe at the interface with the metal wall.

Figure 12.26 shows the design of injection moulding equipment (REP Corporation) [30]. It consists of a plasticating screw section and an accumulator with a plunger and a nozzle. Some injection moulding machines do not have the accumulator and the compound is injected by the screw acting as a plunger.

The characteristics of the machine shown in Figure 12.26 are not only in the mechanical design but more importantly in the mode of the computer control. The main feature of this control recognises non-uniformity of compound in each shot. In the plastication section the mechanical work by the screw and the external heating or cooling are adjusted to raise the temperature of incoming compound to a prescribed level. Then, the compound is transferred to the accumulator by the action of the screw. Because there is no mechanical action or heating or cooling in the accumulator, the temperature stays the same for every shot. Then, the compound is injected into mould by the action of the plunger. The hydraulic pressure pushing the plunger is variable, adjusted to give the same injection speed for every shot. The amount of the shear heating depends upon the rheology of the compound and non-uniformity between the shots gives different temperatures after moulding is filled. For providing uniform vulcanisation for every shot the heating of the mould is adjusted. Throughout the entire process the thermic management is the scheme of the control. Whereas this control scheme is capable of handling non-uniformity among shots, it does not erase the non-uniformity. The non-uniformity itself must be reduced as much as possible at the mixing stage.

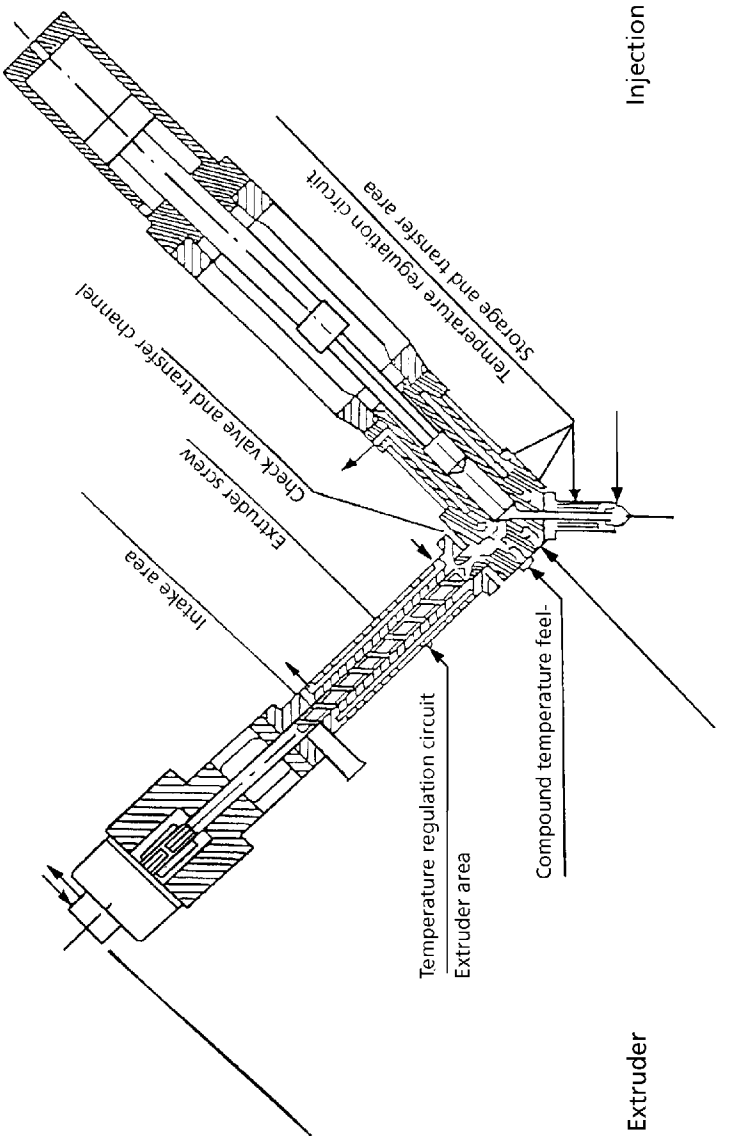

Figure 12.26 Rubber injection moulding head.

Reprinted with permission from J. McConnell and G. Michel, Presented at the 152nd Meeting of the ACS Rubber Division, Cleveland, OH, Fall 1997, Paper No.76. Copyright 1997, Rubber Division of the ACS.

References

1. N. Nakajima, W. J. Shieh and Z. G. Wang, *International Polymer Processing*, 1991, **6**, 4, 290.

2. K. Okubo, *Journal of the Society of the Rubber Industry, Japan*, 1989, **62**, 140.

3. R. Brzoskowski, K. Kubota, K. Chung, J. L. White, F. C. Weissert, N. Nakajima and K. Min, *International Polymer Processing*, 1987, **1**, 3, 130.

4. P. S. Johnson, *Rubber Chemistry and Technology*, 1983, **56**, 3, 575.

5. J. M. McKelvey, *Polymer Processing*, John Wiley and Sons, Inc., New York, 1962.

6. R. Brzoskowski, J. L. White, F. C. Weissert, N. Nakajima and K. Min, *Rubber Chemistry and Technology*, 1986, **59**, 4, 645.

7. M. P. Wagner, *Rubber Chemistry and Technology*, 1976, **49**, 3, 703.

8. K. Kubota, R. Brzoskowski, J. L. White, F. C. Weissert, N. Nakajima and K. Min, *Rubber Chemistry and Technology*, 1987, **60**, 5, 924.

9. *Information for The Rubber Industry*, A.G. Degussa, Geschäftsberich Anorganische Chemieprodukte, Frankfurt, 1983.

10. S. Wolff, *Rubber Chemistry and Technology*, 1982, **55**, 4, 967.

11. ASTM D1646 - 98a
Standard Test Methods for Rubber - Viscosity, Stress Relaxation, and Pre-vulcanisation Characteristics (Mooney Viscometer).

12. N. Nakajima and M. H. Chu, *Rubber Chemistry and Technology*, 1990, **63**, 1, 110.

13. A. I. Medalia, *Rubber Chemistry and Technology*, 1974, **47**, 2, 411.

14. N. Nakajima, Presented at the *International Seminar on Elastomers*, Itoh, Shiznoka, Japan, 1985, 182.

15. R. N. Datta, P. K. Das, S. K. Mandal and D. K. Basu, *Kautschuk Gummi Kunststoffe*, 1988, **41**, 2, 157.

16. N. Nakajima and E. R. Harrell, *Journal of Rheology*, 1982, **26**, 5, 427.

17. A. R. Payne, *Journal of Applied Polymer Science,* 1965, **9**, 6, 2273.

18. R. A. Heinrich, *Measurements and Control*, Imass, Inc., P.O. Box 134, Accord, Hingham, MA 02018, USA, 1985.

19. N. Nakajima, and E. R. Harrell, *Rubber Chemistry and Technology*, 1980, **53**, 1, 14.

20. N. Nakajima, J. J. Scobbo, Jr., and E. R. Harrell, *Rubber Chemistry and Technology*, 1987, **60**, 4, 742.

21. J. D. Ferry, *Viscoelastic Properties of Polymers*, John Wiley and Sons, Inc., New York, 1980.

22. N. Nakajima and E. R. Harrell, *Rubber Chemistry and Technology*, 1982, **55**, 5, 1426.

23. R. Brzoskowski, S. A. Montes, J. L. White and N. Nakajima, *Journal of Non-Newtonian Fluid Mechanics,* 1989, **31**, 43.

24. W. M. Hess, in *Reinforcement of Elastomers*, Ed., G. Kraus, Interscience Publishers, New York, 1965, Chapter 6.

25. S. Montes, J. L. White and N. Nakajima, J*ournal of Non-Newtonian Fluid Mechanics*, 1988, **28**, 183.

26. A. R. Payne and R. E. Whittaker, *Rubber Chemistry and Technology*, 1971, **44**, 2, 440.

27. N. Nakajima and J. J. Scobbo, Jr., *Rubber Chemistry and Technology*, 1988, **61**, 1, 137.

28. N. Nakajima, E. R. Harrell, P. R. Kumler, D. A. Seil and A. H. Jorgensen, *Advances in Polymer Technology*, 1984, **4**, 3/4, 267.

29. ASTM D3616 - 95
Standard Test Methods for Rubber, Raw - Determination of Gel, Swelling Index, and Dilute Solution Viscosity.

30. Thermic Aspects of Rubber Injection Moulding, REP Corporation.

13 Material Testing, Quality Control and Process Control

13.1 Introduction

The purpose of material testing may be for problem solving, quality control or process control. In this chapter the discussion will focus primarily on quality control and process control in support of production. The underlying motivation is possible cost-saving and quality improvement. For the latter the uniformity and reproducibility of quality are the most important. The elimination of waste is also considered.

The activities of quality and process control go hand-in-hand in production as illustrated in Figure 13.1. In relation to the quality control characterisation methods for gum rubber and those for compounds have been given in the earlier chapters. However, characterisation is primarily for problem solving, which requires detailed examination.

For that purpose fundamental research based on a scientific approach must be adopted. Testing in support of production is quite different from characterisation because of many constraints, of which time is one. This aspect will be discussed in section 13.2.

Process control requires monitoring of process parameters. In order to understand the significance of the parameters, it is necessary to know the process mechanisms. The energy aspect and mixing mechanism have been given in the earlier chapters. Some monitoring involves testing of material quality. White [1] reviews the history of rheological instruments for processability and quality control.

13.2 Material testing

The requirements and constraints imposed for testing are:

1. Ease of operation with the possibility of automation.
2. Provision of accurate and reproducible data.
3. Results obtained quickly with instant feedback.

4. Results expressed as simple number(s).

5. Preferably a tester is commercially available and modification, if required, should be minor.

6. Results are meaningful in terms of basic science (viscoelasticity, fracture, molecular architecture, etc.) and processability.

Between the first five and the last item there is a serious conflict. With the simplification imposed on the first five, the test results cannot be fully scientific. However correct the test may be, it is the same as 'a blind man touching an elephant'.

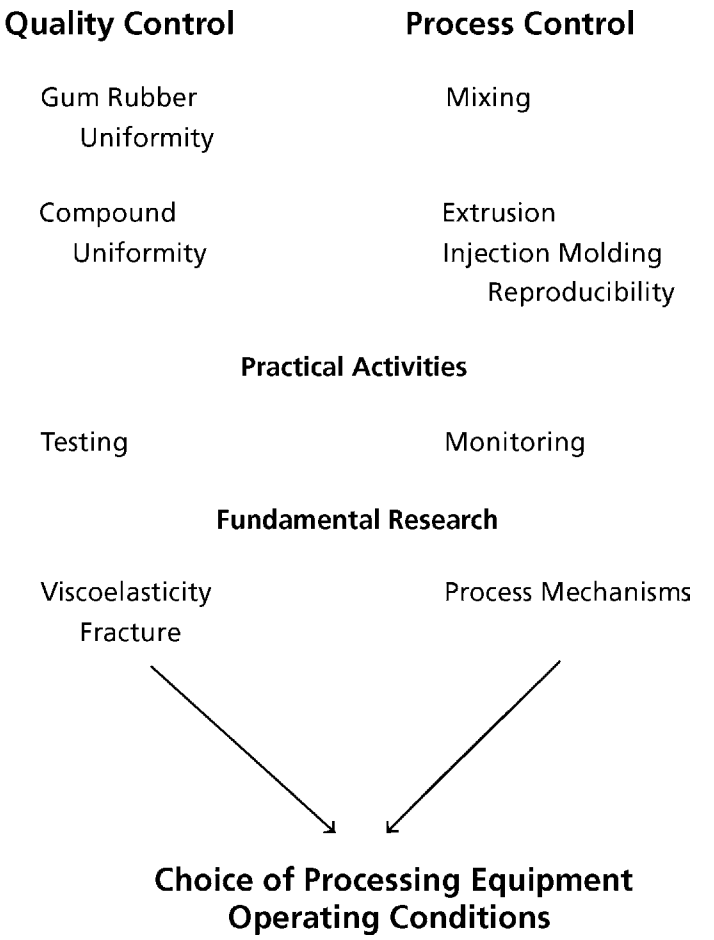

Figure 13.1 Quality Control and Process Control

A mistake is often made in trying to squeeze out information, which is not covered by the test used. Considering processability, there are many aspects of the subject. One test cannot possibly cover every aspect of processability.

It should be obvious that the choice of a test method is of critical importance. The question of which test is appropriate, depends upon a given material and a specific aspect of the process. For the former, a background knowledge of the material, i.e., characterisation, is necessary and for the latter the process mechanism provides the answer.

13.3 Test for the uniformity of gum rubber

There are two aspects in the question of uniformity. The first one is a 'black swan', so-to-speak. If the specification is for the shape of the bird, a black one will not be noticed. This is illustrated in Figure 13.2, by two torque-time curves obtained in the usual Mooney index measurements [2]. These two rubbers give exactly the same torque at 4 minutes of the rotation, e.g., ML (1 + 4), and yet their behaviours are very different. If the specification is the value of ML (1 + 4) only, the 'black swan' goes unnoticed.

What is the physical meaning of the shape of these torque-time curves? Because the rubber in the Mooney rheometer has a complex distribution of stress and strain [3], only an approximate answer can be given. The usual procedure calls for one minute of preheating to 100 °C or to another prescribed temperature before turning the rotor on. However, one minute is not long enough to equilibrate the temperature. Therefore, these curves do not represent the rubber's behaviour at a constant temperature. The following explanation ignores these facts.

Because the Mooney rheometer is a rotational instrument, the deformation is shear. The torque is proportional to shear stress. Since the rotational speed is constant, the time is proportional to shear strain. Therefore, it is a shear stress-strain curve, which is analogous to the more familiar tensile stress-strain curve.

In addition to the torque-rise behaviour the steepness of the curve may be expressed with the torque/time ratio, which is the stress/strain ratio, i.e., modulus. Between the two gum-rubbers in question, there is a significant difference in modulus. The gum rubber giving a steeper curve is stiffer than the other one. The peak may be interpreted as the failure point [4]. The stiffer rubber has a smaller strain to break and the softer rubber is more deformable. The former tends to fall in Region I of mill processability and the latter in Region II. The former may contain macrogel in a significant amount, if it is an emulsion-polymerised diene rubber. See Chapters 4 and 6 for additional information.

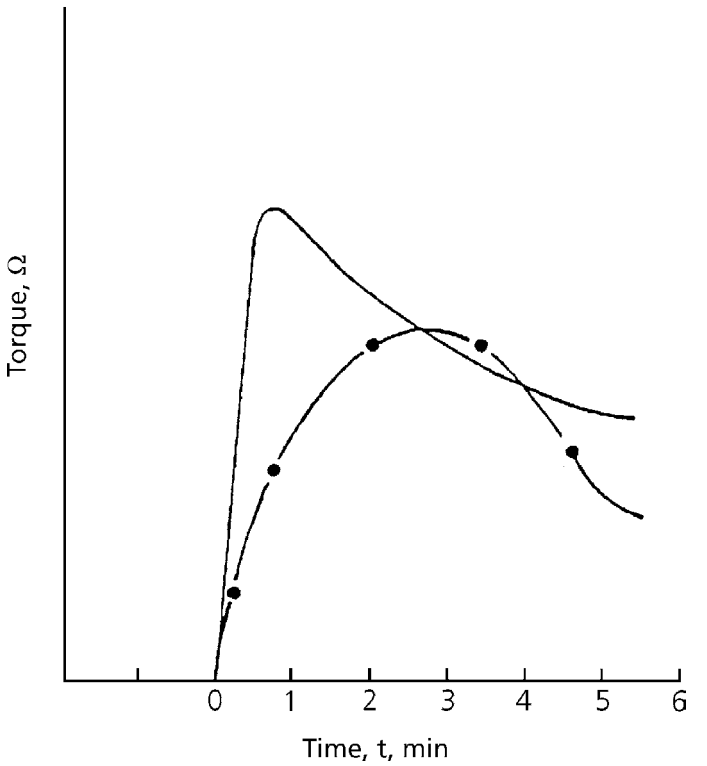

Figure 13.2 Typical Mooney curves; very different viscoelastic properties for the same Mooney indices.

The importance here is to recognise the limitation of the test. In addition to the non-equilibrium temperature of the test and the complex distribution of strain, the curve is measured at 2 rpm, which is an arbitrary time-scale. The material behaviour may be different at other time-scales; this situation is exactly like 'a blind man touching an elephant'. In addition, at this time scale the Mooney rheometer is not very sensitive to a small difference between the gum rubbers. Therefore, this method is for the screening and catching only a gross difference among the samples. The Mooney test is performed for the specification in any event, and therefore, it is proposed here to pay attention to the shape of the curves also.

The next question about uniformity concerns all 'white swans', but of varying sizes. How uniform should the size range be? It translates to the Mooney curves in Figure 13.3, where the dashed curves define the range. The permissible range depends upon the requirements from processing, which may be very severe sometimes but quite accommodating at other times. Only the severest case needs to be discussed. As illustrated in Figure 13.4 [5] the differences among the rubbers are magnified at the lower frequencies. This means that we must use a lower frequency or a longer time for the test to obtain meaningful data.

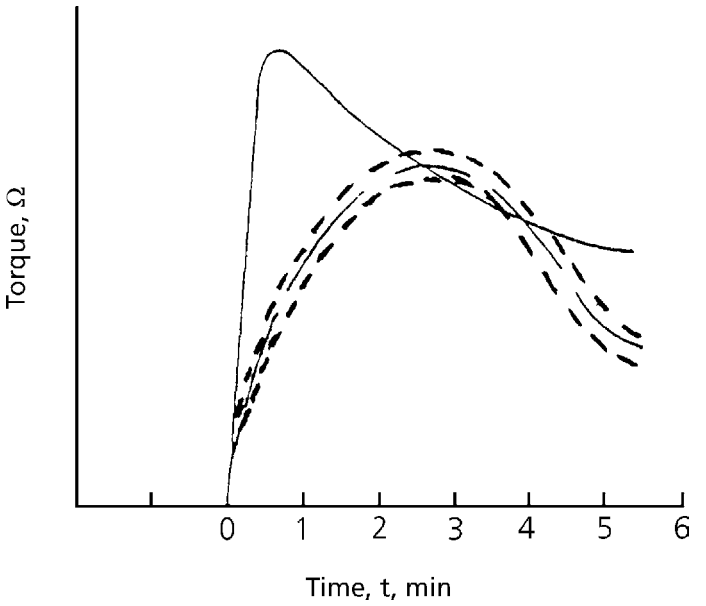

Figure 13.3 Mooney torque-time curves showing permissible range of processability.

Realising the present test is for assisting production, there is a time-limit for testing, which may arbitrarily be set to less than ten minutes.

The commercially available testers for this purpose are rather limited, as is described next.

The usefulness of the slow speed Mooney rheometer for problem solving has been described in Chapter 6. It requires modification of the standard Mooney rheometer with the addition of a 1/40 gear or an electronic speed control. The example in Figure 13.5 shows that 5 minutes of running time may be adequate [6].

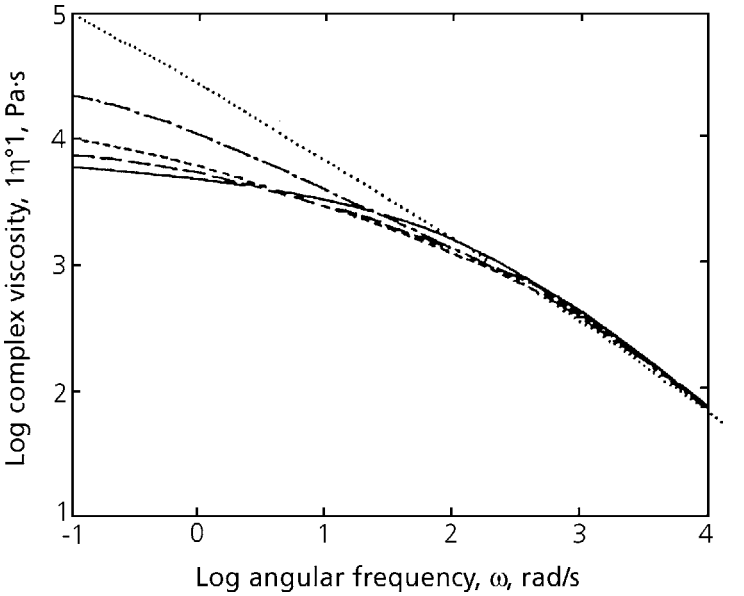

Figure 13.4 Effect of increasing long branching (XL-0-XL-4) on the complex viscosity master curves at 230 °C: (—) XL-0; (- -) XL-1; (—) XL-2; (-·-) XL-3; (.....)XL-4.

Reprinted with permission from E. R. Harrell and N. Nakajima, Journal of Applied Polymer Science, 1984, 29, 3, 995. Copyright 1984, Wiley.

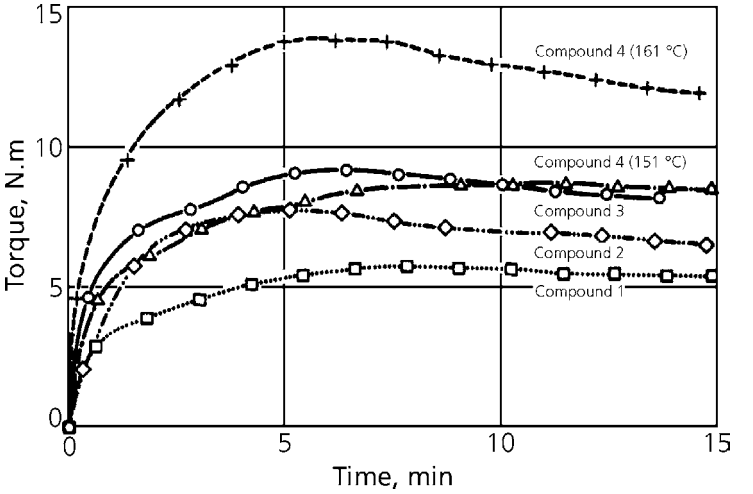

Figure 13.5 Torque-time curves at a very low deformation rate, indicating gel and long branch formation at rotor speed; 0.045 min^{-1}.

Reprinted with permission from N. Nakajima, W. J. Shieh and Z. G. Wang, International Polymer Processing, 1991, 6, 4, 290. Copyright 1991, Hanser Publishers.

The Dynamic Stress Relaxometer (DSR) also provides long time data and promises to be a tester for the same purpose [7]. The oscillating discs may be used if the frequency as low as 10^{-2} rad/s is available. These three tests conform with scientific requirements based on viscoelasticity [7, 8].

The so-called 'Mooney relaxation curve' is another test, which has been the subject of discussion recently. The meaning of this relaxation curve is rather complex and will be discussed in section 13.4.

13.4 Mooney relaxation curve

A proposal to use the Mooney relaxation curve, arises from a realisation that the standard Mooney index alone is not adequate to specify a gum rubber. However, the proposal is based on a convenience rather than a scientific rationale. Since the standard Mooney measurement is made routinely for a given rubber, by stopping the rotation at some time at or after 4 minutes and by holding the rotor at that position, it is hoped that the relaxation curve yields additional information on the material. But what information is gained from the relaxation curve?

As explained earlier the peak of the curve is a failure point [9]. The mode of failure appears like a slippage at the interface between the rotor of the rheometer and the rubber specimen, when it is marked with a 'magic marker'. Because the surfaces of cavity and rotor are serrated, some fracture must have occurred even though the overall behaviour appears to be a slippage. Once the failure occurs, the remaining strain is an unknown quantity. Therefore, the scientific meaning of the relaxation curve becomes obscure.

There is a certain school of thought that as long as the test discriminates one sample from another, scientific significance is unimportant. If the data relates to, for example, a degree of branching the test serves that purpose. Sometimes this approach works. However, the relationship is applicable to only a limited range of variation in material or in the processing conditions. An attempt to interpret scientific meaning of the relationship is futile.

When the rubber is in the melt state, the stress-over-shoot (see section 4.3) occurs and it is not a failure point. A rubber's behaviour may be in the melt state if it is a low MW rubber, at a high temperature or at a low deformation rate.

What the relaxation curve means if the relaxation curve is obtained by stopping the deformation before, at and after the peak of overshoot, had been described in Chapter 6 [10, 11]. The sample was EPR and temperature was 100 °C. The relaxation curve was

dependent upon the deformation rate and the magnitude of deformation, i.e., non-linear viscoelastic behaviour. The relaxation curve was shown to be a manifestation of the stored memory possessed by the material at the time the deformation was stopped. This type of experiment may be useful for a problem solving, but is too involved for the present interest on the material testing.

13.5 Testing for uniformity of compound

Compound testing has two aspects, one is for quality and the other is for reproducibility of the mixing process. Even though both aspects are intimately related, they will be discussed separately.

The primary concern about quality is the degree of dispersion of the fillers. Sometimes premature crosslinking also becomes critical. Both examples have already been described. The dispersion was tested in two different ways; how many bigger particles, i.e., agglomerates, remained was examined with an SEM. The strength of the filler network was examined with the amplitude dependence of the dynamic properties [12]. Both tests require considerable time and are not readily adoptable for use in production areas. A visual inspection of the surface gloss and the compound becoming stretchable have been used for this purpose. There are instruments for determining the former and the latter may be replaced with the moduli at two points, i.e., the shear amplitude at 0.1 and 0.5 in Figure 13.6 [6]. DSR may also be operated at two different strain levels. The measurement takes only a few minutes.

The uniformity in terms of reproducibility involves batch-to-batch as well as in-batch variation. The required size level of the uniformity depends upon the downstream method of processing such as extrusion and injection moulding as already discussed. If the size is in the order of mm^3, the compound may be extruded from a capillary rheometer at a constant speed and the pressure oscillation may be taken as a measure of uniformity.

For a larger size non-uniformity, for example, variation within the batch of internal mixers may appear as a pressure oscillation observed by a pressure-tap at the chamber wall of a mixer [13]. It may also appear as an oscillation of the mixing torque (see Table 3.1 [24]). However, before using these oscillations as a measure of degree of non-uniformity, an independent check by actual sampling of the contents must be done, because the oscillation is also related to the way in which the compound is moved around the mixer. For the batch-to-batch variation, previously mentioned ‘two-point measurements’ of moduli may be used. If the requirement is not very critical, even a one-point measurement may be adequate.

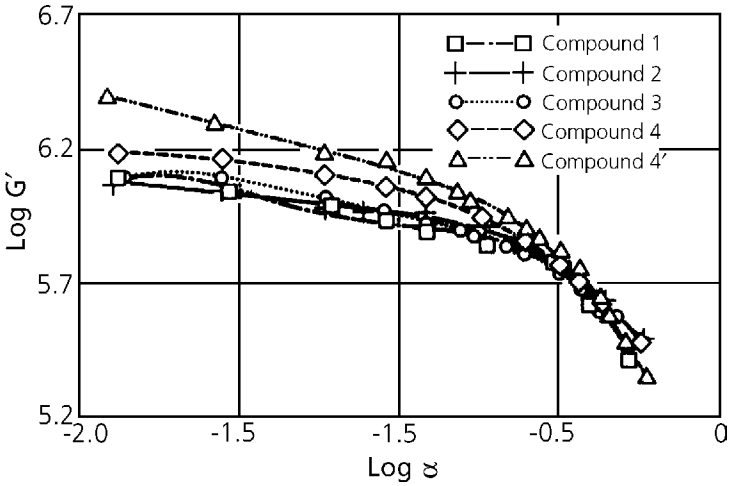

Figure 13.6 Amplitude dependence of shear storage modulus, indicating relative degree of dispersion of fillers.

Reprinted with permission from N. Nakajima, W. J. Shieh and Z. G. Wang, International Polymer Processing, 1991, 6, 4, 290. Copyright 1991, Hanser Publishers.

13.6 Process control

This discussion will be limited to the control of the internal mixer only. Uses of the roll-mill also require control, but in this case, the material is visible to the operator who makes the appropriate adjustments.

The problem with the internal mixer is that the contents are not visible and we must rely on indirect monitoring. As discussed in section 11.2 the total mixing time is not a good criterion, because of the poor reproducibility. The temperature-time curve is important for preventing premature cure. However, a built-in thermocouple at one location may not be accurate enough. In the example described earlier [14], the recorded temperature was 12-39 °C lower than the average temperature of the compound. Also, within the compound there was a temperature distribution estimated to be ±13.5 °C (see section 10.2.3). Therefore, the temperature recording may be only supplementary information for the process control. At present the energy input is the best measure and the compound is dumped at a prescribed total energy input.

Other indicators to monitor are the torque-time curve and the movement of the ram. Also, pressure tapping may be explored. Before discussing these, it is worthwhile to examine some of the causes of time-wise reproducibility problem. Even if the charging of the material is done in the same way each time, the mutual positions of two rotors with respect to wings are not the same. If there is a difference in the rotational speed of the rotors, they meet at the same mutual position after so many revolutions. The question is whether or not the charging may be automated in such a way for the rotors to accept the material at the same mutual position every time.

Also, important is the ease of material movement around the mixing chamber. Stagnation and impinging motions may contribute to the reproducibility problem. This has already been discussed (see section 11.10.3) in conjunction with efficiency of mixing [15].

The amplitude of oscillation in torque-time curve or that of the ram movement decreases as the contents becomes more homogeneous. In order to use these or total energy for deciding the endpoint, the dispersion must be examined ahead of time to assure a satisfactory result. The reproducibility in the same type mixer but different machines may be a problem. There may be a difference in the extent of wear of the rotor blades. The cooling surface may have scale build-up such that the cooling efficiency may be different.

Knowledge of how well the mixing is progressing is an important part of the process control. Various methods have been developed to gauge it with a 'processability index'. These are summarised in Shiga's review [16] and reproduced as Table 13.1.

Among these methods 'the second torque-maximum' has been the most easily identifiable feature. It is called BIT, because the incorporation of the carbon black is practically completed by this time. A distinct change of some properties of the compound is reported to occur at the maximum torque; for example, the maximum in die swell and an increase of the density to a constant value are reported in the mixing of SBR1712 with carbon black N339 [27]. Shiga observed an increase of the resistivity to a constant value in the mixing of EPDM [28, 29]. A detailed work by Cotten showed that the density increased in an asymptotic manner and that at the torque maximum the density was still increasing. Samples were SBR1712 and *cis*-1,4-BR441 mixed with N339. Significant increases of resistivity were observed well past the maximum [32]. A similar observation is reported by Shiga in the mixing of SBR1500 [31].

The second maximum torque is not observed sometimes or is so broad that it is difficult to accurately assign the peak-time. If the BIT is to be used for the process control, its significance should be known ahead of time.

From a very practical point of view, the end of incorporation is often very important, because in many operations the compound is dumped from the internal mixer at this time onto a mixing mill. Subsequently, the dispersion is completed on the mill.

Just when to terminate mixing is a critical question for both the quality and economic stand points. Yet, there is no universal criterion, because the optimum endpoint depends upon both formulation and requirements from the end-use. Jansen and Kraus [19] states, 'It is not always clear what constitutes a good dispersion. At practical black loadings complete separation of every primary structure aggregate from its neighbours is neither possible, nor would it be desirable'. Therefore the endpoint must be predetermined case-by-case.

Table 13.1 Processability Indices (From Reference [31])

Method No.	Report	Sample type
1. Microscopic method ASTM D2663-69 [17]	[18]	
	[19]	SBR, NR, BR
2. Surface roughness	[20]	SBR, NR, BR
3. PMT	[21]	SBR
4. Mooney slope	[21]	SBR
5. Delta Mooney	[22]	SBR
6. BPI	[22]	SBR
7. BIT (t_2pp)	[23]	SBR
8. t′ point	[24]	SBR
9. Bound rubber	[24]	SBR
10. Unit work	[24]	SBR
11. TSSU	[24]	SBR
12. Die swell	[25]	SBR
13. Compound Mooney	[25]	SBR
14. Specific volume	[25]	SBR
15. Resistivity	[26]	SBR
16. *L*-value	[27]	SBR
17. Mechanical properties	[28]	SBR
18. Optical extinction	[19]	SBR

PMT: Initial Mooney peak torque
BPI: Banbury processability index
BIT: Black incorporation time
t′ point: Time to decrease torque oscillation
t_2pp: Time to second power peak
TSSU: Total shear-strain units
L-value: Parameter obtained from cure-rheometer

References

1. J. L. White and I. Soos, *Rubber Chemistry and Technology*, 1993, **66**, 3, 435.

2. ASTM D1646 - 96a
Standard Test Method for Rubber - Viscosity, Stress Relaxation and Pre-Vulcanisation Characteristics (Mooney Viscometer).

3. N. Nakajima and E. R. Harrell, *Rubber Chemistry and Technology*, 1979, **52**, 1, 9.

4. N. Nakajima, *Polymer Engineering and Science*, 1979, **19**, 3, 215.

5. N. Nakajima, *Polymer International*, 1995, **36**, 2, 105.

6. N. Nakajima, W. J. Shieh and Z. G. Wang, *International Polymer Processing*, 1991, **6**, 4, 290.

7. E. R. Harrell, J. P. Porter and N. Nakajima, *Rubber Chemistry and Technology*, 1991, **64**, 2, 254.

8. N. Nakajima and E. R. Harrell, *Rubber Chemistry and Technology*, 1982, **55**, 5, 1426.

9. N. Nakajima and E. A. Collins, *Rubber Chemistry and Technology*, 1977, **50**, 4, 791.

10. N. Nakajima and E. R. Harrell, *Journal of Rheology*, 1983, **27**, 3, 241.

11. N. Nakajima and E. R. Harrell, *Journal of Rheology*, 1986, **30**, 2, 383.

12. A. R. Payne, *Journal of Applied Polymer Science*, 1965, **9**, 6, 2273.

13. S. Toki, M. Takeshita, Y. Morimoto and M. Okuyama, Presented at the 124th ACS Rubber Division Meeting, Houston, TX, Fall 1983, Paper No.37.

14. N. Nakajima, E. R. Harrell and D. A. Seil, *Rubber Chemistry and Technology*, 1982, **55**, 2, 456.

15. N. Nakajima, *Rubber Chemistry and Technology*, 1981, **54**, 2, 266.

16. S. Shiga, *Rubber Chemistry and Technology*, 1992, **65**, 3, 660.

17. ASTM D2663 - 95a
Standard Test Methods for Carbon Black-Dispersion in Rubber.

18. A. I. Medalia, *Rubber Age*, 1965, **97**, 1, 82

19. J. Jansen and G. Kraus, *Rubber Chemistry and Technology*, 1980, **53**, 1, 48.

20. P. C. Vegvari, W. M. Hess and V. E. Chirico, *Rubber Chemistry and Technology*, 1978, **51**, 4, 817.

21. W. Mills and F. Giurco, *Rubber Chemistry and Technology*, 1976, **49**, 2, 291.

22. S. C. Einhorn, *Rubber World*, 1963, **148**, 5, 40.

23. K. C. Beach, L. F. Comper and V. E. Lowery, *Rubber Age*, 1959, **85**, 2, 253.

24. P. R. Van Buskirk, S. B. Turetzky and P. F. Gunberg, *Rubber Chemistry and Technology*, 1975, **48**, 4, 577.

25. I. Pliskin, *Rubber Chemistry and Technology*, 1973, **46**, 5, 1218.

26. M. E. Woods and R. P. Krosky, *Rubber Age*, 1973, **105**, 4, 33.

27. B. L. Lee, *Rubber Chemistry and Technology*, 1979, **52**, 5, 1019.

28. B. B. Boonstra and A. I. Medalia, *Rubber Chemistry and Technology*, 1963, **36**, 1, 115.

29. N. Tokita and I. Pliskin, *Rubber Chemistry and Technology*, 1973, **46**, 5, 1166.

30. S. Shiga and M. Furuta, *Journal of the Society of the Rubber Industry, Japan*, 1982, **55**, 491.

31. S. Shiga, H. Yamada, I. Ichikawa and T. Hikasa, *Journal of the Society of the Rubber Industry, Japan*, 1981, **54**, 587.

32. G. R. Cotten, *Rubber Chemistry and Technology*, 1984, **57**, 1, 118.

14 Mixing of Rubber without using a Mill or Internal Mixer

14.1 Masterbatch

The ultimate purpose of mixing rubber is to disperse filler into the rubber matrix. With carbon black the dispersion process may be stated as,

agglomerate → aggregate

100-10 μm → 100-10 nm

The process of carbon black manufacture may be stated as

primary particle → agglomerate (and pellet)

100-10 nm → 100-10 μm (and larger)

The question is whether or not the primary particles can be directly mixed into the rubber.

The size of latex particles of the emulsion-polymerised rubber is less than 100 nm. This size corresponds to the domain size of rubber after the mixing is completed. It follows that if the primary particles of carbon black are added to rubber latex, satisfactory mixing may be achieved [1]. This is easier said than done.

First of all, the primary particles of carbon black are small, being invisible or at best like smoke. There is a handling problem. If the particles are suspended in water, they tend to flocculate. When the aqueous suspension of carbon black is added to the rubber latex, the mixture tends to consist of flocculates of carbon black and flocculates of rubber particles. The latter flocculation occurs, because the latex contains a minimum amount of emulsifier and thus it has minimum colloidal stability. Any change of the condition tends to bring a loss of stability. Once the separate flocculates are formed, additional mixing is required for improving dispersion. However, this approach offers an opportunity for developing innovative mixing processes.

The main requirement is to keep the same kind of particles, i.e., carbon black - carbon black and rubber - rubber separate and for the different kinds of particles, i.e., carbon black - rubber to attract each other. For this purpose the carbon black particles may be given an electrostatic charge and the rubber particles given the opposite charge. The charging process may be done simultaneously with 'atomising' (mist formation) particles.

A similar process can be developed with silica fillers. The solution-polymerised rubber may be also atomised.

In a recent development by Cabot [2] a rubber latex and a carbon black slurry are co-coagulated in a continuous, rapid mixer with vigorous agitation. The process is particularly suited to NR latex, which has a delicate balance of stability, although in principle, it is applicable to any rubber latex. The advantages over dry mixing are demonstrated in several ways:

(i) capability of dispersing a wider range of fillers including the high surface area/low structure carbon blacks which are very difficult to disperse

(ii) improved macro-dispersion and micro-dispersion

(iii) preservation of rubber MW, particularly for NR and resulting superior resistance to crack growth

(iv) saving of mixing energy and improved cleanness.

The current method of preparing carbon black masterbatch is to grind the agglomerates first and then mix them into rubber. In this process the size of carbon black is much larger than that of the aggregates. Even so, a recent development of wet masterbatch resulted in savings of both mixing energy and better dispersion [3].

14.2 Continuous mixing

The mill mixing and the use of internal mixer have been the major modes of mixing of rubber. However, these methods are not without deficiencies. The mill mixing may be labour-intensive so that it is used when the cost of mixing is not a concern. Therefore, it tends to be used for research and development. In production, it is used when the cost, for other than mixing dominates or when there is a critical requirement for a good dispersion.

The internal mixer has been used for many years. Much experience has been accumulated to make optimal use of the mixer. Significant improvements have been made over the

years. However, there are many inherent deficiencies as discussed already. Major deficiencies are:

(i) the non-uniformity of the contents resulting from the design of the machine and from the nature of the material;

(ii) with a roll-mill (see section 11.2) after each passage, the material is completely removed and recharged. Therefore, mixing proceeds by a step-by-step improvement (see section 11.2). In the internal mixer the material is improved by passing through a gap and is then returned and diluted with unimproved material. This is not a very efficient process. This situation may be visualised by considering the chemical reaction of a reactant A changing to product B. The best efficiency may be obtained by removing B from the reacting system instead of returning and mixing with A:

(iii) the optimal conditions required for incorporation and dispersion are very different. Trying to achieve the best result with the same machine for very different processes requires a compromise

(iv) poor batch-to-batch reproducibility. Even with the same type machines, the mixing results are not necessarily the same

(v) because the chamber volume is cubic and the cooling surface of the chamber is the square of the linear dimension of a machine, scale-up is difficult (see section 11.2). This is especially true, if one recognises the temperature sensitive nature of viscoelastic properties.

All of these deficiencies may be overcome by adopting continuous mixing. In addition there is no downtime for charging and discharging in the continuous operation so that the output rate can be improved.

Continuous mixing is not a new idea, but for many years there existed the Farrel continuous mixer, Figure 14.1 [4] and the Transfermix, Figure 14.2 [5]. In practice these machines have been used for improving dispersion of a compound containing incorporated fillers. Proposed in this section is a completely continuous operation from charging the formulation to discharging a well-mixed compound. In principle, a batch process may be translated into a continuous process, when every operational parameter of the former is known. However, between the batch mixing and continuous mixing of rubber there is a fundamental difference in the material transport. In the batch mixing the material is returned to the milling zone repeatedly. In the continuous mixer the material is moved forward, by conveying screws.

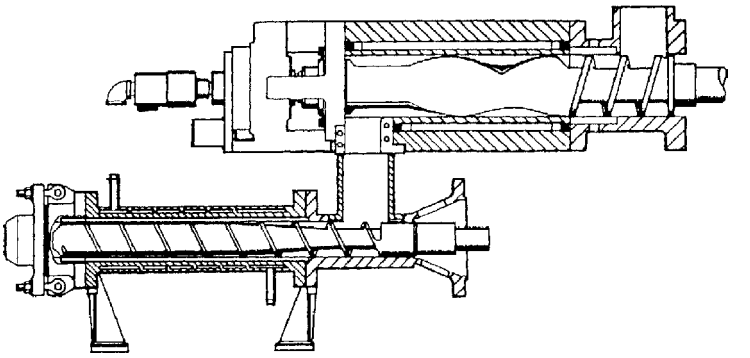

Figure 14.1 Farrel continuous mixer.

Reprinted with permission from P. Hold, Advances in Polymer Technology, 1984, 4, 3/4, 281. Copyright 1984, John Wiley & Sons.

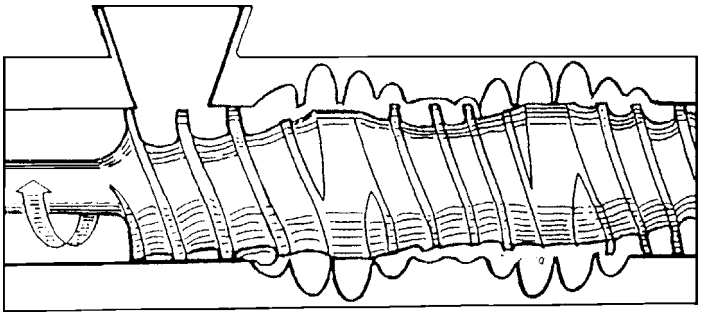

Figure 14.2 Transfermix screw and barrel.

Reprinted with permission from P. S. Johnson, Rubber Chemistry and Technology, 1983, 56, 3, 575. Copyright 1983, Rubber Division of the ACS.

As a first approach a cylindrical barrel rather than the complicated barrel of Transfermix may be chosen. With a single screw extruder a filled channel is required in order to create pressure necessary for feeding material to a mixing zone. This leads to excessive temperature rise. With a twin-screw a starved condition may be used to move the material forward with a minimum of temperature rise. A successful example of the continuous mixing of EPDM with a Werner & Pfleiderer twin screw extruder was described by Tyler [6].

There is a twin-screw mixer-pelletiser for mixing polyolefins and carbon black, see Figure 14.3 [7]. It has a large size and the output rate is comparable to that for the largest batch internal mixer for rubber.

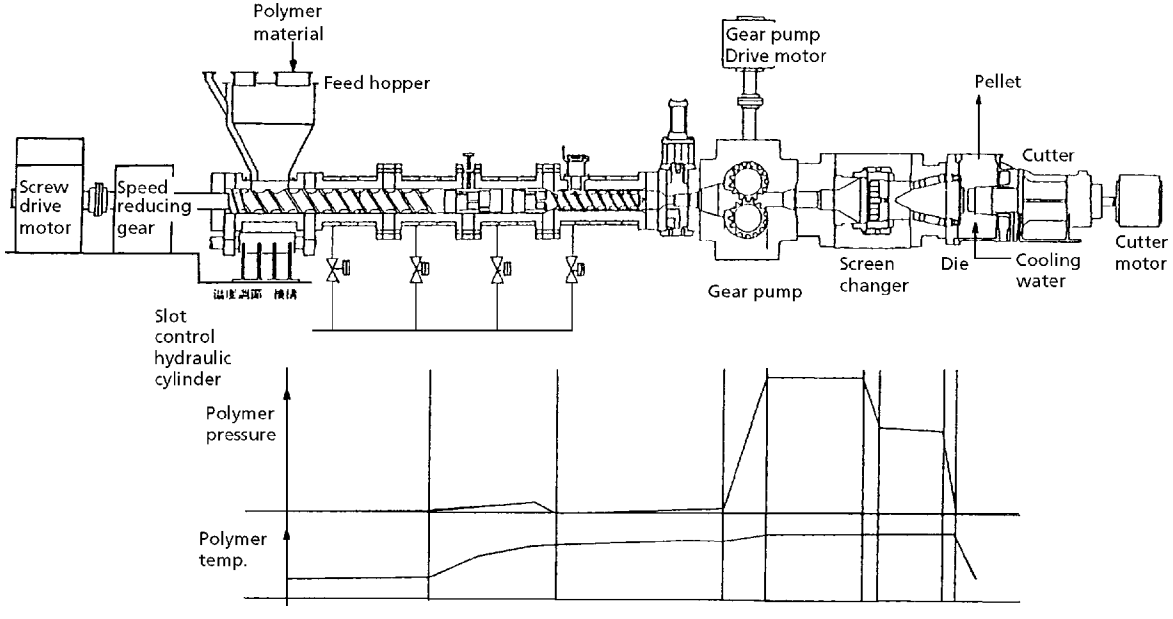

Figure 14.3 JSW CMP Pelletiser.

Reprinted with permission from H. Mizugichi, S. Ogoshi and Y. Mizutani, JSW Technical Review, 1990, 14, 76. Copyright 1990, Japan Steel Works, Ltd.

Because rubber has a much higher viscosity and elastic modulus than those of polyolefins, this machine is not immediately usable for rubber. However, it may be taken as the starting point of the idea and necessary modifications will be discussed next. One significant difference between this machine and other plastic-extruders is the placement of a gear-pump between the die and the screw-head.

The characteristics of the use of the gear pump are:

(i) improved efficiency of increasing pressure for overcoming the die resistance. In the conventional screw extruder, the metering zone is used for this purpose but the reverse flows, i.e., pressure flow and leakage flow reduce the efficiency

(ii) the gear pump maintains a steady output rate through the die. With a screw pump, the pressure level and the output rate are affected by the property of material. Therefore, the material non-uniformity disturbs a steady operation

(iii) With a gear pump taking care of the extrusion through the die, the screw section can be dedicated to mixing.

In developing successful continuous mixing it is important to design a steady process from the beginning to end. This means a strict feed control is a must. One approach is to use a premixed formulation with powdered or pelletised rubber. Maintaining a steady rate of feeding requires a feeding device.

In feeding a bale of rubber a conical extruder may be used for masticating and feeding. However, because the conical extruder is operated with a periodic feeding of bales, it may affect the stability of feeding. If this is the case, mastication may be performed with an extruder and a steady feed achieved with use of a gear pump.

In the incorporation stage, three changes must be brought about, i.e., comminution-lamination, imparting a tacky surface and compaction. When the powdered or pelletised rubber is used, all three must occur. This may require a powerful kneading gear. Pre-masticated rubber it is already in the form of supermolecular flow units which have tackiness, and a relatively mild kneading gear may be sufficient.

The continuous dispersion has already been demonstrated with the Farrel continuum mixer and the Transfermix. There is no need for a feasibility study. The temperature-rise during incorporation should be kept to a minimum. Otherwise the temperature-control during dispersion becomes difficult. The temperature-control by cooling is difficult for the following reasons; for better cooling the channel must be shallow. The shallow passage requires a higher rate of the material transport; otherwise, the output rate is sacrificed.

The high rate contributes to a temperature-rise. Therefore, cooling may not be effective. The distributive mixing is achieved by a rigorous control of feeding of additives. However, non-uniformity can arise within a volume at the feed-port. The volume of the material corresponding to that of the feed-port may be homogenised for example, with the Rapra CTM, see Figure 12.7 [5].

14.3 Handling of new material

This book is about mixing of rubber in traditional rubber processing. In recent years many new materials have been introduced into the field of rubber processing. They are plastic-rubber blends, block or graft copolymers consisting of plastic and rubber segments, soft-rubbers containing large amount of liquid and rubber compounds containing fibrous fillers. The mixing of these materials is not covered in this book. Nevertheless a few comments are in order.

First, mixing of these materials may be very different from what has been described so far. For example, the internal mixer described here is primarily a tangential type. For many of the new materials an intermeshing type may offer an advantage. Also, use of a twin-screw and continuous mixing may be a preferred choice.

Increasing uses of office machines, money-changers, computer-related equipment and medical equipment require relatively small volumes but require a large variety of rubber products each having unique properties. The rubber materials for these applications may be very different from those discussed in this book. However, with understanding of what is different in new materials through characterisation [8, 9 and 10], an insight may be gained for choosing proper mixing operations.

References

1. N. Nakajima, *Journal of the Society of the Rubber Industry, Japan*, 1994, **67**, 3, 163.

2. N. Tokita, M. J. Wang, B. Chung and K. Mahmud, *Journal of the Society of the Rubber Industry, Japan*, 1998, **71**, 9, 522.

3. K. Sone, *Journal of the Society of the Rubber Industry, Japan*, 1998, **71**, 6, 308.

4. *Advances in Polymer Technology*, 1984, **3/4**, front cover.

5. P. S. Johnson, *Rubber Chemistry and Technology*, 1983, **56**, 3, 575.

6. R. C. Tyler, D. W. Tredinnick and F. R. Burbank, Presented at the 148th Meeting of the ACS Rubber Division, Cleveland, OH, Fall 1995, Paper No.61.

7. M. Mizugichi, S. Ogoshi and Y. Mizutani, *Japan Steel Works Technical Review*, 1990, 14, 76.

8. N. Nakajima, R. Babrowicz and E. R. Harrell, *Journal of Applied Polymer Science*, 1992, **44**, 8, 1437.

9. N. Nakajima, *Rubber Chemistry and Technology*, 1996, **69**, 1, 73.

10. N. Nakajima, *Rubber World*, 1996, **215**, 3, 33.

Abbreviations and Acronyms

ABS	Acrylonitrile-butadiene-styrene
ACM	Polyethylacrylate
AN	Acrylonitrile
ARRD	Agerite resin D
ASTM	American Society for Testing and Materials
BET	Brunauer-Emmett-Teller method
BIT	Black incorporation time
BPI	Banbury processability index
cis-1,4-BR	*cis*-1,4-polybutadiene rubber
CF	Conductive furnace black
CO	Epichlorohydrin
CPE	Chlorinated polyethylene
CR	Polychloroprene
CSDP	Carbon-silica dual phase
CSM	Clorosulphonated polyethylene
CTAB	Cetyltrimethylammonium bromide
CTM	Cavity transfer mixer
DBP	Dibutylphthalate
DBPA	Dibutylphthalate absorption
DCPD	Dicyclopentadiene
DOP	Dioctyl phthalate
DSC	Differential scanning calorimeter
DSR	Dynamic stress relaxometer
DSV	Dilute solution viscosity
DTA	Differential thermal analysis
ECO	Epichlorohydrin-ethylene oxide
ENB	Ethylidene norbornene
E/P	Ethylene:Propylene ratio

EP	Epoxide
EPDM	Ethylene-propylene-diene terpolymer
EPM	Ethylene-propylene copolymer
EPR	Ethylene-proplyene rubber
ERD	Eccentric rotating disk
E-SBR	Copolymer of styrene and butadiene made by emulsion polymerisation
ESR	Electron spin resonance
EVA	Ethylene vinylacetate polymer
FEF	Fast extrusion furnace black
FF	Fine furnace black
FFKM	Tetrafluoroethylene-perfluoromethyl vinyl ether
FKM	Vinylidene fluoride type polymer
FPM	Fluoroelastomer
FQ	Fluorosilicone
FT	Fine thermal black
GPC	Gel permeation chromatography
GPF	General purpose furnace black
GPF-HS	General purpose furnace black (high structure)
HAF	High abrasion furnace black
HAF-HS	High abrasion furnace black (high structure)
HAF-LS	High abrasion furnace black (low structure)
IIR	Polyisobutylene
IR	Polyisoprene rubber
IRB	Industry reference black
ISAF	Intermediate super abrasion furnace black
ISAF-HS	Intermediate super abrasion furnace black (high structure)
ISAF-LM	Intermediate super abrasion furnace black (low modulus)
ISAF-LS	Intermediate super abrasion furnace black (low structure)
LALLS	Low angle laser light scattering
L/D	Length:diameter ratio
MBTS	Dibenzothiazyl disulphide
MEK	Methyl ether ketone
MER	Mechanical energy resolver

MQ	Polydimethyl siloxane
M-R	Mass-size relationship
MT	Medium thermal black
MTS	High speed tensile tester
MV	Mooney viscosity
MW	Molecular weight
M_W	Weight average MW
NBR	Acrylonitrile butadiene rubber
NMR	Nuclear magnetic resonance
NR	Natural rubber
P-A	Perimeter-area relationship
PAC	Degree of packing
PDMS	Polydimethyl siloxane
PEN	Degree of penetration
phr	Parts per hundred rubber (by weight)
PMT	Initial Mooney peak torque
PS	Polystyrene
PTT	Passenger tyre tread
PU	Polyurethane
PVC	Polyvinyl chloride
SAF	Super abrasion furnace black
SAF-HS	Super abrasion furnace black (high structure)
SBR	Styrene-butadiene copolymer
SCF	Semi-conducting furnace black
SEM	Scanning electron microscope
SIBR	Styrene-isoprene-butadiene terpolymer
SIR	Standard Indonesian rubber
SPB	syndiotactic 1,2-polybutadiene
SPF	Super processing furnace black
SRF-HS	Semi-reinforcing furnace black (high structure)
S-SBR	Copolymer of styrene and butadiene made by solution polymerisation
T	Polysulphide
T_g	Glass transition temperature

TEM	Transmission electron microscope
TESPT	Bis-(3-[triethyoxysilyl]-propyl-tetrasulphone
TETD	Tetraethyl thiuram disulphide
TFEP	Tetrafluoroethylene-propylene
TMTD	Tetramethyl thiuram disulphide
TSSU	Total shear-strain units
VIC	Variable internal clearance
WLF	Williams-Landel-Ferry

Author Index

F

G

H

I

J

K

L

M

N

O

P

R

S

T

U

V

W

Y

Z

Company Name Index

Main Index

D

E

F

G

H

I

L

M

N

O

P

Q

R

S

T

U

V

W

Y